Modelling Surface Active Species Transport During a Foam Fractionation Process with Reflux

Hamed Rajabi

Supervisor: Dr Paul Grassia

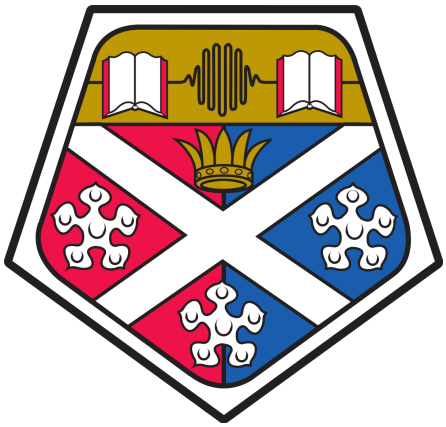

PhD Thesis

Department of Chemical and Process Engineering

University of Strathclyde

September, 2023

Contents

List of figures viii

List of tables ix

Nomenclature x

Abstract xvi

Declaration xviii

Acknowledgements xix

1 Introduction 1

1.1 Motivation 1

1.2 Thesis overview 5

2 Literature review 7

2.1 Surface active components 7

2.1.1 Surfactant properties and applications 9

2.1.2 Surfactant on surface 10

2.1.3 Surfactant in bulk 11

2.2 Foam fractionation 13

2.2.1 Fractionation applications and operation 13
2.2.2 Fractionation as a counter-current separation process 15
2.3 Performance of fractionation 18
2.4 Foam properties 19
2.4.1 Foam structure 20
2.4.2 Young-Laplace law 22
2.4.3 Essential physics governing foam evolution 24
2.4.3.1 Foam drainage 25
2.4.3.2 Film drainage 26
2.4.3.3 Disjoining pressure 28
2.4.3.4 Reynolds model 29
2.5 Foam film interface 31
2.5.1 Gibbs elasticity 32
2.5.2 Marangoni effect 33
2.5.3 Surfactant adsorption 35
2.5.3.1 Gibbs adsorption equation 36
2.5.3.2 Henry isotherm 37
2.5.3.3 Langmuir isotherm 39
2.5.4 Protein adsorption characteristics 40

3 Governing equations **42**
3.1 Velocity field equations 42
3.2 Mass transport equation 47
3.2.1 Mass balance on surface 47
3.2.2 Mass balance in bulk 50

4 Small Péclet-Δ limit **52**
Abstract 52
Highlights 53

4.1 Introduction 53
4.2 Mathematical model 57
4.2.1 Dimensionless groups 58
4.2.2 Velocity fields 61
4.2.3 Modelling of evolution of surfactant in a foam film 63
4.2.4 Combining equations in small $\mathrm{Pe}\,\Delta$ limit 64
4.2.5 Adsorption isotherms 66
4.2.5.1 Approximations to isotherm 66
4.2.5.2 Dimensional variables for isotherms 68
4.2.6 Total amount of surfactant at any film location 69
4.2.7 Overall amount of surfactant at any time 72
4.2.8 Effective concentration at any time 73
4.2.9 Recovery and enrichment 73
4.2.10 Late time behaviour of system 74
4.3 Simulation and benchmarking 76
4.4 Results 78
4.4.1 Global Henry isotherm, no film drainage 79
4.4.2 Global Henry isotherm, with film drainage 80
4.4.3 Local Henry isotherm, no film drainage 82
4.4.4 Local Henry isotherm, with film drainage 84
4.4.5 Quasisteady-state approximation 86
4.4.6 Overall amount of surfactant in film 88
4.4.7 Effect of changing solubility parameter 91
4.4.8 Foam fractionation recovery and enrichment 93
4.4.8.1 Recovery and enrichment over time 94
4.4.8.2 Recovery and enrichment comparison 95
4.5 Conclusion 97

5 Supplementary material for small Péclet-Δ limit **101**

Abstract 101
5.1 Gibbs-Marangoni effect 102
5.1.1 Marangoni stresses 102
5.1.2 Gibbs elasticity 103
5.2 Foam film drainage 103
5.3 Governing equations 105
5.3.1 Continuity and momentum equations 105
5.3.2 Mass transfer equations 107
5.4 Approximations to adsorption isotherms 107
5.5 Nondimensionalization 110
5.6 Numerical solution procedure 111
5.6.1 Separation of variables 113
5.6.2 Initial condition for spectral method 118
5.7 Simulation parameters 119
5.8 Estimating global and local Henry isotherms 120
5.9 Quasisteady state 123
5.9.1 Marangoni flow and film drainage balance 124
5.9.2 Power series expansion for quasisteady evolution 125

6 Large Péclet-Δ limit **128**

Abstract 128
Highlights 129
6.1 Introduction 129
6.2 Mathematical model 136
6.2.1 Dimensionless groups 137
6.2.2 Velocity fields 139
6.2.3 Mass transport equation in a foam film 140
6.2.4 Calculating evolution of separatrix 144
6.2.5 Total amount of surfactant present in foam film 146

6.2.5.1 Extent of coupling between surface and bulk 147
6.2.5.2 Relating bulk surfactant with surface surfactant . . 148
6.2.6 Recovery and enrichment 150
6.3 Results 150
6.3.1 Evolution with time of surfactant on surface 151
6.3.2 Evolution with time of separatrix shapes 153
6.3.3 Evolution with time of area ratio 156
6.3.4 Total amount of surfactant relative to initial amount 158
6.3.4.1 Case without film drainage 159
6.3.4.2 Case with film drainage 160
6.3.5 Effect of time evolution in cases with film drainage 162
6.3.6 Recovery and enrichment 165
6.4 Conclusion 167

7 Supplementary material for large Péclet-Δ limit **173**

Abstract 173
7.1 Nondimensionalization 174
7.2 Early time evolution 175
7.2.1 Early-time evolution during initial time step 175
7.2.2 Behaviour at film surface for initial time step 178
7.2.3 Accuracy for initial time step 182
7.3 Numerical approach after initial time step 183
7.4 Simulation parameters and benchmarking 185
7.4.1 Physicochemical data used in simulations 185
7.4.2 Benchmarking simulations 190
7.4.2.1 Number of Fourier terms 194
7.4.2.2 Size of time steps 195
7.4.2.3 Number of material points in separatrix 195
7.5 Non-linear adsorption isotherm 196

7.5.1 Specifying non-linear isotherm 197
7.5.2 Expected behaviours for non-linear isotherm 198
7.5.3 Non-linear isotherm data for surfactant relative to initial surfactant 199
7.5.4 Non-linear isotherm data for recovery and enrichment 200

8 Summary and conclusions **203**

9 Future work **209**

References **246**

Appendix **247**

A 1 Thinning rate equation for a rigid interface 247
A 2 Equilibrium adsorption behaviour of proteins 251
A 3 Simpler protein adsorption isotherm 253
A 4 Analysing non-linear isotherm for β-LG 255

List of figures

2.1 Surfactant distribution 12

2.2 Foam fractionation column with reflux 14

2.3 Schematic of foam structure 22

2.4 Thin film and adjacent Plateau border 23

2.5 Henry adsorption isotherm 38

2.6 Langmuir adsorption isotherm 39

4.1 Insoluble and soluble surfactant 54

4.2 Dimensionless global and local Henry isotherms 68

4.3 Γ_{tot}, no film drainage, global Henry isotherm 80

4.4 Γ_{tot}, soluble and insoluble, global Henry isotherm 82

4.5 Γ, with and without film drainage, global Henry isotherm 83

4.6 Γ_{tot}, no film drainage, local Henry isotherm 84

4.7 Γ_{tot}, Γ, c and $\delta\, c$, with film drainage, local Henry isotherm 85

4.8 Γ, quasisteady-state, numerical 87

4.9 Γ_{ove}, $\Gamma_{\mathrm{ove}}/\Gamma_{\mathrm{ove},0}$ and c_{eff} comparison 89

4.10 Changing $\mathcal{S}$ effect, global and local Henry isotherms 92

4.11 Γ_{ove}, quasisteady prediction and numerical solution, global Henry . . 92

4.12 Recovery vs enrichment, various solubilities, with film drainage, both global and local Henry isotherms 96

4.13 Recovery vs enrichment, various solubilities, with and without film drainage, different isotherms 97

5.1 Global and local Henry isotherms plotted for a Langmuir fit using experimental adsorption data for SDS 123

6.1 Diagram of a foam film in large $\mathrm{Pe}\,\Delta$ limit 132
6.2 Evolution of dimensionless amount of surfactant on film surface, S_S . 152
6.3 Evolution with time of material points on separatrix 154
6.4 Evolution with time of dimensionless ratio A_b/A_t 156
6.5 $S_T/S_{T,0}$ vs time, no film drainage case 160
6.6 $S_T/S_{T,0}$ vs time, with film drainage case 161
6.7 Recovery vs enrichment, various solubility parameters, different times 165

7.1 $\chi_m = (1 - x_m)/\sqrt{t}$ versus Γ_0 graph 181
7.2 Separatrix shapes calculated using various Fourier terms 194
7.3 RMSD between position of surface material points 194
7.4 A_b/A_t, calculated with various material points 196
7.5 $S_T/S_{T,0}$ vs time, non-linear isotherm 199
7.6 Recovery vs enrichment, various solubilities 201

A 4.1 β-LG adsorption isotherm 256

List of tables

Dimensional nomenclature x
Dimensionless nomenclature xiii

5.1 Dimensional parameters for SDS 121
5.2 Dimensionless parameters for SDS 122

6.1 Time corresponding to maximum $S_T/S_{T,0}$, as well as values of these maxima for solubility parameter $\mathcal{S} = 3$ 163
6.2 Time for maximum $S_T/S_{T,0}$, and values of these maxima for solubility parameter $\mathcal{S} = 3$ 163

7.1 Experimental data for β-L 187
7.2 Dimensional parameters for β-LG 189
7.3 Dimensionless parameters for β-LG 189
7.4 Difference at top of separatrix with time-step size 195

A 4.1 Initial surfactant bulk concentrations and corresponding surface concentrations 256
A 4.2 Initial surfactant surface concentrations and corresponding bulk concentrations 257

Nomenclature

Table : Dimensional

Symbol	Description
A	surface area
a	radius of curvature of Plateau border
$\bar{A}$	molar area
a_i	activity of i^{th} component
α_P	parameter of non-ideality within isotherm for protein
b_{Pj}	adsorption equilibrium constant of protein in state j
$b_{P_{min}}$	adsorption equilibrium constant of protein in first state
b_{avg}	average of b_{Pj} values
B_P	sum of all b_{Pj} values
$\bar{B}_{Peff}$	effective B_P value accounting for non-ideality
c	bulk concentration
c_{Pb}	surfactant concentration in Plateau border's bulk
$\mathcal{D}$	diffusion coefficient
δ	film half-thickness
δ_0	initial film half-thickness
ΔP	excess pressure within foam films
ϵ	surface dilational modulus

$\mathcal{G}$	Gibbs elasticity
Γ	surface concentration
Γ_0	initial surface concentration
Γ_i	surface concentration of i^{th} component
$\bar{\Gamma}_m$	maximum surface concentration
$\bar{\Gamma}_{min}$	minimum surface concentration in local Henry isotherm
$\bar{\Gamma}_{Pmax}$	maximum surface concentration of protein
Γ_{Pb}	surfactant concentration on Plateau border's surface
γ	surface tension of solution
γ_0	surface tension of pure solvent
γ_{Pb}	surface tension of Plateau border surface
K	pre-factor for diverging velocity at early time
κ	diffusivity tensor
$\bar{K}_L$	Langmuir parameter
$\bar{K}_H$	Henry constant
$\bar{K}_{H(glob)}$	global Henry constant
$\bar{K}_{H(loc)}$	local Henry constant
L	film half-length
μ	liquid viscosity
μ_i	chemical potential of i^{th} component
$\mathcal{N}_i$	number of moles of i^{th} component
$\mathcal{N}_i^s$	number of moles of i^{th} component in surface layer
μ_s	surface liquid viscosity
ω	molar surface area
ω_0	molar area for solvent
ω_j	molar area of protein in j^{th} state
ω_{avg}	average of ω_j values
ω_P	average molar surface area of protein

ω_{min}	molar area of protein in first state
ω_{max}	molar area of protein in largest area state
P	pressure
P_c	capillary pressure
P_{Pb}	Plateau border pressure
P_{film}	pressure in film
P_{air}	pressure in bubble
Π	surface pressure
Π_d	disjoining pressure
Π_{el}	electrostatic pressure
Π_{ste}	steric pressure
Π_{vdw}	van der Waals pressure
R_i	radii of curvature
R_{Pb}	radius of curvature around Plateau border
ρ	density
T	temperature
t	time
u	velocity field in x-direction across foam films
$\bar{u}$	average liquid velocity in x-direction
u_s	film's surface velocity
w	velocity field in z-direction
x	distance from centre of film along x-axis
z	distance from middle of film along z-axis

Table : Dimensionless

Symbol	Description
A_b	cross-sectional area in film of material initially in Plateau border
A_t	instantaneous film cross-sectional area
B_{Peff}	dimensionless effective adsorption parameter for protein
c	bulk concentration
c_0	initial bulk concentration
c_{eff}	effective concentration at any time
χ	similarity variable
χ_m	similarity variable following a material point
χ_{max}	similarity variable at maximum velocity
δ	film half-thickness
$\dot{\delta}$	film thinning rate
Δ	initial aspect ratio
Δt	size of time intervals
ϕ_l	foam liquid volume fraction
Γ	surface concentration
Γ_0	initial surface concentration
Γ_1	function in expansion for Γ
Γ_2	function in expansion for Γ
Γ_{min}	minimum surface concentration for local Henry isotherm
Γ_{Pmax}	maximum surface concentration for protein
Γ_{ove}	overall amount of surfactant on and within film
$\Gamma_{ove,0}$	overall amount of surfactant in film at initial time
Γ_{tot}	total amount of surfactant present at any location in film
$\Gamma_{tot,0}$	initial total amount of surfactant present at any location in film
$\Gamma_{tot,\mathrm{Pb}}$	total amount of surfactant present at Plateau border
$\Gamma_{tot,sol}$	difference between total surfactant at any location and at Plateau border

Γ_{mn}	matrix in spectral method
Γ'_{mn}	matrix in spectral method
Γ'^{D}_{mn}	diagonal components of matrix in spectral method
Γ'^{ND}_{mn}	non-diagonal components of matrix in spectral method
Γ''_{mn}	matrix in spectral method
G_n	series involving function of position
G'_n	first derivative of G_n with respect to x
G''_n	second derivative of G_n with respect to x
G_n^{Pb}	Fourier component for Plateau border concentration in spectral method
K_L	Langmuir parameter
$K_{H(glob)}$	global Henry constant
$K_{H(loc)}$	local Henry constant
n	counter over Fourier terms or over configurational states
Pe	Péclet number
$\mathcal{S}$	solubility parameter
S_B	overall amount of surfactant in bulk of film
S_S	overall amount of surfactant on surface of film
S_T	overall amount of surfactant on and within film
$S_{T,0}$	overall amount of surfactant on and within film at initial time
t	dimensionless time
$\tau_{tot,n}$	series involving function of time
$\dot{\tau}_{tot,n}$	time derivative of $\tau_{tot,n}$
θ	surface coverage
θ_P	surface coverage of protein
θ_{avg}	average coverage of protein in a domain of interest
u	velocity in x-direction
u_{end}	horizontal velocity at material point position after first time step
$u_{est,end}$	estimated horizontal velocity at instant $t + \Delta t$

u_{mid}	horizontal velocity at $t = \Delta t/2$
u_s	surface velocity in x-direction
u_{start}	horizontal velocity of material point at start of time step
$V(\chi)$	function giving velocity variation along surface at early time
V_R	film drainage velocity parameter
w	velocity in z-direction
$w_{est,end}$	estimated vertical velocity at instant $t + \Delta t$
w_{start}	vertical velocity of material point at start of time step
x	distance from middle of a film along x-axis
x_m	x-coordinate following a material point
x_{end}	position of material point after first time step
$x_{est,end}$	material point estimate of position in x-coordinate
x_m	position of a material point initially at $x = 1$ after first time step
x_{sep}	x-position of a material point on separatrix
x_{start}	initial position of material point
x_{surf}	x-position of a material point on surface of film
z	distance from middle of a film along z-axis
$z_{est,end}$	material point estimate of position in z-coordinate
z_{sep}	z-position of a material point on separatrix
z_{start}	initial z-position of a material point on separatrix

Abstract

Surface active species can be encountered in various process industries. This can then result in demand for their separation. Most of the conventional separation methods are limited when the separation of surfactant from a dilute solution is required. However, foam fractionation is an economical and environmentally friendly method that can overcome this limitation.

In a fractionation column, bubbles rise, while surfactants adsorb on the surface of the bubbles. Thus, the foamate taken from the top of the column is richer in surfactant concentration than the initial feed. In the foam fractionation system with reflux, which is the subject of this study, a part of this rich foamate is returned to the column. Hence, reflux enriches the interstitial liquid in contact with bubbles. Consequently, the difference in surface concentration of the richer Plateau borders and the leaner adjacent foam films results in a flow of fluid from the Plateau border towards the centre of the film. This is due to the Marangoni stress which arises in turn due to the difference in surface tension in those regions.

In addition, film drainage is the other significant mechanism that occurs, and is due to the much higher curvature of the Plateau borders compared to the neighbouring films. This difference can result in a pressure difference which causes a fluid flow from the films towards the Plateau borders. The interaction between the Marangoni flow and

film drainage can result in the mass transport of surfactants on and within the foam films.

The evolution of insoluble surfactants in this sort of system has previously been studied elsewhere [1]. However, recognition of the fact that surfactants are actually somewhat soluble in water motivated the present study. The novel contribution of this research is to study soluble surfactant transport on and within a foam film during a fractionation process with reflux. This can then lead to the ability of designing more efficient fractionation columns.

The present study is thereby based on the work of Vitasari et al. [1], but with the difference that in the present study, surfactant solubility has also been included. To do this, surfactant transport processes are modelled. Nonetheless, to simplify the mathematical modelling used in the current study, we considered two specific limits. In the first, surfactants are considered to be highly diffusive, at least across the foam films. Hence, they are uniformly distributed across the films [2]. In the second limit however, surfactants are considered to have low diffusivities. Hence, they are only being transported via convection within the foam film, due primarily to flow associated with Marangoni-induced stresses. In addition, we have employed a linear adsorption isotherm to relate surfactant surface and bulk concentrations, albeit with the option to vary that isotherm to capture, at least locally, the behaviour of a non-linear one. Note that each of the above mentioned limits (diffusion-dominated and convection-dominated) is relevant for surfactants with particular characteristics transported in a foam film with a specific geometry. Therefore, the real case is generally somewhere in between the two above mentioned limits. Despite this, these models and the limits we consider can still provide valuable information about surfactant transport which can eventually help with the design of a more efficient fractionation column.

Declaration of Authenticity and Author's Rights

This thesis is the result of the author's original research. It has been composed by the author and has not been previously submitted for the examination which has led to the award of a degree.

Hamed Rajabi **Date**: 13/09/2023

Acknowledgements

First and foremost, I would like to praise and thank God, who has granted me countless blessings and the opportunity to finally accomplish my PhD thesis. I would like to express my heartfelt gratitude and acknowledgement to my supervisor: Dr Grassia. Paul - Thank you for giving me such an opportunity to carry out this interesting project as a PhD student. I am very glad that with your help I could achieve one of the biggest dreams of my life. I cannot thank you enough for your commitment, support and guidance throughout my studies.

A big thanks to my beloved wife and son for bearing with the difficulties I put them through because of my studies. Reyhaneh - If it wasn't for you, I would have never seen the ability in myself to continue my education. Liam - Please forgive me for not being able to spend the time you deserved with you in the most beautiful years of your life. I would like to thank my parents and sisters for their encouragement and support. Mum and dad - Thank you for your emotional and financial support without which it would not have been possible for me to achieve this aim. I hope that in the future I can repay some of your efforts. I would also like to thank my parents-in-law for supporting us in the difficult way we chose.

Finally, I would like to express my deepest appreciation to the University of Strathclyde members, especially Dr. Demos Kivotides who have helped me during this time.

Chapter 1

Introduction

The introduction chapter consists of two sections. In the first section, some general background which describes the importance of the current field of study is explained. Specifically, it includes a brief discussion about surface-active components and their properties, foam fractionation as our target separation technique, surface-active components' adsorption behaviour on a gas/liquid interface and finally, limiting behaviours for modelling surfactant transport on and within the foam film. Moreover, the significance of this study in terms of industrial application is described in brief. In the second section, the structure of the present thesis is outlined.

1.1 Motivation

Surface-active components can be found in nature or synthesised as chemical surfactants, biosurfactants, proteins and enzymes [3–5]. The main common characteristic of surface-active components is their tendency to adsorb to a gas/liquid interface due to having a hydrophobic and a hydrophilic group in their structure [3, 6–8]. Moreover, they can have various characteristics, such as wetting, foaming, micellisation, detergency, corrosion inhibition, lubricity, and viscosity, which makes them the primary choice in many industrial applications [9–13].

On the other hand, their widespread usage in various industries creates a demand for their separation using efficient techniques. This may occur since some surfactants are valuable materials and need to be recovered from a solution, or else, some of them are harmful to the environment and need to be removed from wastewater before disposal [14–16]. The industries using surface-active components range from food, pharmaceutical, waste-treatment, environment-related, and many more [17, 18]. However, as the concentration of surface-active components is low in many cases, utilization of older separation techniques, such as distillation or ultrafiltration is not efficient [19, 20].

One of the promising methods to date to separate surface-active components from an aqueous solution is foam fractionation [21]. This physicochemical process is competitive among other methods used in this area, such as gel-filtration, ion exchange, precipitation, membrane filtration and coagulation in terms of simplicity of the equipment, low-cost, mild operation, and environmental compatibility [22–26]. Furthermore, its applicability when separating a dilute solution [27–29], which is, as mentioned, beyond the limits of other techniques, has made it more attractive.

Foam fractionation is a foam separation technique based on the adsorption of surface-active components on the bubbles' surfaces [21, 30–32]. During the process, bubbles enter at the bottom of the column, and exit at the top as foamate, while becoming richer in surfactant concentration than the initial solution [33]. As already alluded to, this is due to adsorption on the surface of bubbles, with high surface-to-liquid content ratios [34]. However, as was first reported by Lemlich and Lavi [26], to increase the efficiency of a fractionation column, or in particular, to increase its recovery and enrichment, it is beneficial to return a part of the enriched foamate to the column. This is called 'reflux' and puts higher surfactant concentration interstitial liquid in contact with rising bubbles. This will eventually lead to having a higher surfactant concentration foamate at the top of the column than in a case without reflux [35]. However, a lot of interesting physics is happening in foams (particularly in foams

subject to reflux), and to model a fractionation process we need to model that physics.

In a fractionation column, it is most likely to have foam with a low liquid volume fraction [1]. The structure of the aforementioned foam is expected to be as follows. Bubbles have polyhedral shapes and are separated from one another by a thin liquid film called a foam lamella [36, 37]. Three foam films meet symmetrically and form an interstitial channel named the Plateau border. Four Plateau borders meet and form a node [38, 39]. Plateau borders typically have a much larger quantity of liquid than lamellae within the foam [32]. A source of liquid can also be a source of surfactant. This then is the reason why in this study, we consider the Plateau borders as a source of surfactants with effectively constant surfactant concentrations within the Plateau borders [1].

On the other hand, Plateau borders have higher curvatures compared to their adjacent films, which are assumed to be comparatively flat. According to the Young-Laplace law, this causes a liquid flow from the thin films towards the Plateau borders, known as film drainage [40]. Even though the quantity of liquid draining is not high, when surfactants are soluble in bulk liquid, film drainage can play an important role in the final recovery and enrichment of surfactant in the foam films. In the present study, we use Reynolds' model for a rigid interface to obtain an equation for thinning rate or the rate of film drainage [41].

Another important mechanism which is essential in this study is the Marangoni flow. Marangoni stresses occur at a gas/liquid interface due to the inhomogeneities caused by the difference in surface tensions [42, 43]. As previously mentioned, reflux enriches the liquid in Plateau borders resulting in a gradient of surfactant surface concentration and hence a gradient in surface tension between films and the adjacent Plateau borders. As a result, Marangoni stresses bring surfactant from Plateau borders towards the centre of the films [44]. In a fractionation process, it turns out that the Marangoni flow is initially the dominant mechanism compared to the film drainage. However,

after a long time, film drainage and Marangoni flow can reach a balance on the surface corresponding to a quasi-static condition [1].

Up until now, several studies have been carried out on film drainage and its effects on the foam and the foam film stabilization [40, 45–52]. Moreover, the transport of surfactant onto the foam film surface in the presence of film drainage and Marangoni forces has been investigated [1]. However, in previous research, the presence of surfactants in the bulk of the film has been neglected. This has been done even though most common surfactants have a substantial solubility in water, which can change significantly with variations in hydrophobic tail length, head group nature, counterion valence, solution environment, and in addition, temperature [10, 17, 53–55]. Thus, this research aims to address soluble surfactant transport on and within the foam film in a foam fractionation process with reflux.

Overall, to have a better understanding of the surfactant transport process, mathematical modelling and simulation is a must. Modelling a soluble surfactant transport in a fractionation process with reflux is nonetheless a complicated task. However, to be able to simplify it, while simultaneously gaining valuable information which helps us increase the efficiency of the overall process, we take two extreme limits. The first limit is the so-called 'small $\mathrm{Pe}\,\Delta$ limit', where Pe is the Peclet number and Δ is the ratio between half of the film's initial thickness and half of its length. The key feature of this limit is the tendency to have a uniform distribution of surfactant across the film thickness. This can be a reasonable approximation when smaller chemical surfactants with high diffusivities in a very thin film are considered. In this study however, the opposite limit considering larger surface-active components, such as proteins, that tend to correspond to a 'large $\mathrm{Pe}\,\Delta$' value has also been modelled. In this case, surfactants are only transported via convection within the bulk as they have a lesser tendency to diffuse from the surface to the bulk.

1.2 Thesis overview

This thesis is presented under the University of Strathclyde thesis submission regulations. The thesis is organised as follows.

A literature review is provided in Chapter 2. This chapter studies previous research and background information required to carry out the present work. The main topics covered are as follows: Surface-active components and their behaviour on the surface and within the solution bulk, the foam fractionation process, recovery and enrichment calculations for fractionation performance, foam properties, as well as foam film interfaces and their rheology.

In Chapter 3, governing equations are presented and explained. In particular, we use continuity and momentum balance equations to obtain the velocity fields. Then, the obtained velocity field equations are used in relevant mass transport equations to obtain an equation for the evolution of surfactant concentration.

Having derived the governing equations, we solve two limits in the modelling of a soluble surfactant transport on and within the foam film. These limits are presented in the form of the original articles (accepted or submitted), as well as their supplementary material.

Chapter 4 is 'Transport of soluble surfactant on and within a foam film in the context of a foam fractionation process'. This section models the so-called 'small $\mathrm{Pe}\,\Delta$ limit', in which, surfactants are uniformly distributed across the foam film. To carry out calculations in the above mentioned limit, two distinct adsorption isotherms have been used to relate surfactant surface and bulk concentrations. Moreover, the study has been carried out with and without the consideration of film drainage. In brief, Chapter 4 provides the main article published in the journal Chemical Engineering Science, while Chapter 5 provides essential background information, calculations and data used to carry out the research. For instance, mass transport mechanisms and related equations, the

introduction of the adsorption isotherms, nondimensionalization process, a numerical solution procedure, the selection of simulation parameters, as well as an analytical solution for the so-called quasisteady condition can be found in Chapter 5.

Chapter 6 is 'Transport of convected soluble surfactants on and within the foam film in the context of a foam fractionation process'. This chapter takes into account a different limit in which the transport of surfactant within the foam film is convection-dominated. This limit is called the 'large $\mathrm{Pe}\,\Delta$ limit', in which the diffusion across the film is ignored compared to the convection within it. Similar to what was done earlier, supplementary material has also been provided now within Chapter 7. It consists of an alternative method for the early time evolution calculations, a numerical approach to the problem, simulation parameters and benchmarking, as well as using a non-linear adsorption isotherm.

At the end, the findings are summarised in Chapter 8 and the direction for future work is outlined in Chapter 9.

Chapter 2

Literature review

In the present chapter, we focus on the key information from literature required to carry out our study, as well as the background research that has been done relevant to the field. Moreover, the novel contribution of the present study relative to the previous work, and the reason why this study can develop this particular field have also been explained. At the start of the chapter, there is a discussion about surface active components, their properties and their application in industry. Then, we explain foam fractionation as an efficient surfactant separation process. Moreover, some details about foam geometry and foam's key physics have been provided. Furthermore, as the interfacial rheology of foam in the presence of surfactant is an important topic needed for the present study, it is also discussed in detail.

2.1 Surface active components in a solution

In this section, we review 'surface-active components' as they are the materials that can be separated using the method called 'foam fractionation'. Moreover, we review some of the surface-active materials' properties, applications, and alternative methods of separation from an aqueous solution. In this research, 'surfactant' is to be used as a general term, including all surface-active molecules, including small chemicals,

bio-surfactants, or proteins[3–5].

Surfactants are very important substances that everyone encounters in their daily life, e.g. they are one of the main components of detergents. Research on these materials has made great advances over more than the past half-century since an early publication by Schwartz and Perry [56] summarized their chemical, physicochemical and technological properties.

Surfactants are amphiphilic compounds having a hydrophilic (lyophilic) part and a hydrophobic (lyophobic) part [6]. The hydrophilic parts are typically polar groups, while the hydrophobic parts are often formed of hydrocarbon chains [54, 57]. For instance, in an aqueous media, surfactant molecules will migrate to gas/liquid interfaces and orientate in such a fashion as to minimise, as much as possible, the contact between their hydrophobic groups and the liquid [9].

Typical surfactants are classified as anionic, cationic, amphoteric or non-ionic [58]. Apart from traditional chemical surfactants, there are new classes of surfactants, e.g., biosurfactants [4, 5]. Biosurfactants are produced by living organisms and can be categorized based on their chemical structure, including glycolipids, lipopiptides, lipoprotein, phospholipids, natural lipids, polymeric surfactin and fatty acids [7, 59].

Proteins also show surface activity and can be categorized as surface-active components [3, 8]. For instance, the outer surface of a globular protein contains polar and charged amino acid groups. The distribution of these functional groups on the hydrophilic outer shell is usually uneven, with the consequence that some parts of the surface are more hydrophobic than others. Hence, adsorption at the gas/liquid interface happens to allow the more hydrophobic regions on the outer surface to minimize their exposure to the aqueous environment [60].

2.1.1 Surfactant properties and applications

The behaviour of surfactants in an aqueous solution (on the surface and in the bulk), gives them the following properties [9, 13]:

- Wetting
- Foaming/defoaming
- Emulsification/demulsification
- Dispersion/aggregation of solids
- Solubility and solubilisation
- Adsorption
- Micellisation
- Detergency
- Synergistic interactions with other surfactants
- Corrosion inhibition
- Substantivity to fibres and surfaces
- Biocidal properties
- Lubricity
- Stability in highly acidic or alkaline media
- Viscosity modification

The named properties of surface-active components make them the primary choice in various applications, such as [9–12]:

- Domestic, institutional and industrial cleaning products
- Toiletry and personal care products
- Crop protection formulations used in agriculture
- Oil field chemicals
- Food industry e.g., emulsifiers
- Pharmaceuticals
- Emulsion polymers for coatings, inks and adhesives
- Corrosion inhibition

- Medical and pharmaceutical industry
- Nanotechnology

Consequently, this widespread use of surfactants can create a demand for separating them in industry. This can be as a downstream separation for recovery of a valuable surfactant [14, 23, 61], or else for environmental purposes, e.g. to prevent disposal of a surfactant within an industrial effluent [15, 16, 62, 63]. In particular, some of the applications for which surfactants are in demand are remediation of contaminated soil, wastewater and groundwater treatment, bio-separation, removal of ink to permit the recycling of plastic or paper, analytical chemistry, ore flotation and protein recovery in food industries [25, 64].

Some of the conventional surfactant separation techniques include distillation, extraction, ultrafiltration, precipitation, and micro-emulsion formation [25, 26]. However, the main disadvantage of these methods is that the efficiency of these methods decreases rapidly as the concentration of the desired components falls [65]. This limitation encouraged researchers to find alternative methods, such as ion exchange and selective adsorption as well as foam fractionation which has shown great potential for the separation of dilute solutions [28, 29, 66]. In addition to the above-mentioned reason, foam fractionation has other advantages over the traditional separation methods that will be addressed in Sec. 2.2. However, prior to that, we note that surfactants have a specific behaviour on the gas/liquid interface and in the solution bulk, and to be able to study foam fractionation, we need to study these characteristics first.

2.1.2 Surfactant on surface

As has been alluded to earlier, due to the presence of hydrophobic groups in surfactant molecules, they tend to locate at gas/liquid interfaces and orientate in such a fashion as to minimise, as much as possible, the contact between their hydrophobic groups and the (aqueous) liquid. This process is referred to as ‘adsorption’ and results in a

change in the properties at the interface [9]. For instance, the presence of surfactant at a gas/liquid interface can lower its surface tension.

At a gas/liquid interface, surface tension is due to the greater attraction of liquid molecules to each other (due to cohesion) than to the molecules in the gas (due to adhesion) [67]. However, the adsorption of surfactants creates a layer of weakly attracted molecules on the surface and reduces surface tension at the gas/liquid interface. Hence, adsorption is associated with significant energetic changes, as the free energy of a surfactant molecule located at the interface is lower than that of a molecule dissolved in either bulk phase [10, 68, 69].

The adsorption of surfactant on the gas/liquid interface is recognised as the most important characteristic of surface-active components and the key factor in foam-based separation techniques. In addition, surfactants can affect a foam separation technique via facilitating the dispersion of gas and reducing the size of bubbles, changing the velocity and flow regime of bubble rise, and stabilizing foams [70, 71]. Up to now, we mentioned the reasons why a foam separation technique can be good for separating surfactants from a solution. However, despite surfactants' tendency to report to the surface, they are still present in the solution bulk due to their finite solubilities. As our main focus in the present study is to model soluble surfactant transport, we discuss surfactant behaviour in the solution bulk in the next section.

2.1.3 Surfactant in bulk

As is shown in Fig. 2.1b, surfactants are not only present on the surface or gas/liquid interface (air/water interface in the case of Fig. 2.1b) but also dissolved in the bulk [10, 17, 53, 54]. As Miller and Fainerman [72] stated, if the effect produced by the surfactants' polar group is more significant than that of the lipophilic group, the surfactant is soluble in water. Furthermore, it has been found by Tanaka et al. [55] that in addition to the structural physiochemical properties of the surfactants, conditions such

as temperature and pressure can influence surfactant solubility in water.

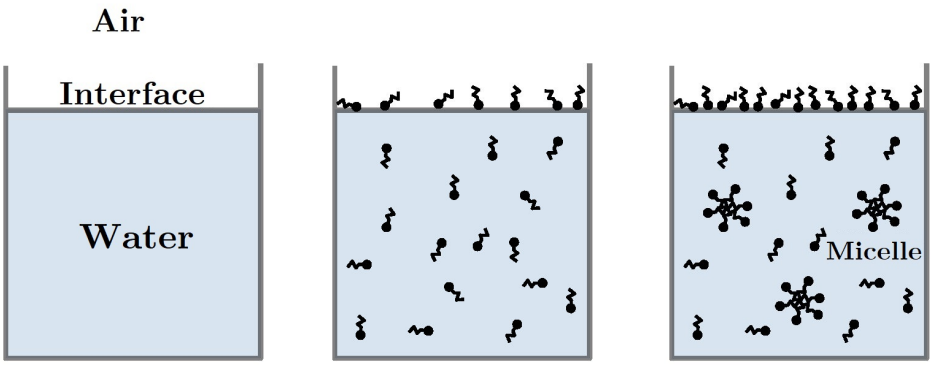

(a) Surfactant concentration zero

(b) Surfactant concentration below CMC

(c) Surfactant concentration above CMC

Figure 2.1: Distribution of surfactant molecules in solution with an increase of surfactant concentration.

Nevertheless, aggregation is the other result of the hydrophilic groups being oriented towards the bulk solution if the surfactant concentration is above a certain level [73]. This limit is called 'critical micelle concentration' (CMC) [74]. Above this concentration, aggregates or so-called micelles are spontaneously formed (see Fig. 2.1c). The formation of micelles reduces the free energy of the solution significantly by reducing the interaction between the hydrophobic groups and surfactants [75]. Hence, before reaching the CMC, the surface tension decreases sharply with the increase of surfactant concentration, but after reaching the CMC, the surface tension stays more or less constant [57]. As a result, in the separation of surfactant using a foam separation technique, we are mostly interested in the solution concentrations less than the CMC: the objective is to have as much surfactant as possible reporting to surfaces, not remaining as micelles in the bulk.

Typically, as the length of a chain in a surfactant increases, the CMC of that surfactant decreases and its surface concentration increases, causing a decrease in the surface tension, or an increase in the so-called surface pressure (i.e. the difference between surface tension without and with surfactant) at a specified surfactant bulk concentration [54, 76].

In summary, surface-active components are very commonly used materials in industry. Thus, we often need to separate them. However, even though various types of these components with different characteristics can be found in nature or synthesized industrially, they share common behaviour when dispersed in a solution, in contact with a gas phase. In particular, they exhibit adsorption behaviour on the surface, and this behaviour is then the basis of certain separation techniques, such as foam fractionation. As a result, the foam fractionation technique is the subject of the next section.

2.2 Foam fractionation

Foam-based separation processes have been utilized to separate and concentrate effectively a variety of constituents from aqueous solutions [27]. Some of these techniques are ion flotation, precipitate flotation, adsorbing colloid flotation and the technique of interest here, foam fractionation [77–81]. In Sec. 2.2.1 we discuss in brief foam fractionation, its applicability and the effective parameters governing it. Moreover, in Sec. 2.2.2 we look at foam fractionation as a counter-current mass transfer process and discuss the effect of reflux on the surfactant mass transfer behaviour.

2.2.1 Fractionation applications and operation

The foam fractionation process in particular (Fig. 2.2), is based on the adsorption of a solute, e.g., surfactant, on the bubbles' surface, which rises through a solution [21, 31, 32]. It is especially advantageous in treating dilute solutions where other separation methods encounter technical or economic limitations [82]. In a fractionation column, bubbles are produced by introducing gas (typically air) at the bottom of the column, through a sparger. Surface-active molecules then adsorb on the surface of the bubbles in a rising foam. The foam is broken or collapsed (typically using either mechanical or chemical methods [83]) at the top of the column. This produces the so-called 'foamate', a solution that is enriched in surfactant concentration [33]. This

enrichment occurs because foam has a relatively high surface area (hence a relatively high amount of adsorbed material) for a specified volume of liquid [34].

However, as alluded to earlier in Sec. 2.1.2, the amount of surfactant recovered during the fractionation process is dependent also on its solubility in the foam film's bulk. Taking into account the amount of surfactant dissolved in the foam film's bulk, alongside the amount present on the surface is the novel contribution of this research. Typically, surfactant surface concentration tends to be in equilibrium with the foam film's bulk liquid concentration [34]. This equilibrium can be expressed using so-called adsorption isotherms and is reviewed later on.

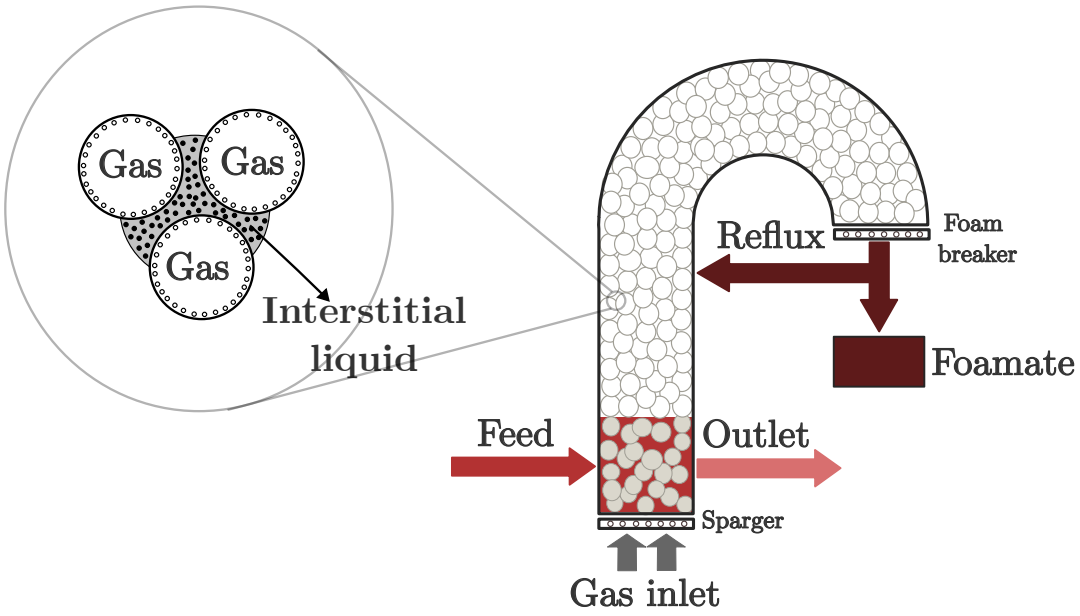

Figure 2.2: Schematic of a typical foam fractionation column with reflux

Foam fractionation is reported to be first used by Ostwald et al. [84] for the separation of albumin from potato and beet juices. This separation method has since then had various applications, such as radioactive effluent purification [85], separation of certain complex organic materials such as proteins and enzymes [86–88], separation of non-polar compounds [89], production of pharmaceutical products [90, 91], environmental problem remediation, e.g., waste water treatment [92], and food processing [93]. One of the key advantages of foam fractionation over other separation methods is,

as has already been alluded to, its effectiveness in separating solutes from very dilute solutions [94].

Some of the process parameters influencing foam fractionation are column length [21], bubble size [95, 96], temperature [80], pH [97–99], contaminants [100], gas flow-rate [101, 102], pressure [96] and external reflux [82]. Among the above-mentioned parameters, reflux is one of the most significant ones and will be discussed in the next subsection.

Generally, foam fractionation can be operated in a batch, or a continuous mode [83, 87]. In the batch mode, a defined volume of surfactant solution is aerated, and in the continuous mode, the surfactant solution is continuously fed into the foam column and eventually, the process reaches a steady state [30].

2.2.2 Fractionation as a counter-current separation process

Overall, foam fractionation can be thought of and modelled as a counter-current separation process in which rising foam contains foam film surfaces and some interstitial bulk liquid, whereas the falling stream has interstitial liquid only [15]. The falling stream can be caused by reflux or can simply be a feed inlet stream in so called stripping mode. Either way, the rising stream can be in contact and possibly in equilibrium with falling liquid. On the other hand, if the falling liquid happens to have an even higher concentration than the liquid within the rising foam, the falling and rising streams are not in equilibrium and a higher degree of separation is possible. [94].

In the 'stripping mode', the aim is to remove surfactant from the feed and as a result feed enters directly into the foam (some distance above the bottom pool). It then mixes with the interstitial liquid and reduces its surfactant concentration while trickling down. Hence the result is a leaner bottom product [31, 103].

Reflux, in general, can either happen due to collapse or drainage of some of the enriched foam, which is called 'internal reflux' [34, 82] or else, by deliberately returning

a fraction of the collapsed foamate to the fractionation column, called 'external reflux' [35]. However, regardless of the mechanism that causes reflux, as was reported by Lemlich and Lavi [26], it can significantly enhance the ability of a foam fractionation device to increase the concentration of surfactants in a foamate [31]. While reflux is happening, the downward flow of surfactant-rich material through the foam liquid channels creates high surfactant concentration gradients between bubbles and their adjacent liquid channels, boosting the mass transport of surfactant onto the bubble surfaces. Moreover, as will be discussed later, this increased mass transport on the surface can cause further surfactant mass transport within the bulk of the bubbles' foam films. However, even if the interstitial liquid in the falling stream is at the same concentration as the interstitial liquid in the rising stream at some location where the two streams are in contact in the column, the overall concentration in the rising stream remains higher than in the falling stream [104]. This is because the rising stream contains surfactant surface excess, not just interstitial liquid and this will contribute to the overall recovery of the fractionation process.

Just as also happens in transfer processes like distillation [31, 105], the fractionation process can be viewed as a sequence of transfer units [35], whereby as mentioned earlier, the falling and rising streams are considered to be at (or near) equilibrium for the streams leaving each unit (albeit not necessarily for the streams entering). With multiple transfer units in sequence [106], the concentration of the falling stream then decreases moving downwards from unit to unit, whereas the overall concentration of the rising stream increases moving upwards from unit to unit. Hence the more units that are present (in effect the taller the foam), the better the separation is expected to become overall.

On the other hand, if the reflux is set up in such a fashion that there happens to be a significant mismatch between the falling and rising stream interstitial liquid concentrations entering a given transfer unit (which is the case to be analysed here), then

we expect to see somewhat more mass transfer between streams within that individual transfer unit. In summary, looking at fractionation from a generic separation viewpoint makes it clear that a fractionation column without reflux acts as a single-stage separation column in which the exiting foamate can be in equilibrium with the relatively low concentration of the bottom liquid pool. However, a separation column with reflux is like a multi-stage column, in which, mass transfer takes place between rising foam and downward interstitial liquid leading to enhanced enrichment [35, 106].

The mass transfer process can be particularly effective when surface active material is transferred from liquid within Plateau borders onto film surfaces. Nonetheless, mass transfer from Plateau border to film surface is not a necessary process for reflux to be effective (but it can enhance the effectiveness of reflux, which is why it is studied here). Indeed in some cases, such as the case studied by Jashnani and Lemlich [104], there might be limits in which film surfaces are already nearly packed with surfactant, in which case mass transfer within the foam is just between the countercurrent streams of interstitial liquids. Here instead transfer between interstitial liquid and film surfaces will be considered as it is yet more effective. As a result, in this study, the "effect of reflux" refers to the reflux effect due to further mass transport from Plateau border to film not merely the benefit caused by contacting two counter-current flows with different overall surfactant concentrations in each.

This study intends to model surfactant separation using a continuous foam fractionation process with reflux. Amongst other things, we will assess recovery and enrichment which are two significant performance parameters of a foam fractionation process that enable us to determine process efficiency. As a result, in Sec. 2.3, we review fractionation performance in brief. In addition, modelling a foam-related system requires a lot of information about the foam's geometry and its physical properties which are the subject of Sec. 2.4.

2.3 Performance of foam fractionation

For the foam fractionation process to be viable, high recovery and enrichment of the desired surfactant are important [107]. Recovery is the proportion of feed surfactant recovered in the foam [61], while enrichment is the ratio of the surfactant concentration in the foam to that of the feed solution [88, 90, 108]. The main goal in a separation process is to shift the process where possible towards higher recoveries and enrichments. However, as we will see, there is often a trade-off involved.

To understand the underlying mechanism of a foam fractionation process, and thereby be able to design the process more efficiently, we need to analyse surfactant mass transport in foam films. However, over and above this, process design also requires process information, such as bubble size distribution, gas hold-up volume, dimensions of the column, initial solution volume and concentration, as well as the foamate volume and concentration [107]. In this study though, we focus just upon modelling surfactant transport on and within a typical foam film in a fractionation column with reflux. As a result, we can gain valuable information about the mass transport of surfactant occurring in a foam film, when that foam film is in contact with a higher concentration interstitial liquid. This then in turn enables us to predict the recovery and enrichment of a typical foam film in a fractionation column. We can also investigate some of the important process parameters, such as optimum residence time or analogously column height.

In the modelling study to be considered here, the concentration of the initial solution is assumed known. Moreover, we can calculate the surfactant concentration for the foam films at each instant, which then corresponds to the foamate concentration. In particular, as we have alluded to, enrichment can be defined as the ratio between the surfactant concentration for a foam film to the initial solution concentration, where the concentration for a foam film can be obtained by knowing the film surface and bulk concentrations and also the volume of the film at each instant. On the other hand,

the calculation of recovery is more complicated, as its common definition needs some additional data, such as the number of foam films broken into foamate or the amount of surfactant that entered the initial solution. However, analysing such data is beyond the scope of the present modelling approach. Therefore, to be able to define a recovery parameter in this research, we calculate the total amount of surfactant in a foam film at each instant. This data can be easily converted to the conventional recovery parameter when the number of foam films exiting a fractionation column as well as the total amount of surfactant entering the initial solution are defined.

To summarise, in a foam fractionation column with reflux, the concentration of interstitial liquid in Plateau borders is higher than the bubbles in contact with it. As a result, mass transfer occurs between interstitial liquid and the adjacent foam films. This then changes foam film concentrations and hence changes the total amount of recovered surfactant. Reflux can thereby affect the recovery and enrichment in a fractionation process, which is what we aim to study here. To proceed with a model for mass transport during a foam fractionation process however, we first need to have some information about the physics of the foam and foam properties, as well as the surfactant adsorption on the gas/liquid interface. These topics are discussed in what follows.

2.4 Foam properties

Despite there being different possible types of foam, we use the term ‘foam’ here to refer to liquid foams. In this context then, ‘foam’ is a well-known gas/liquid dispersed system which is characterized by a highly developed interface, with this interface then determining the foam properties [109]. Foam has several physical features that make it suitable to be used in industry. High specific surface area, low relative or inter-phase slip velocity, large expansion ratio and finite yield stress are some of these properties [36]. Foams show interesting rheological properties: under the application of comparatively small stresses, they behave like a viscoelastic solid, while at higher stresses

they become shear thinning and flow like a liquid [38]. This mechanical behaviour of foams, in combination with a remarkably high surface area and low density, leads to a demand in a variety of applications [110], including for instance, in the food and chemical industries, firefighting, mineral processing, and as templates in structural material science [111].

The study of geometrical and also physiochemical properties of foam and also of foam thin films [112] have been topics of interest among scientists for more than a hundred years. However, investigating the aforementioned features, e.g. inter-phase slip velocity, expansion ratio and yield stress inside the foam can be a difficult task. Although one can approximately measure film thickness, film structure and configuration, some essential thermodynamic parameters defy simple investigations. Some directly measurable characteristic parameters are nonetheless film tension and contact angles between the films and bulk phase [70]. We will make use of film tensions in particular.

To perform a modelling study, it is essential to have sufficient information about foam structure and its material properties. We first discuss foam structure in Sec. 2.4.1, and then in Sec. 2.4.2 explain the Young-Laplace law (which derives from the structure) and its importance in describing forces present within the foam. Further to that, Sec. 2.4.3 discusses foam properties important in the present study for determining how foam evolves and also how foam films evolve.

2.4.1 Foam structure

As already alluded to, foam is a two-phase system in which gas cells are enclosed by liquid [38]. Foams are divided into two major types (see below) according to their liquid volume fraction ϕ_l, which is defined as the ratio of liquid volume to the total volume of the foam. In typical foams, ϕ_l varies from less than 1% to about 35%. The gas fraction in foam is $1 - \phi_l$, and is also known as foam quality [36].

The first type of foam containing higher liquid fractions is known as ‘wet foam’. This

type has spherical bubbles and tends just to persist in very viscous liquids or very limited regions of space. In wet foams, there is very little contact between bubbles [70], and wet foam does not normally exist at distances higher than a few bubble diameters above the liquid pool [32]. Since fractionation columns are typically much taller than this, wet foam is of limited interest in our present study.

Dry foams, on the other hand, begin to appear when ϕ_l is lower than roughly 0.05 [113], although the exact boundary between wet and dry can be subject to interpretation. Dry foams form polyhedral cells with curved faces (lamellae) [114]. The structure of dry foams is generally described by Plateau's laws, as below [39]:

- Bubbles are polyhedral in shape because they are jammed against neighbouring bubbles (Fig. 2.3(a)) [115, 116].
- Bubble faces are thin films that are slightly curved either because of the pressure differences between the bubbles, or simply because their perimeter does not lie in one plane (Fig. 2.3(b,c)) [114].
- Three foam films meet symmetrically at angles of 120° in liquid-filled channels, known as Plateau borders (Fig. 2.3(b,c)) [39].
- The cross-section of each Plateau border is a triangle with concave sides (see Fig. 2.3(c)).
- Four Plateau borders intersect at the vertices (or nodes) of each polyhedral bubble under tetrahedral angles of $\cos^{-1}(-1/3) \approx 109.47^\circ$ (tetrahedral angle, see Fig. 2.3(b)) [38, 70, 117].

To relate foam structure with physical mechanisms in a foam, which in turn determine subsequently how structure evolves, we use a well-known rule, called the 'Young-Laplace law', which is applicable in the context of curved fluid interfaces. We discuss this law next.

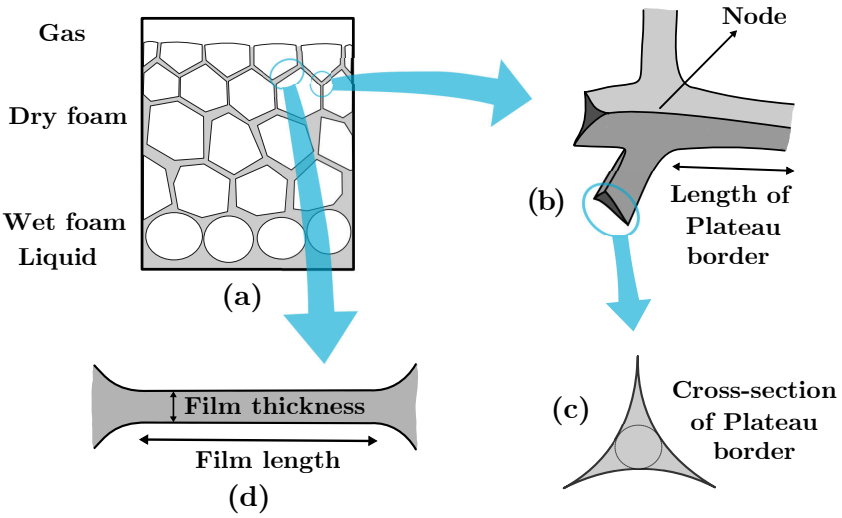

Figure 2.3: Schematic of a foam column (a), which is wet at the bottom and dry at the top, and (b)–(d) are the basic structural elements of the foam.

2.4.2 Young-Laplace law

A gas/liquid interface normally conforms to the Young-Laplace law, which expresses pressure difference (ΔP) across it, and the force of surface tension acting upon an element of surface as below [118–121]:

$$\Delta P = \frac{2\gamma}{\bar{a}} \tag{2.1}$$

where γ is surface tension, and $\bar{a}$ is the mean radius of curvature, related to the two principal radii of interface curvature, R_1 and R_2, by the following expression [36]:

$$\frac{1}{\bar{a}} = \frac{1}{2}\left(\frac{1}{R_1} + \frac{1}{R_2}\right). \tag{2.2}$$

In a three-dimensional system, R_1 and R_2 are orthogonal radii of curvature of the film [42]. Note that, in a film within a foam, which has two surfaces, Eq. (2.1) must be adjusted to:

$$\Delta P = \frac{4\gamma}{\bar{a}}. \tag{2.3}$$

Generally, the Young-Laplace equation indicates a balance between surface tension that tends to reduce the curvature of an interface and a pressure difference, which

tends to bend the interface [114].

On the other hand, the pressure difference between the gas (typically air) in a bubble and liquid in the Plateau border can also be calculated using Eq. (2.1). There is only one interface that is crossed moving from a bubble into a Plateau border. Moreover, typically (at least when the foam is dry) the radius of curvature R_{Pb}, around the Plateau border is much smaller than the radius of curvature along it, and also much smaller than the radii of curvature of the bubble films. In the interest of simplicity then, the film can be considered parallel and planar, so there is typically a negligible difference between pressure of the gas (typically air) bubbles P_{air} and the pressure of the liquid in film P_{film} between them. Meanwhile, the Plateau border can be considered to be curved only in the direction around the Plateau border, in effect then $R_1 \approx R_{\mathrm{Pb}}$ and $R_2 \to \infty$.

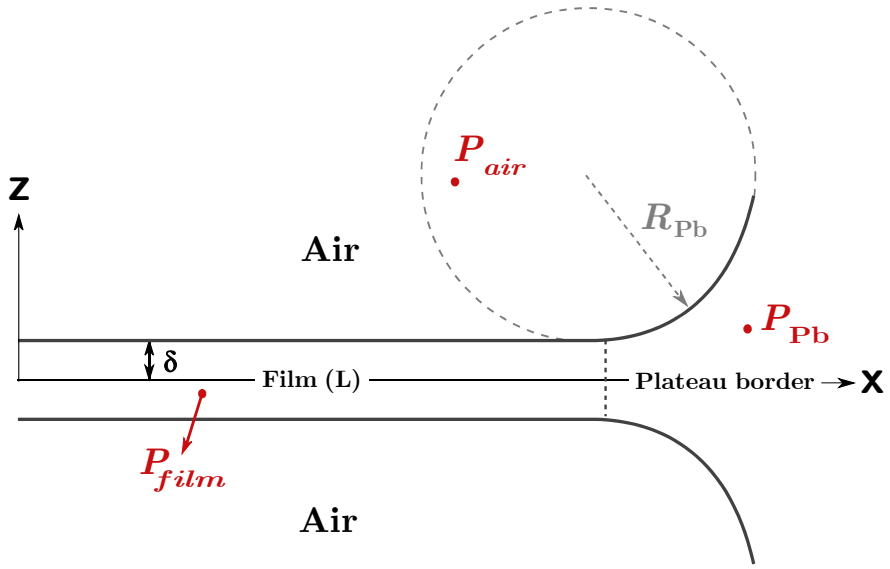

Figure 2.4: Thin film and adjacent Plateau border.

This then results in the following pressure difference ΔP:

$$\Delta P \approx P_c \equiv \frac{\gamma}{a} \tag{2.4}$$

where ΔP is $P_{film} - P_{\mathrm{Pb}}$, where γ is surface tension at the interface of the Plateau border, and where we now use the symbol a to denote $a \approx R_{\mathrm{Pb}}$. Based on Eq. (2.4) it is

clear that the pressure difference is associated with surface tension, so we can identify ΔP with the Plateau border's capillary pressure, which we also denote P_c.

Therefore, in Fig. 2.4, $P_{\mathrm{Pb}} < P_{air}$, $P_{film} \approx P_{air}$, and consequently, $P_{\mathrm{Pb}} < P_{film}$. This follows as we have said since the film has small curvature (i.e. large radius of curvature) which enables us to ignore any pressure difference between the film and gas in bubbles in contact with it, while the curvature around the Plateau border is significant. This relation Eq. (2.4), which essentially follows just from geometry and capillarity, will be discussed further in Secs. 2.4.3.2 to 2.4.3.4: the fact that the pressure in the Plateau border is typically lower than that in the film will be important in those sections, and we will also see that under certain circumstances it might be necessary to adjust the estimate of pressure difference ΔP, away from what Eq. (2.4) predicts.

2.4.3 Essential physics of a foam governing its evolution

Foams are metastable multi-phase systems that evolve by various mechanisms: gas diffusion, film rupture or bubble coalescence, and also, foam and film drainage. The interplay between these mechanisms determines the structure, properties and stability of the foam [122]. However, not all these mechanisms are of equal importance in all situations, meaning that in certain situations the effects of some of these mechanisms can be neglected, e.g. in our study gas diffusion and film rupture/bubble coalescence are to be ignored. However, we discuss them in brief as a part of our overall understanding of the foam behaviour.

Gas diffusion or coarsening happens due to the pressure difference between two adjacent bubbles [123]. This leads then, to the growth of the average bubble radius with time [44, 124], but typically this growth is slow compared e.g. to the residence time of foam films in a fractionation column. Coalescence involves the rupture of a film shared by two adjacent bubbles leading to a new bubble with a volume equal to the sum of the volumes of the bubbles before the film rupture event [38]. Coalescence

is hence driven by the instability of foam films themselves [122]. Foam fractionation however relies upon foam films being sufficiently stable to survive as they flow up through a fractionation column: a foam that is so unstable that coalesces and collapses completely without reaching the top of the column could not be used for fractionation. For simplicity then, the effect of rupture/coalescence is to be neglected here.

On the other hand, foam drainage and in particular film drainage are relevant in our model, as they contribute to processes we wish to study. These are therefore discussed in what follows.

2.4.3.1 Foam drainage

As alluded to in Sec. 2.2, this study is to be carried out under the conditions of a foam fractionation process with external reflux. In this case, reflux liquid will flow through the Plateau border network, under the foam drainage mechanism (driven primarily by gravity), and thereby comes into contact with foam films. Because in this study, we are modelling just surfactant transport on and within the foam films, we do not require full details of the foam drainage process itself. Rather, as we will see, we focus instead upon its effect, namely, contacting surfactant lean films with richer Plateau borders, and the mass transport mechanism which then results from this contact. However it is ultimately foam drainage which provides that supply of surfactant-rich liquid through the Plateau borders. Moreover, the more liquid that flows through those Plateau borders, the thicker they become (which then impacts in turn back on the radius of curvature parameter a, already introduced in Sec. 2.4.2).

The mechanism of foam drainage is hydrodynamical [83] and involves, as we have said, flow through the channels between the bubbles (so-called Plateau borders), as well as through the nodes or intersections of four channels. This flow is driven by gravity and capillarity [38, 123, 125, 126], albeit often with gravity being dominant. The flow meanwhile is opposed by dissipation. Understanding foam drainage provides

information on the relative flow rate between draining and rising liquid within a foam fractionation column [102].

Early models of foam drainage were considered by Leonard and Lemlich [32]. Since then, many researchers have developed the field based on various simplifying assumptions, particularly regarding the nature of the dissipation processes present in Plateau borders and nodes [47, 49, 127–129]. Focussed as they are on flows in Plateau borders, some of these models have disregarded fluid flow from the foam films (lamellae) towards the Plateau borders, as such flows do not contribute much to the overall volume of drained fluid [38]. However, these so-called film drainage flows are essential to consider in the present study, as they turn out to make a contribution to surfactant mass transport on foam films. This is relevant in the present study since, fluid flow from the foam films towards the Plateau borders will carry surfactants, especially when surfactants are soluble in the bulk of the foam film. Film drainage is therefore discussed next.

2.4.3.2 Film drainage

Typically, as we have said, the volume of liquid flowing from foam films into the interstitial channels is small relative to the overall liquid draining through foams. This is because the liquid within the foam films is typically present in a much smaller quantity than the liquid within the Plateau borders. However, flow even of this small quantity can nonetheless have a contribution to the mass transport of surface-active materials on and within the foam films [1, 2]. This then, in turn affects the surfactant recovery and enrichment (see Sec. 2.3) in a fractionation column as the liquid draining from films itself contains surface-active materials. Moreover if films drain to become very thin, they can also be highly enriched, since they carry a given amount of adsorbed surfactant despite having a very small liquid volume. As a result, in the present study, we need to find a model and eventually an equation describing film drainage. Moreover, to understand better the relative importance of considering film drainage in our models,

in the present study, cases both with and without film drainage have been considered.

Following the work of Vitasari et al. [1], in this study, one of the main assumptions is that foam films, despite draining, are parallel and planar. Consequently, due to the Young-Laplace law (see Sec. 2.4.2), the higher curvature of the Plateau border causes the liquid pressure to be lower in the Plateau borders than in the adjacent films (see Fig. 2.4). This then, causes a suction in the Plateau border that drives a flux of liquid from the film into the Plateau border [40].

More generally, the rate of film drainage or the so-called 'film thinning rate' is a result of the Plateau borders' capillary suction, as well as other complex phenomena, such as dimpling and non-uniformity of film thickness [130]. There are experimental methods to measure film drainage, e.g. using a device such as the so-called Scheludko cell [131–134]. These methods lead eventually to empirical formulae for the film thinning rate Besides experimental methods, some researchers have developed film drainage models based on the mobility of the film surface. However, the mobility of the interface is affected by the type of surfactant in the solution. Some surfactants generate rigid interfaces, while others produce mobile interfaces [83, 114]. There are three models of film drainage, namely the Reynolds model for a rigid interface [41, 135], the power law model for a mobile interface [35, 40, 48], and an exponential model [136].

In the present study, we consider comparatively rigid surfaces, due to the significant Marangoni stresses (to be discussed in more detail later) produced by the gradients of surface tension [133]. This assumption has been used and subsequently validated by Tsekov [130], Manev et al. [137]. Moreover, in the foam fractionation context, residence times are typically not terribly large (up to $\approx 20\,\mathrm{s}$ [83]) which is less than characteristic drainage timescales: the surfactants studied tend to create rigid film interfaces, leading to slow film drainage (even slower than the aforementioned typical residence time).

To summarise, film drainage is a capillary-driven film thinning effect transporting liq-

uid towards the Plateau border. If films ever become sufficiently thin however there may be additional forces opposing drainage and preventing foam films from rupturing. These forces are discussed next.

2.4.3.3 Disjoining pressure

If no forces were to oppose the film thinning mechanism, films would simply become thinner and thinner, and eventually unstable films that can rupture would be produced [138]. However, having surface-active materials within the film and adsorbed on film surfaces can produce additional forces between the two surfaces of a film that prevent rupture from happening. In the context of the current study, the foam films will be considered not to reach the thickness in which these forces become relevant compared to the Plateau border capillary suction [1]. However, in the interests of completeness, in the present section, we still discuss such forces in brief.

When the film is thin enough (in the order of tens of nanometres), intermolecular forces act between two interfaces [114]. When measured per unit area, these forces, which prevent two interfacial layers on either side of a film from contacting each other are called 'disjoining pressures' [118]. In essence 'disjoining pressure' can be thought of as an excess pressure in the film relative to that in the bulk solution [139]. Disjoining pressure consists of the net effect of van der Waals, electrostatic, and steric interactions [140–142] as follows:

$$\Pi_d = \Pi_{vdW} + \Pi_{el} + \Pi_{ste} \tag{2.5}$$

where Π_d is net disjoining pressure, Π_{vdW} is van der Waals force per unit area, Π_{el} is electrostatic force per unit area, and Π_{ste} is steric force per unit area.

Van der Waals force is the attraction between two molecules which have induced electrostatic dipoles [140, 143]. As a result, it makes a negative contribution to the disjoining pressure. The second contribution is the electrostatic interaction, which is often significant. This arises because interfaces are generally electrically charged, e.g. be-

cause of the presence of charged species within surfactants. Electrostatic charges with the same sign lead to repulsion and thus have a positive contribution to the disjoining pressure [44]. There is an additional short-range 'structural' repulsive force due to perturbation of the molecular ordering at surfaces. This arises when surfaces contain water molecules adsorbed by hydrogen bonding [142]. For films containing surfactants of low molecular mass, this is associated with steric hindrance between water molecules and the hydrophilic head of the surfactants [114].

If the film reaches an equilibrium thickness, the capillary pressure difference of the Plateau borders (γ/a from Eq. (2.4) or more specifically γ_{Pb}/a, which is the driving pressure for thinning of the foam films), is exactly counterbalanced by Π_d the repulsive net disjoining pressure [144].

Having discussed the pressure difference between the Plateau borders and neighbouring films, as well as the forces opposing it, we can now work out an equation for film drainage rate in a rigid interface.

2.4.3.4 Reynolds model for film drainage

When an adsorbed surfactant is present on an interface, it often happens that strong surface stresses (to be discussed in more detail later on) make it difficult to deform the interface. This is known as a rigid or immobile interface [114]. In the case of a film with rigid interfaces, which is the type of interface considered in the present study, any flow along the film is Poiseuille type. Thus, a no-slip boundary condition can be assumed in the first instance for the purposes of estimating the velocity profile in the film and ultimately the film drainage rate [38]. The film drainage equation for a rigid interface has been developed by Reynolds [41], and is based on the application of the lubrication approximation to the Navier-Stokes equation to obtain the following

equation (the derivation can be found in Sec. A 1) [13]:

$$\frac{\mathrm{d}\delta}{\mathrm{d}t} = -\frac{2\delta^3 \Delta P}{3\mu L^2} \tag{2.6}$$

where ΔP is the pressure difference that is driving thinning of the film, δ is film half-thickness, L is film half-length, and μ is viscosity of the film's bulk. Here, half of the length and thickness of the film have been considered due to the symmetry of the two-dimensional system (see Fig. 2.4).

The pressure difference between film's bulk and Plateau border ΔP, is now the capillary pressure P_c, obtained from Young-Laplace law Eq. (2.4), which is the suction from the Plateau border minus the disjoining pressure Eq. (2.5), that opposes it [145]:

$$\Delta P = P_c - \Pi_d. \tag{2.7}$$

As mentioned in Sec. 2.4.2, the capillary pressure (pressure caused by the difference in curvatures of films and adjacent Plateau borders), can be expressed via the following equation [135]:

$$P_c = \frac{\gamma_{\mathrm{Pb}}}{a} \tag{2.8}$$

where γ_{Pb} is the surface tension at the Plateau border, and a is the radius of curvature around the Plateau border [1]. Note that we are specifically using the surface tension γ_{Pb} at the Plateau border here, anticipating (as we will see later on) that this might differ from the surface tension in the film.

If, as is assumed in the present study, the film is not extremely thin (i.e. not as thin as just tens of nanometres), the disjoining pressure can be neglected compared to the capillary pressure [38]. As a result, the thinning rate equation (Eq. (2.6)) can be expressed using the Plateau border's surface tension and its radius of curvature, as below:

$$\frac{\mathrm{d}\delta}{\mathrm{d}t} = -\frac{2\delta^3 \gamma_{\mathrm{Pb}}}{3a\mu L^2}. \tag{2.9}$$

This completes for now our discussion of film drainage rates, remembering however that film drainage impacts surfactant mass transport during e.g. a foam fractionation process. However this is not the only surfactant mass transport mechanism that is present in a foam fractionation process, particularly one with reflux. The so-called Marangoni effect is also a very important mechanism that drives mass transport of surface-active materials. It will be described in Sec. 2.5.2. To explain the Marangoni effect though, we first need to explain some background on interfacial rheology of foam film interfaces. This is discussed next.

2.5 Foam film interface

One mechanism by which a surfactant aids foaming is by creating a gradient in surface tension, which enables the surface to resist tangential stresses [146]. A film without surfactant has uniform surface tension and tends to be unstable against rupture [147]. In the presence of surfactant though, a disturbance on the surface (e.g. a thin spot on a film) will create a temporary gradient in surfactant surface concentration and hence, a gradient in surface tension (see Sec. 2.5.2). As a result, there will be a flow towards the thin spot in the film, which can then slow down the drainage of the foam film around that region.

What is needed then is a technique for determining how the amount of surfactant on an interface impacts the surface tension or some other rheological property of the surface. Common techniques for studying interfaces containing surface-active components are ellipsometry [148], neutron reflectometry [60, 149], X-ray reflectivity [150], Brewster angle microscopy [151], surface tension measurements [152], atomic force microscopy (AFM) [153], total internal reflection fluorescence (TIRF) microscopy [154] and sum frequency generation (SFG) spectroscopy [155]. Regardless of which technique is deployed, the aim is to determine amounts of surfactant adsorbed and corresponding surface tensions and/or interfacial stresses.

2.5.1 Gibbs elasticity

Interfacial rheology involves establishing a functional relationship between interfacial stress, deformation and rate of deformation, often expressed in terms of elasticity and viscosity coefficients [156]. Two main types of deformation of fluid elements in a two-dimension system are [146]:

- Shear: changes in shape at a constant area or volume
- Compression/dilation: changes in area or volume at a constant shape

The surface dilational modulus, ϵ is defined as the increase in surface tension for a small relative increase in surface area A [157]. Hence, ϵ is a measure of the resistance of a film to change in its area [158, 159] and gives a measure of the stiffness of the interface against a dilational compression or expansion [146, 160]. Surface dilational modulus can be expressed as:

$$\epsilon = \frac{\mathrm{d}\gamma}{\mathrm{d}\ln A} \tag{2.10}$$

where $\ln A$ is the logarithm of area of the bubble surface [161]. For an oscillatory imposed change in $\ln A$, the surface dilational or viscoelasticity modulus is a complex number [158], accounting for both the elasticity and the viscosity contribution [159, 162, 163]. In the simplest case (considered in the present study), when the modulus is purely elastic and an equilibrium state is assumed between the surface tension and the surface concentration of surfactant, dilational modulus can be substituted by the Gibbs elasticity modulus as follows [164–168]:

$$\mathcal{G} \approx -\frac{\mathrm{d}\gamma}{\mathrm{d}\ln \Gamma} \tag{2.11}$$

where $\mathcal{G}$ is a Gibbs-Marangoni parameter and has the same dimension as γ. Also, Γ here is the surface concentration of surfactant, often termed the "surface excess". Note that if total amount of surfactant adsorbed on the surface is fixed, then any changes in $\ln \Gamma$ are opposite to changes in $\ln A$. As can be seen in Eq. (2.11), therefore, Gibbs

elasticity is calculated from the surface tension variations as a response to surfactant surface concentration changes and hence to area changes of the drop [161]. Although Gibbs elasticity is not constant over the entire domain of possible Γ values, it can be assumed to be almost constant over any relatively small domain of surface concentrations.

In summary, surface tension and surface concentration are related to one another. This concept is important to understand Marangoni flow which happens whenever there are variations in surface tension due to variations of surface concentration, which would happen for instance as a result of reflux. The Marangoni effect is described next.

2.5.2 Marangoni effect

On a film interface, regions of either higher or lower surface tensions can be created as a result of an external disturbance or external reflux [44]. One way of quantifying the different surface tensions is to define the so-called surface pressure Π, as:

$$\Pi = \gamma_0 - \gamma \tag{2.12}$$

where γ_0 and γ are the surface tensions of the pure solvent and the solution containing surfactant, respectively [168].

Since addition of surfactant reduces surface tension, it is clear that Π is positive. Moreover, if a disturbance alters the surface concentration of surfactant locally, it also alters γ and hence alters Π. Spatial inhomogeneities in the surface tension will immediately drive surfactant molecules toward the region of lower surface concentrations (or equivalently toward the region of lower surface pressure). This then compensates for the inhomogeneities on the surface.

The above-mentioned effect is known as the Marangoni effect and was first described by Marangoni [169], and subsequently considered also by others [43, 45, 49]. By pre-

venting interfaces of films from becoming denuded of surfactant, it is believed to be one of the most important mechanisms in foam stability [123]. The Marangoni effect is also important within surfactant mass transport models [42]. Indeed the surface redistribution of surfactant can also entrain underlying liquid. If the surfactant is somewhat soluble in bulk liquid (as will be assumed in the present work), then this entrainment also contributes to surfactant mass transport within the bulk.

Spatial gradients in surface tension lead to stress. The so-called Marangoni stress typically needs to be balanced by the viscous shear stress upon the liquid in the bulk of the film and surface viscous stress, as presented in the following equation [170, 171]:

$$\mu \left(\frac{\partial u}{\partial z} \right) \Bigg|_{z=\delta} = \frac{\partial \gamma}{\partial x} + \mu_s \frac{\partial^2 u_s}{\partial x^2} \tag{2.13}$$

where μ is the liquid viscosity, γ is the surface tension, u is the liquid velocity component along the film direction (x-axis), z is the coordinate from the centre of the film across the film thickness, δ is the film half-thickness, and x is the coordinate from the centre of the film along its length (see Fig. 2.4). Moreover, μ_s is the surface viscosity and u_s is the velocity on the film surface.

The physical origin of the surface viscosity is that the adsorption of many species to the surface will increase the interface's resistance to flow. However, the surface viscosity appears to be less important compared to the Marangoni effect, which is dominant for typical surfactant systems even with low concentrations [172]. Consequently, the Marangoni stress equation (Eq. (2.13)) can be simplified to the following equation [1, 45, 51]:

$$\mu \left(\frac{\partial u}{\partial z} \right) \Bigg|_{z=\delta} = \frac{\partial \gamma}{\partial x}. \tag{2.14}$$

In summary, Marangoni flow on a foam film say, occurs when there is a gradient of concentration of surface-active material on the surface, hence a gradient of surface tension. In the present study, due to considering foam films in a foam fractionation system

with reflux, the concentration of surface-active material on the surface of the Plateau border, Γ_{Pb} is higher than that on the surface of the foam film Γ. The Marangoni flow tends to bring material from the surface of the Plateau border towards the centre of the film. This also induces a flow of bulk fluid which, at least near the surface, is in the same direction as the surface flow itself. When the Marangoni effect dominates other mechanisms such as film drainage, the surfactant is thereby transported from the Plateau border towards the centre of the film [1]. On the other hand, film drainage when present opposes this flow and tends to transport material back toward the Plateau border (see Sec. 2.4.3.2).

2.5.3 Surfactant adsorption

Thus far we have discussed how surface tension or equivalently surface pressure is affected by surfactant surface concentration. However, what we have not yet described is how to quantify how much surfactant is adsorbed for a given amount of surfactant in the bulk. As will be discussed further in Chapter 3, to develop a model for surfactant transport, we need to know the relationship between surfactant surface concentration and bulk concentration. The general way that such a relationship is obtained is now discussed.

Generally, thermodynamics of the adsorption layers can provide so-called equations of state, which relate surface tension or analogously surface pressure (Eq. (2.12)) to the surface layer composition [173]. Then, with the application of the so-called adsorption isotherms, we can relate the amount of surfactant adsorbed on the surface to the corresponding amount dissolved in the bulk [44, 174]. The difference between the chemical potential of a surfactant at a film interface and in the bulk phase acts as a driving force for the transport of surfactant from bulk to interface. This situation continues until equilibrium between surface and bulk is reached. Among the approaches used for quantifying equilibrium surfactant adsorption, the construction of an adsorption isotherm is a popular one. To construct such an isotherm, the amount of surfactant ad-

sorbed on a surface is specified as a function of the concentration of the solution from which the surfactant is adsorbed, typically over a wide range of solution concentrations [175]. Further details are given in the following sections.

2.5.3.1 Gibbs adsorption equation

We now describe an important equation relating surface tension, surface concentration and bulk concentration. The starting point for obtaining this is the general Gibbs-Duhem equation which describes the relationship between changes in temperature, pressure and chemical potential for components in a thermodynamic system [176–179]. The Gibbs-Duhem equation at a constant temperature and pressure results in the following equation:

$$\mathrm{d}\gamma = -\frac{1}{A}\sum \mathcal{N}_i \mathrm{d}\mu_i \tag{2.15}$$

where γ is surface tension, A is the interfacial area, $\mathcal{N}_i$ is the number of moles of the i^{th} component, and μ_i is its chemical potential [180]. This equation (Eq. (2.15)) enables us to relate surface tension with surface concentrations and chemical potentials of the components covering the area. Now, the thermodynamic relationship between the interfacial tension γ, and surface concentration Γ, at a constant temperature and pressure can be found using the so-called Gibbs adsorption equation as follows [112, 181]:

$$\mathrm{d}\gamma = -\sum \left(\frac{\mathcal{N}_i}{A}\right) \mathrm{d}\mu_i = -\sum \Gamma_i \, \mathrm{d}\mu_i \tag{2.16}$$

Using an expression for the chemical potential μ_i of any component i, in terms of the activity a_i, at a specified temperature T, leads to the following equation [182–184]:

$$\mathrm{d}\gamma = -RT \sum \Gamma_i \, \mathrm{d} \ln a_i \tag{2.17}$$

where R is the ideal gas constant. For special cases, such as the adsorption of a single non-ionic surfactant in a pure solvent at a low concentration (below CMC), the activity

can be replaced by the concentration c, leading to the following equation [185–187]:

$$\Gamma = -\frac{1}{RT}\left(\frac{\mathrm{d}\gamma}{\mathrm{d}\ln c}\right). \tag{2.18}$$

This equation demonstrates how the quantities Γ and γ, and the bulk concentration c, are all related. However, Eq. (2.18) becomes more useful still to predict the equation of state relationships when linked with adsorption isotherms. These isotherms, as we have alluded to, provide information relating surfactant concentration on the surface, Γ, with its bulk concentration c [44].

Nonetheless, obtaining reliable equilibrium surface tension data as a function of $\ln c$ is an important step [93]. This can be done at each selected concentration c, by observation of the dynamic tension of a solution until it reaches a constant value [188, 189]. Values of Γ as a function of c then follow and can be compared against models. Some of the models that are used to represent the adsorption behaviour of surfactants up to now are the Henry, Langmuir and Frumkin isotherms [93]. The Henry and Langmuir isotherms in particular will be discussed shortly.

To summarise, we used thermodynamics to obtain a relationship between surface tension and surface and bulk concentrations. However, to be able to use the relationship to make predictions, we also need to know an additional relationship between surface and bulk concentrations. Hence, in what follows we discuss adsorption isotherms which, as mentioned, provide the necessary relationship between surface and bulk. Some commonly used adsorption isotherms are described below.

2.5.3.2 Henry isotherm

Henry's law was originally formulated as a simple linear relationship between gas solubility in a liquid and its pressure [190]. An analogous relationship is also applicable for the adsorption of a surfactant surface concentration at the interface Γ, as a function

of its bulk concentration c, and is known as the Henry isotherm [191].

$$\Gamma = K_H c \tag{2.19}$$

where K_H is the Henry constant, and c is the bulk concentration. Here, K_H can be used as a simple measure of the surface activity of a surfactant: larger K_H implies more surface active. It also represents the thickness of the bulk solution (of concentration c), which contains as much surfactant as in a surface monolayer with surface concentration Γ [93]. This linear isotherm can be used in the range of very low surface coverage, θ. Surface coverage is a fraction, namely the number of adsorbed molecules actually on a surface, divided by the number of molecules corresponding to a filled monolayer on that surface. Fig. 2.5 shows the typical linear relationship between surface and bulk concentrations in a Henry adsorption isotherm.

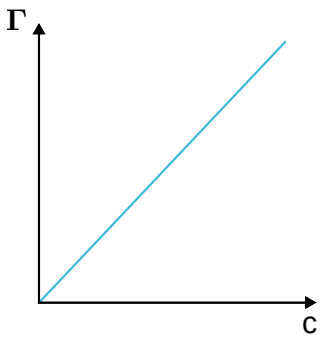

Figure 2.5: Henry adsorption isotherm

Using the Gibbs adsorption equation for an ideal (usually dilute) solution, without aggregation or micellization, one can derive the following surface equation of state for the Henry isotherm, using Eqs. (2.18) and (2.19) [93, 181]:

$$\Pi = \gamma_0 - \gamma = RTK_H c = RT\Gamma \tag{2.20}$$

where Π is the surface pressure and γ_0 is the surface tension of pure solvent (water

typically). Considering that $\Gamma = 1/\bar{A}$, where $\bar{A}$ is the molar area, one obtains:

$$\Pi\bar{A} = RT. \tag{2.21}$$

Some limitations of using the Henry isotherm are that it is only valid up to a certain concentration, and it is not able to impose an upper limit on Γ [93]. To overcome this, more complicated nonlinear models have been developed [192–197]. A widely used nonlinear model is described next.

2.5.3.3 Langmuir isotherm

The equilibrium Langmuir isotherm for a single-component adsorption system can be written as follows [198, 199]:

$$\Gamma = \Gamma_m \frac{\bar{K}_L c}{1 + \bar{K}_L c} \tag{2.22}$$

where Γ_m is the maximum surface excess, and $\bar{K}_L$ is the so-called Langmuir parameter. Here, $\Gamma_m \bar{K}_L$ is a measure of the surface activity, or the surfactant's ability per unit concentration c, to decrease the surface tension γ [93]. For c much greater than $\bar{K}_L^{-1}$ however, the amount of adsorbed surfactant Γ, remains almost fixed at Γ_m. Fig. 2.6 shows the typical relationship between surface and bulk concentrations in a Langmuir adsorption isotherm.

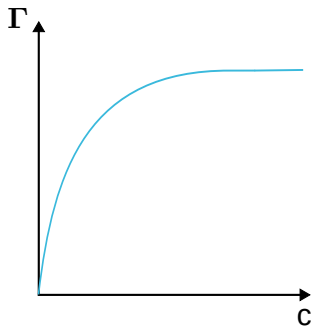

4

Figure 2.6: Langmuir adsorption isotherm

The analogous surface equation of state for the Langmuir isotherm is the so-called Szyszkowski equation [181, 200, 201]

$$\Pi = \gamma_0 - \gamma = RT\Gamma_m \ln\left(1 + \bar{K}_L c\right) \tag{2.23}$$

$$\Pi = \gamma_0 - \gamma = -RT\Gamma_m \ln\left(1 - \frac{\Gamma}{\Gamma_m}\right) \tag{2.24}$$

where Π is the surface pressure and γ_0 is the surface tension of air/pure liquid interface ($\gamma_0 = 72.3 \pm 0.2\,\mathrm{mN/m}$ in the case of water [159]).

The Langmuir isotherm is one of the simplest nonlinear isotherms that has shown reasonable agreement with experimental data [202]. Overall, it often gives a reasonable fit for surface concentration Γ, versus concentration c, even for higher concentrations. This fit can be observed for methods which directly measure surface concentrations [203], as well as other indirect methods (e.g. a fit of Π vs c data to Eq. (2.23)).

To summarise, having discussed both Henry and Langmuir adsorption isotherms, we now are able to relate surface and bulk concentrations, at least for comparatively small surfactant molecules which typically show a straightforward surface-to-bulk relationship. However, it turns out that the relationship between surface and bulk concentrations can be more complicated for larger molecules such as proteins, as is discussed next.

2.5.4 Protein adsorption characteristics

The adsorption of proteins at a liquid interface and their behaviour in the adsorbed state play an important role in many biological and technological processes, especially in the food and pharmaceutical industries. Moreover, proteins are often used as surface-active agents in foam and emulsion-based products [204].

Overall, the adsorption behaviour of proteins is very different from the behaviour typical of simpler surfactant molecules. The different behaviour is due to the structural

reorganization and strong electrostatic or hydrophobic interactions between adsorbed protein molecules at an interface [205]. This can be due to the ability of proteins to unfold and adsorb at the interface, as well as their ability to form viscoelastic interfacial films through intermolecular interactions [206].

Some of the associated complications are outlined in the appendix. In Sec. A 2, we present the general equilibrium adsorption behaviour of proteins. Then, we try to apply some simplifications to obtain an approximate Langmuir-like adsorption isotherm for them in Sec. A 3, which is analysed further in Sec. A 4. As is discussed, due to the complicated nature of protein adsorption behaviour, although fitting a Langmuir isotherm cannot always provide a very accurate result, it can still help us model the process using a relatively straightforward isotherm. In the mass transport calculations in later chapters, we will employ only straightforward isotherms, even when considering proteins.

In summary, surfactants report to the surface as surface excess. Hence, we can use this characteristic to separate them from an aqueous solution. However, to set up a model for the transport of surfactants on and within the foam film, we need to understand all the above-mentioned physics of foam and the physical chemistry of surfactants. Having understood the above-mentioned concepts, in the next chapter, we start to bring all of them together to derive governing equations that enable us to model mathematically surfactant transport behaviour.

Chapter 3

Governing equations

Having carried out a literature review on foams in general and especially foam fractionation, we now need to derive governing equations to define our models. To do this, we need to derive velocity fields using continuity and momentum equations, as well as mass transport equations on and within the foam films.

3.1 Velocity field equations

Having now defined the relevant equations for film drainage (Eq. (2.9)), Marangoni effect (Eq. (2.14)), and Gibbs elasticity (Eq. (2.11), with Gibbs elasticity assumed for simplicity to be constant in our domain of interest), we can now proceed to derive an equation for surfactant mass transport on and within the foam film. To do this though, we first need to derive velocity fields using the continuity equation and a momentum balance, treating for simplicity a two-dimensional system (given that exact film shapes and sizes vary in any case from film to film). Even so, a thin film can be a complicated physical system, not least when the film shape itself deforms. However, a reasonable simplification is to assume a lubrication approximation neglecting shape deformation. Then by considering just the dominant terms in the governing equations and neglecting less important ones, we are able to derive a mathematical approximation that can be

comparatively simple to analyse [207]. In our case study, we use a lubrication approximation as follows [1, 41, 44, 52]:

- The film-thickness (or half-thickness δ), is very small when compared to its length (or half-length L), e.g., $\delta \ll L$;
- Gravity and inertial forces are negligible when compared to viscous forces due to the small Reynolds number;
- The fluid in the film is assumed to be Newtonian (with constant viscosity and incompressible);
- The gas/liquid interfaces are rigid and parallel;
- The transversal velocity (along the z-axis) w, is small in comparison to the longitudinal velocity (along the x-axis) u;
- The variation of u with respect to z is much higher than that with respect to x, i.e., $\partial u/\partial z \gg \partial u/\partial x$. The same principle applies to the second-order derivative, i.e., $\partial^2 u/\partial z^2 \gg \partial^2 u/\partial x^2$;
- The x-component of the velocity field u, is maximum at $z = 0$, i.e. $\partial u/\partial z|_{z=0} = 0$;
- The z-component of the velocity field w, is $w(x, z = 0) = 0$ along the midplane of the film, and due to film drainage $w(x, z = \delta) = \mathrm{d}\delta/\mathrm{d}t$ at the gas/liquid interface;
- Due to the presence of surfactant, the stress at the film interface is driven by surface tension gradients (Marangoni stresses, see Eq. (2.14)), i.e., $\mu\, \partial u/\partial z|_{z=\delta} = \partial\gamma/\partial x$, but surface viscosity is not relevant.

The continuity equation for the thin liquid film in a two-dimensional system is:

$$\frac{\partial u}{\partial x} + \frac{\partial w}{\partial z} = 0. \tag{3.1}$$

The general Navier-Stokes equations for the thin liquid film and a two-dimensional system in x and z directions ignoring the gravity are:

$$\rho\left(\frac{\partial u}{\partial t}+u\frac{\partial u}{\partial x}+w\frac{\partial u}{\partial z}\right)=-\frac{\partial P}{\partial x}+\mu\left(\frac{\partial^2 u}{\partial x^2}+\frac{\partial^2 u}{\partial z^2}\right), \tag{3.2}$$

$$\rho\left(\frac{\partial w}{\partial t}+u\frac{\partial w}{\partial x}+w\frac{\partial w}{\partial z}\right)=-\frac{\partial P}{\partial z}+\mu\left(\frac{\partial^2 w}{\partial x^2}+\frac{\partial^2 w}{\partial z^2}\right). \tag{3.3}$$

Under the set of assumptions aforementioned, the Navier-Stokes equations will reduce to the equation of motion in the lubrication approximation, as follows [208]:

$$\frac{\partial P}{\partial x}=\mu\frac{\partial^2 u}{\partial z^2}, \tag{3.4}$$

and

$$\frac{\partial P}{\partial z}=0. \tag{3.5}$$

Eq. (3.5) states that there is no pressure gradient across the film thickness. To obtain the velocity component along the x-axis, we start by integrating Eq. (3.4) with respect to z, while applying the following boundary conditions:

$$\left.\frac{\partial u}{\partial z}\right|_{z=0}=0, \tag{3.6}$$

and

$$\mu\left.\frac{\partial u}{\partial z}\right|_{z=\delta}=\frac{\partial \gamma}{\partial x}, \tag{3.7}$$

leading to the following result:

$$\frac{1}{\delta}\frac{\partial \gamma}{\partial x}z=\mu\frac{\partial u}{\partial z}. \tag{3.8}$$

We can now perform an integration of Eq. (3.8) with respect to z:

$$u=\frac{z^2}{2\mu\delta}\frac{\partial \gamma}{\partial x}+u(x,z=0), \tag{3.9}$$

where $u(x, z = 0)$ is an integration constant for a specific position along the x-axis. To determine this integration constant, we need to consider the equation describing the thinning of a lamella as follows [40]:

$$\frac{\partial \delta}{\partial t} = -\left(\bar{u}\frac{\partial \delta}{\partial x} + \delta\frac{\partial \bar{u}}{\partial x}\right), \tag{3.10}$$

where $\bar{u}$ is the average velocity of the liquid in the x-direction. Due to the assumption of a flat film, the film thickness is constant along the x-axis ($\partial\delta/\partial x = 0$), resulting in:

$$\bar{u} = -\frac{x}{\delta}\frac{\mathrm{d}\delta}{\mathrm{d}t}. \tag{3.11}$$

By averaging u in Eq. (3.9) for a specific position along the x-axis, and combining it with Eq. (3.11), we obtain the integration constant $u(x, z = 0)$ as follows:

$$u(x, z = 0) = -\frac{x}{\delta}\frac{\mathrm{d}\delta}{\mathrm{d}t} - \frac{1}{\delta}\int_0^\delta \frac{z^2}{2\mu\delta}\frac{\partial \gamma}{\partial x}\mathrm{d}z. \tag{3.12}$$

If we now combine Eq. (3.9) with Eq. (3.12), we obtain the following equation giving the velocity component along the x-axis:

$$u = -\frac{x}{\delta}\frac{\mathrm{d}\delta}{\mathrm{d}t} + \frac{1}{\mu}\left(\frac{z^2}{2\delta} - \frac{\delta}{6}\right)\frac{\partial \gamma}{\partial x}. \tag{3.13}$$

From Eq. (3.13), it becomes clear that the velocity component along the x-axis u, is dependent on film drainage effects (first term on the right-hand side), coupled with the effect of surface tension gradients present at the gas/liquid interface (second term on the right-hand side). Due to the presence of surfactant at the film interface, the surface tension gradient gives a Marangoni stress, originating due to the gradient of surface concentration along the film interface. We assume that the relationship between surface concentration Γ, and surface tension γ, obeys [1, 52]:

$$\frac{\mathrm{d}\gamma}{\mathrm{d}\ln\Gamma} \approx -\mathcal{G}, \tag{3.14}$$

where $\mathcal{G}$ is the so-called Gibbs elasticity (see Sec. 2.5), assumed here to be constant. We can now rewrite Eq. (3.13), as:

$$u = -\frac{x}{\delta}\frac{\mathrm{d}\delta}{\mathrm{d}t} + \frac{\mathcal{G}}{\mu}\left(\frac{z^2}{2\delta} - \frac{\delta}{6}\right)\frac{\partial \ln \Gamma}{\partial x}. \tag{3.15}$$

With knowledge of the horizontal component of the velocity field u, its vertical component w, can now be determined. Combining the continuity equation (Eq. (3.1)) with Eq. (3.15), w is obtained as follows:

$$w = \frac{z}{\delta}\frac{\mathrm{d}\delta}{\mathrm{d}t} + \frac{\mathcal{G}}{\mu}\left(\frac{z^3}{6\delta} - \frac{z\delta}{6}\right)\frac{\partial^2 \ln \Gamma}{\partial x^2}. \tag{3.16}$$

If we set $z = \delta$ in Eq. (3.16), as expected, we obtain the expression for the vertical velocity of the interface dictated by the drainage mechanism, $w|_{z=\delta} = \mathrm{d}\delta/\mathrm{d}t$, where $\mathrm{d}\delta/\mathrm{d}t$ has a negative value due to film thinning.

We can now easily determine the horizontal surface velocity u_s, by setting $z = \delta$ in Eq. (3.15), resulting in:

$$u_s = -\frac{x}{\delta}\frac{\mathrm{d}\delta}{\mathrm{d}t} - \frac{\mathcal{G}}{3\mu}\frac{\delta}{}\frac{\partial \ln \Gamma}{\partial x}. \tag{3.17}$$

From Eq. (3.17), it now becomes clear that there is a competition between Marangoni stresses and film drainage effects on the film surface. Typically, $\partial \ln \Gamma/\partial x > 0$ (at least in the domain $x > 0$ in Fig. 2.4). This is due to reflux through the Plateau borders, meaning Plateau borders are enriched in surfactant relative to adjacent films. On the other hand, film thinning yields negative drainage rates, $\mathrm{d}\delta/\mathrm{d}t < 0$. In order to solve Eq. (3.17), information regarding the film drainage rates is needed, either through the use of empirical formulae in the literature, or theoretical estimations as previously introduced in Sec. 2.4.3.4.

3.2 Mass transport equation

Having derived velocity fields, we now proceed to derive an equation for surfactant mass transport at the gas/liquid interface, as well as an equation for surfactant mass transport in the bulk.

3.2.1 Surfactant mass balance at the gas/liquid interface

The general differential equation representing the transport of surfactant at the surface of a foam film can be defined as follows:

$$\frac{\partial \Gamma}{\partial t} + \frac{\partial (u_s \Gamma)}{\partial x} = - \mathcal{D} \left. \frac{\partial c}{\partial z} \right|_{z=\delta}, \tag{3.18}$$

where Γ is the concentration of surfactant at the interface, also known as surface excess and u_s is the horizontal component of the velocity field at the interface, previously derived in Eq. (3.17). The term on the right-hand side of Eq. (3.18) represents surfactant exchange between the film's surface and subsurface layers due to diffusion. Here, c is the surfactant bulk concentration, and $\mathcal{D}$ is the diffusivity coefficient. For surfactant exchange to occur between surface and bulk, surfactant needs to diffuse to or from the subsurface layer first. Below the CMC (which is always assumed to be the situation in this study), having an unsaturated film surface can result in instantaneous adsorption of surfactant from the subsurface layer [1]. Therefore, the dynamics of this mass transfer process will be limited by the diffusion of surfactant to the subsurface layer. However, what this means is that in the limit in which surfactant diffusion within the film's bulk is slow when compared to the Marangoni flow, surfactant exchange between bulk and surface is severely restricted. Another way of restricting this is to have barely any surfactant (and hence barely any surfactant concentration gradient) in the bulk. This is referred to as the insoluble surfactant case. As a result, in the insoluble surfactant case just as in the case with slow diffusion, the diffusion term on the right-hand side of Eq. (3.18) can be ignored and the mass transport equation is simplified to the following

equation:

$$\frac{\partial \Gamma}{\partial t} + \frac{\partial (u_s \Gamma)}{\partial x} = 0. \tag{3.19}$$

In order to solve Eq. (3.19), information regarding the fluid velocity at the liquid gas interface provided in Sec. 3.1 is needed. Within the present context of studying foam fractionation via reflux, considering draining films with Marangoni stresses on their interfaces, the fluid velocity at the film interface u_s, can be estimated using Eq. (3.17). Knowledge of the initial surfactant surface concentration Γ_0, along with boundary conditions for Γ (discussed below) are also required.

During a foam fractionation process with reflux, the concentration of surfactant in the bulk and on the surface of the Plateau borders is kept high (i.e. higher than Γ_0 initially in the films) by the downward flow of surfactant-rich material through the Plateau borders. Therefore, it is reasonable to assume that Plateau borders act as surfactant reservoirs (particularly in consideration of the fact that, they typically contain more liquid than the significantly thinner films do). Due to this, with the fractionation process running continuously, for a specific height in the column, Plateau borders can be assumed to maintain relatively constant values of surfactant concentration, both at their interfaces Γ_{Pb}, and (to be discussed shortly) within their bulk c_{Pb}. On symmetry grounds at the centre of the film ($x = 0$), we expect $\partial \Gamma / \partial x = 0$. Another important remark is that the surface velocity u_s, at the mid point of the surface (i.e., at $x = 0$) can be assumed to be zero again due to the film symmetry. It then follows from Eq. (3.19) that $\partial \ln \Gamma / \partial t|_{x=0} + \partial u_s / \partial x|_{x=0} = 0$.

By combining the estimation for the surface velocity in Eq. (3.17), accounting for film drainage, and the Marangoni stresses at the gas/liquid interface, with the surfactant mass balance in Eq. (3.19), we obtain the second-order partial differential equation governing the concentration at the film surface Γ, as follows:

$$\frac{\partial \Gamma}{\partial t} = \frac{1}{\delta} \frac{\mathrm{d}\delta}{\mathrm{d}t} \left(\Gamma + x \frac{\partial \Gamma}{\partial x} \right) + \frac{G\delta}{3\mu} \frac{\partial^2 \Gamma}{\partial x^2}. \tag{3.20}$$

Vitasari et al. [1] obtained this equation within the context of foam fractionation with reflux, but considering just insoluble surfactant. This means that surfactant molecules are present only on the film surfaces. Concentration in the bulk (and hence gradients of concentration in the bulk, and diffusive fluxes that such gradients might otherwise induce), are then negligible. Under these assumptions, the above-mentioned study provided insights into the evolution with time of the surfactant surface concentration Γ. Of course, in that study, surfactant exchange between the film bulk and film surface was disregarded (due to the assumption of insoluble surfactant).

Under the stated assumption though (insoluble surfactant), it was verified that, for rigid interfaces leading to comparatively slow film drainage (as is also assumed in the present study), the Marangoni flows initially dominate over film drainage effects, allowing the Marangoni mechanism to pull surfactant from the Plateau border, onto the film surface. This then leads to an increase of the surfactant concentration Γ, and consequently an increase in the overall amount of surfactant on the films, and a decay in the Marangoni flow. This system eventually however reaches a quasi-steady state, in which residual Marangoni flows are eventually balanced by drainage effects. This then allows (given the comparatively slow drainage in the rigid film case) an almost uniform surfactant distribution Γ on the film surface, close to the surface concentration in the Plateau border Γ_{Pb}.

In summary, by assuming that films have comparatively rigid interfaces and so drain slowly, foam fractionation with reflux can enrich the bubble surfaces with surfactant, and maintain an enriched surface over time. However, real surfactants are soluble, meaning that there will be surfactant molecules not only at the gas/liquid interfaces but also dissolved within the bulk of the foam films. Due to this, we now also need to consider mass transport equations in bulk of the films. This is the novel contribution of the present study.

3.2.2 Surfactant mass balance in the bulk

The differential equation representing the transport of surfactant within the bulk of a foam film can be defined as follows:

$$\frac{\partial c}{\partial t} + u.\nabla c = \kappa.\nabla^2 c, \tag{3.21}$$

where c is the surfactant concentration within the film bulk, t is time, u is the velocity field within the film bulk, and κ is the diffusivity tensor containing the surfactant diffusivity coefficient (assumed constant) $\mathcal{D}$, and is defined as follows:

$$\kappa = \begin{pmatrix} \mathcal{D} & 0 \\ 0 & \mathcal{D} \end{pmatrix}. \tag{3.22}$$

This mass balance equation takes into account the passive advection of surfactant with the velocity field u, along with diffusion effects within the film bulk. Due to the thin film geometry, $\delta \ll L$, the diffusion effects will be stronger in the z-direction. This then is why we write Eq. (3.22) as a tensor (even though for now it is an isotropic tensor): when we scale the governing equations differently in the directions along and across the film (as is typically done in lubrication theory [209–212]), the result will appear anisotropic.

Initial and boundary conditions are again required. The initial bulk concentration c_0, is assumed to be in equilibrium with the initial surface concentration Γ_0, according to an adsorption isotherm. Certainly, owing to reflux, c_0 will be less than the analogous concentration c_{Pb} in the Plateau border. Regarding boundary conditions, approaching the interface, the instantaneous bulk concentration $c|_{z=\delta}$ (where recall δ is the film half thickness) is in equilibrium with the instantaneous surface concentration Γ, again considering an adsorption isotherm. On symmetry grounds along the midplane $\partial c/\partial z|_{z=0} = 0$. Boundary conditions on c in the x-direction are not necessarily required owing to the diffusion in the z-direction dominating diffusion in the x-direction

(as a result of having thin geometry).

In summary, we have set up the flow field equations and the general form of the mass transport equations both on the surface and within the bulk. What we have not yet done is explain in detail how surface and bulk mass transport might couple. This will be done in the chapters to follow. It turns out that there are two distinct limiting cases or extreme cases in which that coupling is relatively easy to determine, although the coupling is also different in those different limiting cases. Thus there are two extreme limiting cases with different physics that are presented in the following chapters (Chapters 4 and 6), along with supplementary material related to each of them (Chapters 5 and 7, respectively). These then constitute the main results chapters of the thesis.

Chapter 4

Transport of soluble surfactant on and within a foam film in the context of a foam fractionation process

"This chapter consists of published material: [H. Rajabi, P. Grassia, "Transport of soluble surfactant on and within a foam film in the context of a foam fractionation process." Chemical Engineering Science, vol.265, 118171, 2023. https://doi.org/10.1016/j.ces.2022.118171]"

Abstract

This study models soluble surfactant transport on and within a foam film during a foam fractionation process. Marangoni flow drives surfactant onto the film, and also surfactant concentration is assumed to be uniform across the thin foam film. Adsorption isotherms are used to couple mass transfer equations, so as to determine the evolution of the total amount of surfactant (surface plus bulk) at any film location. Surfactant transport is considered both in the absence and presence of film drainage. It is observed that having soluble surfactant slows down evolution of Marangoni-driven flow

compared to cases assuming insoluble surfactant. This is because in soluble surfactant cases, surfactants diffuse to the bulk even whilst being transferred by Marangoni flow onto the film surface. Furthermore, it is observed that a quasisteady state typically occurs after a long time, such that Marangoni flow and film drainage flow become comparable.

Highlights

- Foam fractionation with reflux is modelled for a soluble surfactant
- Reflux induces Marangoni-driven surfactant transfer from Plateau border to film
- Two isotherms (global and local Henry) relate surfactant on and within foam film
- Surfactant transfer slowed by solubility and by local Henry isotherm
- Film drainage reduces surfactant recovery but improves enrichment

4.1 Introduction

The separation of surface-active components is essential in numerous industries, such as waste treatment, food, pharmaceutical, environmental-related, and many more [108, 202, 213]. One of the important methods to separate surfactants from an aqueous solution is foam fractionation [21, 183, 214]. This physicochemical process is often competitive compared to other methods used in this area, namely ultrafiltration, ion exchange, precipitation, membrane filtration and coagulation [17, 24]. This is primarily due to the simplicity of the equipment, low cost and mild operating conditions, as well as environmental compatibility [22, 23]. Furthermore, the applicability of this method in the separation of dilute solutions, beyond the limits of the other techniques, has made it an attractive alternative [27, 94]. Indeed the foam fractionation process

has various applications, such as radioactive effluent purification [85], separation of hydrophobic proteins and enzymes [86–88, 214], separation of non-polar compounds [89], production of pharmaceutical products [90, 91], environmental problem remediation, [15, 92] and food processing [93].

Foam fractionation is based on the adsorption of a surfactant on the bubble surface, as bubbles rise through a solution [31]. The recovered liquid from the top of the column (foamate) is richer in surfactant than the remaining liquid [33]. Moreover, utilization of reflux can increase significantly the separation ability of a foam fractionation device, and thus increase the concentration of the foamate [26, 34, 35, 82]. In a fractionation column with reflux, part of the surfactant rich foamate is collapsed and returned to the column. Then, it drains through Plateau borders, where it mixes with any liquid already in those Plateau borders and increases the Plateau border surfactant concentration. This in turn can enhance the surfactant concentration on the foam film surfaces and within the bulk of the foam films. As a result, reflux improves the overall foam fractionation process efficiency. This then is the reason why in this study, we focus on the foam fractionation process with reflux.

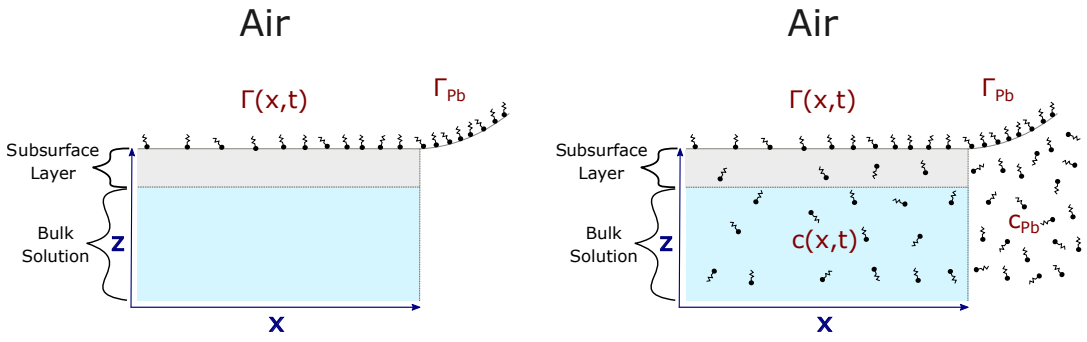

(a) Insoluble surfactant **(b)** Soluble surfactant

Figure 4.1: Insoluble (a) and soluble (b) surfactant distributed on a foam film surface and, where applicable, within the bulk of the foam film. Here Γ and Γ_{Pb} are surface concentrations of surfactant on the film and Plateau border, while c and c_{Pb} are the bulk concentration in the film and Plateau border, respectively. In the present work, Γ on the film depends on coordinate x and time t. Also, c in the film depends on x and t, but is taken to be almost independent of coordinate z. The figure is not to scale as in reality, the film thickness is much smaller than its length.

This study considers the case of comparatively dry foams with typically polyhedral bubbles [70, 117]. Foam films can then be treated as being thin (i.e. thickness much smaller than length) and are in contact at their edges with Plateau borders. Fig. 4.1 shows a schematic figure of such a film, indicating how either insoluble or soluble surfactant might be distributed on and within the foam film. Here Γ and Γ_{Pb} are surfactant surface concentrations on the film and in the Plateau border, and c and c_{Pb} are analogous bulk concentrations. Due to reflux, Γ is typically different from Γ_{Pb}, and c is typically different from c_{Pb}.

There are various physical mechanisms influencing surfactant transport from Plateau-border-to-film and vice versa. For instance, Marangoni flows due to differences between Γ and Γ_{Pb}, leading in turn to differences in surface tension, have been studied by Vitasari et al. [1], Grassia et al. [46], Elfring et al. [167], Vitasari et al. [170], Karakashev et al. [172]. Several studies have also been carried out on film drainage and its effects on foam and foam film stabilization [40, 49, 135]. By the same token, the transport of surfactant onto the foam film in the presence of both Marangoni forces and film drainage has been studied [1, 167, 170, 172]. However, even though we know surfactants are soluble [36, 215], in most previous studies, surfactant transport into the bulk of the film has been neglected [1, 45, 216–218]. Many typical surfactants have nevertheless a substantial solubility in water which can then impact on flow behaviour [17, 54, 55, 219].

In the case of *insoluble* surfactants, the work of Vitasari et al. [1] developed a model for how quickly surfactants move onto the foam film, which is schematically presented in Fig. 4.1a. This model has been developed both in the absence and the presence of film drainage and has revealed that the surfactants can usually move onto the foam films quickly compared to typical bubble residence times in a fractionation column. However, when film drainage is present, it competes against the Marangoni effect and slows down the surfactant transport on the foam surface. An equilibration of surfactant

concentration between the Plateau border and the film is achieved after a sufficiently long time, at least in the absence of film drainage. Moreover, in the presence of film drainage, a quasisteady-state surfactant concentration is reached with a lower surfactant concentration in the film than in the Plateau border. Despite all the achievements of this model, the lack of consideration of any surfactant inside the bulk of the film has led us to present the current model, in which surfactant solubility and its transport inside the bulk are considered (Fig. 4.1b). In addition, a model has been developed here for the behaviour of the soluble surfactant approaching a quasisteady-state configuration at long times, albeit compared to a model already presented by Vitasari et al. [1], some modifications are required in order to account for surfactant solubility.

The present model considers in particular the diffusive transport of soluble surfactant into the bulk of the foam film. Diffusive transport from surface to bulk can in principle occur at different rates relative to Marangoni and film drainage flow, but the specific limit that we will look at here is when surfactants can diffuse very quickly across a thin film, even though any diffusion along the film is very slow. As we explain later on, mathematically, we can express this in terms of the product of a Péclet (Pe) number and a film aspect ratio (Δ), with this product being a small parameter. Hence, we call it a small $\mathrm{Pe}\,\Delta$ limit. To use the model to investigate the performance of foam fractionation for a soluble surfactant, we define (later on) recovery and enrichment factors which are quantities often measured in fractionation studies [36, 82, 83, 108].

This study is laid out as follows. Firstly, Sec. 4.2 deals with the theory used in mathematical models of soluble surfactant transport. That section is divided into several subsections and explains important dimensionless parameters and governing equations and uses them in the so-called small $\mathrm{Pe}\,\Delta$ limit to develop an equation for the evolution of the total amount of surfactant at every position along a film. After that Sec. 4.3 deals with the numerical simulation approach to solve the model and explains some benchmarking methods to check the validity of the simulation approach. Then, Sec. 4.4

presents results and discussion, while Sec. 4.5 provides the conclusions of this study.

4.2 Mathematical model for soluble surfactant transport

In this section, we revisit the relevant transport equations that have been developed by Vitasari et al. [1], albeit extending that work to consider the possibility of surfactant being present in the bulk. Note however that the work of Vitasari et al. [1], whilst retaining much of the essential physics of flow and mass transfer on foam films, involves a number of significant simplifications, and we will highlight these as we develop the model to be used here.

Sec. 4.2.1 identifies key dimensionless groups controlling the behaviour of the system under consideration. Here we utilise dimensionless groups previously identified by Vitasari et al. [1]. However, a newly introduced solubility parameter is a key parameter also employed in our model. Then, we look at the flow fields in Sec. 4.2.2. Since the physical mechanisms that drive the flow fields are Marangoni flow and film drainage, some background to these mechanisms is discussed in the supplementary material Secs. 5.1 and 5.2. Sec. 4.2.3 describes mass transfer equations on the foam film and within the bulk. Modelling of insoluble surfactant transport on the foam surface only is reviewed in supplementary Sec. 5.3. However, returning to the soluble case in Sec. 4.2.4, analysis of the small $\mathrm{Pe}\,\Delta$ limit, which is the main novel contribution of this study compared to previous studies, is presented. Sec. 4.2.5, meanwhile, consists of a new approach to obtaining a linear adsorption isotherm by modifying the Langmuir adsorption isotherm. In particular, we start with a Langmuir isotherm and make approximations, which we call respectively a global Henry isotherm and local Henry isotherm. This approach enables us to have the convenience of working with a linear isotherm, albeit one which is still a good representation of the original Langmuir isotherm over a concentration range of interest. Detailed explanations of these approx-

imations can be found in supplementary Sec. 5.4. Subsequently, Sec. 4.2.6 presents a new variable called "total amount of surfactant at any film location", which accounts for surface and bulk taken together at a specific position along the foam film. This then is the variable for which we solve. The solutions are ultimately obtained in terms of variables recast in dimensionless form, as described in supplementary Sec. 5.5 with a solution being obtained numerically via a method outlined in supplementary Sec. 5.6. Parameters to use within the solution are discussed in Secs. 5.7 and 5.8. Another key quantity that accounts for the overall amount of surfactant on the surface and within the bulk in a specific time has been introduced in Sec. 4.2.7: this quantity is measured over the entire film, not just at a specific location. Moreover, surfactant effective concentration is presented in Sec. 4.2.8, giving a measure of the extent to which adsorption enhances surfactant concentration over and above bulk liquid. This then leads within Sec. 4.2.9 into a discussion of surfactant recovery and enrichment during fractionation. Finally, Sec. 4.2.10 deals with the system's behaviour at late times, while the details of those late-time solutions can be found in supplementary Sec. 5.9.

4.2.1 Dimensionless groups

Here key dimensionless groups that appear in the model are presented. One of the parameters controlling the behaviour of the system is the Péclet number [220] which is obtained here based on comparing convective surfactant transport by the Marangoni effect to the diffusive transport of surfactant (see supplementary Sec. 5.1.1). In the present model, the Péclet number (Pe) is expressed as follows:

$$\mathrm{Pe} = \frac{\mathcal{G}\delta_0/\mu L}{\mathcal{D}/\delta_0} \tag{4.1}$$

where $\mathcal{G}$ is Gibbs elasticity parameter (surface tension change per change in logarithm of surfactant surface concentration), δ_0 is initial film half-thickness, μ is liquid viscosity, L is film half-length and $\mathcal{D}$ is diffusivity coefficient. Péclet number can be thought

of as being the ratio between characteristic velocity for Marangoni flow (along the film) and characteristic velocity for diffusion (across the film) and is typically a relatively large number (see Table 5.2). Meanwhile, the initial aspect ratio between film half-thickness and film half-length is defined as:

$$\Delta = \delta_0 / L \tag{4.2}$$

where δ_0 is initial film half-thickness, and L is film half-length. Here Δ is typically a very small number as the film is considered to be extremely thin. This small number then causes the product of Pe and Δ to be a relatively small number.

The other significant parameter is the solubility parameter which is defined as below:

$$\mathcal{S} = \frac{\delta_0}{\Gamma_{\mathrm{Pb}} / c_{\mathrm{Pb}}} \tag{4.3}$$

where δ_0 is initial film half-thickness, Γ_{Pb} is surfactant surface concentration at the Plateau border, and c_{Pb} is surfactant bulk concentration at the Plateau border. This is a key parameter for this work, describing the amount of dissolved surfactant relative to the amount of surfactant on the surface. This parameter is physically the film thickness relative to a depletion length associated with transferring surfactant between bulk and surface.

Insoluble surfactant has $\mathcal{S} \to 0$, whereas a highly soluble one has $\mathcal{S} \to \infty$. Note that for values of $\mathcal{S} \ll 1$, even though it is possible to compute the amount of surfactant in the interior of the film, there is so little surfactant in the interior compared to the surface that one might as well treat the surfactant as totally insoluble. By contrast, computing what is happening in the interior of the film is much more relevant for larger $\mathcal{S}$ values. For the parameters that we examine here, it turns out that $\mathcal{S}$ is an order of magnitude or so greater than unity (see Table 5.2).

As already alluded to, film drainage can also be relevant to the surfactant transport

process (see supplementary Sec. 5.2). Hence, we also define a dimensionless film drainage velocity parameter, denoted V_R. It is defined such that the typical ratio between drainage flow velocity [221] and Marangoni flow velocity is on the order of V_R. Here V_R is expressed as follows:

$$V_R = \frac{2\,\delta_0 \gamma_{\mathrm{Pb}}}{3\,a\mathcal{G}} \tag{4.4}$$

where δ_0 is the initial film's half-thickness, γ_{Pb} is surface tension at the Plateau border, a is the Plateau border's radius of curvature and $\mathcal{G}$ is Gibbs elasticity. This is usually a small parameter (see Table 5.2), suggesting that film drainage-driven surfactant transport is typically rather slower than Marangoni-driven surfactant transport. That said, in the case of soluble surfactant, it turns out that there are mechanisms by which Marangoni-driven transport can be slowed down also, so that in relative terms, film drainage-driven transport might become important even though V_R is small. This is a point to which we return later on. Remember also that the focus here is upon foam fractionation with reflux. Increasing the amount of reflux flowing through a fractionation column causes the Plateau borders to swell, increasing a and hence reducing V_R and thus reducing the impact that any film drainage has.

Having defined the dimensionless groups, we also make all system variables dimensionless. We scale horizontal coordinates by the film half-length and vertical coordinates using the film's initial half-thickness. Moreover, we scale surfactant concentrations in the bulk and on the surface by surfactant concentrations in the bulk of the Plateau border and on the surface of the Plateau border, respectively. Velocities along the film are also nondimensionalized using a Marangoni velocity scale. Time is nondimensionalized using the ratio between the film half-length and the Marangoni velocity scale. The full details of the nondimensionalization can be found in supplementary Sec. 5.5. In the dimensionless system, it turns out that the film half-length and the initial film half-thickness are set to unity, and surfactant concentrations in the bulk and

on the Plateau border surface are also set to unity. Note that from now on, we only use dimensionless variables unless specified otherwise.

4.2.2 Velocity fields

A review of the derivation of dimensional governing equations is explained in supplementary Sec. 5.3. However, here we present the equations in dimensionless form. The equations giving velocity fields in the x and z directions (the directions are as indicated in Fig. 4.1) are based on lubrication theory and turn out to be [1]:

$$u = -x\frac{\dot{\delta}}{\delta} + \left(\frac{\delta}{6} - \frac{z^2}{2\delta}\right)\frac{\partial \ln \Gamma}{\partial x} \tag{4.5}$$

$$w = z\frac{\dot{\delta}}{\delta} + \left(\frac{z^3}{6\delta} - \frac{z\delta}{6}\right)\frac{\partial^2 \ln \Gamma}{\partial x^2} \tag{4.6}$$

where u, w are dimensionless velocities in x, z directions. Also, $\dot{\delta}$ is dimensionless rate of change of film half-thickness, δ is dimensionless film half-thickness, and Γ is dimensionless surfactant surface concentration on the film. Note that w at $z = 0$ is zero, while at $z = \delta$, it equals $\dot{\delta}$.

Since Γ might have an a priori unknown variation with x, Eqs. (4.5) and (4.6) indicate that velocities are a priori unknown functions of position and time. Because we are dealing with surfactants that are being advected on the surface, we need to know about surface velocity. By setting $z = \delta$ in Eq. (4.5), we obtain an equation for surface velocity u_s as follows:

$$u_s = -x\frac{\dot{\delta}}{\delta} - \frac{\delta}{3}\left(\frac{\partial \ln \Gamma}{\partial x}\right). \tag{4.7}$$

To proceed we also need to know the value of δ at any given time t. The Reynolds drainage formula for a rigid surface [40] gives in dimensionless form:

$$\dot{\delta} = -V_R\,\delta^3 \tag{4.8}$$

where the respective solution for the film half-thickness is:

$$\delta = (1 + 2V_R t)^{-1/2}. \tag{4.9}$$

Note the considerable simplifications (see Secs. 5.2 and 5.3 for details) that have gone into all these equations. Foam films are not only assumed to be thin (so lubrication theory applies), but in addition their thickness is treated as being spatially uniform, albeit varying in time. In reality foam film thickness can vary spatially as the foam film drains [51, 222, 223]. However describing that process involves the complication that the film surface becomes curved, and a normal stress boundary condition relating pressure to surface tension and curvature is then required at the surface. Here instead we simplify as per Vitasari et al. [1] by retaining only tangential surface stresses (due to the Marangoni effect associated with gradients of surfactant surface concentration). We also assume as per Vitasari et al. [1] that the film drains as if it were a uniform thickness squeeze film.

Yet another simplification is that Eqs. (4.5) and (4.6) are two-dimensional equations (one dimension along the film, and one dimension across it). In reality flow is three-dimensional (two dimensions along the film and one dimension across it). The difficulty however is that the exact three-dimensional flow field that results depends on the film's shape, and specifically how many edges it has. Given that there will be considerable variation from film to film, not only in terms of film size, but also number of edges, we have for simplicity assumed a two-dimensional flow field here.

Having determined expressions for the velocity fields, we can now start to address the dimensionless mass transfer equations on and within the film surface.

4.2.3 Modelling of evolution of surfactant in a foam film

To investigate the evolution of surfactants, we use the dimensionless surfactant mass balance equations within the bulk and on the film surface. The dimensionless surfactant mass balance in the bulk follows a general mass transfer equation [220, 224, 225]:

$$\frac{\partial c}{\partial t} + \nabla.(\mathbf{u}\, c) = \frac{1}{\mathrm{Pe}} \nabla.(\kappa.\nabla c) \tag{4.10}$$

$$\kappa \equiv \begin{pmatrix} \Delta & 0 \\ 0 & \Delta^{-1} \end{pmatrix}$$

where c is dimensionless surfactant concentration in the bulk, t is dimensionless time, $\mathbf{u} = (u, w)$ is dimensionless velocity in the bulk in x and z directions and Δ is the initial aspect ratio. A dimensionless diffusivity tensor (κ) has appeared in the equation because of the nondimensionalization of the mass transfer equation using different characteristic lengths in x and z directions. Therefore, the coefficients of the diffusion terms in x and z directions are Δ/Pe and $1/(\mathrm{Pe}\,\Delta)$, respectively.

As Δ is typically an extremely small number (i.e. the film is assumed to be very thin) and Pe is a relatively large number (see Table 5.2), Δ/Pe is an extremely small number. This makes the diffusive flux in the x direction along the film negligible in all cases. Convection then dominates the mass transfer in that direction, and moreover since we have used a simplified flow field (as explained in Sec. 4.2.2), we have thereby simplified the convective mass flux. However, when $\mathrm{Pe}\,\Delta$ is a reasonably small number, the diffusive flux in the z direction across the film becomes significant. Thus, small $\mathrm{Pe}\,\Delta$ refers to the case in which there is a high diffusive flux across the thin film, even though the diffusive flux along it is negligible. This then is the case to be considered here, as will be discussed further in Sec. 4.2.4. The dimensionless mass transfer equation for

surfactant in the bulk can now be simplified as:

$$\frac{\partial c}{\partial t} + \frac{\partial (uc)}{\partial x} + \frac{\partial (wc)}{\partial z} = \frac{1}{\mathrm{Pe}\,\Delta} \frac{\partial^2 c}{\partial z^2}. \tag{4.11}$$

Here c varies in the x direction, but only very weakly in the z direction due to $\mathrm{Pe}\,\Delta$ being small.

As well as accounting for surfactant in the bulk, we also must account for surfactant on the surface. Thus, we write general dimensionless surfactant mass balance on the surface as follows [226, 227]:

$$\frac{\partial \Gamma}{\partial t} + \frac{\partial (u_s \Gamma)}{\partial x} = -\frac{\mathcal{S}}{\mathrm{Pe}\,\Delta} \left. \frac{\partial c}{\partial z} \right|_{z=\delta} \tag{4.12}$$

where Γ is dimensionless surfactant surface concentration, u_s is dimensionless velocity on the surface and $\mathcal{S}$ is the solubility parameter. Some previous works have ignored the term on the right hand side, which represents transport of surfactant from the surface into the bulk [1, 201, 216–218, 228]. Here however that term must be retained. Nonetheless, one effect which is ignored in the present study is surfactant surface diffusion [171]. The reason is that diffusion along the surface is generally much weaker than Marangoni flow on the surface.

It is clear from the form of Eq. (4.12) that we cannot in general solve for Γ unless we also solve Eq. (4.11), and we know specifically how c varies with both x and z. Here however, as already alluded to earlier, we make a simplifying assumption namely the small $\mathrm{Pe}\,\Delta$ limit, which allows us to progress the analysis even prior to solving for c. This is the subject of the next section.

4.2.4 Combining equations in the small $\mathrm{Pe}\,\Delta$ limit

Here we model the evolution of surfactants on and within the foam film making use of the small $\mathrm{Pe}\,\Delta$ assumption. To have a set of equations for the evolution of surfactant,

regardless of whether in the bulk or on the surface, we combine mass transfer equations for the bulk and surface together. To do this, we integrate Eq. (4.11) over z from 0 to δ, which results in:

$$\delta \frac{\partial c}{\partial t} + cw|_{z=\delta} + \frac{\partial}{\partial x}\left(c \int_0^\delta u \, \mathrm{d}z\right) = \frac{1}{\mathrm{Pe}\,\Delta} \frac{\partial c}{\partial z}\bigg|_{z=\delta}. \tag{4.13}$$

Notice here that in the final term on the left hand side, the term in c has been taken outside the integral sign. This is because as already mentioned, in the small $\mathrm{Pe}\,\Delta$ limit, the value of c tends to vary only weakly across the film thickness. As Sec. 4.2.2 discussed, and as can be obtained from Eq. (4.6), w at $z = 0$ is zero (because of the symmetry of the model), and w at $z = \delta$ is $\dot{\delta}$.

By combining two terms of the left-hand side of Eq. (4.13) and multiplying both sides of the equation by the $\mathcal{S}$ parameter, we obtain:

$$\frac{\partial}{\partial t}(c\,\mathcal{S}\delta) + \frac{\partial}{\partial x}\left(c\,\mathcal{S} \int_0^\delta u \, \mathrm{d}z\right) = \frac{\mathcal{S}}{\mathrm{Pe}\,\Delta} \frac{\partial c}{\partial z}\bigg|_{z=\delta}. \tag{4.14}$$

The term on the right-hand side of the equation is the diffusive flux from the surface to the bulk, which is the negative of the diffusive flux from the bulk to the surface as appears in Eq. (4.12). The combination of Eq. (4.12) and Eq. (4.14) leads to the following equation:

$$\frac{\partial}{\partial t}(\Gamma + c\,\mathcal{S}\delta) + \frac{\partial}{\partial x}\left(u_s\Gamma + c\,\mathcal{S} \int_0^\delta u \, \mathrm{d}z\right) = 0. \tag{4.15}$$

From Eq. (4.15), we can see that the rate of surfactant change in the bulk and on the surface is related to the convection flows, both in the bulk and on the surface. However, we can only progress if we can identify a relationship connecting Γ and c. This can be done with an adsorption isotherm, which is the subject of the next section.

4.2.5 Adsorption isotherms

So far, we have presented the evolution of surfactant in the form of a single equation (Eq. (4.15)). However, as this formula incorporates both Γ and c, we need an adsorption isotherm to link these two quantities together. Here we choose to express the isotherm in dimensionless form, which leads, as we will see shortly, to a rather simple relationship between these quantities Γ and c. The derivation of the original dimensional form and an explanation of how it is made dimensionless can be found in supplementary Secs. 5.4 and 5.5.

As Sec. 5.4 explains, we start with a nonlinear adsorption isotherm called the Langmuir isotherm. This is a commonly used adsorption isotherm, which describes the relationship between surfactant surface and bulk concentrations [93, 229, 230]. The Langmuir isotherm is characterized by a so-called Langmuir parameter that quantifies the affinity for the adsorption and also by a maximum amount of surface concentration or surface excess. It is however possible to simplify the nonlinear isotherm to a linear one as we now go on to explain.

4.2.5.1 Approximations to the isotherm

Significant simplifications will arise in the governing equations if we manage to replace the Langmuir isotherm with a straight line. To do this, we use two distinct approaches. First, we use a straight line to join the origin of a c, Γ plot (see Fig. 4.2) to the conditions c_{Pb} and Γ_{Pb} at the Plateau border. This we call a global Henry isotherm approximation. In the other approach, we construct a tangent to the Langmuir adsorption isotherm, again at the Plateau border conditions, which we call a local Henry approximation. The detail of how we did this and a schematic representation can be found in supplementary Sec. 5.4 and Fig. 4.2, respectively. Here as mentioned the approximate isotherms are to be used in a nondimensional form, such that c_{Pb} and Γ_{Pb} are in effect, both normalized

to unity. In this case, the global Henry isotherm in dimensionless form turns out to be:

$$\Gamma = c. \tag{4.16}$$

The local Henry isotherm is only slightly more complicated. We define a (dimensionless) local Henry constant ($K_{H(\mathrm{loc})}$) to be the slope of the (nondimensionalized) Langmuir adsorption isotherm at the point at which we construct the tangent, and it turns out to become:

$$K_{H(\mathrm{loc})} = \frac{1}{1 + K_L} \tag{4.17}$$

where K_L is a dimensionless Langmuir parameter (see supplementary Sec. 5.5 for how it is obtained). One of the features of a local Henry isotherm (evident in Fig. 4.2) is that even if we approach low concentrations, we have a minimum but still nonzero surface coverage. The minimum amount of surfactant surface concentration for a local Henry isotherm (Γ_{min}), in dimensionless form, becomes:

$$\Gamma_{\mathrm{min}} = \frac{K_L}{1 + K_L}. \tag{4.18}$$

Via Eqs. (4.17) and (4.18), the dimensionless local Henry isotherm becomes:

$$\Gamma = K_{H(\mathrm{loc})} c + \Gamma_{\mathrm{min}}. \tag{4.19}$$

Note that Γ_{min} is just $1 - K_{H(\mathrm{loc})}$.

The dimensionless Langmuir parameter K_L is what controls the value of $K_{H(\mathrm{loc})}$, and as can be seen from Eqs. (4.17) and (4.18), when it is small ($K_L \ll 1$), the local Henry constant ($K_{H(\mathrm{loc})}$) becomes almost unity, and the minimum amount of surfactant surface concentration (Γ_{min}) becomes negligible. Hence, according to Eqs. (4.16) and (4.19), local and global Henry isotherms would become almost identical. On the other hand, if K_L is large ($K_L \gg 1$), it follows that $K_{H(\mathrm{loc})}$ is small, whereas Γ_{min} is

close to unity. There is now quite some difference between the global and local Henry isotherms.

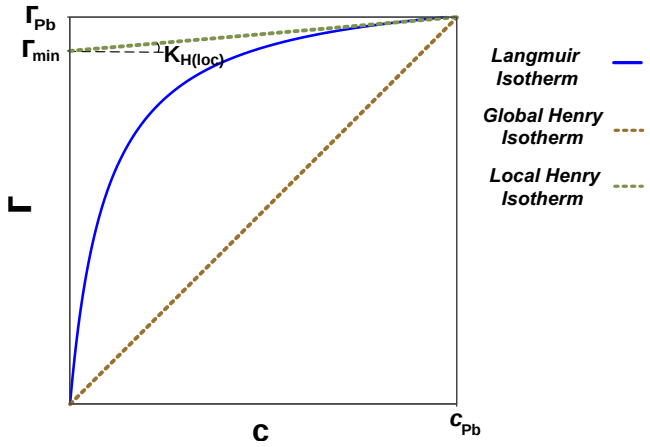

Figure 4.2: Schematic of dimensionless global and local Henry isotherms drawn for a specific Langmuir adsorption isotherm. In the dimensionless system c_{Pb}, Γ_{Pb} and the slope of the global Henry isotherm (in effect, the global Henry constant) are all unity. However, the slope of the local Henry isotherm (the local Henry constant) is smaller than unity.

4.2.5.2 Considering dimensional variables for isotherms

The above discussion has been formulated, as we have said, in terms of dimensionless variables, with c_{Pb} and Γ_{Pb} in effect normalized to unity. However, it is also useful to consider what it means in terms of dimensional variables (such as Sec. 5.4 considers). Using a fractionation process with reflux tends to ensure that the surfactant concentration of the Plateau border is richer than in a system without reflux. In that case, and given that the purpose of fractionation is after all, to concentrate surfactant, the (dimensional) c_{Pb} and Γ_{Pb} are pushed towards the higher surfactant concentration part of the Langmuir adsorption isotherm plot, where surfactant surface concentration no longer changes significantly with changes in bulk concentration. In this situation, provided the concentration c in the foam film is not too far away from c_{Pb}, then the tangent to the Langmuir isotherm at the Plateau border concentration or, in other words, the so-called local Henry isotherm describes the system's behaviour realistically (see e.g. Fig. 5.1). On the other hand, a relatively dilute system could be considered, such that the surfactant concentration in the Plateau border is not exceedingly rich even in spite

of reflux. In that case the (dimensional) c_{Pb} and Γ_{Pb} are pushed towards the lower surfactant concentration part of the Langmuir adsorption isotherm plot, where the slope of the isotherm is now rather larger. This incidentally tends to increase surfactant depletion length, which would decrease the value of $\mathcal{S}$ defined via Eq. (4.3). However, the relevant point here is that the Langmuir isotherm, global Henry isotherm and local Henry isotherm are all then rather similar, so the global Henry isotherm (which mathematically speaking is a little simpler than the others) would provide an acceptable approximation.

To summarize we have defined so-called global and local Henry isotherms which, at least in certain parameter domains, are reasonable approximations to an overarching Langmuir isotherm. Although we could formulate a surfactant transport model utilising a Langmuir isotherm directly, we elect here to work with the global and local Henry isotherms instead. This is convenient as we will see, because it leads to a governing equation that is linear. Indeed in certain cases, i.e. without film drainage, we will see that it is even possible to obtain exact analytical solutions, in the form of series expansions. In any case, now that we have defined the link between the amount of surfactant on the surface and in the bulk and, we proceed to look at the total amount of surfactant (surface and bulk taken together) and how it evolves.

4.2.6 Determining total amount of surfactant at any film location

When a fractionation system is used to recover surfactant, the distribution of surfactant between surface and bulk within the foam film is less significant than the total amount of recovered surfactant and how much the foamate is enriched. To begin to address this, we define a variable (Γ_{tot}), which is the total amount of surfactant present at any location in the film (or strictly speaking half the total amount at that location, because we consider just half of the thickness here). This can be expressed formally as:

$$\Gamma_{\mathrm{tot}} = \Gamma + \mathcal{S} \int_0^{\delta} c \, \mathrm{d}z \tag{4.20}$$

where Γ is dimensionless surfactant surface concentration, c is dimensionless bulk concentration, $\mathcal{S}$ is dimensionless solubility parameter and δ is dimensionless film thickness.

For the small $\mathrm{Pe}\,\Delta$ limit, such that surfactants in the bulk are evenly distributed across the film, Eq. (4.20) can be simplified as:

$$\Gamma_{\mathrm{tot}} = \Gamma + \mathcal{S}\,\delta\,c, \tag{4.21}$$

an approximation already used in Eq. (4.15). Note that only if we consider insoluble surfactant ($\mathcal{S} \to 0$), does the value of Γ_{tot} become almost equal to the amount of surfactant on the surface ($\Gamma_{\mathrm{tot}} \approx \Gamma$). For any other $\mathcal{S} > 0$, the values of Γ_{tot} and Γ differ. We can however, eliminate Γ and c from Eq. (4.15) in favour of Γ_{tot}, making use of the earlier defined adsorption isotherms.

Moreover, once the value of Γ_{tot} is known, it can be broken down into its separate components associated with Γ and c. To show how to do this, we use the local Henry isotherm (Eq. (4.19)) to derive the relevant equations. This is done because equations can be easily transformed to those for the global Henry isotherm if required, merely by setting $K_{H(\mathrm{loc})} = 1$ and $\Gamma_{\mathrm{min}} = 0$. Via Eqs. (4.19) and (4.21), we obtain:

$$\Gamma = \left(\Gamma_{\mathrm{tot}} + \frac{\Gamma_{\mathrm{min}}\mathcal{S}\delta}{K_{H(\mathrm{loc})}}\right)\left(1 + \frac{\mathcal{S}\delta}{K_{H(\mathrm{loc})}}\right)^{-1} \tag{4.22}$$

$$c = \frac{(\Gamma_{\mathrm{tot}} - \Gamma_{\mathrm{min}})}{K_{H(\mathrm{loc})}}\left(1 + \frac{\mathcal{S}\delta}{K_{H(\mathrm{loc})}}\right)^{-1}. \tag{4.23}$$

The combination of Eqs. (4.15), (4.22) and (4.23), using also Eqs. (4.5) and (4.7) gives, after some algebra, the equation for the evolution of Γ_{tot} which becomes:

$$\frac{\partial\Gamma_{\mathrm{tot}}}{\partial t} = \left(1 + \frac{\mathcal{S}\delta}{K_{H(\mathrm{loc})}}\right)^{-1}\left(\frac{\delta}{3}\right)\frac{\partial^2\Gamma_{\mathrm{tot}}}{\partial x^2} + \frac{\dot{\delta}}{\delta}\left(x\frac{\partial\Gamma_{\mathrm{tot}}}{\partial x} + \Gamma_{\mathrm{tot}}\right). \tag{4.24}$$

Eq. (4.24) is a parabolic partial differential equation. Despite being linear, it is not

always possible to solve analytically, given that coefficients depend on x and also implicitly on t, remembering here that δ varies with time, at least when the film is draining. As a result, a method of solving this equation numerically has been applied, specifically a "spectral method" [231]. In this method, the solution of the equation is expressed as a finite expansion of some set of basis functions: we employed a Fourier series. Details of the numerical procedure are found in supplementary Sec. 5.6. When the film is not draining at all, so that $\delta \equiv 1$ and $\dot{\delta} \equiv 0$, the situation is simpler still: each term in the Fourier series expansion then decouples and evolves independently of the others. A separation of variables solution then results, and so in effect, an exact analytical solution is obtained. This situation applies regardless of whether we employ a global or local isotherm, although the rate of evolution for each Fourier term is influenced by the choice of isotherm.

We also require initial and boundary conditions. We know that before the foam fractionation process starts, there is an initial total amount of surfactant on the film surface and in the film bulk which we denote $\Gamma_{\mathrm{tot},0}$ and which is assumed to be uniform with x. Specifically $\Gamma_{\mathrm{tot},0}$ is selected to reflect that there is less surfactant in the film initially compared to the corresponding amount in the Plateau border, remembering here that the Plateau border has been enriched by reflux. This difference between film and Plateau border provides (via the Marangoni effect) the main driving force for surfactant transport from the relatively surfactant rich Plateau border towards the relatively surfactant lean film. Note that given the value of $\Gamma_{\mathrm{tot},0}$, we can use Eqs. (4.22) and (4.23) to determine the corresponding initial surface concentration Γ_0 and initial bulk concentration c_0. Alternatively we can use Eq. (4.21) to recover $\Gamma_{\mathrm{tot},0}$ for given Γ_0 and c_0. Remember that within all these equations, the value of δ is unity initially (see Eq. (4.9)).

The boundary condition of the model at $x = 0$ is $\mathrm{d}\Gamma_{\mathrm{tot}}/\mathrm{d}x|_{x=0} = 0$, which is due to the symmetry at the centre of the film. We also need a boundary condition at $x = 1$ where

the film meets the Plateau border. The challenges of imposing a boundary condition at this particular point have been discussed by Ruschak [232, 233]: even though flow in the film is a lubrication flow with near parallel streamlines, flow in the Plateau border meniscus itself is generally two-dimensional. Here in the interests of simplicity, we impose $\Gamma_{\mathrm{tot}}|_{x=1} = \Gamma_{\mathrm{tot,Pb}}$, where as already mentioned in Sec. 4.2.5.1, we assume throughout that the dimensionless c_{Pb} and Γ_{Pb} are fixed at unity. In other words, the Plateau border is treated as a reservoir of surfactant [1]. The basis for this assumption however is that there might be rather more liquid in Plateau borders than in films, at least when films are thin: surfactant exchange from Plateau border to film is assumed to affect concentrations in the film, but has little impact on concentrations within the bulk of the border. A consequence of this though is that $\Gamma_{\mathrm{tot,Pb}}$, i.e. the total amount of surfactant at the location at which Plateau borders connect with films is actually weakly time-dependent if films gradually become thinner over time. Specifically it follows from Eq. (4.21) that $\Gamma_{\mathrm{tot,Pb}} = (1 + \mathcal{S}\,\delta)$ where δ is given via Eq. (4.9).

4.2.7 Determining overall amount of surfactant at any time

In order to assess the fractionation process performance, we need to calculate the overall amount of surfactant throughout the film (surface plus bulk) at each time. This is obtained by integrating Γ_{tot} over the film half-length (which is unity in our dimensionless system). Thus

$$\Gamma_{\mathrm{ove}} = \int_0^1 \Gamma_{\mathrm{tot}}\,\mathrm{d}x. \tag{4.25}$$

In what follows, we call Γ_{ove} the overall amount of surfactant, although strictly speaking it is the overall amount within a film half-length and half-thickness.

This quantity depends on time and hence upon the duration for which the film and Plateau border are in contact as reflux proceeds. This duration is dependent on process parameters, such as fractionation column length and velocity of bubbles through it [61]. Thus, calculating Γ_{ove} as a function of time can help to design or operate a more

efficient fractionation column. Note that later on, we also compare the ratio between the overall amount of surfactant at each time and the overall amount of surfactant at the initial time, and we denote this $\Gamma_{\mathrm{ove}}/\Gamma_{\mathrm{ove},0}$. This measures the extent to which the surfactant recovered in the film is increased by contacting the film with a surfactant rich Plateau border. Note that because of the way we select the initial condition and also the way we normalize length in the dimensionless system, the value of $\Gamma_{\mathrm{ove},0}$ is actually the same as $\Gamma_{\mathrm{tot},0}$.

4.2.8 Determining effective concentration at any time

Another parameter that helps us evaluate foam fractionation performance is a so-called surfactant effective concentration (c_{eff}). This quantity tells us how rich the foamate is at any instant. It can be expressed as the overall amount of surfactant on the surface and in the bulk at a specific instant, divided by the volume of the film. As we are dealing with a two-dimensional system with film half-length equal to unity, the volume can be just expressed in terms of the film half-thickness (δ). This leads to

$$c_{\mathrm{eff}} = \int_0^1 \Gamma_{\mathrm{tot}}/(\mathcal{S}\,\delta)\,\mathrm{d}x \equiv \Gamma_{\mathrm{ove}}/(\mathcal{S}\,\delta). \tag{4.26}$$

Note that according to Eq. (4.21), the value of effective concentration c_{eff} only matches the bulk concentration within the film in the limit when $\mathcal{S}\,\delta \gg 1$, i.e. for soluble surfactants and films that are not too thin. Otherwise c_{eff} exceeds the bulk concentration.

4.2.9 Recovery and enrichment

Using the definitions in Secs. 4.2.7 and 4.2.8 we can proceed to determine recovery and enrichment which are quantities often used to assess fractionation performance [36, 44, 82, 108]. In this study, enrichment is defined as the ratio between the effective concentration of the foamate at each instant relative to the initial feed bulk concentration (c_{eff}/c_0). Recovery on the other hand is taken to be measured just by the value

of Γ_{ove}, which specifically is the overall amount of surfactant recovered per film (or strictly speaking, per half-film length and half-film thickness). This differs from a conventional definition of recovery which would be the overall amount of surfactant recovered in the foamate relative to the overall amount fed to the fractionation column [36, 44, 83]. Clearly, if we know the overall amount of surfactant recovered per film and also the number of foam films that enter the foamate, then we have a measure of the amount of surfactant recovered, which can be compared with the amount originally in the feed. Hence recovery per film Γ_{ove} is proportional to the conventional definition of recovery, but it can be defined conveniently in the current model without needing to specify either the total number of foam films recovered or the overall quantity of surfactant in the feed. To summarize, in this work Γ_{ove} represents recovery and c_{eff}/c_0 represents enrichment. As we will see later on, generally, there is a competition between recovery and enrichment (see Sec. 4.4.8), with high solubility parameter $\mathcal{S}$ favouring recovery and low solubility parameter $\mathcal{S}$ favouring enrichment.

Values of Γ_{tot}, Γ_{ove} and c_{eff}, as well as enrichment and recovery which derive from them, evolve with time and can approach a final state in the limit of very long times. This could either be a final steady state in the absence of film drainage, with an equilibrium between the Plateau border and film, or if there was film drainage, a quasisteady-state balance could be reached, as we discuss next.

4.2.10 Late time behaviour of the system under consideration

Recall that in Vitasari et al. [1], the Marangoni flow is found to be the dominant contribution to the flow field at short times. However, at longer times, Marangoni tends to decay, such that a balance between Marangoni flow and film drainage flow then occurs, which leads the system into a quasisteady-state situation. Note that strictly speaking, this is indeed a quasisteady state rather than a true steady state, since the surfactant surface concentration continues to evolve, albeit slowly, even after Marangoni and film drainage flow balance. The difference in the present study is that surfactants are present

in the bulk too. As a result, not only does the Marangoni-driven surface flow turn out to have slower impact on the surfactant surface concentration owing to surfactant escaping into the bulk (see Sec. 4.4.1 and later sections), but also film drainage removes liquid and hence surfactants from the bulk as drainage proceeds. Thus, although there is still an eventual balance between Marangoni flow and film drainage, this will happen at longer times compared to the insoluble surfactant case [1], and will also be further from equilibrating with the Plateau border (i.e. further from the state reached in the absence of film drainage). Note also that investigating the quasisteady state is primarily of interest in the case of the global Henry isotherm. This is because (as we will see later on, see Sec. 4.4.3 onwards) in the local Henry isotherm case, the impact of the Marangoni effect upon surfactant transport is slowed down even more significantly than in the global Henry isotherm case. Hence, for a local Henry isotherm, a balance between Marangoni flow and film drainage flow would likely only be realized at times much later than a typical residence time in a foam fractionation process. The following analysis focusses therefore on the global Henry case.

Note that thus far we have focussed primarily upon a partial differential equation for Γ_{tot} (see Eq. (4.24)). Nonetheless using Eqs. (4.22) and (4.23) it is also possible to obtain analogous equations for Γ and c. If we are searching for a quasisteady state, it is easier to work in terms of Γ not Γ_{tot}. This is because the boundary conditions for Γ are time-independent even with film drainage, whereas those for Γ_{tot} are not. Specifically for Γ we find, still using the global Henry isotherm,

$$\frac{\partial \Gamma}{\partial t} = (1+\mathcal{S}\delta)^{-1}\left(\frac{\dot{\delta}}{\delta}\Gamma + \left(\frac{\delta}{3}\right)\frac{\partial^2 \Gamma}{\partial x^2}\right) + \frac{\dot{\delta}}{\delta}\left(x\frac{\partial \Gamma}{\partial x}\right). \tag{4.27}$$

Here Eq. (4.27) is the general unsteady equation for the evolution of Γ. It is necessary to explore whether or not this equation approaches a quasisteady state at a sufficiently long time. A description of the approximate analytical solution of Eq. (4.27) at late times can be found in supplementary Sec. 5.9. In addition, further discussion and a

comparison between analytical and numerical solutions are presented in Sec. 4.4.5.

This completes setting up the model in the small $\mathrm{Pe}\,\Delta$ limit. After deriving the equations for the evolution of Γ_{tot} (or equivalently Γ or c), we need to use simulations to calculate Γ_{tot} (or equivalently Γ or c) at every film position and every instant. These simulations are described next.

4.3 Simulation and benchmarking

Parameters corresponding to sodium dodecyl sulphate (SDS) have been used for simulation purposes within this study. SDS is one of the most studied anionic surfactants, and hence, relevant parameters are readily available in the literature [165, 203, 234–249]. The origin of some of the important parameters used in our simulation and the related tables can be found in supplementary Sec. 5.7.

Recall from Sec. 4.2.6 that a spectral method has been used to solve Eq. (4.24). Full details of the method are given in Sec. 5.6. In our simulation, 38 Fourier terms have been used. Having generated the Fourier series, we can reconstruct the spatial variation of the solution from the Fourier series. To do this, we have evaluated at 500 spatial points throughout the film half-length. For the most part, 38 Fourier terms evaluated at 500 spatial points capture the surfactant distribution adequately, except for very slowly evolving systems at very early times (see e.g. Fig. 4.6 later on). Moreover, we have typically solved out to 20 dimensionless time units for the process duration divided into time steps of 0.001 dimensionless units. Time stepping is done via the fourth order Runge-Kutta method [250]. Note that based on the parameters we have chosen, each time unit is equivalent to $0.125\,\mathrm{s}$ (see Table 5.1) thereby considering surfactant transport processes taking on the order of seconds. Note however that in certain cases (e.g. in Figs. 4.5 and 4.11 and also in Secs. 4.4.5, 4.4.6 and 4.4.8), more than 20 time units have been considered to enable us to investigate the system's behaviour for somewhat longer times.

To benchmark our numerical method, we have compared our simulation with an alternative method called the "material point" method, which had previously been used for the evolution of Γ in an insoluble case [1]. As a result, this particular comparison has been made for the case in which the solubility parameter ($\mathcal{S}$) is set to zero. These two numerical methods yielded almost the same results for Γ with a maximum relative difference of 3×10^{-5}. Details of the material point method can be found elsewhere [1].

We have carried out another benchmark using two analytical solutions for the case without film drainage: note that obtaining these analytical solutions relies on having a linear isotherm (either a global Henry isotherm or a local Henry isotherm, but not the Langmuir isotherm which is nonlinear). Neglecting film drainage simplifies Eq. (4.24) and enables us to solve it analytically. The analytical solutions involve a complementary error function (erfc) approach or else (as mentioned in Sec. 4.2.6) a separation of variables solution approach, which results in a Fourier series solution. Both approaches are valid, but the complementary error function tends to be more convenient to use at early times, whereas the Fourier series is more convenient at later times. Details of these analytical solutions can be found in Vitasari et al. [1]. Further discussion of solutions in the absence of film drainage can also be found in Sec. 4.4, e.g. Secs. 4.4.1 and 4.4.3.

Yet another benchmark used a case in which Marangoni flow has been switched off, but film drainage could still occur. This means that there is no mechanism driving surfactant transfer from the Plateau border toward the centre of the film. However, the transfer of surfactants from the film to the Plateau border still happens due to film drainage. This turns out to lead to an analytical solution, in which Γ_{tot} is directly proportional to δ, as can be easily verified from Eq. (4.24) upon dropping the Marangoni term. Comparing the spectral method with the analytical solution in the so-called "no Marangoni" case has confirmed the consistency of the method once again.

Having thereby benchmarked the spectral method solution, we now consider the results that it predicts, including in cases which cannot be readily solved analytically.

4.4 Results

In this section, simulations for the evolution of the total amount (Γ_{tot}) of soluble surfactant have been carried out. As already alluded to, dimensional parameters for the system, assuming the surfactant is sodium dodecyl sulphate (SDS), are presented in supplementary Sec. 5.7 and Table 5.1. Dimensionless parameters are then reported in Table 5.2. The solubility parameter ($\mathcal{S}$, see Sec. 4.2.1) turns out to be 8.696, the local Henry constant ($K_{H(\mathrm{loc})}$, see Sec. 4.2.5.1) is 8.77×10^{-2}, and the film drainage velocity parameter (V_R, see Sec. 4.2.1) turns out to be 0.0063. The global Henry constant is unity by definition. Other dimensionless parameters obtained for the system are also presented in Table 5.2 including a check that the parameter $\mathrm{Pe}\,\Delta$ really is smaller than unity.

To compare analogous conditions for different adsorption isotherms, we set the initial bulk concentration equal to half of the Plateau border's bulk concentration ($c_0 = 0.5$) as the reference concentration. Therefore, Γ_0 is calculated to be 0.5 and 0.9561 for the global and the local Henry isotherms, respectively (Eqs. (4.16) and (4.19) and also Sec. 5.8). In the local Henry isotherm case, note that Γ_0 is already quite close to unity, which has implications that we discuss later on. Regardless of whether we consider a global or local Henry isotherm case, once we know Γ_0 and c_0, we now proceed to calculate the evolution of Γ_{tot}. The evolution of Γ and c can also be calculated using Eqs. (4.22) and (4.23).

We begin this section by presenting the results for the case of the global Henry isotherm in the absence of film drainage in Sec. 4.4.1. Then, we discuss the global Henry isotherm case in the presence of film drainage in Sec. 4.4.2. After that, we consider the local Henry isotherm, first without film drainage and then with film drainage in

Secs. 4.4.3 and 4.4.4, respectively. An approximation to a quasisteady-state situation is also presented in Sec. 4.4.5. Details of how the quasisteady-state equations have been derived can be found in supplementary Sec. 5.9. Then, in Sec. 4.4.6, we quantify the overall amount of surfactant in the film at any instant as well as the effective concentration, and compare the various soluble surfactant cases and the insoluble ones, with and without film drainage. Moreover, we investigate the effect of varying the solubility parameter upon the foam fractionation process: the results of this particular parametric study are found in Sec. 4.4.7. Finally, the performance of the fractionation column in terms of recovery and enrichment has been investigated and compared for different cases in Sec. 4.4.8.

4.4.1 Global Henry isotherm, no film drainage

We first neglect film drainage in the interests of simplicity, while also using the global Henry isotherm. It is reasonable to neglect film drainage as a first approximation, because the V_R parameter is generally small. For the present case, within Eq. (4.24) we can set $\delta = 1$, $\dot{\delta} = 0$ and we replace $K_{H(\mathrm{loc})}$ by unity, which simplifies Eq. (4.24) considerably. Results are plotted in Fig. 4.3.

Even though in this case Marangoni-driven transport is occurring along the film, it is accompanied by diffusion taking place across the film. Thus surfactant effectively escapes from the surface into the bulk of the film, and so does not accumulate quite so rapidly on the surface itself. Hence, compared to the insoluble surfactant case that has been presented by Vitasari et al. [1], the rate of evolution of Γ_{tot} is slowed down by a $1 + \mathcal{S}$ factor which is significantly greater than unity. This is as expected because the extent of the slow down depends upon how much surfactant enters the bulk, which in turn depends on solubility.

Note that the value of Γ_{tot} at the edge of the film where it adjoins the Plateau border remains constant in this particular system without film drainage. The constant value

is in fact just $1 + \mathcal{S}$, and so is higher for a more soluble surfactant. The system also reaches a spatially uniform concentration Γ_{tot} at very long times, equilibrating with the Plateau border. However, the time scale to reach this uniform concentration is much longer than in the insoluble case considered by Vitasari et al. [1]. When surfactant is soluble as in Fig. 4.3, even at 20 time units some nonuniformities are still evident, and equilibrium is still not reached.

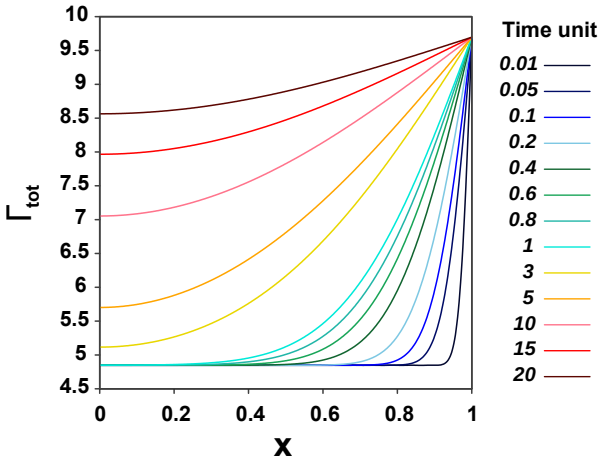

Figure 4.3: Γ_{tot} evolution, calculated for the no film drainage case using a global Henry isotherm.

This completes discussion of the case with a global Henry isotherm without film drainage. In what follows, we still consider the global Henry isotherm, but now, in the presence of the film drainage.

4.4.2 Global Henry isotherm, with film drainage

When film drainage is happening along with Marangoni flow, the surfactant transport process (see Fig. 4.4a) can be split into three stages of time. In the first stage at early time, there is a large concentration gradient near the boundary but no concentration gradient at the centre. Therefore, there is a strong Marangoni flow near the boundary which dominates the film drainage by a large amount. However, as there is still no Marangoni flow near the centre of the film, the effect of even comparatively weak film drainage can decrease slightly the value of Γ_{tot} in this zone (Fig. 4.4a). It is noted

further that, unlike the case considered in Sec. 4.4.1, there is now also continuous reduction in Γ_{tot} at the Plateau border. This is just associated with the thinning process (Eqs. (4.9) and (4.21) with Γ and c both unity at the Plateau border).

During the second stage occurring at intermediate times, the surfactant concentration gradient has now reached the centre of the film. The time scale needed for this to occur is however longer in the case of soluble surfactant than it is for insoluble surfactant (contrast Fig. 4.4a and Fig. 4.4b): the reasons for this slower evolution in the soluble case have already been discussed in Sec. 4.4.1. During this second stage, the Marangoni flow driving surfactant onto the film is the dominant effect. This follows because there is still a significant difference between surface tension at the centre of the film and surface tension at the Plateau border, owing to the difference between the amount of surfactant in these zones. The film drainage, whilst present, is weaker than the Marangoni flow because of the slow film thinning rate.

In the third and final stage at later times, as the difference between concentrations along the surface becomes less and the Marangoni flow decays, film drainage is now comparable to the Marangoni flow but acts in the opposite direction. This situation might lead to a quasisteady state, to be discussed further in Sec. 4.4.5.

Particularly during this third stage, it is interesting to compare the soluble surfactant case in Fig. 4.4a with the insoluble case in Fig. 4.4b. When surfactant is insoluble, the amount at any spatial location always appears to increase with time as Fig. 4.4b shows. As has already been mentioned above, in the soluble case however, this is not the case, as can be seen in Fig. 4.4a particularly when focussing on the region close to the Plateau border. At later times, because a significant amount of surfactant has transferred from the film surface to the film bulk, and because the film is itself draining, surfactant can actually be lost from the film.

Indeed the overall amount of surfactant in the film (Γ_{ove}) (see Sec. 4.4.6 for details) might start to decrease if the process continues for long enough. This would happen

regardless of the amount of surfactant actually on the surface Γ, which always increases (see Fig. 4.5). Solubility might therefore actually have an adverse effect on overall surfactant recovered via foam fractionation if the film is draining and the process is left to run for too long in time, a point to which we return in Sec. 4.4.8.

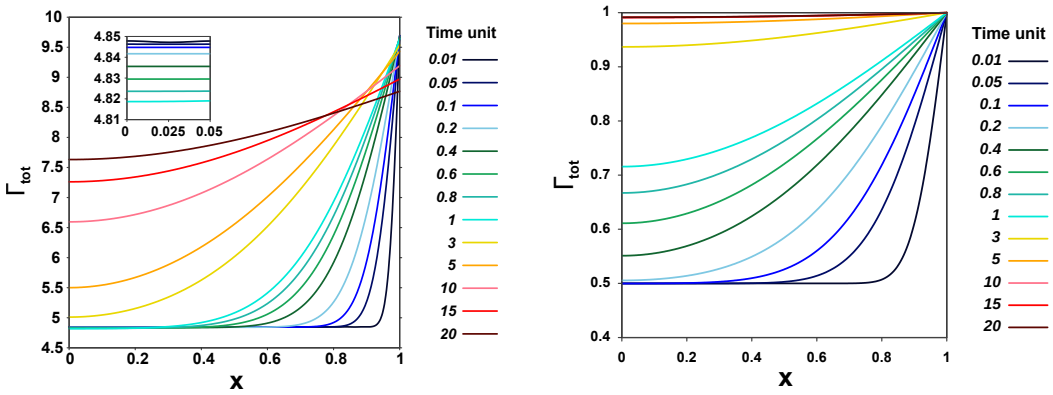

(a) Soluble surfactant **(b)** Insoluble surfactant

Figure 4.4: Γ_{tot} evolution, calculated for the soluble and insoluble surfactant cases using a global Henry isotherm.

Detail of what is happening to surfactant concentration Γ on the surface can be seen in Fig. 4.5. The advantage of plotting Γ instead of Γ_{tot} is that, even with film drainage present, the value of Γ at the Plateau border does not depend on time. Hence an easier comparison between cases with and without film drainage can be performed. It is clear that in the presence of film drainage, the value of Γ is slightly lower than in the absence of film drainage. Moreover, in the case with film drainage, slight nonuniformities persist in Γ even at very late times: Fig. 4.5 extends up to 100 time units rather than just 20 units as in Fig. 4.4. Late time behaviour of the system is discussed further in Sec. 4.4.5.

This completes for now our analysis of the global Henry isotherm case. In what follows we switch to the local Henry isotherm, without film drainage in the first instance.

4.4.3 Local Henry isotherm, no film drainage

In the local Henry isotherm case (Eq. (4.19)), Γ_{min} is not zero, and the initial amount of Γ (denoted Γ_0) for a given c_0 is rather higher than for the global Henry isotherm.

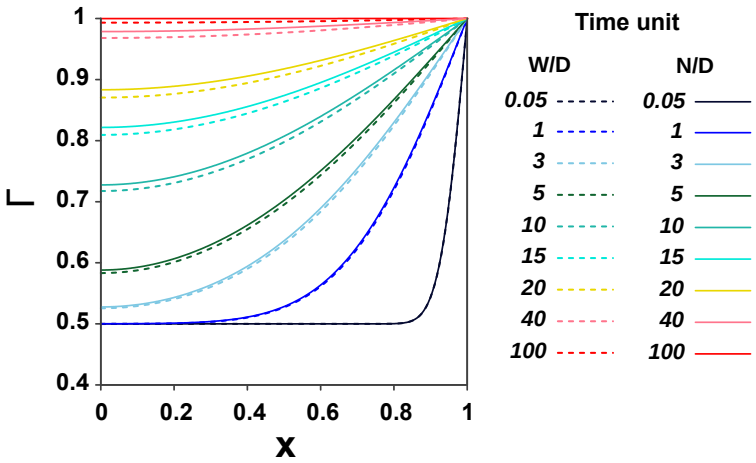

Figure 4.5: Γ evolution, calculated with film drainage (W/D) and with no film drainage (N/D) using a global Henry isotherm.

As a result, Γ_{tot} in the local Henry isotherm case starts initially from a slightly higher amount than for the global Henry isotherm. In addition, in our simulation, the local Henry constant ($K_{H(\text{loc})}$) is determined to be 8.77×10^{-2}, a relatively small number (see Table 5.2). This makes the surfactant concentration gradient on the surface and hence the Marangoni term much smaller than in the global Henry isotherm case. In the global Henry isotherm case, and without film drainage, the evolution has been slowed down by a $1+\mathcal{S}$ factor because of the solubility. However, in the local Henry isotherm case, it is slowed down by a $1 + \mathcal{S}/K_{H(\text{loc})}$ factor (see Eq. (4.24)), which is a much more significant slow down. The issue is that there is now very little capacity to store additional surfactant on the surface, because Γ itself is already relatively high. Hence most of surfactant that is gained contributes to increasing the concentration c within the bulk of the film. Due to this very slow evolution, we see apparent oscillation at early times within Fig. 4.6. However, this is an artifact of using a limited number of Fourier components. Strictly speaking we need more Fourier components at those early times [251–253], but the oscillations soon decay away.

As can be seen in Fig. 4.6 (by contrast with Fig. 4.3), the local Henry isotherm starts from a slightly higher initial Γ_{tot} than the global Henry isotherm does. This is owing to having a higher Γ_0. However the main effect here is that the rate of increase of Γ_{tot}

is much slower than for the global Henry isotherm. Therefore, even after 20 time units, the Marangoni-driven surfactant transport has only just barely managed to reach the centre of the film.

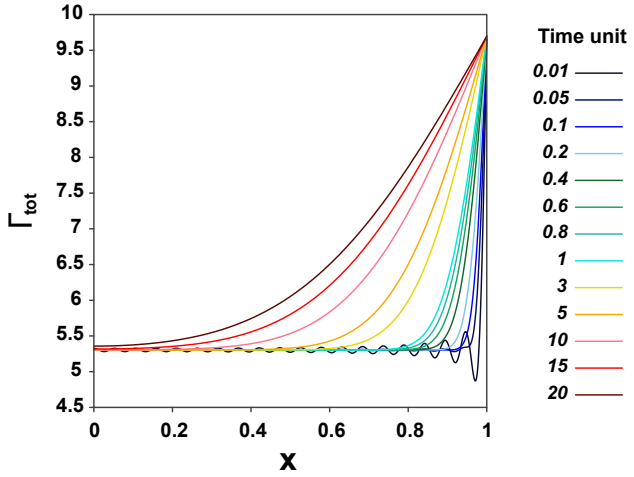

Figure 4.6: Γ_{tot} evolution, calculated for the no film drainage case using local Henry isotherm.

4.4.4 Local Henry isotherm, with film drainage

Now, we consider the case of a local Henry isotherm in the presence of film drainage. In this case, again, having a small local Henry constant slows down the Marangoni flow. Apparent oscillations (which are numerical artifacts due to having a fixed number of Fourier terms) can again occur in this particular system, but to avoid them we simply started plotting from slightly later times. At the centre of the film, we can now see a reduction over time in Γ_{tot} due to film drainage. This reduction is now much more significant than in Fig. 4.4a, which was obtained for a global Henry isotherm. The fact that a reduction might be seen suggests it may be important to manage carefully the foam film residence time in order to optimize the surfactant recovered, a point we return to discuss in Secs. 4.4.6 and 4.4.8. Another possibility to consider to mitigate this is increasing the reflux flow through the system, which (see Sec. 4.2.1) thickens the Plateau borders and so can reduce the parameter V_R and hence the film drainage rate.

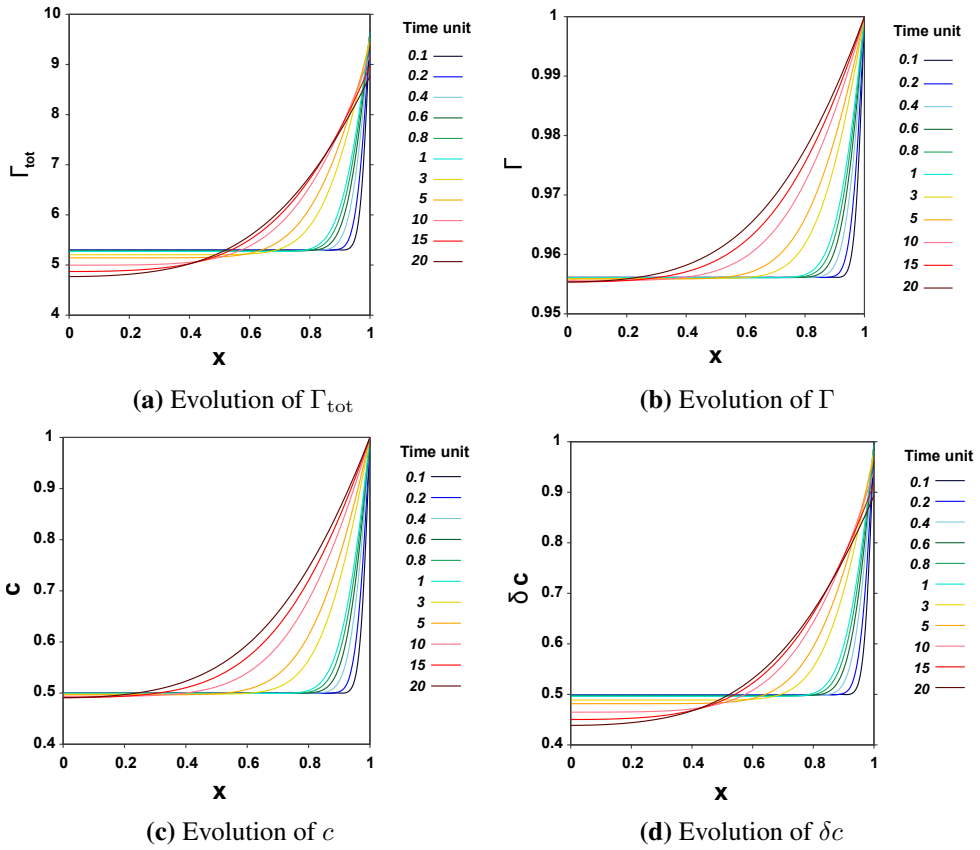

(a) Evolution of Γ_{tot} **(b)** Evolution of Γ

(c) Evolution of c **(d)** Evolution of δc

Figure 4.7: Evolution of Γ_{tot}, Γ, c and $\delta\, c$, calculated for the case with film drainage, and using a local Henry isotherm.

The value of Γ_{tot} is comprised (see Eq. (4.21)) of surfactant on the surface Γ plus surfactant in the bulk $\mathcal{S}\,\delta\, c$, where recall $\mathcal{S}$ is given within Table 5.2 and the evolution of δ is given by Eq. (4.9). To understand these separate contributions to Γ_{tot}, the evolution of Γ, c and $\delta\, c$ are shown in Figs. 4.7b to 4.7d. It can be seen in Fig. 4.7b that the Γ values are always relatively high (i.e. close to unity), as the surface already has a significant amount of surfactant since the initial time. Over time, there is a slight Marangoni-driven increase in Γ at positions neighbouring the Plateau border, remembering here that the value of Γ at the Plateau border itself is fixed. On the other hand, there is a slight decrease in Γ close to the centre of the film owing to film drainage.

Meanwhile, it can be seen in Fig. 4.7c, that changes in c are proportional to the changes in Γ. However, the range of c values encountered (from just less than 0.5 up to 1) is

much larger than the range of Γ. However, we can see in Fig. 4.7d that it is δc which mirrors most closely the value of Γ_{tot}. This reveals that the evolution of Γ_{tot}, obtained from Eq. (4.21), is significantly affected by both surfactant concentration in the bulk and by film drainage.

To date we have analysed numerically the behaviour of surfactant on and within foam films up to some finite time. However it is also of interest to know how the system behaves in the limit of long times. Specifically, we want to obtain an approximate analytical solution for late times. This is the subject of the next section.

4.4.5 Quasisteady-state approximation for soluble surfactant

Here we discuss the expected long-time behaviour of the system, and compare it with the numerical results of the spectral method. The case without film drainage is simple because the film equilibrates with the Plateau border. Hence the case we consider here (as already alluded to in Sec. 4.2.10) is the one with film drainage.

The late-time behaviour for insoluble surfactant with film drainage has previously been discussed by Vitasari et al. [1]. In that study, it is explained that there is a quasisteady-state balance between Marangoni flow and film drainage terms at late times. A similar analysis can be carried out for a case with soluble surfactant (full details are in Sec. 5.9). A complication is that (as we have already seen) soluble surfactant slows down the evolution of the Marangoni term, and hence delays the process of Marangoni and film drainage coming into balance. Under these circumstances (as already explained in Sec. 4.2.10), we choose to consider the global Henry isotherm case. In the local Henry isotherm case, as we have likewise explained, the evolution of the Marangoni term is slowed down even more. Marangoni and film drainage would then only balance after very long times indeed, which would likely exceed the residence time of a foam film within a foam fractionation process.

In a system containing soluble surfactants, when film drainage is active, the relevant

parameter to consider when determining whether a quasisteady state is likely to occur turns out to be $\mathcal{S}\,V_R$. We know that V_R is typically a small parameter while $\mathcal{S}$ is typically greater than unity. If $\mathcal{S}\,V_R$ is a very large parameter, film drainage effectively dominates Marangoni flow (this case is similar to the no Marangoni case discussed in Sec. 4.3). The case of our interest is therefore, when $\mathcal{S} > 1$, but $\mathcal{S}\,V_R$ is still small compared to unity. The parameter values in Table 5.2 indicate that this is indeed the case, so Marangoni flow and film drainage can then eventually come into balance. The derivation of the approximate solution itself is presented, as we have said, in supplementary Sec. 5.9.

Moreover, as Sec. 4.2.10 already explains, the approximate solution is expressed in terms of Γ rather than Γ_{tot}, which is convenient because Γ has a boundary condition that is independent of time. This approximate solution is a series expansion in powers of the small parameter V_R. When V_R vanishes, the only steady state solution is to have Γ equal to unity, i.e. equilibration between the film and Plateau border. For small but nonzero V_R, perturbations to Γ written as $V_R\Gamma_1$ (first order correction) and $V_R^2\Gamma_2$ (second order correction) occur. Here Γ_1 and Γ_2 turn out to be functions of x and of δ but not explicitly of time (although δ itself depends on time, making the solution for Γ quasisteady). The value of Γ_2 also depends on the solubility parameter $\mathcal{S}$, although it turns out that Γ_1 does not depend on $\mathcal{S}$ (see Sec. 5.9 for details).

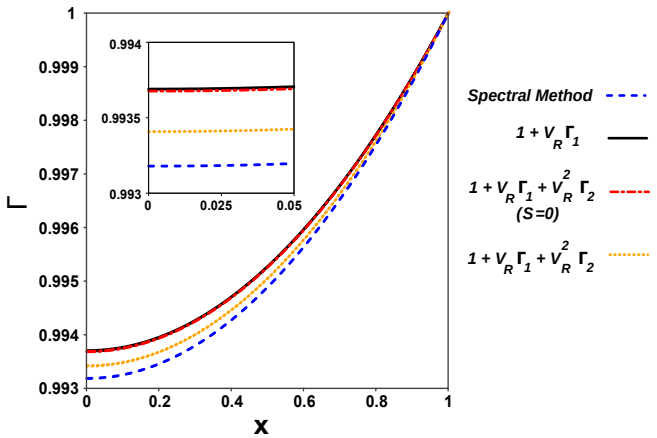

Figure 4.8: Profile of Γ calculated using a quasisteady-state approximation and numerically via a spectral method at 100 time units using a global Henry isotherm.

In Fig. 4.8, we can see a comparison between the results of the numerical solution and the approximate solution obtained in supplementary Sec. 5.9. The data shown here correspond to 100 time units, for which a quasisteady state is likely to be a reasonable approximation, even in the case of a soluble surfactant. As can be seen, the values of Γ that have been predicted with the series expansion solutions are slightly larger than the values obtained numerically from the spectral method. However, including the second-order correction gives a better fit to the numerical solution result than including just the first-order correction does. The relative difference between Γ calculated from first-order correction and the one calculated using the numerical method at $x = 0$, which has the greatest difference out of any x value, is equal to 5.47×10^{-4}, while the analogous difference for the second-order correction is 2.35×10^{-4}. It can also be seen that taking into account the solubility is required to have a more accurate approximation, as when the solubility parameter is ignored all together, there is a much smaller difference between the first-order and second-order corrections (see Sec. 5.9.2 for details).

4.4.6 Quantifying overall amount of surfactant in the film

Although profiles of Γ_{tot}, Γ and/or c plotted against x as considered to date are relevant to study, what is of primary interest for the performance of a fractionation process is the overall amount of surfactant accounting for the entire film. In this section, overall amounts of surfactant, for different cases have been compared with each other. These cases consist of global and local Henry isotherms, with or without film drainage as well as soluble and insoluble surfactant cases.

The first comparison is for the overall amount of surfactant recovered per film (Γ_{ove}) calculated by Eq. (4.25). Another comparison is the ratio of the overall amount of surfactant in the film with respect to its initial amount ($\Gamma_{\mathrm{ove}}/\Gamma_{\mathrm{ove},0}$): this is a measure of how much extra surfactant is recovered as a result of Plateau-border-to-film mass transfer induced by reflux. In addition, surfactant effective concentration (c_{eff}) has been calculated via Eq. (4.26) and compared in different cases: this measures how enriched

the foam film is compared to an equivalent volume of bulk solution within the film itself.

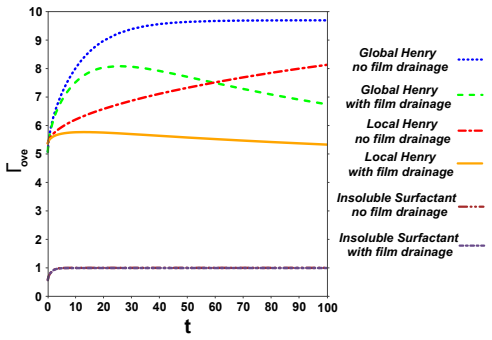

(a) Evolution of Γ_{ove}

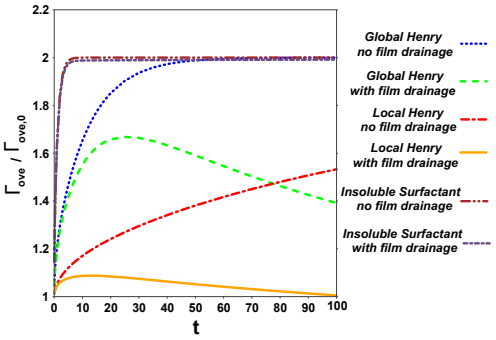

(b) Evolution of $\Gamma_{\mathrm{ove}}/\Gamma_{\mathrm{ove},0}$

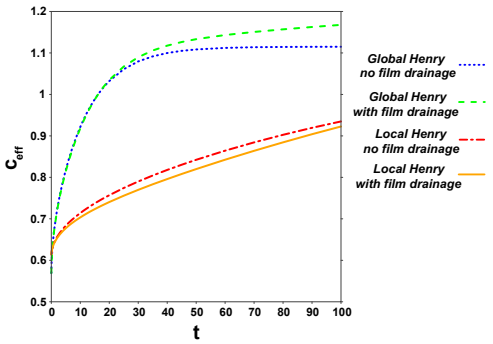

(c) Evolution of c_{eff}

Figure 4.9: Evolution of Γ_{ove}, $\Gamma_{\mathrm{ove}}/\Gamma_{\mathrm{ove},0}$ and c_{eff}, calculated for soluble and insoluble cases, global and local Henry isotherm, and with and without film drainage.

Fig. 4.9a shows Γ_{ove} for different cases up to 100 time units. As is expected and can be seen from Fig. 4.9a, using a global Henry isotherm rather than a local Henry isotherm, leads to faster growth in the amount of surfactant at early times. However, in the global Henry isotherm case with film drainage, despite the comparatively fast initial increase, surfactant later decreases after reaching a maximum. A decrease at late times is also seen in the local Henry isotherm case, but there is now barely any growth in Γ_{ove} at all before the decrease begins.

Another observation is that in the soluble cases, when film drainage is absent, the global and local Henry isotherm cases should eventually reach the same overall amount of surfactant. However, the local Henry isotherm case evolves slowly and so on the time scale of Fig. 4.9a still remains some way away from what is recovered the global

Henry case. This implies that the surfactant recovered by the fractionation process would be sensitive to the residence time (or equivalently fractionation column length and/or bubble rise velocity). Note also that the lesser amount of surfactant predicted to be accumulated in the local Henry case has resulted when comparing the local and global cases at the same value of $\mathcal{S}$. For a particular surfactant though, switching from a local to a global isotherm corresponds to lowering the target surfactant concentration (in dimensional variables) and, as has been explained in Sec. 4.2.5.2, this could lead to an even lower $\mathcal{S}$ in the global Henry isotherm case. Finally, as is expected, the insoluble cases have the least overall amount of surfactant, there now being no surfactant in the bulk, while the differences between cases without and with film drainage cases are also very small.

We use another comparison, the overall amount of surfactant at each time divided by the overall amount at the initial time ($\Gamma_{\mathrm{ove}}/\Gamma_{\mathrm{ove},0}$), that can be seen in Fig. 4.9b. This quantity indicates, as we have said, the amount of surfactant recovered at any given time relative to the state of the films at initial time, and hence the impact that the reflux has had on the Plateau-border-to-film mass transfer. As can be seen in Fig. 4.9b, although the insoluble surfactant cases have much smaller Γ_{ove} at any given time compared to the soluble surfactant cases, their $\Gamma_{\mathrm{ove}}/\Gamma_{\mathrm{ove},0}$ values grow more rapidly, with very little difference between cases without and with film drainage.

The next most rapidly growing $\Gamma_{\mathrm{ove}}/\Gamma_{\mathrm{ove},0}$ occurs for the soluble surfactant case with a global Henry isotherm but without film drainage. The analogous value of $\Gamma_{\mathrm{ove}}/\Gamma_{\mathrm{ove},0}$ for a global Henry isotherm with film drainage starts out similar but then peaks and decreases. Choosing a residence time close to the time of the peak would ensure that recovery is benefitting from Plateau-border-to-film mass transfer induced by reflux.

The slowest growing cases for $\Gamma_{\mathrm{ove}}/\Gamma_{\mathrm{ove},0}$ are those for a local Henry isotherm, especially when film drainage is present, in which case $\Gamma_{\mathrm{ove}}/\Gamma_{\mathrm{ove},0}$ barely grows at all. In the case without film drainage, $\Gamma_{\mathrm{ove},0}$ is actually slightly higher for a local Henry

isotherm than for a global Henry isotherm, which means that $\Gamma_{\text{ove}}/\Gamma_{\text{ove},0}$ for the local isotherm at long times should always end up just slightly lower than for the global one. However, at 100 units of time the local Henry isotherm case is still quite some way from its final state.

The comparison of c_{eff} (Eq. (4.26)) in various cases can be seen in Fig. 4.9c, just considering cases with soluble surfactant. This gives a measure of how rich of the foamate is in surfactant, regardless of the actual amount of surfactant recovered. It is clear that longer residence times enrich the foamate, even if less surfactant is recovered. There is now relatively little difference between cases without and with film drainage, suggesting that even though drainage might be detrimental to the total amount of surfactant recovered, it is not detrimental to the concentration of what is recovered, and in fact sometimes it is beneficial.

4.4.7 Effect of changing solubility parameter

Recall that the main novelty of this study is the fact that we introduced the solubility parameter ($\mathcal{S}$). We know (see Eq. (4.3)) that the solubility parameter is dependent on the initial film half-thickness and Plateau border's surface and bulk concentrations. Even though, in the particular system of interest here, we estimated the solubility parameter in Table 5.2 to be 8.696, it is important to do a parametric study with respect to the solubility parameter.

In Fig. 4.10, we used various solubility parameters to show the effect on the evolution of $\Gamma_{\text{ove}}/\Gamma_{\text{ove},0}$ for both global and local Henry isotherms. Note that these comparisons have been made specifically in the case with film drainage, although unlike Fig. 4.9b we only considered times up to 20 time units.

By increasing the solubility parameter, the overall amount of surfactant in the film increases, but this effect is scaled out in Fig. 4.10 by comparing $\Gamma_{\text{ove}}/\Gamma_{\text{ove},0}$, rather than just Γ_{ove}. It can be seen from Fig. 4.10a for the global Henry isotherm case, that

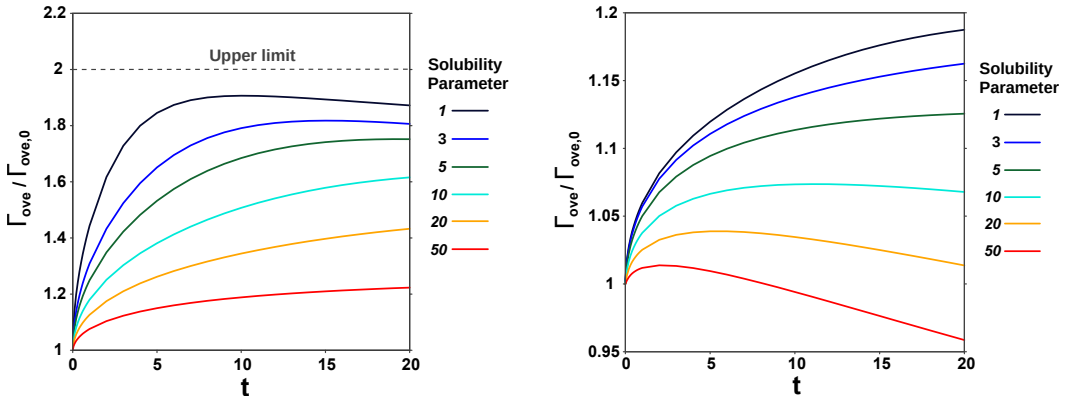

(a) Global Henry isotherm **(b)** Local Henry isotherm

Figure 4.10: Effect of changing $\mathcal{S}$ on $\Gamma_{ove}/\Gamma_{ove,0}$ using global and local Henry isotherms (the upper limit shown is the highest theoretical $\Gamma_{ove}/\Gamma_{ove,0}$ corresponding to the film and Plateau border equilibrating).

systems with higher solubility parameter evolve more slowly, which is in line with expectations.

In Fig. 4.10b meanwhile, using the local Henry isotherm, Marangoni flow is slowed down very greatly, so the system is dominated by film drainage in the case when the solubility parameter is high. As a result, we lose surfactant from the film as the process evolves. Loss of surfactant from the film occurs sooner for higher values of the solubility parameter.

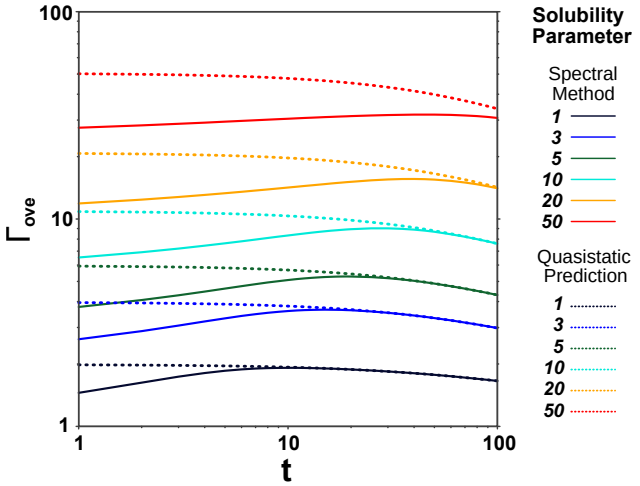

Figure 4.11: Γ_{ove} vs time t, calculated using a quasisteady prediction and compared with numerical solution. A global Henry isotherm is used and various $\mathcal{S}$ values are considered.

In Fig. 4.11, in addition to numerical data from the spectral method, we also plot the

quasisteady prediction (see Sec. 5.9) for Γ_{ove} as a function of time for several $\mathcal{S}$, with data extending now up to 100 time units. Eventually, the system does approach a quasisteady state. However, as shown in Fig. 4.11, in the cases with larger solubility parameters, Γ_{ove} calculated using the numerical solution only matches with the Γ_{ove} calculated from the quasisteady prediction at rather late times.

4.4.8 Foam fractionation recovery and enrichment

Recovery and enrichment are important quantities that can be used to assess foam fractionation performance [34, 36, 44, 61, 83]. As Sec. 4.2.9 mentions, enrichment is the ratio between surfactant concentration in a foamate to the initial feed solution concentration and, in our model, is quantified as c_{eff}/c_0. Meanwhile Γ_{ove} is used here to represent the recovery of the fractionation column at any instant. Again as Sec. 4.2.9 explains, strictly speaking this quantifies surfactant recovery per film, but it can be readily converted back to a more conventional definition of recovery once the number of films entering the foamate and the overall surfactant amount entering the feed are specified.

Note that recovery and enrichment usually follow opposite trends [107, 108] and so, in a given system, to increase one we need to sacrifice the other. If we change the fractionation operation in some way however, we may be able to improve the recovery and enrichment performance. Changing residence time in the fractionation column and/or operating the fractionation with reflux as assumed here are possible ways of doing that. In fact, the recovery and enrichment at the initial instant in a column operated with reflux turn out to give a good representation of what the recovery and enrichment would be over a wide domain of times in an equivalent column without reflux. This follows because in the case without reflux, there is no Marangoni driving force tending to transfer surfactant from the Plateau border to the film. Any changes in recovery and enrichment over time then rely on film drainage which is comparatively weak. By the same argument, if operating with reflux is ever to be beneficial in recovery and

enrichment terms for the mass transfer from Plateau border to film, then it is necessary for residence time of foam films in a fractionation column to be sufficiently long for Marangoni flows to have taken effect.

In what follows, we present two sets of comparisons. First, we investigate the evolution of recovery and enrichment in the global and local Henry isotherm cases, both with film drainage. After that, we compare recovery and enrichment for the global and local Henry isotherms with and without film drainage, but just at selected times. In both sets of comparisons, different values of solubility $\mathcal{S}$ are considered across the domain $0.1 \leq \mathcal{S} \leq 50$.

4.4.8.1 Evolution of recovery and enrichment over time

As shown in Fig. 4.12a for the global Henry isotherm, there is a clear benefit in allowing the films to reside in the system for around 20 time units or more. The recovery vs enrichment curve has moved upward and to the right relative to the recovery vs enrichment in the initial state.

That said, the benefit of mass transfer from Plateau border to film induced by reflux is realised sooner in systems with small $\mathcal{S}$, i.e. low solubility. In systems like that there is little advantage in extending the residence time much beyond 20 time units. At even longer times and for these low solubilities, we do see further slight improvements in enrichment due to film drainage, but the improvements are attained only slowly. On the other hand, for larger $\mathcal{S}$ values there is still benefit in extending residence time out to 50 or 100 time units. In systems with larger $\mathcal{S}$, the Marangoni flow induced by the reflux itself impacts the system more slowly, and so may need longer residence times to take effect.

In the local Henry isotherm case (Fig. 4.12b), the situation is somewhat different. We now have more surfactant on the surface initially, which impacts the initial recovery vs enrichment curve, particularly at low solubilities for which systems are dominated by

the surface rather than the bulk.

Indeed, across the full set of solubilities, the difference between the initial state and the state even at 100 time units is quite modest. We can divide the results plotted in Fig. 4.12b into three broad domains: low solubilities (on the bottom right of the figure), moderate solubilities (in the middle), and high solubilities (on the top left). In the low solubility domain (bottom right) there is little benefit of mass transfer from Plateau border to film induced by reflux at all. The system is dominated by the surfactant on the surface, but for the local Henry case, the surface concentration on the film already starts off very close to the surface concentration on the Plateau border, so barely changes over the course of time.

In the moderate solubility domain (middle of Fig. 4.12b) we do see a gradual shift over time of the recovery vs enrichment curve, with longer times (even as long as 100 time units) being beneficial. Note that the equivalent solubilities in the global Henry isotherm case Fig. 4.12a had already converged after 20 time units, but in the local Henry case by contrast, the evolution is slowed down somewhat, hence the reason longer times are needed.

On the top left of Fig. 4.12b we see cases which even by 100 time units have barely shifted away from the initial state. This is because the effects of large solubility combined with a local Henry isotherm now slow down the Marangoni-driven evolution very significantly, meaning that mass transfer from Plateau border to film caused by reflux is yet to impact the system. To benefit from this particular reflux effect at all, systems like this would need very long residence times indeed.

4.4.8.2 Comparison of recovery and enrichment of different systems at selected times

In this section, comparisons between different isotherms and with and without film drainage have been made. We examine the plots at just 20 and 100 time units.

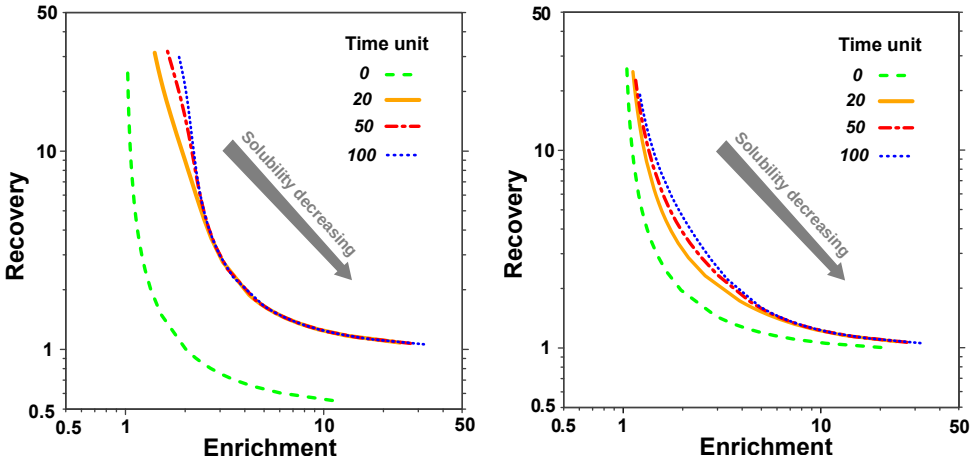

(a) Global Henry with drainage **(b)** Local Henry with drainage

Figure 4.12: Recovery vs enrichment plotted for various solubilities ($0.1 \leq \mathcal{S} \leq 50$) and evolving over time.

We know that by construction there is no difference between cases with and without film drainage at the initial time. What Fig. 4.13a makes clear however is that there is still little difference between these cases even at 20 time units. Thus the main difference we see here at 20 time units is between the global and local Henry isotherm cases. This then manifests itself in the domain of larger solubilities (towards the top left of the figure). In the global Henry case, the film had already begun to acquire surfactant due to Marangoni-driven reflux (which is then beneficial for recovery and enrichment), but this has not yet happened in the local Henry isotherm case.

Meanwhile at 100 time units as can be seen in Fig. 4.13b, for less soluble surfactant (bottom right of the figure) there is little difference between the results for the two different types of isotherm. What we can see however is that cases with film drainage are being enriched slightly compared to cases without film drainage.

Still at 100 time units but now for higher solubilities (top left of the figure), differences between the global and local Henry isotherm cases remain apparent. However, differences between cases with and without drainage are also clearly seen, with film drainage leading to less recovery. This is particularly evident in the local Henry isotherm case, for which loss of surfactant from the film via drainage has not been compensated by

gain of surfactant via reflux-induced Marangoni flow.

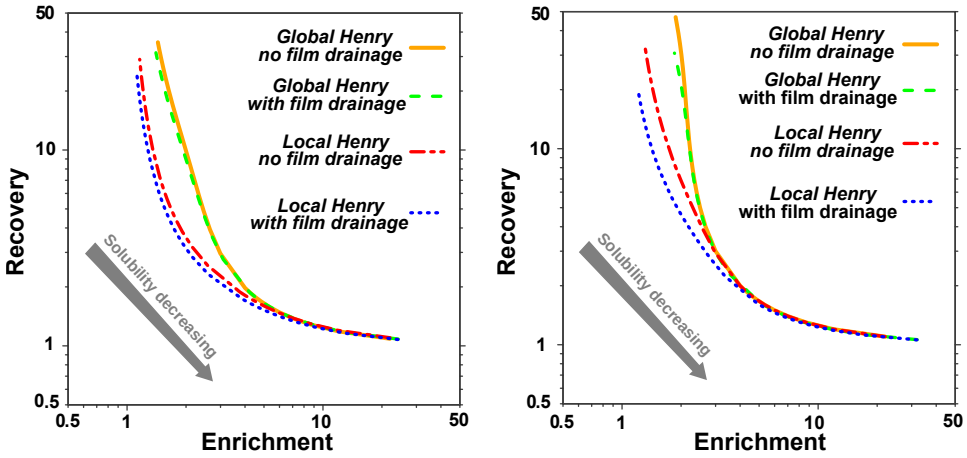

(a) At 20 time units **(b)** At 100 time units

Figure 4.13: Recovery vs enrichment plotted for various solubilities ($0.1 \leq \mathcal{S} \leq 50$) for systems using different isotherms and with and without film drainage.

4.5 Conclusion

Simulation of soluble surfactant transport on and within a foam film in the context of a foam fractionation column with reflux has been carried out. Reflux produces a Marangoni flow that drives surfactant onto the film. Despite incorporating tangential stresses that drive the Marangoni flows, the model remains nevertheless highly simplified: lubrication theory is used to determine flow fields, but films are assumed to remain uniform thickness, so film surface curvatures and normal stresses associated with them are not invoked. Likewise a two-dimensional flow field is assumed, recognising that the exact three-dimensional flow field that would otherwise result is sensitive to film size and also to number of edges a given film has. Variation from film to film is thereby expected.

The parameters used in the simulations were taken from relevant literature. As mentioned, this simulation assumes soluble surfactant, unlike previous work [1] which considered insoluble surfactant only. However, solubilities of different systems vary, and can be quantified by a solubility parameter ($\mathcal{S}$). Moreover, a simplifying assump-

tion has been applied in our modelling and simulations, namely, a small $\mathrm{Pe}\,\Delta$ limit, in which a uniform surfactant concentration across the film thickness is obtained. This is what should happen in a sufficiently thin film when the diffusive transport across the film is fast compared to the Marangoni flow along it.

Our simulations consider two different adsorption isotherms: a global Henry isotherm and a local Henry isotherm. Both can be considered to arise from an overarching non-linear isotherm (e.g. a Langmuir isotherm). The local Henry isotherm in particular is a new approach in which we use the local slope of the actual surfactant adsorption isotherm data and it gives a better approximation to the true isotherm in the higher range of concentrations. This is useful because in a typical foam fractionation process with reflux, the concentration in the Plateau border could well be situated at a point on Langmuir isotherm which is not too far from saturation, such that there is just a comparatively small change in surfactant surface concentration with respect to change in surfactant bulk concentration. As a result, a local Henry adsorption isotherm gives a better approximation in this domain of interest, while a global Henry isotherm still works reasonably well for significantly lower surfactant concentrations. Note also however that, for a given surfactant, decreasing surfactant concentration may also imply a decrease in the solubility parameter.

For each adsorption isotherm, two different cases are considered here, namely, no film drainage and with film drainage. Drainage, when included, is accounted for in a simplified fashion, i.e. still assuming the film remains uniform thickness but treating it now as a squeeze film. In the film drainage case, the amount of surfactant recovered by the film is less than in the case without film drainage, although the effective concentration of surfactant may be higher. The case without film drainage eventually equilibrates with the Plateau border, whereas the case with film drainage eventually approaches instead a quasisteady state. This quasisteady-state solution can be applied for later times when Marangoni flow and film drainage flow come into balance. The surfactant

on and within the film then evolves only slowly with time due to a dependence of the quasisteady solution on the film thickness. Increasing the solubility parameter tends however to reduce the amount of surfactant on the surface in the quasisteady state, and moves the system further from equilibrium with the Plateau border.

There is however a question as to whether the quasisteady state is even reached in a typical residence time of a foam film in a fractionation column. Indeed, it has been found that the solubility reduces the impact of the Marangoni flow acting along the surface and so slows down the Marangoni-driven evolution. The reason is that the surfactant carried along the surface tends not to accumulate there but instead can escape into the bulk. This effect is particularly noticeable for the local Henry isotherm, as there is then little capacity for surfactant to accumulate on the surface, so a great deal necessarily escapes to the bulk. There also tend to be very low gradients in surfactant concentration along the surface in the local Henry isotherm case which slows Marangoni flows.

Moreover adding film drainage (which opposes Marangoni flow) slows the evolution even more compared to a case without drainage. Even though drainage is itself nominally weak, because it acts across the whole film thickness, its impact in mass transfer terms is not necessarily less than that of the Marangoni flow.

Higher solubilities give at any specified time, less growth in the overall amount of surfactant relative to its initial amount. This is due to the previously mentioned fact that higher solubilities slow down the Marangoni flow. Moreover, as film drainage is now in relative terms more important, there will be a bigger deviation at later times from conditions applicable in the Plateau border. The film drainage might even cause the reduction of the total amount of surfactant recovered after a certain time, particularly in cases with significantly slowed down Marangoni flows. This then impacts on the amount of surfactant recovered. However, despite the decreasing recovery, the enrichment always increases because both film drainage and Marangoni flow contribute to

having richer films.

In summary, the results of the study can help to understand the evolution of surfactants on and within foam films during foam fractionation with reflux. It is seen that reflux is beneficial for fractionation even of soluble surfactants. However, systems exhibiting a global Henry isotherm (or an isotherm approximating to one) benefit more from reflux than systems with a local Henry isotherm (or likewise an isotherm approximating to one). Indeed the local Henry isotherm case would only benefit from Plateau border to film mass transfer induced by reflux if residence times are very long. This knowledge can help to improve design and operation of fractionation columns.

Although an often overlooked element, i.e. the solubility parameter $\mathcal{S}$, has been included in the model considered here, other improvements to the model are nonetheless still possible. For instance, the small $\mathrm{Pe}\,\Delta$ assumption employed here is a reasonable assumption but would only be true in a sufficiently thin film. The value of the diffusivity coefficient is moreover another factor that might adversely affect the applicability of the small $\mathrm{Pe}\,\Delta$ assumption. Generally, bulkier molecules tend to have smaller diffusivity coefficients. Therefore, Péclet number and hence $\mathrm{Pe}\,\Delta$ for those bigger molecules (e.g. fractionation of a protein) can be much greater than for a comparatively small molecule such as SDS as has been considered here. In addition, by introducing the local Henry isotherm, we have tried to use the simplicity of a linear isotherm and simultaneously improve its accuracy over the global Henry isotherm for a higher range of concentrations. Nonetheless taking in account the full nonlinearity of the adsorption isotherm would be another means to improve this model. Additional improvements would involve relaxing some of the simplifying assumptions already mentioned above, e.g. allowing film thicknesses to be non-uniform rather than uniform, and allowing flow fields to be three-dimensional rather than two-dimensional.

Chapter 5

Transport of soluble surfactant on and within a foam film in the context of a foam fractionation process: Supplementary material

"This chapter consists of published material: [H. Rajabi, P. Grassia, "Transport of soluble surfactant on and within a foam film in the context of a foam fractionation process." Chemical Engineering Science, vol.265, 118171, 2023. https://doi.org/10.1016/j.ces.2022.118171]"

Abstract

In this supplementary section, we have reviewed some of the essential background concepts useful in understanding the present study, such as Marangoni stress, Gibbs elasticity and foam film drainage (Secs. 5.1 and 5.2). After that, a review of the governing equations in dimensional form and how to obtain approximate adsorption isotherms are presented (Secs. 5.3 and 5.4). Then, the nondimensionalization procedure is explained

(Sec. 5.5). Following that, the numerical solution procedure for the equation of the evolution of the total amount of surfactant at any location (Γ_{tot}) is explained in detail (Sec. 5.6). Then, values for simulation parameters relevant to a system containing sodium dodecyl sulphate (SDS), along with corresponding parameters for approximate adsorption isotherms for SDS are presented (Secs. 5.7 and 5.8). Finally, an approach to quasisteady state is discussed (Sec. 5.9).

5.1 Gibbs-Marangoni effect

The Gibbs-Marangoni effect (or simply Marangoni effect) is explained already in Sec. 2.5.2. However we retain the section to follow as it is a **part of our published article.**

The Gibbs-Marangoni effect refers to the forces that occur due to inhomogeneities in the free surface energy of a liquid surface, i.e. due to gradients in the surface tension [254]. This manifests itself via a Marangoni stress and Gibbs elasticity as described below.

5.1.1 Marangoni stresses

The Marangoni stresses typically need to be balanced by the viscous shear stress upon the bulk liquid in the film as presented in the following equation [43, 170, 255]:

$$\mu \left(\frac{\partial u}{\partial z} \right) \Bigg|_{z=\delta} = \frac{\partial \gamma}{\partial x} \tag{5.1}$$

where x is the distance from the centre of the film along the film, z is the distance from the centre of the film across the film (see Fig. 4.1), μ is liquid viscosity, u is liquid velocity along the film, δ is film half-thickness, and γ is surface tension. Eq. (5.1) will be used to provide a boundary condition that is then needed to obtain the velocity field: later on it is copied over to Eq. (5.10) leading ultimately to velocity fields in

Eqs. (5.13) to (5.15) in Sec. 5.3.1. These latter equations are also reproduced in the main text Sec. 4.2.2 albeit in dimensionless form. For compactness of notation, we use the same symbols (x, z, δ, u, etc.) to denote dimensional variables here, but dimensionless variables in the main text.

5.1.2 Gibbs elasticity

Gradients of surface tension arise through having gradients in the concentration of surfactant adsorbed on the surface, i.e. gradients in the so called surface excess. That then gives a measure of the stiffness of the interface against a dilational compression or expansion [146, 158–161]. In the case when the surface tension variation is purely elastic, a Gibbs elasticity modulus can be defined [164–168].

$$\mathcal{G} \approx -\frac{\mathrm{d}\gamma}{\mathrm{d}\ln\Gamma} \tag{5.2}$$

where $\mathcal{G}$ is the Gibbs parameter [168], γ is surface tension, and Γ is surfactant surface excess. Eq. (5.2) allows us later on to replace surface tension with surface excess in the equations for velocity field in Sec. 5.3.1, ultimately leading to the dimensionless equations in Sec. 4.2.2. Again, for compactness of notation, we use the same symbol Γ to denote dimensional surface excess here, but dimensionless surface excess in the main text.

5.2 Foam film drainage

Foam film drainage is explained in Sec. 2.4.3.2 and a detailed derivation of the thinning rate can be found in Sec. A 1. However, we retain the section to follow as it is a **part of our published article.**

In the main text of this study, we have used a specific model for foam film drainage (i.e. for foam film thickness versus time; see Sec. 4.2.2). The purpose of the present

section is to explain how that model came about.

So-called Plateau borders located at the edge of the films, have much higher curvatures than those of the films connected to them. This will create a lower pressure in the Plateau borders than within the films and will drive capillary suction effects and hence film drainage. Some film drainage models include the Reynolds model [221] for a rigid interface which is utilised in the present study, and the Breward-Howell model for a mobile interface [40, 48, 118, 256], albeit not used here. The film drainage that develops for a rigid interface is based on the application of the conventional Reynolds lubrication theories to develop the following equation [49]:

$$\frac{\mathrm{d}\delta}{\mathrm{d}t} = -\frac{2\delta^3 \Delta P}{3\mu L^2} \tag{5.3}$$

where t is time, δ is film half-thickness, L is film half-length, μ is film bulk viscosity, and ΔP is pressure difference driving the drainage mechanism in the film. Typically, this involves a capillary term [40] and a disjoining term [257, 258]. For newly formed foam films which are not yet exceedingly thin, the disjoining pressure is negligible. Therefore, the driving pressure difference will become [164]:

$$\Delta P = \frac{\gamma_{\mathrm{Pb}}}{a} \tag{5.4}$$

where γ_{Pb} is the surface tension of the Plateau border, and a is the Plateau border's radius of curvature. Solving Eq. (5.3) with the initial condition, $\delta|_{t=0} = \delta_0$ results in:

$$\delta = \delta_0 \left(1 + \frac{4}{3}\frac{\gamma_{\mathrm{Pb}}\delta_0^2}{\mu L^2 a} t\right)^{-1/2}. \tag{5.5}$$

Here Eq. (5.5) is the dimensional form of the film half-thickness equation. It is presented in nondimensional form in Sec. 4.2.2.

5.3 Governing equations

Governing equations are explained in more detail in Chapter 3. as they are essential to our modelling. However, we retain the section to follow as it is a **part of our published article.**

In this section governing equations are presented in dimensional form. These equations are used in nondimensional form in the main text Sec. 4.2, but for compactness of notation, deploying the same symbols as are used here. The nondimensionalization process is explained in Sec. 5.5.

5.3.1 Continuity and momentum equations

Following Vitasari et al. [1], we make standard lubrication theory assumptions for the continuity and Navier-Stokes equations as follows:

$$\frac{\partial u}{\partial x} + \frac{\partial w}{\partial z} = 0, \tag{5.6}$$

$$\frac{\partial P}{\partial x} = \mu \frac{\partial^2 u}{\partial z^2} \tag{5.7}$$

and

$$\frac{\partial P}{\partial z} = 0. \tag{5.8}$$

Here w denotes vertical velocity component, P denotes pressure and u, x and z are as defined previously.

The following boundary conditions are applied to solve the above equations:

$$\left(\frac{\partial u}{\partial z}\right)\bigg|_{z=0} = 0 \tag{5.9}$$

and

$$\mu \left(\frac{\partial u}{\partial z}\right)\bigg|_{z=\delta} = \frac{\partial \gamma}{\partial x} \tag{5.10}$$

which is a copy of Eq. (5.1). The thinning rate of the foam film, according to Breward and Howell [40] obeys the following generic equation :

$$\frac{\partial \delta}{\partial t} = -\left(\bar{u}\frac{\partial \delta}{\partial x} + \delta\frac{\partial \bar{u}}{\partial x}\right) \tag{5.11}$$

where t is time, δ is film half-thickness, and $\bar{u}$ is average liquid velocity across the foam films. Here however the thickness of the foam film is assumed to be uniform ($\mathrm{d}\delta/\mathrm{d}x = 0$). As a result, Eq. (5.11) reduces to:

$$\bar{u} = -\frac{\dot{\delta}}{\delta}x \tag{5.12}$$

where $\dot{\delta}$ is defined as the thinning rate. By solving the above set of equations, the following velocity fields are obtained in x and z directions:

$$u = -\frac{x}{\delta}\frac{\mathrm{d}\delta}{\mathrm{d}t} + \frac{\mathcal{G}}{\mu}\left(\frac{\delta}{6} - \frac{z^2}{2\delta}\right)\frac{\partial \ln \Gamma}{\partial x} \tag{5.13}$$

$$w = \frac{z}{\delta}\frac{\mathrm{d}\delta}{\mathrm{d}t} + \frac{\mathcal{G}}{\mu}\left(\frac{z^3}{6\delta} - \frac{z\delta}{6}\right)\frac{\partial^2 \ln \Gamma}{\partial x^2} \tag{5.14}$$

where $\mathcal{G}$ is the Gibbs parameter and can be obtained from Eq. (5.2). Moreover, by setting $z = \delta$ in Eq. (5.13), an equation for the surface velocity u_s will be obtained as follows:

$$u_s = -\frac{x}{\delta}\frac{\mathrm{d}\delta}{\mathrm{d}t} - \frac{\mathcal{G}\delta}{3\mu}\frac{\partial \ln \Gamma}{\partial x}. \tag{5.15}$$

This defines velocity fields, provided we know how surfactant is distributed. Next, to keep track of surfactant distribution, we introduce mass transfer equations in the bulk and on the foam surface.

5.3.2 Mass transfer equations for soluble surfactants on & within the foam film

Having obtained the velocity fields in the bulk and on the surface, we present mass transfer equations for surfactants likewise in the bulk and on the surface. Here equations are presented in dimensional form, with dimensionless analogues in the main text Sec. 4.2.3. Soluble surfactant mass transfer in the bulk obeys the following equation:

$$\frac{\partial c}{\partial t} + \nabla.(\mathbf{u}\, c) = \nabla.(\mathcal{D}\nabla c) \tag{5.16}$$

where c is surfactant concentration in the bulk, t is time, $\mathbf{u} = (u, w)$ is velocity in the bulk in x and z directions, and $\mathcal{D}$ is diffusivity coefficient. Meanwhile, mass transfer on the surface obeys:

$$\frac{\partial \Gamma}{\partial t} + \frac{\partial (u_s \Gamma)}{\partial x} = \mathcal{D}\, \frac{\partial c}{\partial z}\bigg|_{z=\delta}. \tag{5.17}$$

This equation indicates that surfactant surface concentration changes due to convection along the surface and a diffusion flux from or to the bulk.

To obtain a set of equations describing the evolution of surfactants with time, we need to combine Eqs. (5.16) and (5.17) using an adsorption isotherm, to be discussed shortly, see Sec. 5.4. Moreover, velocity equations (Eq. (5.13), Eq. (5.14), Eq. (5.15)) are substituted into the mass transfer equations. These ultimately lead to the equations that we solve in the main text.

5.4 Approximations to adsorption isotherms

In this section, we work out linear approximations to a Langmuir adsorption isotherm in order to combine mass transfer equations in the bulk and on the surface (Eqs. (5.16) and (5.17)). The Langmuir adsorption isotherm is generally a better fit to the adsorption behaviour of a surfactant/surface active material than the rather simpler Henry

isotherm is [175]. However, its nonlinearity causes some computational complexity. On the other hand, the Henry adsorption isotherm being linear is easier to compute with, but typically leads to accurate results only for low surfactant concentrations [230]. However, the aim of foam fractionation with reflux is typically to achieve the highest possible concentrations. To extend the isotherm's applicability to higher concentrations, and simultaneously keep the simplicity that the Henry adsorption isotherm offers, we propose to replace the Langmuir isotherm with approximated linear adsorption isotherms. We use two distinct approximations in the modelling. These approximations aim to obtain a reliable but straightforward relationship between the surfactant concentrations in the bulk and on the foam surface.

The general equation for Langmuir adsorption isotherm relating Γ and c is [93, 229, 230]:

$$\Gamma = \Gamma_m \frac{\bar{K}_L c}{1 + \bar{K}_L c} \tag{5.18}$$

where $\bar{K}_L$ and Γ_m are parameters, respectively a so-called Langmuir parameter and a maximum surface excess.

The first approximation we now make is termed a global approximation. It consists of a straight line joining $(c, \Gamma) = (0, 0)$ to $(c, \Gamma) = (c_{\mathrm{Pb}}, \Gamma_{\mathrm{Pb}})$ in a surfactant surface concentration versus bulk concentration plot (see e.g. Fig. 5.1 within Sec. 5.8 later on). Here c_{Pb} is the bulk surfactant concentration at the Plateau border, and Γ_{Pb} is the surfactant surface concentration at the Plateau border. This straight line has a slope (that we call a global Henry constant, $\bar{K}_{H(\mathrm{glob})}$) as follows:

$$\bar{K}_{H(\mathrm{glob})} = \frac{\Gamma_{\mathrm{Pb}}}{c_{\mathrm{Pb}}} = \frac{\Gamma_m \bar{K}_L}{1 + \bar{K}_L c_{\mathrm{Pb}}}. \tag{5.19}$$

The approximate isotherm which is obtained using the global Henry constant is:

$$\Gamma = \bar{K}_{H(\mathrm{glob})} c. \tag{5.20}$$

The global Henry approach underestimates the values of Γ for any c in the domain of $0 < c < c_{\mathrm{Pb}}$. However, this remains a reasonable approximation for sufficiently low concentrations in the Plateau border (i.e. sufficiently low c_{Pb} such that $\bar{K}_L c_{\mathrm{Pb}}$ is rather smaller than unity).

The second approximation is a local approximation, which is a tangent line to the Langmuir isotherm at $(c, \Gamma) = (c_{\mathrm{Pb}}, \Gamma_{\mathrm{Pb}})$: again see e.g. Fig. 5.1 later on within Sec. 5.8. This has a slope (that we call a local Henry constant, $\bar{K}_{H(\mathrm{loc})}$) given by:

$$\bar{K}_{H(\mathrm{loc})} = \left.\frac{\mathrm{d}\Gamma}{\mathrm{d}c}\right|_{c=c_{\mathrm{Pb}}} = \frac{\Gamma_m \bar{K}_L}{(1+\bar{K}_L c_{\mathrm{Pb}})^2} = \frac{\Gamma_{\mathrm{Pb}}}{c_{\mathrm{Pb}}(1+\bar{K}_L c_{\mathrm{Pb}})}. \tag{5.21}$$

This is a factor $1 + \bar{K}_L c_{\mathrm{Pb}}$ smaller than the global Henry constant. As a result, local Henry constant matches global Henry constant only when $\bar{K}_L c_{\mathrm{Pb}} \ll 1$ and otherwise is smaller than the global Henry constant. Now, the relationship between surface and bulk concentrations (local Henry isotherm) becomes:

$$\Gamma = \bar{K}_{H(\mathrm{loc})} c + \bar{\Gamma}_{\mathrm{min}}. \tag{5.22}$$

This equation has an intercept (a minimum value for Γ in the limit of $c \to 0$, denoted $\bar{\Gamma}_{\mathrm{min}}$) as follows:

$$\bar{\Gamma}_{\mathrm{min}} = \frac{\Gamma_{\mathrm{Pb}} \bar{K}_L c_{\mathrm{Pb}}}{1+\bar{K}_L c_{\mathrm{Pb}}}. \tag{5.23}$$

As we can see from Eq. (5.22), the value of Γ decreases moving towards lower bulk concentrations but never becomes less than $\bar{\Gamma}_{\mathrm{min}}$. In the domain of $c < c_{\mathrm{Pb}}$, the local approximation overestimates Γ for any c, but is a reasonable approximation when c is close to c_{Pb}. In fact in the present study it is unlikely that we would encounter values of c exceedingly small compared to c_{Pb}. This is because we are focussing upon using reflux to contact surfactant rich liquid in Plateau borders with somewhat less surfactant rich liquid in films, but the films always contain at least some level of surfactant in them to start with.

To summarise, we worked out two linear adsorption isotherms starting from a non-linear adsorption isotherm. Thus far we have presented the isotherms in dimensional form, although it is possible to nondimensionalize them: dimensionless analogues are presented in the main text Sec. 4.2.5.1. General details about nondimensionalizing the system are given in Sec. 5.5 with specific details about values of parameters needed for the calculations being given in Secs. 5.7 and 5.8. Once those parameter values are set, it becomes possible to use the isotherms as given in Sec. 4.2.5.1 to combine mass transfer equations in the bulk and on the surface, which is done in Sec. 4.2.4.

5.5 Nondimensionalization

Here we present a description of how to nondimensionalize the variables and equations used in our model (and thereby obtain the governing equations in main text Sec. 4.2).

- We make x (distance along the film) dimensionless with respect to film half-length L, and z (distance across the film) dimensionless with respect to initial film half-thickness δ_0.
- Velocities u in the x direction are nondimensionalized with respect to $\mathcal{G}\delta_0/\mu L$, while velocities w in the z direction are nondimensionalized with respect to $\mathcal{G}\delta_0^2/\mu L^2$.
- Times t are made dimensionless with respect to $\mu L^2/\mathcal{G}\delta_0$.
- Surfactant concentrations in the film c are made dimensionless with respect to the surfactant concentration in the bulk of the Plateau border c_{Pb}. Note that the Plateau border is treated as a surfactant reservoir. Thus, its concentration is assumed to be constant.
- Surfactant concentrations on the film surface Γ are made dimensionless with respect to the Plateau border surface concentration Γ_{Pb}.
- When films are draining, we make instantaneous film half-thickness δ dimen-

sionless with respect to the initial film half-thickness δ_0.

- The parameters of the local Henry isotherm, namely the local Henry constant $\bar{K}_{H(\mathrm{loc})}$ and the minimum amount of surface concentration ($\bar{\Gamma}_{\mathrm{min}}$) are made dimensionless with respect to $\Gamma_{\mathrm{Pb}}/c_{\mathrm{Pb}}$ and Γ_{Pb}, respectively. The dimensionless analogues we denote $K_{H(\mathrm{loc})}$ and Γ_{min}, respectively.

- K_L represents the nondimensional Langmuir parameter obtained from the product of dimensional Langmuir parameter and Plateau border bulk concentration ($\bar{K}_L c_{\mathrm{Pb}}$). Note that $K_{H(\mathrm{loc})}$ and Γ_{min} can be obtained in terms of K_L: see main text Eqs. (4.17) and (4.18).

After nondimensionalization, we proceed to solve the equation for the evolution of the total amount of surfactant, Γ_{tot} (with surface and bulk taken together) as given by Eq. (4.24) in the main text. Detail of how to solve Eq. (4.24) using a spectral method is the subject of the next section.

5.6 Numerical solution procedure for calculating evolution of Γ_{tot}

This section gives the numerical solution procedure for the evolution of Γ_{tot} Eq. (4.24) working now in dimensionless variables. To proceed we divide the total amount of surfactant at any location (Γ_{tot}) in two parts. The first part is $\Gamma_{\mathrm{tot,sol}}(x,t)$, which is the difference between dimensionless total amount of surfactant at any film location and the equivalent amount at the Plateau border: this is what will be obtained as the solution from the numerical method. The second part is $\Gamma_{\mathrm{tot,Pb}}(t)$, which is the dimensionless total amount of surfactant at the Plateau border. Thus we have:

$$\Gamma_{\mathrm{tot}} = \Gamma_{\mathrm{tot,sol}} + \Gamma_{\mathrm{tot,Pb}}. \tag{5.24}$$

Here, in the dimensionless system, $\Gamma_{\mathrm{tot,Pb}}$ is $1+\mathcal{S}\,\delta$ (see Sec. 4.2.6 in main text), which is a known value at each time. It can be seen from the boundary condition at $x = 1$, namely that $\Gamma_{\mathrm{tot}} = \Gamma_{\mathrm{tot,Pb}}$, that at a long time, provided film drainage is not too strong, the system comes typically quite close to equilibrium. The value of Γ_{tot} approaches $\Gamma_{\mathrm{tot,Pb}}$ and so the $\Gamma_{\mathrm{tot,sol}}$ term becomes relatively small at long time. Now, we combine Eq. (4.24) with Eq. (5.24), which results in:

$$\begin{aligned}\frac{\partial}{\partial t}\left(\Gamma_{\mathrm{tot,sol}}+\Gamma_{\mathrm{tot,Pb}}\right) = \left(\frac{\dot{\delta}}{\delta}\right)\left(x\frac{\partial \Gamma_{\mathrm{tot,sol}}}{\partial x}+\Gamma_{\mathrm{tot,sol}}+\Gamma_{\mathrm{tot,Pb}}\right)\\ +\frac{\delta}{3(1+\mathcal{S}\delta/K_{H(\mathrm{loc})})}\left(\frac{\partial^2 \Gamma_{\mathrm{tot,sol}}}{\partial x^2}\right)\end{aligned} \tag{5.25}$$

which can be simplified as follows:

$$\frac{\partial \Gamma_{\mathrm{tot,sol}}}{\partial t} = \left(\frac{\dot{\delta}}{\delta}\right)\left(x\frac{\partial \Gamma_{\mathrm{tot,sol}}}{\partial x}+\Gamma_{\mathrm{tot,sol}}+\Gamma_{\mathrm{Pb}}\right)+\frac{\delta}{3(1+\mathcal{S}\delta/K_{H(\mathrm{loc})})}\left(\frac{\partial^2 \Gamma_{\mathrm{tot,sol}}}{\partial x^2}\right). \tag{5.26}$$

Note that Γ_{Pb} on the right hand side of this equation is normalized to unity in the dimensionless system considered here. However, it is convenient to continue to write it as Γ_{Pb} as a reminder of how this term originates. Note also that we have used here the more general form of the equation for the evolution of Γ_{tot}, which is the one for the local Henry isotherm. This is because the equation given can be easily transformed to the equivalent one for the global Henry isotherm merely by setting $K_{H(\mathrm{loc})} = 1$ and $\Gamma_{\mathrm{min}} = 0$.

To tackle Eq. (5.26), we use the separation of variables method. This ultimately results in a set of equations (see Eq. (5.44) along with Eq. (5.43) and Eqs. (5.45) to (5.49)) in a format that we can solve. For completeness, full details of how to derive these equations are included below.

5.6.1 Separation of variables

The separation of variables method has been used to express $\Gamma_{\mathrm{tot,sol}}$ as a series involving functions of position $(G_n(x))$ and time $(\tau_{\mathrm{tot},n}(t))$ as follows:

$$\Gamma_{\mathrm{tot,sol}} = \sum_{n=1}^{\infty} G_n(x)\tau_{\mathrm{tot},n}(t). \tag{5.27}$$

From this equation, solutions for $\Gamma_{\mathrm{tot,sol}}$ and hence for Γ_{tot} can be reconstructed. Now, by substitution of Eq. (5.27) into Eq. (5.26), the following equation is obtained:

$$\begin{aligned}\sum_{n=1}^{\infty} G_n(x)\dot{\tau}_{\mathrm{tot},n}(t) =& \frac{\dot{\delta}}{\delta}\left(x\sum_{n=1}^{\infty} G_n'(x)\tau_{\mathrm{tot},n}(t) + \sum_{n=1}^{\infty} G_n(x)\tau_{\mathrm{tot},n}(t) + \Gamma_{\mathrm{Pb}}\right) \\ &+ \frac{\delta}{3(1+S\delta/K_{H(\mathrm{loc})})}\left(\sum_{n=1}^{\infty} G_n''(x)\tau_{\mathrm{tot},n}(t)\right)\end{aligned} \tag{5.28}$$

where $\dot{\tau}_{\mathrm{tot},n}(t)$ is the derivative of $\tau_{\mathrm{tot},n}(t)$ with respect to time, $G_n'(x)$ and $G_n''(x)$ are first- and second-order derivatives of $G_n(x)$ with respect to position. We choose $G_n(x)$ to be trigonometric functions and hence write $\Gamma_{\mathrm{tot,sol}}$ as a Fourier series on a dimensionless interval $0 \leq x \leq 1$ [259]. Moreover, according to the symmetry of the system and the boundary conditions, we consider $G_n(x)$ as an expansion in terms of $\cos\left(\frac{n\pi}{2}x\right)$ with $n = 1, 3, 5, ...$ [260].

This transforms Eq. (5.27) to:

$$\Gamma_{\mathrm{tot,sol}} = \sum_{n=1}^{\infty} \cos\left(\frac{n\pi}{2}x\right)\tau_{\mathrm{tot},n}(t). \tag{5.29}$$

Thus, $\Gamma_{\mathrm{tot,sol}}$ can be considered as a Fourier series with $\tau_{\mathrm{tot},n}$ as a coefficient of the Fourier series at every instant t. Now, in order to substitute Eq. (5.29) into Eq. (5.28), we need to calculate, $\partial\Gamma_{\mathrm{tot,sol}}/\partial t$, $\partial\Gamma_{\mathrm{tot,sol}}/\partial x$ and $\partial^2\Gamma_{\mathrm{tot,sol}}/\partial x^2$ as follows:

$$\frac{\partial\Gamma_{\mathrm{tot,sol}}}{\partial t} = \frac{\partial}{\partial t}\sum_{n=1}^{\infty} \cos\left(\frac{n\pi}{2}x\right)\tau_{\mathrm{tot},n}(t) = \sum_{n=1}^{\infty} \cos\left(\frac{n\pi}{2}x\right)\dot{\tau}_{\mathrm{tot},n}(t) \tag{5.30}$$

$$\frac{\partial \Gamma_{\text{tot,sol}}}{\partial x} = \frac{\partial}{\partial x} \sum_{n=1}^{\infty} \cos\left(\frac{n\pi}{2}x\right) \tau_{\text{tot},n}(t) = \sum_{n=1}^{\infty} -\left(\frac{n\pi}{2}\right) \sin\left(\frac{n\pi}{2}x\right) \tau_{\text{tot},n}(t) \quad (5.31)$$

$$\frac{\partial^2 \Gamma_{\text{tot,sol}}}{\partial x^2} = \frac{\partial^2}{\partial x^2} \sum_{n=1}^{\infty} \cos\left(\frac{n\pi}{2}x\right) \tau_{\text{tot},n}(t) = \sum_{n=1}^{\infty} -\left(\frac{n\pi}{2}\right)^2 \cos\left(\frac{n\pi}{2}x\right) \tau_{\text{tot},n}(t). \quad (5.32)$$

Now, using orthogonality principles [261] and by multiplying Eq. (5.28) by $\cos\left(\frac{m\pi}{2}x\right)$ with $m = 1, 3, 5, ...$, and integrating it over $0 \leq x \leq 1$, the equation will be transformed into a set of first-order differential equations for $\tau_{\text{tot},n}$ with respect to time as follows [262, 263]:

$$\begin{aligned}
&\int_0^1 \Gamma_{\text{tot,sol}} \cos\left(\frac{m\pi}{2}x\right) \mathrm{d}x = \int_0^1 \sum_{n=1}^{\infty} \cos\left(\frac{m\pi}{2}x\right) \cos\left(\frac{n\pi}{2}x\right) \tau_{\text{tot},n}(t)\, \mathrm{d}x \\
&= \sum_{n=1}^{\infty} \frac{\tau_{\text{tot},n}(t)}{2} \int_0^1 \left[\cos\left(\frac{(m+n)\pi}{2}x\right) + \cos\left(\frac{(m-n)\pi}{2}x\right)\, \mathrm{d}x\right] \\
&= \sum_{n=1}^{\infty} \frac{\tau_{\text{tot},n}(t)}{2} \left[\frac{2}{(m+n)\pi} \sin\left(\frac{(m+n)\pi}{2}\right) + \frac{2}{(m-n)\pi} \sin\left(\frac{(m-n)\pi}{2}\right)\right]
\end{aligned} \quad (5.33)$$

where the terms on the right-hand side of Eq. (5.33) are zero when $n \neq m$, and $\tau_{\text{tot},m}/2$ when $n = m$. In addition,

$$\begin{aligned}
&\int_0^1 x \frac{\partial \Gamma_{\text{tot,sol}}}{\partial x} \cos\left(\frac{m\pi}{2}x\right) \mathrm{d}x \\
&= \int_0^1 \sum_{n=1}^{\infty} -\left(\frac{n\pi}{2}x\right) \cos\left(\frac{m\pi}{2}x\right) \sin\left(\frac{n\pi}{2}x\right) \tau_{\text{tot},n}(t)\, \mathrm{d}x.
\end{aligned} \quad (5.34)$$

When $n = m$, the respective terms on right-hand side of Eq. (5.34) become:

$$\int_0^1 -\left(\frac{m\pi}{2}x\right) \sin\left(\frac{m\pi}{2}x\right) \cos\left(\frac{m\pi}{2}x\right) \tau_{\text{tot},m}(t)\, \mathrm{d}x = -\frac{\tau_{\text{tot},m}}{4} \quad (5.35)$$

while, for $n \neq m$, the respective terms on the right-hand side of Eq. (5.34) become:

$$\begin{aligned}
&\sum_{n=1}^{\infty} -\left(\frac{n\pi}{2}\right)\left[\frac{2}{(m+n)^2\pi^2}\sin\left(\frac{(m+n)\pi}{2}\right)\right. \\
&-\frac{1}{(m+n)\pi}\cos\left(\frac{(m+n)\pi}{2}\right) \\
&\left.-\frac{2}{(m-n)^2\pi^2}\sin\left(\frac{(m-n)\pi}{2}\right)+\frac{1}{(m-n)\pi}\cos\left(\frac{(m-n)\pi}{2}\right)\right]\tau_{\mathrm{tot},n}(t).
\end{aligned} \tag{5.36}$$

Here Eq. (5.36) can be simplified as follows:

$$\sum_{n=1}^{\infty}\left[\frac{n}{2(m+n)}\cos\left(\frac{(m+n)\pi}{2}\right)-\frac{n}{2(m-n)}\cos\left(\frac{(m-n)\pi}{2}\right)\right]\tau_{\mathrm{tot},n}(t). \tag{5.37}$$

We know that $\cos\left(\frac{(m+n)\pi}{2}\right) = (-1)^{\left(\frac{m+n}{2}\right)}$ and $\cos\left(\frac{(m-n)\pi}{2}\right) = (-1)^{\left(\frac{m-n}{2}\right)}$. This indicates that the ratio between $\cos\left(\frac{(m+n)\pi}{2}\right)$ and $\cos\left(\frac{(m-n)\pi}{2}\right)$ is $(-1)^n$, where $n = 1, 3, 5, ...$, so $(-1)^n = -1$. Hence, Eq. (5.37) can be simplified as follows:

$$\sum_{n=1}^{\infty}\left[(-1)^{\left(\frac{m+n}{2}\right)}\left(\frac{mn}{m^2-n^2}\right)\right]\tau_{\mathrm{tot},n}(t), \tag{5.38}$$

and this is what we equate to the left hand side of Eq. (5.34). Thus arising from Eq. (5.34) we have diagonal terms of the form Eq. (5.35) and non-diagonal terms of the form Eq. (5.38).

Moreover,

$$\begin{aligned}
&\int_0^1 \frac{\partial^2\Gamma_{\mathrm{tot,sol}}}{\partial x^2}\cos\left(\frac{m\pi}{2}x\right)\mathrm{d}x \\
&=\sum_{n=1}^{\infty} -\int_0^1\left(\frac{n\pi}{2}\right)^2\cos\left(\frac{m\pi}{2}x\right)\cos\left(\frac{n\pi}{2}x\right)\tau_{\mathrm{tot},n}(t)\,\mathrm{d}x \\
&=\sum_{n=1}^{\infty} -\left[\frac{n^2\pi}{(m+n)}\sin\left(\frac{(m+n)\pi}{2}\right)+\frac{n^2\pi}{(m-n)}\sin\left(\frac{(m-n)\pi}{2}\right)\right]\left(\frac{\tau_{\mathrm{tot},n}(t)}{4}\right).
\end{aligned} \tag{5.39}$$

The right-hand side of Eq. (5.39) is zero when $n \neq m$, and $-m^2\pi^2\tau_{\mathrm{tot},m}/8$ when

$n = m$. Finally,

$$\int_0^1 \frac{\partial \Gamma_{\mathrm{tot,sol}}}{\partial t} \cos\left(\frac{m\pi}{2}x\right) \mathrm{d}x = \int_0^1 \sum_{n=1}^{\infty} \cos\left(\frac{m\pi}{2}x\right) \cos\left(\frac{n\pi}{2}x\right) \dot{\tau}_{\mathrm{tot},n}(t)\, \mathrm{d}x$$
$$= \sum_{n=1}^{\infty} \left[\frac{2}{(m+n)\pi} \sin\left(\frac{(m+n)\pi}{2}\right) + \frac{2}{(m-n)\pi} \sin\left(\frac{(m-n)\pi}{2}\right)\right] \frac{\dot{\tau}_{\mathrm{tot},n}(t)}{2} \tag{5.40}$$

where the right-hand side of Eq. (5.40) is zero when $n \neq m$ and $\dot{\tau}_{\mathrm{tot},m}/2$ when $n = m$.

We also need to express Γ_{Pb} in terms of a Fourier series to substitute it in Eq. (5.26):

$$\Gamma_{\mathrm{Pb}} = \sum_{n=1}^{\infty} G_n^{\mathrm{Pb}} \cos\left(\frac{n\pi}{2}x\right). \tag{5.41}$$

Now, we perform the same Fourier projection procedure for Γ_{Pb} to obtain the Fourier components (G_n^{Pb}) as follows:

$$\int_0^1 \Gamma_{\mathrm{Pb}} \cos\left(\frac{m\pi}{2}x\right) \mathrm{d}x = \sum_{n=1}^{\infty} \int_0^1 G_n^{\mathrm{Pb}} \cos\left(\frac{m\pi}{2}x\right) \cos\left(\frac{n\pi}{2}x\right) \mathrm{d}x \tag{5.42}$$

where the right-hand side of Eq. (5.42) is zero when $n \neq m$ and is $G_m^{\mathrm{Pb}}/2$ when $n = m$. In the dimensionless system, the surfactant surface concentration at the Plateau border is always unity ($\Gamma_{\mathrm{Pb}} = 1$), thus:

$$G_m^{\mathrm{Pb}}/2 = \left(\frac{2}{m\pi}\right) \sin\left(\frac{m\pi}{2}\right), \tag{5.43}$$

where for odd values of m as considered here, $\sin\left(\frac{m\pi}{2}\right)$ alternates between 1 and -1.

Here, upon substituting Eqs. (5.33), (5.34), (5.39), (5.40) and (5.43) into Eq. (5.26) and rearranging, it transforms to a system of first-order differential equations with respect to t. As a consequence, we write Eq. (5.28) in tensorial notation as below:

$$\dot{\tau}_{\mathrm{tot},m} = 2\left[\frac{\dot{\delta}}{\delta}\left(x\Gamma'_{mn} + \Gamma_{mn}\right) + \frac{\delta}{3(1 + \mathcal{S}\delta/K_{H(\mathrm{loc})})}\Gamma''_{mn}\right] \tau_{\mathrm{tot},n} + 2\frac{\dot{\delta}}{\delta} G_m^{\mathrm{Pb}}/2 \tag{5.44}$$

where ${}_{x}\Gamma'_{mn}$, Γ_{mn} and Γ''_{mn} are matrices and are defined as follows:

$$ {}_{x}\Gamma'_{mn} = {}_{x}\Gamma'^{\mathrm{D}}_{mn} + {}_{x}\Gamma'^{\mathrm{ND}}_{mn} \tag{5.45} $$

$$ {}_{x}\Gamma'^{\mathrm{D}}_{mn} = \begin{cases} -\frac{1}{4} & \text{if } n = m \\ 0 & \text{if } n \neq m \end{cases} \tag{5.46} $$

$$ {}_{x}\Gamma'^{\mathrm{ND}}_{mn} = (-1)^{\left(\frac{m+n}{2}\right)} \left(\frac{mn}{m^2 - n^2} \right) \tag{5.47} $$

where superscript indices D and ND refer to diagonal and non-diagonal terms, respectively. It can be seen from Eq. (5.47) that the non-diagonal terms are anti-symmetric. In addition,

$$ \Gamma_{mn} = \begin{cases} \frac{1}{2} & \text{if } n = m \\ 0 & \text{if } n \neq m \end{cases} \tag{5.48} $$

$$ \Gamma''_{mn} = \begin{cases} -\frac{m^2\pi^2}{8} & \text{if } n = m \\ 0 & \text{if } n \neq m \end{cases} \tag{5.49} $$

so these involve diagonal terms only.

This set of equations can be readily solved numerically, but to obtain a solution, an initial condition is required. As surfactants are assumed here to be uniformly distributed on the undeformed interfaces [45], we can assume that $\Gamma_{\mathrm{tot,sol}}(x, 0) = \Gamma_{\mathrm{tot},0} - \Gamma_{\mathrm{tot,Pb}}$, where the initial $\Gamma_{\mathrm{tot,Pb}}$ is $1 + \mathcal{S}$ and where $\Gamma_{\mathrm{tot},0}$ is the initial condition in the film. Using these values, an initial condition for each component $(\tau_{\mathrm{tot},n}|_{t=0})$ can be determined as discussed below.

5.6.2 Initial condition for the spectral method

To cast the initial condition in the form of a Fourier series, we proceed as follows:

$$\Gamma_{\mathrm{tot,sol}}|_{t=0} = \sum_{n=1}^{\infty} \cos\left(\frac{n\pi}{2}x\right) \tau_{\mathrm{tot},n}|_{t=0}. \tag{5.50}$$

Following the same procedure that we used to take a Fourier expansion of $\Gamma_{\mathrm{tot,Pb}}$ or analogously of Γ_{Pb} (see e.g. Eq. (5.43)), we obtain:

$$\tau_{\mathrm{tot},m}|_{t=0} = \frac{4\left(\Gamma_{\mathrm{tot},0} - \Gamma_{\mathrm{tot,Pb}}\right)}{m\pi} \sin\left(\frac{m\pi}{2}\right). \tag{5.51}$$

This can also be expressed in terms of the dimensionless initial amount of surfactant adsorbed on the surface (Γ_0) rather than in terms of the initial total amount of surfactant ($\Gamma_{\mathrm{tot},0}$). To do this, we use Eq. (4.22) from the main text. Also, dimensionless $\Gamma_{\mathrm{tot,Pb}}$ at the initial instant equals $1 + \mathcal{S}$ as we have already mentioned, and dimensionless δ (which appears in Eq. (4.22)) at the initial time equals unity. That simplifies Eq. (5.51) to the following equation:

$$\tau_{\mathrm{tot},m}|_{t=0} = \frac{4(1 + \mathcal{S}/K_{H(\mathrm{loc})})\left(\Gamma_0 - 1\right)}{m\pi} \sin\left(\frac{m\pi}{2}\right). \tag{5.52}$$

Here m is just an arbitrary variable. Thus, to obtain the initial $\tau_{\mathrm{tot},n}$ within equation Eq. (5.52), we simply replace m by n.

To summarise, we now have a set of equations in dimensionless form which can be used to compute evolution of surfactant on and within the film in a foam fractionation system with reflux. However, these equations contain a number of dimensionless parameters (amongst them solubility $\mathcal{S}$, local Henry constant $K_{H(\mathrm{loc})}$, and also scaled film thickness δ, which depends in turn on a film drainage parameter V_R, see Eq. (4.4) in the main text). To determine the actual values of all those dimensionless parameters, and also to relate the dimensionless system back to the original dimensional one,

we first need estimates of all relevant dimensional parameters. This is done in what follows.

5.7 Selection of simulation parameters

Dimensional parameters used in this study have been taken from relevant literature, such as Vitasari et al. [1], Weaire and Hutzler [38], Durand and Stone [165], Chang et al. [202], and are summarized in Table 5.1. Then these parameters were nondimensionalized and dimensionless values used for simulation purposes (see Table 5.2). The sources of some of the key parameters are discussed below.

The critical micelle concentration (CMC) of SDS is reported to be around $8.2\,\mathrm{mol\,m^{-3}}$ at ambient temperature ($25^{\circ}\mathrm{C}$) [73, 93, 234, 235]. Thus, we assume a typical bulk concentration of the Plateau border to be $8\,\mathrm{mol\,m^{-3}}$, which is just less than the CMC. We have used the surface excess data versus bulk concentration reported by Nilsson [247] which were obtained from a direct measurement method using a radiotracer. Using these data, the corresponding Γ_{Pb} for the assumed c_{Pb} then becomes $4.6 \times 10^{-6}\,\mathrm{mol\,m^{-2}}$.

Shear viscosity of the liquid and equilibrium surface tension at the Plateau border are taken to be $10^{-3}\,\mathrm{Pa\,s}$ and $38 \times 10^{-3}\,\mathrm{N\,m^{-1}}$, respectively, as reported by Shen et al. [243]. The Gibbs elasticity of SDS is determined at various concentrations by a few studies [165, 264]. Although Gibbs elasticity is actually variable and depends on surface concentration, it is possible to consider a roughly constant Gibbs elasticity for a smaller range of concentration changes. Thus, we set the Gibbs elasticity ($\mathcal{G}$) in this study to be as reported by Durand and Stone [165], namely $40{\times}10^{-3}\,\mathrm{N\,m^{-1}}$. SDS diffusivity coefficient ($\mathcal{D}$) is also reported by Shen et al. [243] and Liu and Shen [198] to be around $8 \times 10^{-10}\,\mathrm{m^2\,s^{-1}}$.

It has been reported by Durand and Stone [165] that a typical initial film half-thickness

is $20 \times 10^{-6}\,\mathrm{m}$. However, estimates can vary because, according to Reynolds equation Eq. (5.3), films thin quite quickly at the beginning and then the thinning rate slows down. Given this, we will consider a film half-thickness of $5 \times 10^{-6}\,\mathrm{m}$ somewhat smaller than the value reported by Durand and Stone [165]. This ensures that the surfactant has the opportunity to diffuse quickly across the film, and the assumption of small $\mathrm{Pe}\,\Delta$ which underpins the entire model used here is satisfied. Film half-length and Plateau border radius of curvature have also been taken from Breward and Howell [40]: values are reported in Table 5.1.

Using the parameters in Table 5.1 and the definitions in Sec. 4.2.1 in main text, the value for $\mathrm{Pe}\,\Delta$ turns out to be 0.25 (see Table 5.2), which is a small parameter. In addition, Δ/Pe is calculated to be 4×10^{-6}. That verifies that longitudinal diffusion is indeed negligible. Moreover, the film drainage velocity parameter V_R (definition in Sec. 4.2.1) turns out to be 0.0063 (again see Table 5.2), which is a small parameter.

A number of other parameters within Table 5.1 and Table 5.2 are sensitive to surfactant adsorption behaviour. As we will be using two different approaches to calculate adsorption isotherms for SDS, an explanation of how the various parameters are obtained comes next.

5.8 Estimating global and local Henry isotherms for SDS

A schematic of the local and global Henry isotherms can be seen in Fig. 5.1. In this figure, a Langmuir adsorption isotherm is fitted to the experimental SDS adsorption data taken from Nilsson [247]. The dimensional Langmuir parameter $\bar{K}_L$ and maximum surface excess $\bar{\Gamma}_m$ obtained from these data are reported in Table 5.1. Using the dimensional c_{Pb} and Γ_{Pb} also reported in Table 5.1, we can compute dimensional

Table 5.1: Dimensional parameters taken from Vitasari et al. [1], Weaire and Hutzler [38], Durand and Stone [165], Chang et al. [202], Shen et al. [243].

Dimensional Parameters	Symbol	Value	Unit
Characteristic time scale	$\mu L^2/\mathcal{G}\delta_0$	0.125	s
Film half-length	L	5×10^{-3}	m
Initial film half-thickness	δ_0	5×10^{-6}	m
Liquid viscosity	μ	1×10^{-3}	$\mathrm{Pa\,s}$
Surfactant surface concentration at the Plateau border	Γ_{Pb}	4.6×10^{-6}	$\mathrm{mol\,m^{-2}}$
Bulk concentration in the Plateau border	c_{Pb}	8	$\mathrm{mol\,m^{-3}}$
Initial surfactant surface concentration on the film for global Henry isotherm	$\Gamma_{0(\mathrm{glob})}$	2.3×10^{-6}	$\mathrm{mol\,m^{-2}}$
Initial surfactant surface concentration on the film for local Henry isotherm	$\Gamma_{0(\mathrm{loc})}$	4.398×10^{-6}	$\mathrm{mol\,m^{-2}}$
Initial surfactant concentration in the film	c_0	4	$\mathrm{mol\,m^{-3}}$
Radius of curvature of the Plateau border	a	5×10^{-4}	m
Surface tension at the Plateau border	γ_{Pb}	38×10^{-3}	$\mathrm{N\,m^{-1}}$
Gibbs parameter	$\mathcal{G}$	40×10^{-3}	$\mathrm{N\,m^{-1}}$
Diffusivity coefficient	$\mathcal{D}$	8×10^{-10}	$\mathrm{m^2\,s^{-1}}$
Langmuir parameter	$\bar{K}_L$	1.3	$\mathrm{m^3\,mol^{-1}}$
Maximum surface concentration	Γ_m	5.05×10^{-6}	$\mathrm{mol\,m^{-2}}$
Global Henry constant	$\bar{K}_{H(\mathrm{glob})}$	575×10^{-9}	m
Local Henry constant	$\bar{K}_{H(\mathrm{loc})}$	50.5×10^{-9}	m
Minimum surface concentration for local Henry isotherm	$\bar{\Gamma}_{\mathrm{min}}$	4.2×10^{-6}	$\mathrm{mol\,m^{-2}}$

parameters relevant to approximate isotherms that will replace the Langmuir isotherm. The relevant parameters are defined in Sec. 5.4 and include a global Henry constant $\bar{K}_{H(\mathrm{glob})}$, a local Henry constant $\bar{K}_{H(\mathrm{loc})}$ and a minimum surface concentration $\bar{\Gamma}_{\mathrm{min}}$.

Dimensional values can also be converted to dimensionless form, with values reported in Table 5.2. The values for local and global Henry constants become 8.77×10^{-2} and unity, respectively. In addition, the dimensionless Langmuir parameter K_L and dimensionless Γ_{min} (see Sec. 5.5) are calculated to be 10.4 and 0.9123, respectively. Moreover, using the assumed dimensional δ_0, c_{Pb} and Γ_{Pb}, the solubility parameter ($\mathcal{S}$) is estimated (see Eq. (4.3) in main text) to be 8.696 for SDS using both global and local Henry isotherms.

Table 5.2: Dimensionless parameters, calculated using the data from Table 5.1. For compactness of notation, some of the dimensionless quantities here ($\Gamma_{0(\mathrm{glob})}$, $\Gamma_{0(\mathrm{loc})}$ and c_0) are denoted with the same symbol as their dimensional analogues.

Dimensionless Parameters	Symbol	Value
Initial surfactant surface concentration on film for global Henry isotherm	$\Gamma_{0(\mathrm{glob})}$	0.5
Initial surfactant surface concentration on film for local Henry isotherm	$\Gamma_{0(\mathrm{loc})}$	0.9561
Initial surfactant bulk concentration in film	c_0	0.5
Initial total amount of surfactant for global Henry isotherm	$\Gamma_{\mathrm{tot},0(\mathrm{glob})}$	4.848
Initial total amount of surfactant for local Henry isotherm	$\Gamma_{\mathrm{tot},0(\mathrm{loc})}$	5.304
Solubility parameter	$\mathcal{S}$	8.696
(Initial) aspect ratio	Δ	1×10^{-3}
Péclet number	Pe	250
Coefficient of diffusion term in x direction	Δ/Pe	4×10^{-6}
Reciprocal of coefficient of diffusion term in z direction	$\mathrm{Pe}\,\Delta$	0.25
Film drainage velocity parameter	V_R	0.0063
Dimensionless Langmuir parameter	K_L	10.4
Local Henry constant	$K_{H(\mathrm{loc})}$	8.77×10^{-2}
Minimum surface concentration for local Henry isotherm	Γ_{min}	0.9123

For both approximate isotherms, the dimensionless initial bulk concentration is set to be half of the Plateau border bulk concentration ($c_0 = 0.5$). However, in the local Henry isotherm, the dimensionless initial surface concentration ($\Gamma_{0(\mathrm{loc})}$) is then calculated to be 0.9561 (using Eq. (4.19) in main text), which is greater than the equivalent amount for the global Henry isotherm ($\Gamma_{0(\mathrm{glob})}$) which equals 0.5 (using Eq. (4.16). Moreover, initial $\Gamma_{\mathrm{tot,Pb}}$, which is $1 + \mathcal{S}$ using both isotherms, is calculated to be 9.696, while $\Gamma_{\mathrm{tot},0}$ for global and local Henry isotherms, is determined to be 4.848 and 5.304, respectively (see Eq. (4.21) in main text).

The above results mean that in the case of the local Henry isotherm, the surface already has an amount of surfactant close to its maximum capacity. As a result, there is little spatial variation of surfactant along the surface, and hence less driving force for Marangoni flow. As a result, even though the local Henry isotherm case has a

greater initial amount of surfactant $\Gamma_{\mathrm{tot},0}$, its subsequent rate of increase is relatively slow compared to the global Henry isotherm case, which is an effect also seen in the main text Sec. 4.4.6 for overall surfactant on the film for instance.

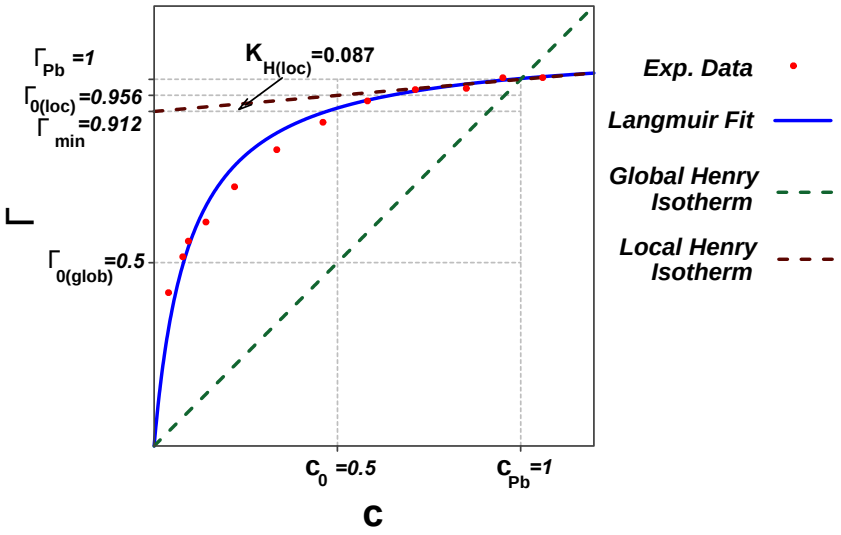

Figure 5.1: Global and local Henry isotherms plotted for a Langmuir fit using experimental adsorption data for SDS [247]. Dimensional values of c_{Pb} and Γ_{Pb} are reported in Table 5.1, but when data are converted to dimensionless form as is done here, c_{Pb} and Γ_{Pb} are both scaled to unity. Meanwhile c_0 is dimensionless initial bulk concentration, and $\Gamma_{0(\mathrm{glob})}$ and $\Gamma_{0(\mathrm{loc})}$ are dimensionless initial surfactant surface concentrations for global and local Henry isotherms respectively. Note that $\Gamma_{0(\mathrm{glob})}$ is identical to c_0 by construction, but $\Gamma_{0(\mathrm{loc})}$ is larger. Other parameters used can be found in Table 5.2.

5.9 Quasisteady state for soluble surfactant

Consider a case with a global Henry isotherm. Marangoni flow typically dominates at early times because the film drainage is typically weak. Later on, though, Marangoni flow decays, and eventually, there is a quasisteady balance between Marangoni flow and film drainage. However, this balance is expected to depend on the parameters $\mathcal{S}$ and V_R. In Sec. 5.9.1, it is explained what conditions are needed in order to achieve a quasisteady state in the case of a soluble surfactant. Then Sec. 5.9.2 presents an approximate analytical solution for the quasisteady behaviour of dimensionless Γ. The results obtained from this section are utilised in Sec. 4.4.5 and in Fig. 4.11.

5.9.1 Balance between Marangoni flow and film drainage for a quasisteady state

Here, as mentioned, we consider the quasisteady state using the global Henry isotherm. We know that for $\mathcal{S} \ll 1$, surfactant effectively acts as insoluble. For the case of insoluble surfactants, we can find a solution to the quasisteady state elsewhere [1]. However, large $\mathcal{S}$ tends to weaken the influence of the Marangoni flow, which slows down the evolution of Γ_{tot}. This comes about as follows. Even though flow induced by Marangoni stress causes the gradients of surfactant surface concentration to decay, when surfactant escapes from the surface into the bulk, the impact upon the surface is lessened, and so these gradients now decay more gradually. On the other hand, film drainage is typically weak (i.e. the parameter V_R is small) regardless of whether surfactant is soluble or insoluble. As a result, the competition between Marangoni flow and film drainage can be expressed in terms of $\mathcal{S}$ and V_R. Two different cases can be considered. The first case is when $\mathcal{S}$ is so large, that $\mathcal{S}\,V_R \gg 1$. The other case has $\mathcal{S} > 1$, but $\mathcal{S}\,V_R$ is still small compared to unity.

In the first case, solubility has caused the influence of Marangoni to weaken so much that it is even weaker than the drainage term. Hence, the system is dominated by film drainage. This case is also studied by Vitasari et al. [1], so we will not consider it in detail here. In Vitasari et al. [1], the film is divided into two zones, one of them away from the edge of the film where an assumption of no Marangoni flow is applicable, and near the edge of the film adjacent to the Plateau border, where the Marangoni flow becomes important again.

By contrast, the other case mentioned earlier with $\mathcal{S} > 1$ but $V_R \ll 1$ (and with $\mathcal{S}\,V_R$ still remaining much less than unity) behaves differently. In this case, Marangoni (although weakened by solubility) remains the dominant effect at early times. It is only later on that drainage might become relevant after Marangoni flow decays (and as already noted, this decay might be particularly slow when the surfactant is soluble).

The case of the local Henry isotherm turns out to be similar, except that the parameter $\mathcal{S}$ is now replaced by $\mathcal{S}/K_{H(\mathrm{loc})}$, where $K_{H(\mathrm{loc})}$ is typically a parameter that is rather smaller than unity. As a result, this causes $(\mathcal{S}/K_{H(\mathrm{loc})})V_R \gg 1$, which indicates the film drainage now dominates Marangoni flow. In spite of this, as discussed earlier, there may still be a zone near the Plateau border in which Marangoni retains importance. Nonetheless any Marangoni-driven evolution of that zone is now slowed down so much, that it would only tend to impact after a very long time, which is unlikely to be relevant on the scale of residence times in a fractionation column. Hence in what follows we consider the global Henry isotherm case.

5.9.2 Power series expansion for the quasisteady evolution of Γ

Here we work out an approximate solution for the evolution of surfactant surface concentration (Γ) within the quasisteady state. The reason why we develop a solution for Γ rather than Γ_{tot} is that the boundary conditions of Γ are time independent, making it easier to identify quasisteady behaviour.

The solution for the quasisteady evolution of Γ can be obtained by expanding Γ in powers of V_R, which is a small parameter. We start from the equation for the evolution of surfactant surface concentration using the global Henry isotherm (see Eq. (4.27) in the main text):

$$\frac{\partial \Gamma}{\partial t} = (1+\mathcal{S}\delta)^{-1}\left(\frac{\dot{\delta}}{\delta}\Gamma + \left(\frac{\delta}{3}\right)\frac{\partial^2 \Gamma}{\partial x^2}\right) + \frac{\dot{\delta}}{\delta}\left(x\frac{\partial \Gamma}{\partial x}\right). \tag{5.53}$$

Now, we expand the solution for Γ in the following form:

$$\Gamma = 1 + V_R\,\Gamma_1 + V_R^2\,\Gamma_2 + ... \tag{5.54}$$

where $V_R \ll 1$ and where Γ_1 and Γ_2 are functions to be determined. Here clearly, we are expanding Γ in powers of V_R. We assume that at a long time, there is no explicit

dependence of Γ on time (only implicit dependence due to Γ depending on δ, with δ depending on time via Eq. (4.8)). Hence Eq. (5.53) gives:

$$\begin{aligned}
&- V_R\delta^3\left(V_R\frac{\partial\Gamma_1}{\partial\delta}+V_R^2\frac{\partial\Gamma_2}{\partial\delta}\right)\\
&=(1+\mathcal{S}\delta)^{-1}\left[-V_R\delta^2(1+V_R\Gamma_1+V_R^2\Gamma_2)+\frac{\delta}{3}\left(V_R\frac{\partial^2\Gamma_1}{\partial x^2}+V_R^2\frac{\partial^2\Gamma_2}{\partial x^2}\right)\right]\\
&- V_R\delta^2\,x\left(V_R\frac{\partial\Gamma_1}{\partial x}+V_R^2\frac{\partial\Gamma_2}{\partial x}\right).
\end{aligned}\tag{5.55}$$

Collecting terms at order V_R gives:

$$0=(1+\mathcal{S}\delta)^{-1}\left(-\delta^2+\frac{\delta}{3}\frac{\partial^2\Gamma_1}{\partial x^2}\right)\tag{5.56}$$

which requires:

$$\frac{\partial^2\Gamma_1}{\partial x^2}=3\delta\tag{5.57}$$

from which it follows:

$$\Gamma_1=\frac{3}{2}\delta(x^2-1).\tag{5.58}$$

This satisfies required boundary conditions $\partial\Gamma_1/\partial x|_{x=0}=0$, and $\Gamma_1=0$ at $x=1$.

Note that $\partial\Gamma_1/\partial\delta=\Gamma_1/\delta$. Note further that $x\,\partial\Gamma_1/\partial x=2\Gamma_1+3\delta$. Gathering terms at order V_R^2 now gives:

$$-\delta^2\Gamma_1=(1+\mathcal{S}\delta)^{-1}\left(-\delta^2\Gamma_1+\frac{\delta}{3}\frac{\partial^2\Gamma_2}{\partial x^2}\right)-\delta^2(2\Gamma_1+3\delta)\tag{5.59}$$

from which it follows:

$$\frac{\partial^2\Gamma_2}{\partial x^2}=(3\delta\,(2\Gamma_1+3\delta)-3\delta\,\Gamma_1)(1+\mathcal{S}\delta)+3\delta\,\Gamma_1.\tag{5.60}$$

The equation simplifies to:

$$\frac{\partial^2\Gamma_2}{\partial x^2}=6\delta\,\Gamma_1\left(1+\frac{\mathcal{S}\delta}{2}\right)+9\delta^2(1+\mathcal{S}\delta)\tag{5.61}$$

which upon substituting for Γ_1 simplifies again to:

$$\frac{\partial^2 \Gamma_2}{\partial x^2} = 9\delta^2 x^2 \left(1 + \frac{\mathcal{S}\delta}{2}\right) + \frac{9\delta^3 \mathcal{S}}{2}. \tag{5.62}$$

This then integrates to:

$$\Gamma_2 = \frac{3}{4}\delta^2(x^4 - 1)\left(1 + \frac{\mathcal{S}\delta}{2}\right) + \frac{9}{4}\mathcal{S}\delta^3(x^2 - 1) \tag{5.63}$$

which satisfies boundary conditions $\partial\Gamma_2/\partial x|_{x=0} = 0$, and $\Gamma_2 = 0$ at $x = 1$.

Here, as was expected, Γ_1 is negative, which means the film drainage causes Γ to fall below unity. Note that Γ_1 is entirely independent of $\mathcal{S}$, so any $\mathcal{S}$ dependence of the solution for Γ only appears at order V_R^2, not at order V_R.

Again, Γ_2 is negative, so the second-order correction makes Γ even smaller than $1 + V_R\Gamma_1$. Moreover, Γ_2 exhibits dependence on $\mathcal{S}$: increasing $\mathcal{S}$ makes the magnitude of Γ_2 larger, i.e. makes Γ even smaller. However, in the case of $\mathcal{S} > 1$, one might have to wait until quite long time to see this quasisteady state (because the entire evolution is slowed down). It can be seen from Eq. (5.63) that the largest difference between the first-order and the second-order correction, for given $\mathcal{S}$ and given δ, happens at $x = 0$. This difference can be obtained as $V_R^2(\frac{21}{8}\mathcal{S}\delta^3 + \frac{3}{4}\delta^2)$. Cases with nonzero $\mathcal{S}$ (i.e. soluble surfactant, with the $\mathcal{S}$ value reported in Table 5.2) therefore exhibit much bigger difference from the first-order correction than the insoluble surfactant case does. A comparison between the approximate analytical solution and the numerical solution can be found in Fig. 4.8.

Chapter 6

Transport of convected soluble surfactants on and within the foam film in the context of a foam fractionation process

"This chapter consists of published material: [H. Rajabi, R. Rosario, P. Grassia, "Transport of convected soluble surfactants on and within the foam film in the context of a foam fractionation process," Chemical Engineering Science, vol.281, 119100, 2023. https://doi.org/10.1016/j.ces.2023.119100]"

Abstract

This study models convective transport of soluble surfactant in a foam fractionation system with reflux. Owing to reflux, initial surfactant concentration in films is lower than in Plateau borders. Marangoni flows and film drainage flows arise convecting surfactant both on the film surface and in the bulk. An interface is set up within the film bulk called a separatrix: this divides two regions of uniform surfactant concentration,

one with concentration equal to that of the initial film and one with concentration equal to that in the Plateau border. The evolution of the separatrix is tracked to determine surfactant recovery and enrichment for the film. Surfactant lean films benefit most from Plateau-border-to-film mass transfer induced by reflux. However for films that are initially comparatively surfactant rich, recovery might actually decrease at long times owing to film drainage. Nonetheless surfactant lean films and those containing surfactant with only moderate solubility benefit from Plateau-border-to-film mass transfer caused by reflux even despite film drainage.

Highlights

- Foam fractionation with reflux is modelled for a convected soluble surfactant
- Convection occurs on film surface and within bulk of foam films
- Separatrix divides material in bulk from newly arrived material from Plateau border
- Solutions that are leaner in surfactant benefit from reflux
- Foam drainage can cause surfactant recovery to decrease at longer times

6.1 Introduction

Foam separation techniques have been identified as alternatives to more conventional separation processes such as ion exchange and ultrafiltration [265], particularly because of their efficiencies in dealing with dilute aqueous systems [266]. Due to these advantages, these methods have recently been finding their place in various sectors such as pharmaceutical, environmental-related and biochemical industries [267–275]. One of the foam separation methods which is the subject of the present study is foam fractionation. Foam fractionation is a physicochemical process in which surface-active

chemicals are separated from an aqueous solution by adsorption on bubbles rising in a column [183]. As there are no solvents other than water existing during this process, it can be considered as a "green" process in sustainability terms [30]. Some of the advantages of foam fractionation are low capital cost, low energy requirement and subsequently low operational costs [265]. As a result, there have been various studies carried out in this field [14, 15, 21–23, 30, 95, 102, 214, 276–278].

Some of these studies show a potential benefit of foam fractionation by returning part of the so called foamate back into the fractionation column, known as reflux [26]. Reflux, effectively puts into contact a rising stream of leaner bottom solution and a falling stream of enriched collapsed foamate [35]. Rich liquid is then travelling through a network of Plateau borders contacting the foam films. Thus, there is an opportunity for further enrichment of the foamate [1, 2, 26, 33–35, 82, 94, 106].

Plateau borders referred to above specifically are liquid channels embedded within the foam where three films meet [38, 279], and as we have said, they form a network. Due to often having a higher liquid volume compared to the liquid in the films adjacent to them, Plateau borders may to an extent be considered as surfactant reservoirs [1]. Plateau borders can therefore in principle transfer significant surfactant to adjacent films as reflux proceeds. However to achieve this surfactant transfer, flow must occur from Plateau border to film. For the purpose of this work, we use the term "surfactant" to encompass any surface-active molecule including big, bulky molecules like proteins which are often targeted for separation by fractionation [22, 23, 95, 277]. These then are the molecules that, for reflux to be effective, must flow from Plateau border to film.

Although, in line with previous work [1, 2], we focus the discussion here on foam fractionation with reflux, the results are also relevant to foam fractionation operated in another mode, namely stripping mode [91, 94, 103]. In stripping mode a feed is provided to a fractionation column and flows down through Plateau borders, contacting foam films as it flows. As with reflux, surfactant is again transferred from Plateau

borders to films. However the objective now is not so much to enrich the films, but rather to remove surfactant from the liquid in the Plateau borders. This mode of operation would for instance be relevant for removing a surface active contaminant from a wastewater stream. For the most part in what follows, for simplicity we discuss reflux, even though stripping is also relevant.

Despite the potential advantages of foam fractionation over other separation methods, in view of the complicated flows that arise in the presence of reflux, the process of foam fractionation with reflux requires more research. In particular, it is useful to have a modelling study which can predict the extent to which reflux permits foam films to become enriched in surfactant, under different sets of conditions encountered during fractionation. This can subsequently help us to design and operate a more efficient fractionation column in the future. Specifically the model to be used in the present work has been built upon two previous modelling studies on film scale surfactant transport during foam fractionation with reflux [1, 2], and in what follows we review them.

The main effect that was included in those studies was Marangoni flow taking surfactant rich material from Plateau border into the film. Moreover, film drainage which thins the film and which causes a flow towards the Plateau border, opposes Marangoni flow on the surface. In Vitasari et al. [1], the authors worked out the evolution of an insoluble surfactant over just the surface of a foam film. They also discussed a so called quasi-steady state for cases in the presence of film drainage, in which a balance on the film surface eventually happens between Marangoni flow and film drainage. However, the fact that surfactants have some level of solubility was neglected. Solubility must however affect the transport behaviour, which thereby affects the foam fractionation process.

Later, Rajabi and Grassia [2] considered the solubility of surfactants within a foam film in addition to their presence on the surface. Marangoni-driven and film drainage-driven surfactant transport again occur, but transport now occurs not just on the foam

film surface, but in the bulk of the foam film as well. However the study of Rajabi and Grassia [2] focussed on a particular limit in which surfactant also diffuses rapidly across the foam film. This limit could be quantified in terms of dimensionless groups corresponding to a small $\mathrm{Pe}\,\Delta$ number, where Pe denotes Péclet number (measuring the ratio between convective and diffusive transport) and Δ is the film thickness to film length aspect ratio. It was identified by Rajabi and Grassia [2] that this particular limit would be a reasonable approximation for smaller surfactant molecules (which tend to have comparatively high diffusivity coefficients) being transported across particularly thin films. What was found by Rajabi and Grassia [2] is that the impact of Marangoni flow is slowed down due to the solubility, compared to the case considering insoluble surfactants. The reason for this slow down was found to be surfactant escaping into the bulk of the film, once the Marangoni flow transported it from the Plateau border onto the film. It was also confirmed that the quasi-steady state condition introduced by Vitasari et al. [1] can also occur, after a sufficiently long time: Marangoni-driven and film drainage-driven transport are then effectively in balance.

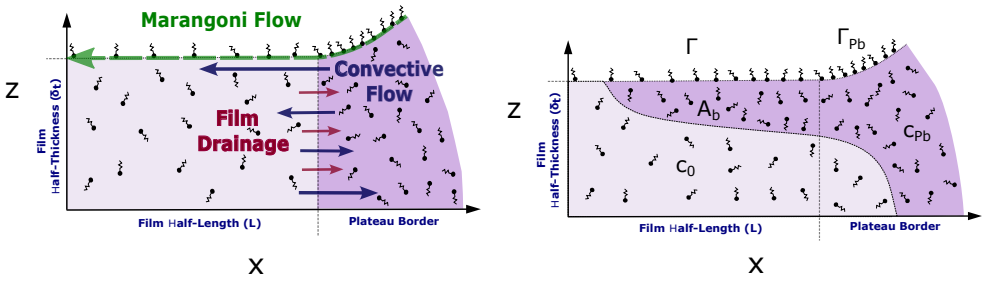

(a) Initial stage **(b)** Later stage

Figure 6.1: Diagram of a foam film in the large $\mathrm{Pe}\,\Delta$ limit. Here $A_b(t)$ is at time t the area in the film with the Plateau border's surfactant concentration c_{Pb} as opposed to the initial film concentration c_0. The figure is not drawn to scale: in reality film half-length is orders of magnitude larger than film half-thickness.

However, there could be an opposite limit in which $\mathrm{Pe}\,\Delta$ is relatively large. This limit is relevant in cases with relatively small diffusivity coefficient, e.g. for bigger molecules such as proteins [280]. It could also be relevant for foam films shortly after they are formed, such that the film is still in the process of draining, and hence could be quite some way from a final thickness. This limit is the subject of and the novel

contribution of the present study (see Fig. 6.1). Diffusion across the film is now relatively slow and, as a consequence, transport from the film surface to the film bulk is relatively slow. Hence, what happens on the surface turns out to be identical to what has been discussed by Vitasari et al. [1] (albeit distinct from the system considered by Rajabi and Grassia [2] which has small rather than large $\mathrm{Pe}\,\Delta$). Flow is affected by competition between Marangoni-driven and film drainage-driven transport on the surface. However the Marangoni and film drainage flow fields are not just confined to the surface but exist in the bulk as well. Since, similar to Rajabi and Grassia [2], surfactants are now treated as soluble and present in the bulk, the aforementioned flow fields necessarily convect surfactant in the bulk. In the large $\mathrm{Pe}\,\Delta$ limit considered here, convection (not diffusion) is the dominant transport mechanism in the bulk. Indeed, as we will see, convection plays an important role in transferring surfactants from the bulk of the Plateau border into the bulk of the film.

A point to emphasise is that, since the flow on the surface here is identical to what was found in the prior work by Vitasari et al. [1], the flow field in the bulk also turns out to be the same. In effect therefore the results to be obtained here could have been obtained by post-processing the results of Vitasari et al. [1]. However such post-processing was never attempted by Vitasari et al. [1]: for an insoluble surfactant as considered in that work, any motion in the bulk is irrelevant to surfactant transport. The novelty of the present work is therefore to consider soluble surfactant, for which transport in the bulk is certainly relevant, surfactant in the bulk now being passively convected.

In the model considered here, we start with a situation in which the Plateau border is surfactant rich and the film is surfactant lean (Fig. 6.1a). Marangoni stresses offset by film drainage set up a convective flow field. Convection then carries surfactant rich material from Plateau border to film and carries surfactant lean material from film to Plateau border (Fig. 6.1b). The net effect is that the film is enriched. This then is the process we wish to model.

Note that what we are trying to describe here (analogously to the work of Vitasari et al. [1], Rajabi and Grassia [2]) is specifically the microscale process of surfactant transfer between an individual Plateau border and an adjacent foam film. We are not endeavouring at this stage to incorporate this microscale behaviour into a fractionation model at the entire process scale. In a typical fractionation column there will be a multitude of foam films and a multitude of Plateau borders, and the surfactant content of each depends on where in the fractionation column they are located, and also on the time elapsed since the fractionation process started. Sufficiently long after start up, a continuous fractionation system with reflux should settle into a steady state operation. However the time scale for that to happen presumably relies on residence times of flowing foam films passing up through the entire column and likewise residence times of flowing liquid (within Plateau borders) passing down through the column. This is not however what is focussed upon here.

The intention here is to keep the models as simple as possible, while still endeavouring to capture the main transport processes that are expected to occur. The models used by Vitasari et al. [1], Rajabi and Grassia [2] were likewise greatly simplified, and analogous simplifications will be employed here (see also Sec. 6.2.3 for further discussion of some of the simplifications employed).

Two-dimensional rather than fully three-dimensional flow fields will for instance be considered. Given however that films in a real foam have different shapes and sizes, capturing the full three-dimensional geometry of the flow on each and every film would be challenging in any case. Films are also to be treated as having a spatially uniform thickness, albeit with that thickness changing over time. There are of course models in the literature that study the fluid mechanics of a draining foam film in a much more sophisticated fashion accounting for non-uniformities in thickness (see e.g. Yeo et al. [51], Frankel and Mysels [222], Joye et al. [223]): film surfaces are no longer flat leading also to pressure jumps across them. The film shape and the surfactant mass

transport must then be determined together. These sorts of complications have been neglected in previously mentioned work on foam fractionation [1, 2] and will be neglected again here also. Indeed we assume the film geometry and how it evolves is known, and focus just on surfactant mass transport. As we have alluded to though, the models to be used here still capture key physics, such as Marangoni flow, drainage flow and convective surfactant transport.

One aspect that will however differ here from previous work are the physicochemical parameters that we assume. Previous work [1, 2] utilised parameters relevant to the common surfactant SDS. For the simulations here however, we use parameters relevant to the protein beta-lactoglobulin (β-LG) [281]. As a much bigger molecule than SDS, this has lower diffusivity [280], and as a result can readily meet criteria for having large $\mathrm{Pe}\,\Delta$ which is the basis of our model. Physicochemical data for β-LG are readily available, since it is a widely studied protein in foam and interface science [76, 149, 152, 158, 159, 161, 162, 205, 280, 282–284] and it has also been used in the context of foam fractionation [24, 61]. As has been mentioned though, we will often use the generic term "surfactant" to keep the discussion more general: the model we present requires large $\mathrm{Pe}\,\Delta$ but is not tied to any specific material, provided parameter values are available.

This study is laid out as follows. Sec. 6.2 outlines the mathematical theory used in the study of convected soluble surfactant transport, which is based on adapting the works of Vitasari et al. [1] and Rajabi and Grassia [2] to this new convection-dominated system. In Sec. 6.2 equations are mainly presented in dimensionless form, but the nondimensionalisation process itself is presented in Sec. 7.1 of the supplementary material. Technical details of numerical algorithms employed are also relegated to supplementary material. Algorithms already used by Rajabi and Grassia [2] can be adapted supplemented with some additional features, so any discussion of algorithms in the supplementary material is focussed on those additional features. In particular the chal-

lenge of carrying out the calculations at early times is discussed Sec. 7.2. Other than that, the numerical approach is similar to what Vitasari et al. [1] and Rajabi and Grassia [2] have already done. However here algorithms take account also of mass transfer by convection in the bulk of the foam film, and a discussion of that can be found in Sec. 7.3 of the supplementary material: convection in the bulk did not need to be addressed in the work of Vitasari et al. [1], but it certainly must be considered here, so the discussion of Sec. 7.3 covers that. In addition, Sec. 7.4 deals with selecting simulation parameters and benchmarking. Returning to the main text, results and discussion are presented in Sec. 6.3, with some supplementary results in Sec. 7.5. Finally Sec. 6.4 deals with conclusions of the study.

6.2 Mathematical model for convected soluble surfactant transport

This study models convected soluble surfactant transport on and within a foam film. We first present in Sec. 6.2.1 essential dimensionless groups used to carry out the study. Derivation of the velocity fields in the bulk and on the surface of the foam film are discussed elsewhere [1]. However, due to their importance within the current study, they are also mentioned here in brief (Sec. 6.2.2). Mass transfer equations are presented in Sec. 6.2.3. As will be discussed in detail later, due to the Marangoni-driven and film drainage-driven convective flows in the bulk of the film, two regions form within the bulk. One region remains at the initial bulk surfactant concentration and the other region has a higher bulk concentration corresponding to the concentration found in the bulk of the Plateau border. The novel contribution of the present work is to model, simulate and analyse the evolution of these separate regions in the bulk and the subsequent effect on the fractionation process performance. We assess the size of these two regions by examining a cross section of the foam film, looking at the total area of the cross section of the film and also the areas corresponding to each of these

regions. The details of computing these two regions and the surfactant they contain can be found in Secs. 6.2.4 and 6.2.5. Finally Sec. 6.2.6 deals with overall measures of fractionation performance, namely recovery and enrichment.

6.2.1 Dimensionless groups

Definitions of dimensionless groups that have been used in this study are identical to the ones used by Rajabi and Grassia [2]. However here we are looking at a different parameter regime. Hence we present the dimensionless groups in brief.

The first dimensionless group is Péclet number. It is obtained [285] based on balancing surfactant transport by Marangoni effects along the film in the x-direction, and diffusive transport of surfactant across the film, in the z-direction (the directions are as indicated in Fig. 6.1), and can be expressed as follows:

$$\mathrm{Pe} = \frac{\mathcal{G}\delta_0/\mu L}{\mathcal{D}/\delta_0} \tag{6.1}$$

where $\mathcal{G}$ is Gibbs parameter (that measures sensitivity of surface tension to surface concentration) [157, 166], δ_0 is initial film half-thickness, μ is liquid viscosity, L is film half-length and $\mathcal{D}$ is diffusion coefficient (in this case for β-LG). In fractionation applications, Péclet number is typically a relatively large number, especially for proteins that due to their bigger molecule sizes have smaller diffusion coefficients [286] (see Table 7.3 in the supplementary material for a typical value of Pe). Meanwhile, Δ is the initial aspect ratio between film half-thickness and film half-length, and is defined as:

$$\Delta = \delta_0/L \tag{6.2}$$

where δ_0 is initial film half-thickness, and L is film half-length. In a typical foam film Δ is a relatively small parameter (see Table 7.3). However here, as can be seen in Sec. 7.4.1 (and in particular in Table 7.3), in the particular limit of interest, the product

of Pe and Δ remains a relatively large number which is in line with our assumptions.

Another parameter relevant to this study is the solubility parameter $\mathcal{S}$. Solubility parameter describes the typical amount of dissolved surfactant relative to the amount of surfactant on the surface, and is defined as below:

$$\mathcal{S} = \frac{\delta_0}{\Gamma_{\mathrm{Pb}}/c_{\mathrm{Pb}}} \tag{6.3}$$

where δ_0 is initial film half-thickness, Γ_{Pb} is surfactant surface concentration at the Plateau border, and c_{Pb} is surfactant bulk concentration at the Plateau border: both Γ_{Pb} and c_{Pb} are dimensional quantities here, although later on we will also define dimensionless analogues of them. Note that for a given Γ_{Pb} an insoluble or almost insoluble surfactant will have a very small c_{Pb} and hence a very small $\mathcal{S}$, but a more soluble surfactant will have a larger c_{Pb} and hence a larger $\mathcal{S}$ value. Formally $\Gamma_{\mathrm{Pb}}/c_{\mathrm{Pb}}$ is a depletion length (extent of a bulk region containing an equivalent amount of surfactant as the surface itself), and $\mathcal{S}$ is then the ratio of the actual geometric extent to that depletion length. As Table 7.3 makes clear, in systems of interest $\mathcal{S}$ turns out to be a dimensionless parameter on the order of magnitude of unity, and we will allow it to vary during the course of this study.

Finally dimensionless film drainage velocity parameter (V_R) is the ratio between velocity of film drainage under the action of capillary suction and typical velocity of Marangoni convection at the start of the process, which can be expressed as follows:

$$V_R = \frac{2\,\delta_0 \gamma_{\mathrm{Pb}}}{3\,a\mathcal{G}} \tag{6.4}$$

where δ_0 is the initial film half-thickness, γ_{Pb} is surface tension at the Plateau border, a is the Plateau border's radius of curvature and $\mathcal{G}$ is Gibbs elasticity. As Table 7.3 makes clear, V_R is typically a small parameter. At least early on in the process then, film drainage is a weaker effect than Marangoni flow. Moreover since the drainage velocity

parameter is low (in other words, film drainage flow is slow), effects of drainage require quite some time before impacting the system.

To summarise, Table 7.3 gives the typical values of dimensionless groups, and is based on dimensional parameter values obtained from literature (see Tables 7.1 and 7.2).

In line with what has been done in Vitasari et al. [1] and Rajabi and Grassia [2], in addition to defining the above dimensionless groups, we also make all the system's variables dimensionless. The process of nondimensionalisation is again similar to Vitasari et al. [1] and Rajabi and Grassia [2] and can be found in Sec. 7.1. Briefly, we scale horizontal coordinates by the film half-length and vertical coordinates using the film's initial half-thickness. In addition, the crossectional areas within the bulk of the foam film are nondimensionalised with respect to the initial film area. Meanwhile, we scale surfactant concentrations in the bulk and on the surface of the film by surfactant concentrations in the bulk and on the surface of the Plateau border, respectively. Velocities along the film have also been nondimensionalised using the Marangoni velocity scale, but transverse velocities have an additional factor of aspect ratio included in the scaling. Time is nondimensionalised using the ratio between the film half-length and the Marangoni velocity scale. Note from Table 7.2 that the characteristic time scale is actually rather short, significantly shorter in fact than was the case in Rajabi and Grassia [2], owing to focussing on not quite so thin films in the present work which admit higher velocities along them. Certainly typical film residence times in a foam fractionation column are likely to be many dimensionless time units.

Note that from now on, we only use dimensionless variables unless specified otherwise.

6.2.2 Velocity fields

To work out the velocity fields in the bulk and on the surface, we use the same approach taken by Vitasari et al. [1]. The physical mechanisms that drive the flow fields are Marangoni stresses and film drainage. Details of these mechanisms are discussed

elsewhere [2]. To derive the velocity fields, a lubrication approximation has been used which leads to the dimensionless velocity fields in the bulk as follows:

$$u = -x\frac{\dot{\delta}}{\delta} + \left(\frac{\delta}{6} - \frac{z^2}{2\delta}\right)\frac{\partial \ln \Gamma}{\partial x} \tag{6.5}$$

$$w = z\frac{\dot{\delta}}{\delta} + \left(\frac{z^3}{6\delta} - \frac{z\delta}{6}\right)\frac{\partial^2 \ln \Gamma}{\partial x^2} \tag{6.6}$$

where u and w are dimensionless vertical and horizontal velocity components in the bulk and Γ is dimensionless surfactant surface concentration. Here also δ is dimensionless film half-thickness and $\dot{\delta}$ is dimensionless rate of change of δ with time. By the same token and using Eq. (6.5) with $z = \delta$, the velocity field u_s on the surface becomes:

$$u_s = -x\frac{\dot{\delta}}{\delta} - \frac{\delta}{3}\left(\frac{\partial \ln \Gamma}{\partial x}\right). \tag{6.7}$$

Note that in the present model, even though we are considering a soluble surfactant, the velocity fields here are unchanged from those considered by Vitasari et al. [1] for an insoluble surfactant. This is because (unlike the work of Rajabi and Grassia [2] which allowed surfactant to diffuse readily between bulk and surface), here it turns out that surfactant fails to diffuse off or onto the surface on time scales of interest. Thus as far as setting up the velocity field is concerned, the surfactant might as well be insoluble. What is different from Vitasari et al. [1] is that this same velocity field, established as a result of conditions on the surface, now transports surfactant both on the surface and in the bulk. Hence, we move on to the mass transfer equation.

6.2.3 Mass transport equation in a foam film

The general dimensionless mass transfer equation for surfactant in the bulk can be expressed as follows [220]:

$$\frac{\partial c}{\partial t} + \frac{\partial (uc)}{\partial x} + \frac{\partial (wc)}{\partial z} = \frac{\Delta}{\mathrm{Pe}}\frac{\partial^2 c}{\partial x^2} + \frac{1}{\mathrm{Pe}\,\Delta}\frac{\partial^2 c}{\partial z^2} \tag{6.8}$$

where, c is surfactant concentration in the bulk (which recall is made dimensionless here with respect to the analogous concentration in the Plateau border), Pe is Péclet number and Δ is initial aspect ratio. In the limit of interest of the present study, $\mathrm{Pe}\,\Delta$ (see Table 7.3) is large and $\mathrm{Pe}\,/\Delta$ is extremely large. Hence diffusion terms in both x and z directions are negligible. Moreover, using the continuity equation for an incompressible liquid, Eq. (6.8) turns out to give $\mathrm{D}c/\mathrm{D}t = 0$, which means that following an element of fluid, there will be no change in the concentration with time.

The general mass transfer equation on the surface is as follows [2]:

$$\frac{\partial \Gamma}{\partial t} + \frac{\partial (u_s \Gamma)}{\partial x} = -\frac{\mathcal{S}}{\mathrm{Pe}\,\Delta} \left.\frac{\partial c}{\partial z}\right|_{z=\delta} \tag{6.9}$$

where Γ is surfactant concentration on the film surface (again made dimensionless using the analogous Plateau border surface concentration) and $\mathcal{S}$ is the solubility parameter defined earlier. The term on the right-hand side of the above equation is the diffusive flux from the bulk to the surface (in the z direction). It turns out to be negligible due to the large $\mathrm{Pe}\,\Delta$ assumption (with $\mathcal{S}$ being order unity here). This then confirms that, at least on the time scale of interest for Marangoni flow and film drainage, there is not any diffusive transport from surface to bulk. As Eq. (6.9) shows, the larger the value of $\mathcal{S}$, the more likely it is that bulk-to-surface transport becomes relevant, but here $\mathrm{Pe}\,\Delta$ is much larger than $\mathcal{S}$, so convection along the surface is much faster than any bulk-to-surface transport (which ultimately requires diffusion to be active).

As already alluded to, as far as mass transport on the surface is concerned, the system is then equivalent to the insoluble case which has already been considered by Vitasari et al. [1]. Combination of Eq. (6.9) and Eq. (6.7) and using the mentioned assumptions in Vitasari et al. [1] leads to the following mass transfer equation on the surface:

$$\frac{\partial \Gamma}{\partial t} = \left(\frac{\delta}{3}\right) \frac{\partial^2 \Gamma}{\partial x^2} + \frac{\dot{\delta}}{\delta} \left(x \frac{\partial \Gamma}{\partial x} + \Gamma \right). \tag{6.10}$$

Eq. (6.10) has initial and boundary conditions defined as follows:

$$\begin{aligned} &\Gamma(x, t=0) = \Gamma_0 \\ &\Gamma(x=1, t) = 1 \\ &\delta(t=0) = 1 \\ &u_s(x=0, t) = 0 \Rightarrow \left.\frac{\mathrm{d}\Gamma}{\mathrm{d}x}\right|_{x=0} = 0, \end{aligned} \tag{6.11}$$

where in particular $\Gamma_0 < 1$ so that the film starts off leaner than the Plateau border. The value of δ evolves according to $\dot{\delta} = -V_R \delta^3$ [2] and hence

$$\delta = (1 + 2V_R\, t)^{-1/2} \tag{6.12}$$

where recall V_R is a relatively small parameter, so δ evolves comparatively slowly.

As can be seen from Eq. (6.10), the evolution of surfactant on the surface is due to a competition between Marangoni flow and film drainage. Eq. (6.10) is a parabolic partial differential equation. A method of solving this equation numerically has been applied, specifically a "spectral method" [287] (details can be found in Rajabi and Grassia [2]).

As was mentioned previously, this study uses a similar set of simplifying assumptions used previously by Vitasari et al. [1] and Rajabi and Grassia [2] (two-dimensional system, lubrication approximation, film surface remains flat, etc.).

One significant simplification that we highlight, is the assumed boundary condition in Eq. (6.11) that the Plateau border surface remains at (dimensionless) surface concentration unity. To justify this, it is important to recall a physical picture of how foam fractionation with reflux operates. Foam films rise up through the fractionation column, whilst simultaneously reflux liquid drains down through a network of Plateau borders, and we are looking at the mass exchange process between the two. For sufficient reflux flow, it can be the case that there is more liquid in the Plateau borders

than in the films [1]. Similarly there can be more liquid flux (and also more surfactant flux) in the Plateau borders than in the films [278]. As a result, the relative change in surfactant content in the comparatively surfactant lean films should be greater than the relative change in surfactant content in the surfactant rich Plateau borders. Even though the Plateau border surfaces do lose surfactant to the films, the surfactant remaining on them is carried down under gravity, and so is replaced by additional surfactant arriving from higher up. In effect therefore Plateau borders are approximated here as being surfactant reservoirs. Ultimately though what the boundary condition in Eq. (6.11) attempts to capture is the notion that Plateau borders are richer in surfactant than films.

Here of course since surfactant is soluble, we do not consider just surfactant transport on surfaces, but also surfactant transport in the bulk. That said, even though the surfactant is soluble here, we reiterate that there is no transfer between bulk and surface on the time scale of interest due to the large $\mathrm{Pe}\,\Delta$ assumption. Convection between the bulk of the film and the bulk of the Plateau border is still permitted, but to the extent that the Plateau border is treated as a surfactant reservoir, what we must focus upon here is surfactant convection in the bulk of the film. Treating a Plateau border as a reservoir, as is done here, is arguably more relevant for foam fractionation with reflux than for foam fractionation in stripping mode (see Sec. 6.1 for a discussion of stripping mode; removing surfactant from Plateau borders such that they become leaner is an inherent part of stripping mode). Even when reflux is considered though, it is necessary to establish what is happening on the surface first, and then use those surface conditions to determine how surfactant is transported in the bulk.

On the surface though, as was the case with Vitasari et al. [1], we have already mentioned that there is a competition between Marangoni flow and film drainage. Due to the dominance, at least early on, of Marangoni flow, there is a flow on the surface in the direction from the Plateau border towards the centre of the film.

The physics that the model describes is as follows. In general a gradient in surfactant

concentration is present on the surface. This gradient then is what sets up a flow field, and that flow field is what causes a convective flow also in the bulk. Comparatively close to the surface, the bulk flow carries fluid from the Plateau border towards the film. This fluid is richer in surfactant than the film itself, as reflux in foam fractionation tends to keep the Plateau border's concentration (c_{Pb}) higher than the bulk film concentration (c_0). Here in fact we work in a dimensionless system in which c_{Pb} becomes unity, and c_0 also turns out (as we discuss later) to be the same as dimensionless Γ_0 (with $\Gamma_0 < 1$ here). Thus a new region in the bulk with the Plateau border's concentration appears, and is carried towards the centre of the film. However to compensate the incoming flow from the Plateau border, a leaner concentration fluid exits the film into the Plateau border. The latter flow is not from locations near the surface ($z = \delta$), but instead mainly from locations closer to the midplane of the film ($z = 0$) with concentration c_0 as we have said.

As can be seen in Fig. 6.1b, the film is divided into two regions with distinct concentrations. One region has area A_b. The other has area $A_t - A_b$, where A_t here is the total area, or more specifically A_t is the total area of a half-length and half-thickness of film. Owing to the way in which we make the system dimensionless, in fact A_t is identical to δ as given by Eq. (6.12), or if the film is not draining, A_t and δ are fixed at unity. In any case, once we know these areas A_b and $A_t - A_b$ we can also figure out how much surfactant is in the film. The boundary that divides these regions is to be called the separatrix, and to determine what the areas are we need to work out what the evolution of the separatrix is.

6.2.4 Calculating evolution of separatrix

As can be seen from Fig. 6.1a, the boundary which separates bulk and Plateau border concentrations is initially a vertical line which passes through $x = 1$ at the edge of the film (where it meets the Plateau border). As already alluded to, we call this boundary a separatrix. However during the foam fractionation process with reflux, the shape of

this boundary changes continuously due to the effects of convective flow in the bulk. As mentioned, close to the surface, a flow of uniform concentration (in dimensionless form, $c_{\mathrm{Pb}} \equiv 1$) is pulled towards the centre of the film, while around the midplane of the film, fluid (with lower concentration c_0) moves out of the film towards the Plateau border. In the no film drainage case, the amount of fluid entering matches the amount leaving. However in the case with film drainage, the amount leaving is always slightly more than the amount entering. Nonetheless, since the fluid leaving tends to be leaner in surfactant than the fluid entering, there is still a possibility to use reflux to recover more surfactant in the film.

As mentioned previously, we need a model for how the separatrix evolves and then knowing the shape of the separatrix we must calculate the areas A_b and $A_t - A_b$. As a result, we track a number of initially uniformly distributed material points on the separatrix with time. The general equations for how these material points evolve and hence how the separatrix is convected are as below (the details of implementing these equations numerically can be found in supplementary Sec. 7.3):

$$\mathrm{d}x_{\mathrm{sep}}/\mathrm{d}t = u(x_{\mathrm{sep}}, z_{\mathrm{sep}}) \tag{6.13}$$

$$\mathrm{d}z_{\mathrm{sep}}/\mathrm{d}t = w(x_{\mathrm{sep}}, z_{\mathrm{sep}}) \tag{6.14}$$

where x_{sep} and z_{sep} are x and z positions of the material points on the separatrix and u and w are velocity fields in the x and z directions. However at initial time, the velocity field Eq. (6.5) turns out to be singular, leading instantaneously to an infinite velocity [220]. Hence, at early times, the numerics are difficult to handle and we need a bespoke method to evolve the separatrix early on. The relevant method is addressed in supplementary Sec. 7.2.

Having defined the separatrix, it is now easy to calculate the size of the respective regions containing surfactant with the Plateau border's concentration and containing

surfactant with the initial bulk concentration. This is discussed next.

6.2.5 Total amount of surfactant present in the foam film

In what follows we determine the size of the bulk regions containing surfactant with the Plateau border's concentration and containing surfactant with the initial bulk concentration, the regions themselves being sketched in Fig. 6.1b. The amount of surfactant in the bulk then immediately follows. However this does not represent the total amount of surfactant in the film, since we must also account for surfactant on the surface. This is again determined in what follows.

At a specific dimensionless time t, the total dimensionless amount of surfactant contained in the film, S_T, is the sum of the surfactant S_S on the film surface and S_B in the film bulk

$$S_T = S_S + S_B. \tag{6.15}$$

In particular S_S can be obtained from the following formula

$$S_S = \int_0^1 \Gamma \, \mathrm{d}x. \tag{6.16}$$

Here, S_S is identical to what has previously been worked out in Vitasari et al. [1]. However the dimensionless amount of surfactant S_B contained in the film bulk is a new concept not considered by Vitasari et al. [1] and can be calculated as follows:

$$S_B = \mathcal{S} \int_0^1 \int_0^1 c \, \mathrm{d}x \, \mathrm{d}z \tag{6.17}$$

where $\mathcal{S}$ is solubility parameter (Eq. (6.3)), c is dimensionless concentration of surfactant in the bulk. Note in particular the prefactor $\mathcal{S}$ appearing in this equation which follows owing to the way the system has been nondimensionalised. An analogous prefactor appears in the work of Rajabi and Grassia [2].

Within Eq. (6.17), c has different values either side of the separatrix (in dimensionless variables, unity on one side, and c_0 on the other), but in each of those regions c itself is spatially uniform. Hence in each region, c can be taken outside the integration, and the integrals then merely compute areas, respectively A_b and $A_t - A_b$. At the initial instant, $A_b = 0$ and $S_B = \mathcal{S}\, c_0 A_t$. Immediately after that, A_b starts to grow and $A_t - A_b$ falls. Note also the difference between c in this study and in Rajabi and Grassia [2]: $c(x,t)$ in Rajabi and Grassia [2] was in instantaneous equilibrium with $\Gamma(x,t)$, but here it is not, remaining fixed instead at either unity or c_0.

Thus far in this section we have considered surface S_S and bulk S_B contributions separately. However it is important also to understand how they are coupled. This is discussed in Secs. 6.2.5.1 and 6.2.5.2.

6.2.5.1 Extent of coupling between surface and bulk

Above we mentioned a difference between the present model and the work of Rajabi and Grassia [2]. Note another important difference from Rajabi and Grassia [2] here. The flow fields that convect surfactant in the bulk here can be determined entirely from knowledge of Γ and δ (see Eqs. (6.5) and (6.6)). However Γ and δ both evolve in the present model entirely independently of solubility $\mathcal{S}$ as Eqs. (6.10) and (6.12) make clear. Consequently there is only one-way coupling here: the surface drives the bulk, but the bulk does actually not influence the surface. The separatrix shape that we compute is $\mathcal{S}$ independent, as is the integral term in Eq. (6.17). The only $\mathcal{S}$ dependence in S_B therefore is due to the multiplicative prefactor $\mathcal{S}$ outside the integral. This means that we can solve for the separatrix shape just once, and we then know S_B for all $\mathcal{S}$ values: in effect we are post-processing the results of Vitasari et al. [1] here. Of course the value of S_S here is also independent of $\mathcal{S}$ and so must be the same S_S as computed by Vitasari et al. [1] for an insoluble case. Since S_T is nothing more than the sum of S_S and S_B, it can also be obtained for all $\mathcal{S}$ by doing a computation just once.

The situation is rather different from the regime considered by Rajabi and Grassia [2]. Coupling was much stronger there such that the bulk could also affect the surface. The evolution equation for Γ that resulted then depended explicitly on $\mathcal{S}$, so to evaluate the various amounts of surfactant present (S_S, S_B and S_T) it was necessary to compute a separate solution for each different value for $\mathcal{S}$, a rather more laborious process.

6.2.5.2 Relating bulk surfactant with surface surfactant

Returning to the problem at hand, thus far we have explained how to obtain the amount of surfactant in the bulk and the amount of surfactant on the surface, but not specifically how it might be possible to relate the two. In order to relate the surface and bulk surfactant concentrations, generally speaking we need an adsorption isotherm [93, 229, 230]. Especially when we are dealing with proteins rather than simple surfactant molecules, isotherms can take rather complicated forms [159, 163, 288]. Specifically what the isotherm does [289] is to relate the equilibrium amount of surfactant on the surface to the equilibrium amount of surfactant in the bulk.

However, in the dimensionless system with which we are working, the equilibrium amount of surfactant on the surface of the Plateau border and in the bulk of the Plateau border are both unity by construction. Any isotherm that we select must respect that. Even with that constraint though, there are still different isotherms that could be used. However following Rajabi and Grassia [2], we will simplify the model and use what we call a global Henry adsorption isotherm. The global Henry isotherm in dimensionless form then requires that at equilibrium $\Gamma = c$. However a feature of the surfactant mass transfer model employed in the present work is that there is no general requirement at any instant for there to be equilibrium between surface and bulk. Equilibrium might still apply between the surface and a subsurface immediately adjacent to it. However diffusion is considered too slow on times scales of interest for equilibrium across the entirety of the bulk to be achieved.

Hence, in the specific model used here, we only ever utilise the isotherm to relate the amount of surfactant on the film surface initially with the amount in the film bulk initially. Using the global Henry isotherm this turns out to be in dimensionless form $\Gamma_0 = c_0$, where Γ_0 and hence c_0 are necessarily less than unity: owing to reflux through the Plateau borders, the film starts off leaner in surfactant than the Plateau border. Any other isotherm could be chosen and would just give us a rather more complicated relation [159, 163, 288] between Γ_0 and c_0 (see Sec. 7.5 for an example). The requirement to have $\Gamma_0 < 1$ and $c_0 < 1$ in the dimensionless system here would however be retained.

By coupling the isotherm with the evolution with time of the separatrix shape, we now have a definitive formula for the amount of surfactant in the bulk, namely

$$S_B = \mathcal{S}[A_b + c_0(A_t - A_b)] = \mathcal{S}[A_b + \Gamma_0(A_t - A_b)] \tag{6.18}$$

where the global Henry isotherm has been assumed, i.e. c_0 is the same as Γ_0. We then use Eq. (6.16) to obtain S_S, and Eq. (6.15) to obtain S_T.

The way we proceed here is to set various different values for Γ_0. The value of Γ at any given position and time depends of course on Γ_0, but is, as we have mentioned, independent of the bulk, i.e. independent of $\mathcal{S}$. Since flow fields depend on Γ (Eqs. (6.5) and (6.6)), and since flow fields also advect the separatrix (Eqs. (6.13) and (6.14)), the areas A_b and $A_t - A_b$ at any instant depend on Γ_0 in a non-trivial way. Thus the way that S_B in Eq. (6.18) evolves over time is likewise affected by the value of Γ_0 in a non-trivial way. Meanwhile the evolution of S_S (Eq. (6.16)) depends on the instantaneous values of Γ which again are sensitive to the choice of Γ_0. Determining how the evolution of overall amount of surfactant S_T (i.e. the sum of S_S and S_B via Eq. (6.15)) is affected by different Γ_0 is therefore less straightforward than determining how the evolution of S_T is affected by different $\mathcal{S}$.

Having now quantified the amount of surfactant, in the next section we present how we

define recovery and enrichment of a fractionation process with respect to the parameters discussed earlier.

6.2.6 Recovery and enrichment

Recovery and enrichment are two quantities which are often used to evaluate the performance of a foam fractionation process [5, 33]. In this study, total amount of surfactant, S_T is a measure at any instant of the recovery per foam film (or in fact part of a foam film, as we are using film half-length and half-thickness in our model). It also can be converted to the conventional recovery definition by specifying the number of foam films leaving the fractionation column [2]. Meanwhile, enrichment is the ratio between surfactant concentration in the foamate to the initial feed solution concentration and hence, enrichment can be quantified as $S_T/(\mathcal{S}\, c_0 A_t)$, where $\mathcal{S}$ is solubility parameter (Eq. (6.3)), c_0 is initial solution concentration (and in our case is equal to Γ_0) and A_t is instantaneous cross sectional area of a film half-length and half-thickness. We can see from the form of the equations (Eqs. (6.15), (6.16) and (6.18)), enrichment and recovery are dependent on solubility parameter, initial surfactant concentration and film half-thickness (given via Eq. (6.12)). Results for recovery and enrichment will be discussed later (Sec. 6.3.6).

Now, having defined the model, we solve it numerically using the procedure that we have already established in previous work [2] along with some additional methodology to evolve the separatrix (see also supplementary Secs. 7.2 and 7.3) and the parameter values that we use are given in supplementary Tables 7.2 and 7.3 within Sec. 7.4.1. Benchmarking is also done within supplementary Sec. 7.4.2, so we turn now to results.

6.3 Results

In this section, results are discussed in the following order. We start by considering the evolution with time of the total amount of surfactant on the surface of a foam

film in Sec. 6.3.1. Then Sec. 6.3.2 discusses the evolution within the film bulk of the so called separatrix with time, while Sec. 6.3.3 explains the evolution with time of A_b/A_t, where A_b is the area of the region containing material initially in the Plateau border's bulk but then advected into the film. This is then normalised by the total cross sectional area A_t. The effects of initial surface concentration Γ_0, and solubility parameter $\mathcal{S}$, on the evolution of total amount of surfactant in the film S_T, measured relative to initial amount of surfactant $S_{T,0}$, are discussed in Sec. 6.3.4. We then analyse in Sec. 6.3.5 the effect of time evolution upon systems with various different initial surfactant concentrations and different solubility parameters. Then Sec. 6.3.6 considers recovery and enrichment in a foam fractionation process.

6.3.1 Evolution with time of the total amount of surfactant on the surface of a film

The evolution with time of the dimensionless amount of surfactant on the surface S_S (Eq. (6.16)), is simulated and plotted in Fig. 6.2. More specifically we plot $1 - S_S$, this being a quantity which we know decays over time. The evolution of S_S is the same as what happens for an insoluble surfactant and has previously been investigated by Vitasari et al. [1]. However, due to the effect that evolution of surfactant on the surface has on the advection of surfactants in the bulk, we discuss S_S here in brief. The results for the cases with no film drainage and with film drainage are displayed in Fig. 6.2a and Fig. 6.2b, respectively.

By comparing Fig. 6.2a with Fig. 6.2b, at early time, the evolution of S_S is very similar for the cases not including or including film drainage effects. This is to be expected from Vitasari et al. [1], due to the dominance of Marangoni flow on the surface of the film over any film drainage effects at early times. However, as time continues to evolve and Marangoni flow becomes weaker, the competition between Marangoni flow and film drainage in the case with film drainage (Fig. 6.2b) slows down the evolution

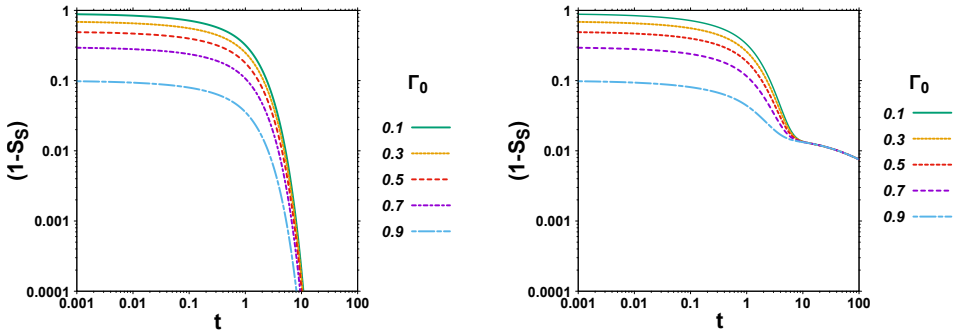

(a) No film drainage **(b)** With film drainage

Figure 6.2: Evolution with time of the dimensionless amount of surfactant on the film surface, S_S. Here, $1 - S_S$ is plotted for various Γ_0 versus time t in a log-log scale to emphasise the difference between the no film drainage and with film drainage case at late time. Values of other model parameters, e.g. V_R in the case with drainage, are as per Table 7.3.

of S_S slightly, compared to the no film drainage case (Fig. 6.2a). The main differences between the two cases are observed at later times though. In the case without film drainage (Fig. 6.2a), the surface evolves quickly towards a uniform surfactant distribution, in dimensionless form $\Gamma(x) \rightarrow \Gamma_{\mathrm{Pb}} \equiv 1$, with no surfactant concentration gradients remaining to keep pulling material onto the surface (hence $S_S = 1$). On the other hand, when film drainage is considered, S_S will only approach this final state rather more slowly. This is due to the fact that, at later times, a quasi-steady state between weak remaining Marangoni effects and slow film drainage is reached [1]. This prevents the surface from reaching a completely uniform concentration, at least as long as the film keeps draining.

Fig. 6.2 also shows that the parameter Γ_0 affects at least slightly the dimensionless time it takes for the film surface to reach a uniform surfactant distribution without film drainage. Here, as Γ_0 is increased, leading to less discrepancy between the Plateau border surface and the film surface, the time to reach a uniform surfactant distribution on the surface is less, albeit this time is only a weak function of Γ_0. On the other hand, in the case with film drainage it is apparent that the quasi-steady state once it is attained is independent of Γ_0, as the curves for all the different Γ_0 values collapse together.

6.3.2 Evolution with time of the separatrix shapes

Since in this study surfactants are considered to be soluble, they are present in the bulk too. Thus, it is necessary to understand how surfactants in the bulk are transported due to the advection flow driven by surfactant transport on the surface. The results presented in Fig. 6.3 reflect the passive advection of points in the separatrix, where recall the separatrix is the boundary separating material that has arrived from the Plateau border from material that was originally in the film. These material points are initially distributed along the line at the edge of the film ($x = 1$), but move due to the advective flow in the bulk, generated either by Marangoni stresses on the surface alone, e.g. the no film drainage case (Fig. 6.3a for $\Gamma_0 = 0.1$), or due to the interplay between those Marangoni stresses and film drainage, e.g. the film drainage case (Fig. 6.3b again for $\Gamma_0 = 0.1$). As mentioned already, in this study, transport in the bulk is considered to be purely advective, because surfactant diffusive transport from the surface to the film bulk has been neglected (large $\mathrm{Pe}\,\Delta$ limit).

Overall, it can be seen in Fig. 6.3 that the separatrix is pulled towards the the left, i.e. towards the centre of the film over time, at least at locations close to the surface ($z = \delta$). However for locations close to the midplane of the film ($z = 0$), it is pulled to the right over time and ultimately out of the film. This is caused mainly due to the effect of Marangoni flow which is leftward on the surface, and rightward near the midplane. Film drainage if present, also competes with Marangoni near the surface, but cooperates with Marangoni near the midplane.

Results for the case with no film drainage, in Fig. 6.3a, show that, at early times, Marangoni flow is rapid, so the separatrix evolves quickly initially. At later times, Marangoni flow becomes much slower as the surfactant surface concentration gradients weaken as a result of the gradual enrichment of surfactant on the film surface. The separatrix shape therefore evolves increasingly slowly over time, as Fig. 6.3a shows, until it reaches a final steady shape for which Marangoni effects are no longer present

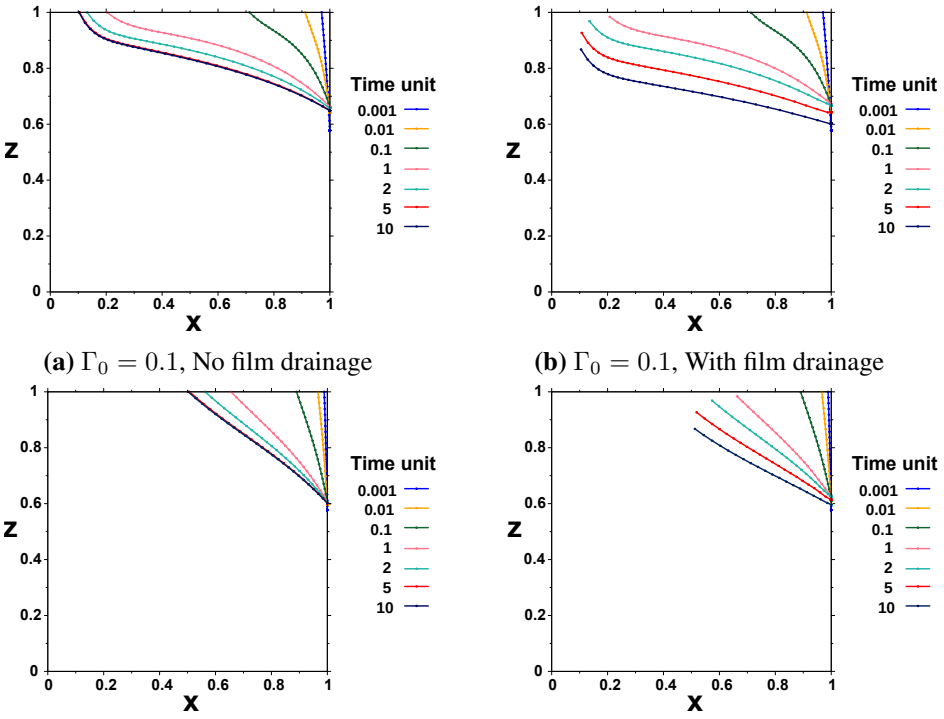

(a) $\Gamma_0 = 0.1$, No film drainage

(b) $\Gamma_0 = 0.1$, With film drainage

(c) $\Gamma_0 = 0.5$, No film drainage

(d) $\Gamma_0 = 0.5$, With film drainage

Figure 6.3: Evolution with time of the material points on the separatrix, assuming points initially equally spaced on the boundary separating the film and Plateau border bulks (initially at $x = 1$). The parameter values used here are taken from supplementary Tables 7.2 and 7.3.

because a surface uniformly covered in surfactant ($\Gamma \to \Gamma_{\mathrm{Pb}} \equiv 1$) is achieved. After that, there is no more convective exchange of material between the film and Plateau border.

In the case in which film drainage is included in the model along with Marangoni effects (Fig. 6.3b), at early times, flow due to Marangoni effects dominates film drainage. However as a result of an ongoing competition between Marangoni-driven flow and film drainage opposing it, the evolution of the separatrix shape is slightly slower.

Proceeding towards later times, the decrease in the vertical coordinate of the leftmost and topmost point in the separatrix (point at the film surface; see Fig. 6.3b) now shows the film becoming progressively thinner as time evolves, due to film drainage effects. This same leftmost and topmost separatrix point also of course migrates horizontally. However from about $t \approx 5$ onward, the material on the surface of the film is barely moving horizontally at all, due to film drainage and Marangoni effects coming into a

quasi-steady balance on the surface [1]. Although the top left of the separatrix then no longer moves leftwards, material points lower down in the separatrix (within the film bulk) are still moving rightwards towards the Plateau border, as a result of ongoing film drainage in the bulk. As well as moving rightwards though, these same points are also moving downwards and this is the main effect we see in Fig. 6.3b at later times.

In Figs. 6.3c and 6.3d we show analogous data but for $\Gamma_0 = 0.5$ (instead of $\Gamma_0 = 0.1$). The main effect we see is that the separatrix is pulled less strongly to the left as Γ_0 increases. There is also a weak effect in the z direction (evident by comparing the right hand end of the separatrix in Figs. 6.3c and 6.3d with the right hand end of the separatrix in Figs. 6.3a and 6.3b). At any given time, increasing Γ_0 seems to move the right hand end of the separatrix downward very slightly relative to cases with smaller Γ_0. However this is a much weaker effect than what is seen in the horizontal.

In summary, at early times, there is rapid surfactant exchange between the Plateau border and film bulks, dominated by Marangoni effects pulling material with dimensionless concentration $c_{\mathrm{Pb}} \equiv 1$ from the Plateau border into the film, at least for locations near the surface. Meanwhile for locations closer to the midplane of the film, material of dimensionless concentration c_0 (with $c_0 = \Gamma_0$ here) is pulled out of the film into the bulk of the Plateau border due to continuity. At later times, material inside the film is being pulled into the bulk of the Plateau border throughout, although locations near the midplane tend to be moving faster than those near the surface. As has been noted, different regions within the film have different concentrations, although those concentrations do not themselves evolve with time. As a result, by calculating just the areas of those regions we are able to calculate total amount of surfactant in the bulk of the film. Therefore in the next section we focus on these areas and how they evolve over time.

6.3.3 Evolution with time of area ratio A_b/A_t

In this section, the evolution with time of the area ratio A_b/A_t is presented. Recall that A_b here is the area within the film containing material that was initially in the bulk of the Plateau border. Meanwhile (see Sec. 6.2.3), the total area A_t has a straightforward evolution which is due to the film drainage: indeed in a no film drainage case, it is constant, equal to unity in the dimensionless system used here. Data are presented in Fig. 6.4. Specifically data for cases without film drainage and cases with film drainage are found in Fig. 6.4a and Fig. 6.4b, respectively.

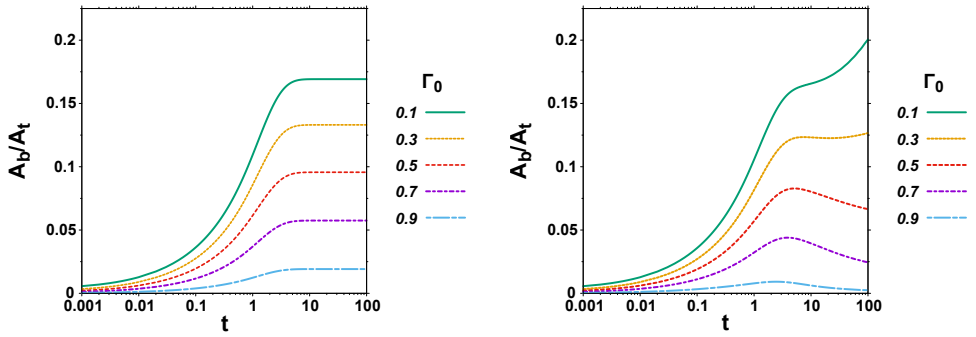

(a) No film drainage **(b)** With film drainage

Figure 6.4: Evolution with time of the dimensionless ratio A_b/A_t. The parameter values used here are taken from supplementary Tables 7.2 and 7.3.

Results with no drainage, with the value of A_t now equal to unity at all times, are shown in Fig. 6.4a. We see that A_b/A_t increases significantly at early times. At later times though, A_b/A_t eventually reaches a final steady value. The final steady value of A_b/A_t is dependent on the dimensionless initial uniform surfactant concentration along the film surface, Γ_0. Smaller values of Γ_0 (less surfactant initially on the film surface) will lead to higher values of A_b/A_t being achieved, i.e. more material being pulled from the Plateau border surface onto the film surface.

In the case where film drainage is included, A_b/A_t has a similar behaviour at early times (as observed in Fig. 6.4b), due to the dominance of Marangoni effects over film drainage effects early on. Indeed Marangoni effects manage to produce a significant amount of mass transfer even before the film has had time to drain substantially. How-

ever, as has also been observed in Secs. 6.3.1 and 6.3.2, the early time evolution is now slightly slower due to the competition between Marangoni flow and film drainage. Major differences in A_b/A_t for the two cases are however observed at late times, when the film drainage effect can no longer be neglected (see Fig. 6.4b). To analyse the effect of Γ_0 on A_b/A_t, it is helpful now to write the rate of change of A_b/A_t with time as follows:

$$\frac{\mathrm{d}}{\mathrm{d}t}\left(\frac{A_b}{A_t}\right) = \frac{1}{A_t}\left(\frac{\mathrm{d}A_b}{\mathrm{d}t} - \frac{A_b}{A_t}\frac{\mathrm{d}A_t}{\mathrm{d}t}\right). \tag{6.19}$$

As long as Marangoni flow dominates, $\mathrm{d}(A_b/A_t)/\mathrm{d}t$ is always positive, so that A_b/A_t increases with time. At this stage, both terms on the right hand side of Eq. (6.19), i.e. both $\mathrm{d}A_b/\mathrm{d}t$ and $-(A_b/A_t)\,\mathrm{d}A_t/\mathrm{d}t$ are positive. However, at late time for the case with film drainage, the second term on the right hand side is positive, but the first term on the right hand side can become negative. Hence, the sign of Eq. (6.19) depends on the relative magnitude of these two terms. Since in the cases with smaller Γ_0, the value of A_b/A_t at any given time is larger (i.e. more surfactant exchange has taken place), the second term on the right hand side of Eq. (6.19) is larger and hence A_b/A_t remains an increasing function of time. The opposite happens for the cases with larger Γ_0, the value of A_b/A_t is then lower, and hence the second term on the right hand side of Eq. (6.19) is less important than the first term: the right hand side of Eq. (6.19) is then negative, and so the value of A_b/A_t can decrease at long times. Knowing the value of A_b/A_t and how it behaves with time is of interest, since A_b/A_t turns out to determine the average concentration of dissolved surfactant in the film bulk which can be obtained from $c_0 + (c_{\mathrm{Pb}} - c_0)A_b/A_t$. Of course in the dimensionless system here, $c_{\mathrm{Pb}} \equiv 1$ and $c_0 = \Gamma_0$.

In summary in the case with no film drainage, at early times, A_b/A_t increases quickly at first, increasing the overall amount of surfactant in the film, since material of concentration c_0 is being substituted by material of higher concentration, $c_{\mathrm{Pb}} \equiv 1$. At later times, the system reaches a steady state, where A_b/A_t reaches a final steady value. Fur-

thermore, as we decrease Γ_0, the early-time rate of growth of A_b/A_t becomes faster, leading also to higher final values of A_b/A_t in the late-time limit. In the case where film drainage effects are present, a slightly slower initial increase is observed for A_b/A_t compared to the no film drainage case. At later times, once the film drainage effects start to become more significant in relative terms, two different situations can be observed depending on the value of Γ_0. In cases with smaller Γ_0, the value of A_b/A_t continues to increase, while it decreases at longer times in cases with larger Γ_0.

Having now considered the areas of two regions within the bulk with uniform but different concentrations, now we can calculate the amount of surfactant in the bulk, as well as the overall amount of surfactant on the surface plus the bulk. This is discussed in the next section.

6.3.4 Total amount of surfactant relative to initial amount

Now, we proceed to analyse the influence of the solubility parameter $\mathcal{S}$ (Eq. (6.3)) and initial surfactant concentration Γ_0, on the total amount of surfactant contained in the film S_T (surface plus bulk). Specifically, we plot total amount of surfactant (S_T) relative to its initial value ($S_{T,0}$), for different $\mathcal{S}$ and Γ_0 (see Figs. 6.5 and 6.6). This ratio $S_T/S_{T,0}$ is a measure of how Plateau-border-to-film mass transfer induced by reflux affects the recovery of a fractionation process over time relative to the initial recovery prior to any benefit from this effect of reflux. The larger this ratio, the more the system benefits from reflux. However the other relevant factor in cases with film drainage is thinning of the film, which can result in a decrease of the total amount of surfactant in the film, and subsequently, a decrease in the recovery over time. First, we present the results of the no film drainage case in Sec. 6.3.4.1. Then, the case with film drainage will be discussed in Sec. 6.3.4.2.

In this study, using relevant data from literature (see Tables 7.2 and 7.3), a base case estimate for the solubility parameter $\mathcal{S}$ (as per the definition in Eq. (6.3)) turned out to

be 3.09. To investigate the effect of solubility parameter being varied about the base case, we selected values $\mathcal{S} = 3$ and $\mathcal{S} = 30$ for the no film drainage case. In this particular case, we did not explore solubility parameters smaller than $\mathcal{S} = 3$, because the completely insoluble case has been solved by Vitasari et al. [1]. We know already what happens there: $S_T/S_{T,0}$ grows over time from unity to Γ_0^{-1}, at least in the absence of film drainage. In the case with film drainage, behaviour is more complex, and so to elucidate the behaviour a little more, we look at a wider domain of $\mathcal{S}$, namely $\mathcal{S} = 0.03$, $\mathcal{S} = 0.3$, $\mathcal{S} = 3$ and $\mathcal{S} = 30$.

6.3.4.1 Case without film drainage

The results of the no film drainage case are presented in Fig. 6.5 for two different solubility parameters, 3 and 30 as we have said. What we see in each case is that $S_T/S_{T,0}$ increases with time and then eventually reaches a final steady state value. The final steady state value becomes larger as the initial surfactant amount Γ_0 becomes smaller. Moreover the final steady state value also becomes larger as the solubility $\mathcal{S}$ decreases. However the final steady state value of $S_T/S_{T,0}$ always falls short of Γ_0^{-1} (the value attained for an insoluble surfactant [1]).

The final amount of surfactant in the film can be calculated by considering the final values resulting from Eqs. (6.15) to (6.18). This then leads to the equation $S_T = \Gamma_{\mathrm{Pb}} + \mathcal{S}(c_{\mathrm{Pb}} A_b + c_0(A_t - A_b))$, where A_b now specifically denotes a final area. This final S_T value can also be written in the form $S_T = \Gamma_{\mathrm{Pb}} + \mathcal{S}\, c_{\mathrm{Pb}} A_t - \mathcal{S}(c_{\mathrm{Pb}} - c_0)(A_t - A_b)$. In our dimensionless system Γ_{Pb} and c_{Pb} are unity, A_t is also unity (in the absence of film drainage), and c_0 is the same as Γ_0. Hence, with those substitutions $S_T = 1 + \mathcal{S} - \mathcal{S}(1 - \Gamma_0)(1 - A_b)$. Recall also (see Sec. 6.2.5.1) that the only $\mathcal{S}$ dependence here is the dependence showing explicitly: the value of A_b is sensitive to Γ_0 but not sensitive to $\mathcal{S}$.

By similar arguments, in our dimensionless system $S_{T,0} = (1 + \mathcal{S})\Gamma_0$. It is clear now

that the ratio $S_T/S_{T,0}$ always falls short of Γ_0^{-1}, and the amount it falls short grows as $\mathcal{S}$ grows. In a hypothetical case in which A_b/A_t became as large as unity, $S_T/S_{T,0}$ could attain the value Γ_0^{-1}. However we know from Fig. 6.4a that A_b/A_t never becomes that large. The other way to prevent $S_T/S_{T,0}$ falling short of Γ_0^{-1} is to have Γ_0 itself approaching unity. However the difference between the initial surfactant concentration on the film and the concentration in the Plateau border is then so small, that there is essentially no benefit to derive from Plateau-border-to-film mass transfer induced by reflux.

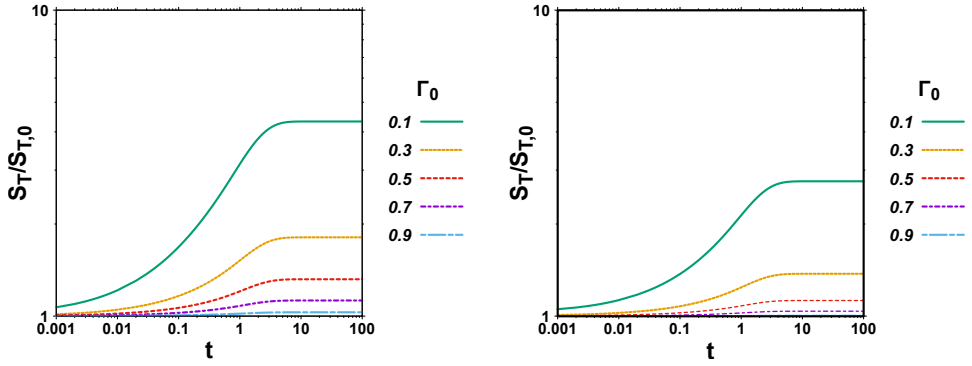

(a) $\mathcal{S} = 3$ **(b)** $\mathcal{S} = 30$

Figure 6.5: Total amount of surfactant (S_T) relative its initial value ($S_{T,0}$) versus time, calculated for surfactants with solubility parameters, 3 and 30 and for various values of Γ_0, in the no film drainage case.

In summary, the total amount of surfactant in the film S_T increases when solubility $\mathcal{S}$, is increased, but the relative amount, S_T/S_{T0} actually decreases. We observe that high solubility results in having more surfactant in the film initially, but simultaneously that reduces the factor by which reflux can then increase the recovery over time.

6.3.4.2 Case with film drainage

Regarding the case in which film drainage is included (Fig. 6.6), at early times the behaviour of $S_T/S_{T,0}$ is similar to what is seen when film drainage effects are neglected. However the rate of increase of $S_T/S_{T,0}$ is slightly less than in the no film drainage case, because of the competition between Marangoni flow and film drainage, which slightly slows down the evolution of S_T.

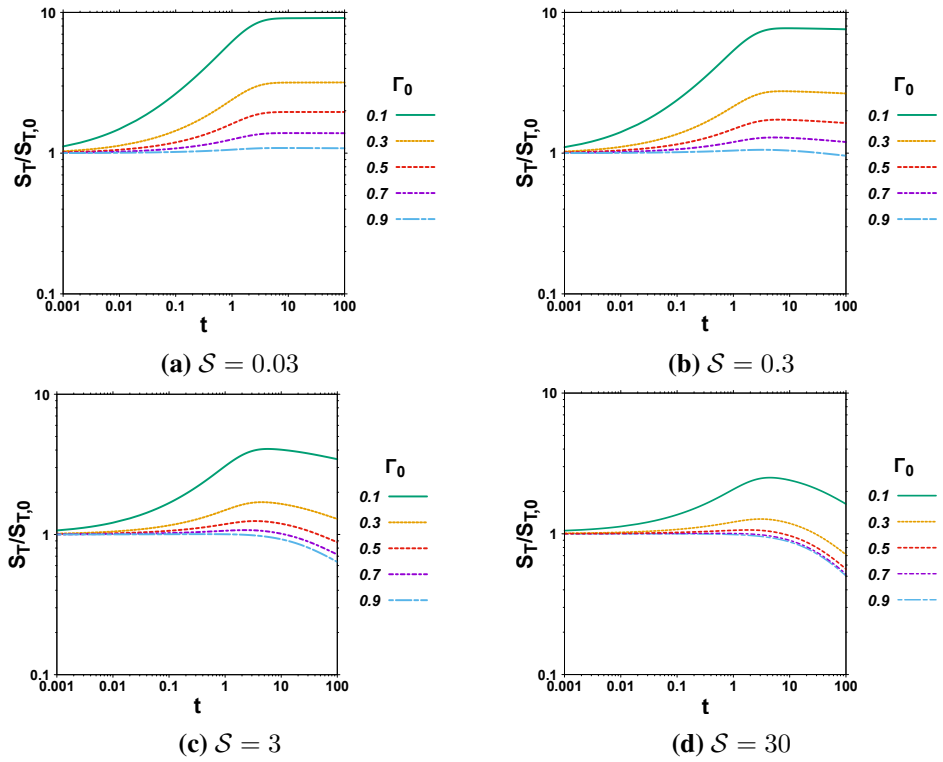

(a) $\mathcal{S} = 0.03$ **(b)** $\mathcal{S} = 0.3$

(c) $\mathcal{S} = 3$ **(d)** $\mathcal{S} = 30$

Figure 6.6: Total amount of surfactant S_T relative to its initial value $S_{T,0}$ versus time, calculated for surfactants with solubility parameters, 0.03, 0.3, 3 and 30 and for various values of Γ_0, in the case with film drainage. The drainage velocity parameter V_R is given in supplementary Table 7.3.

At later times though, a decrease in $S_T/S_{T,0}$ is observed. This is due to the fact that, after reaching a (quasi-steady) balance on the surface, the main effect influencing the amount of surfactant is film drainage from the bulk. Hence, the total amount of surfactant or equivalently surfactant recovery of the film decreases from this time onward. For the less soluble surfactant cases (Figs. 6.6a and 6.6b), the late time decrease in $S_T/S_{T,0}$ is comparatively small. This is due to the fact that in cases with only moderate solubility, although film drainage is indeed removing material from the bulk, there is now barely any surfactant in the bulk to start with. However the reduction at late times is more significant in the more soluble surfactant cases. The other important factor affecting the late-time behaviour is the initial surfactant concentration. In fact, most of the surfactant loss from the bulk is from locations near the midplane of the film containing surfactant with the initial bulk concentration c_0 (equal to Γ_0 in the dimensionless system here). As a result, films with lower initial bulk concentration tend

to lose only surfactant lean material, whereas films with higher initial concentration stand to lose more surfactant.

Once sufficient material is lost from the bulk, the surfactant recovery S_T for a film might even become less than the initial amount $S_{T,0}$. As Fig. 6.6 shows, this typically happens for the cases with higher solubilities $\mathcal{S}$ and higher initial surface concentrations Γ_0. Even when that happens though, there might still be a benefit for the film in enrichment terms, as we will see later on.

In summary, in cases with film drainage, surfactant recovery reaches a maximum around the time that a quasi-steady state is reached, then decreases. In cases with higher solubility parameters, due to the same reason mentioned in Sec. 6.3.4.1, the increase of $S_T/S_{T,0}$ up to the quasi-steady state is less. However its decrease from that time onward is higher: when $\mathcal{S}$ is large, most of the surfactant is contained in the bulk, and we are specifically losing surfactant from the bulk. Overall, more soluble cases are more sensitive to film drainage.

6.3.5 Effect of time evolution in cases with film drainage

In this section, we investigate in more detail how $S_T/S_{T,0}$ and also S_T itself are affected by the fractionation process time evolution. We focus on the case with film drainage, since this is the case which exhibits interesting non-monotonic behaviour. We have chosen just two values of the solubility parameter $\mathcal{S}$, namely 3 and 30, as these are cases in which the non-monotonic behaviour is more evident. The times when $S_T/S_{T,0}$ and S_T reach a maximum for various values of Γ_0 are identified, along with the maximum values themselves. Moving to later times, values of $S_T/S_{T,0}$ at 10 and 100 time units are also presented for selected $\mathcal{S}$ and Γ_0 within Tables 6.1 and 6.2.

Looking at Tables 6.1 and 6.2 separately, reveals the fact that in each case there is a certain time corresponding to the maximum S_T or equivalently maximum $S_T/S_{T,0}$,

Table 6.1: Time for maximum $S_T/S_{T,0}$ and maximum S_T, as well as values of these maxima are reported. In addition values of $S_T/S_{T,0}$ at 10 and 100 time units are given. Here Γ_0 takes values 0.1, 0.5 and 0.9, solubility parameter $\mathcal{S} = 3$ and film drainage is assumed to occur.

Γ_0	0.1	0.5	0.9
$S_{T,0}$	0.4061	2.0034	3.6007
Time of max $S_T/S_{T,0}$	5.78	3.44	0.40
Max $S_T/S_{T,0}$	4.0734	1.2465	1.0055
Max S_T	1.6542	2.4973	3.6205
$S_T/S_{T,0}$ at $t = 10$	4.0224	1.1934	0.9245
$S_T/S_{T,0}$ at $t = 100$	3.4430	0.8805	0.6374

Table 6.2: Time corresponding to the maximum $S_T/S_{T,0}$ and maximum S_T, as well as values of these maxima are reported. In addition values of $S_T/S_{T,0}$ at 10 and 100 time units are given. Here Γ_0 takes values 0.1, 0.5 and 0.9, solubility parameter $\mathcal{S} = 30$ and film drainage is assumed to occur.

Γ_0	0.1	0.5	0.9
$S_{T,0}$	3.1061	15.5034	27.9007
Time of max $S_T/S_{T,0}$	4.46	1.82	0.01
Max $S_T/S_{T,0}$	2.5062	1.0647	1.0002
Max S_T	7.7846	16.5061	27.9053
$S_T/S_{T,0}$ at $t = 10$	2.4041	0.9700	0.8752
$S_T/S_{T,0}$ at $t = 100$	1.6270	0.5619	0.5027

and this time is highly dependent on the value of Γ_0. For lower Γ_0 values, longer time is required for the maximum to happen. What leads to the maximum in $S_T/S_{T,0}$ is the following. Initially, Marangoni effects dominate, hence $S_T/S_{T,0}$ increases. However film drainage is also taking surfactant out from the bulk. After some time, the amount of surfactant being removed from the film due to film drainage outweighs the amount brought in as a result of Marangoni flow on the surface and any associated convective flow in the bulk. Choosing smaller Γ_0 drives a stronger Marangoni flow, so it then takes longer for film drainage to dominate over it.

Moreover, it is confirmed that, as Fig. 6.6 also shows, systems with lower Γ_0 eventually reach a higher maximum value of $S_T/S_{T,0}$. This means that the cases with lower Γ_0 gain in relative terms more surfactant due to reflux, despite the fact that total amount of surfactant in these cases is less than cases with higher initial concentrations.

Looking now towards even longer times, e.g. $t = 10$ and $t = 100$, less of the surfactant

that was gained is subsequently lost in the cases with lower Γ_0. This is again due to having leaner bulk in these cases. For instance, in the case with $\Gamma_0 = 0.1$ and solubility parameter $\mathcal{S}$ equal to 3, at 10 and 100 times units respectively, $S_T/S_{T,0}$ is approximately 1% and 15% less, relative to its maximum amount. However the analogous amount for $\Gamma_0 = 0.9$ is around 8% and 36% less at 10 and 100 time units, respectively. Leaner solutions therefore not only benefit more from reflux up to the maximum, but also lose less surfactant as the process continues. As a result enrichment (see definition in Sec. 6.2.6) in these cases can be high without much decrease over time in their recovery (to be discussed later on in Sec. 6.3.6). On the other hand, solutions that were richer initially e.g. $\Gamma_0 = 0.9$ lose more surfactant later on, and indeed they can lose so much surfactant that they end up by $t = 10$ or $t = 100$ with less than they had initially. Overall, it can be seen that leaner solutions benefit more from foam fractionation with reflux.

Now, instead of looking at Table 6.1 and Table 6.2 individually, we can compare them to gauge the effect of different solubilities. In fact the initial total surfactant amount $S_{T,0}$, in the systems which contain higher solubility surfactants are significantly higher. Hence, as far as recovery is concerned, even without benefitting from Plateau-border-to-film mass transfer induced by reflux, surfactants with higher solubilities can be recovered to a greater extent than lower solubility surfactants. Plateau-border-to-film mass transfer induced by reflux merely increases that recovery, i.e. the maximum S_T is even higher than $S_{T,0}$. However, as can be seen in Table 6.2, the time when $S_T/S_{T,0}$ for more soluble surfactants reaches a maximum is significantly less than cases with lower solubilities. This is due to the fact that in these cases the contribution from the film bulk is more important than in low solubility cases. As a result, the effect of losing surfactant from the bulk due to the film drainage can be seen sooner.

This is more obvious in systems with higher Γ_0 which need very little time at all to reach a maximum in $S_T/S_{T,0}$. For instance, in the case with $\Gamma_0 = 0.9$ and solubility

parameter $\mathcal{S}$ equal to 30 say, the time required to reach the maximum is just 0.01 time units and the maximum amount of S_T itself is only around 0.02% higher than the amount of surfactant at initial time $S_{T,0}$. In addition, in higher solubility cases, more surfactant is lost at longer times. For instance, approximately 12% and 49% of surfactant relative to its peak amount will be lost after 10 and 100 time units in this last mentioned case ($\Gamma_0 = 0.9$ and $\mathcal{S} = 30$). Thus, for these cases there is barely any benefit for having long residence time if increasing the recovery is our primary goal in foam fractionation. However, as is discussed next (Sec. 6.3.6), reduction of recovery even in these cases can still be offset by increased enrichment as the film thins.

6.3.6 Recovery and enrichment

We now consider recovery and enrichment which as was discussed in Sec. 6.2.6 are important parameters for assessing performance of a fractionation process: formal definitions are given in Sec. 6.2.6. In Fig. 6.7, we have plotted recovery versus enrichment for various solubility parameters ($0.1 \leq \mathcal{S} \leq 50$) at different times, assuming film drainage is present, and for two different initial surfactant concentrations (Γ_0), namely 0.1 and 0.5. We do not consider $\Gamma_0 = 0.9$ here, because Plateau-border-to-film mass transfer induced by reflux is expected to have only very modest benefit in that case.

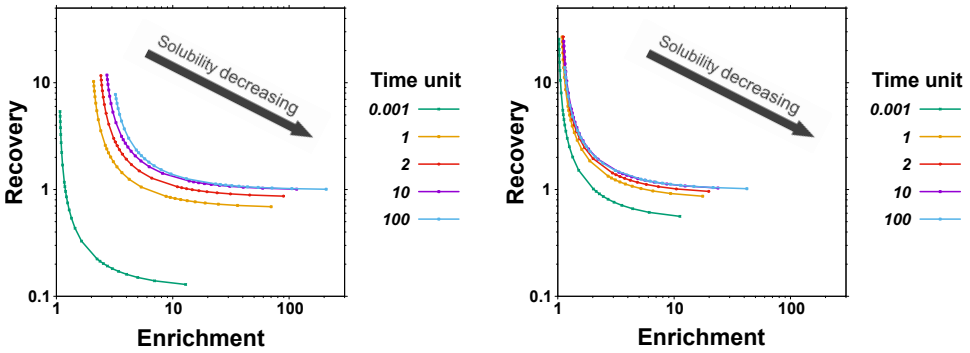

(a) $\Gamma_0 = 0.1$ **(b)** $\Gamma_0 = 0.5$

Figure 6.7: Recovery versus enrichment, plotted for various solubility parameters ($0.1 \leq \mathcal{S} \leq 50$) at different times.

We can see that there is a trade off between recovery and enrichment. As a result, to

increase one, we generally need to decrease the other. High solubility parameter $\mathcal{S}$ leads to high recovery but low enrichment, whereas low solubility parameter leads to low recovery but high enrichment. Nonetheless, in the presence of reflux, recovery and enrichment benefit as time evolves: the recovery-enrichment curves are pushed upwards and to the right. However the extent of that benefit depends on the initial surface concentration (Γ_0): there is much more benefit when Γ_0 is small (Fig. 6.7a) than when it is larger (Fig. 6.7b).

The other observation is that in all cases, after around $t = 10$ further benefits in the recovery versus enrichment plot are limited: the $t = 10$ and $t = 100$ curves lie close to one another, so are a little difficult to distinguish in the plots. Between $t = 10$ and $t = 100$, as film drainage continues to remove material from the bulk, in the high solubility part of the plot there is a modest decrease in recovery, while in the low solubility part of the plot there is a modest increase in enrichment. To summarise then, the effect seen at longer times, is an enhancement of enrichment at the expense of recovery. Long times (i.e. many units of dimensionless time) are needed to see this though, since (as already noted in Sec. 6.2.1) drainage flow is comparatively slow.

It is worth remembering also here that throughout data have expressed in terms of dimensionless time. The conversion back to dimensional time using typical parameter estimates is given in Table 7.2. For the given parameter values, dimensionless $t = 100$ corresponds to only around 1 s of dimensional time. Even this is short compared with a typical residence time that might be expected for a foam film in a fractionation column. Hence not just in Fig. 6.7, but in Figs. 6.2 to 6.6 and in Tables 6.1 and 6.2 also, it is actually the long-time limiting behaviour that is of particular interest for typical fractionation applications.

6.4 Conclusion

Simulation of convected soluble surfactant transport on and within a foam film has been carried out in the context of a foam fractionation process with reflux (or analogously, a foam fractionation process operated in stripping mode). This study builds on related models developed and published earlier [1, 2]. However the main novelty of the present study is that here mass transfer of soluble surfactant in the bulk of a foam film due to convective flow is taken into account. The convective flow happens as a result of an interplay between Marangoni flow and film drainage on the surface of the foam film, albeit with the resulting flow fields then extending into the bulk. The parameters used for the simulation purposes were taken from relevant literature [158, 159, 162, 205, 280, 283]: see supplementary Sec. 7.4.1 for details. Here also dimensionless parameters that were identified as being particularly relevant to system behaviour were the solubility parameter $\mathcal{S}$ and initial surface surfactant concentration Γ_0, so various values of these parameters have been considered. Note that we are referring to "surfactant" generically in this work, but the main application considered here is protein separation, e.g. β-LG.

In general, this study tackles a specific limit, namely large $\mathrm{Pe}\,\Delta$, in which diffusion of surfactant from the surface of a foam film into the bulk is ignored, so convection dominates. For simplicity and following on from the work Rajabi and Grassia [2], we have selected a Henry isotherm to relate the bulk and surface concentrations. However we could have used another adsorption isotherm at the expense of making the relationship between bulk and surface non-linear [194, 288, 290]: adsorption isotherms for proteins in particular are often rather complex [159, 163, 288]. Here though specifically the isotherm is needed to relate initial surface and initial bulk concentrations. The consequence of switching to a non-linear isotherm would be to have less bulk concentration for a given surface concentration (see Sec. 7.5 for an example). Thus we would recover less surfactant from the bulk than the model here predicts.

In addition, in line with previous literature [1, 2], two different cases during this study have been considered, namely, a no film drainage case and a case with film drainage. The main difference between these two cases is that there is more surfactant on the surface and in the bulk of the film in the case without film drainage than with film drainage. Indeed, in the film drainage case, so much surfactant can be lost at late times, that even less is recovered than was present initially. Even so, there can still be a benefit in terms of enrichment.

In this study, within the bulk, we track a locus that we call a separatrix, which forms a boundary between two regions with uniform, but different concentrations. These regions are the one with the Plateau border's concentration and the one with the initial film concentration (the Plateau border's concentration is higher than that of the film, due to reflux). The separatrix evolves with time as a result of the convective flow extending into the bulk, thereby defines how the areas covered by the aforementioned regions change with time. Knowing the areas enables us in turn to calculate the amount of surfactant in the bulk and subsequently, the overall amount of surfactant in the film (surface and bulk together).

As surfactant evolution on the surface has previously been investigated elsewhere [1], we mostly focus on what happens in the bulk and its effect on the overall amount of surfactant. It has been found that over time, the top of the separatrix is pulled towards the centre of the film, while for locations closer to the midplane of the film, the separatrix is pulled instead towards the Plateau border. This is as expected consistent with the direction of convective flow in the bulk. The parameter that has most influence upon the evolution of the separatrix is found to be the initial surfactant surface concentration Γ_0, that causes the driving force for setting up Marangoni flows. Lower surfactant surface concentrations create a larger driving force on the surface, hence, a stronger convective flow towards the centre of the film, at least for locations close to the surface. This then causes the separatrix to displace more and results in having more fluid

with the Plateau border's concentration arriving in the bulk of the film.

It has also been found that higher initial surfactant concentration Γ_0 and higher solubility parameter $\mathcal{S}$ lead to having more initial overall amount of surfactant on and within the film, but less overall amount of surfactant relative to the initial amount. In the no film drainage case, the overall amount of surfactant relative to the initial amount increases up to a point and then reaches a steady state. However, in the case with film drainage, surfactant amount relative to initial amount decreases after reaching a maximum.

To analyse the effects due to drainage at later time when this decrease happens, we determined the time at which the overall amount of surfactant relative to the initial amount reaches a maximum, and also the decrease in amount of surfactant afterwards. It has been observed that in the cases with higher initial surfactant concentration Γ_0, and higher solubility parameter $\mathcal{S}$, the time to reach maximum is less, and the amount of surfactant being lost from the film afterwards is greater. Thus, in cases with higher Γ_0 and higher $\mathcal{S}$, the residence time optimising the surfactant recovery is much lower, and the negative effects of extending residence time to longer times are also more significant. Hence we can say that these cases are more sensitive to the residence time (or equivalently to the fractionation column length). However the system has been made dimensionless on a scale such that typical residence times will likely be well beyond that optimum time. Moreover this is merely an optimum for recovery: longer residence times can still lead to better enrichment. Indeed, this study revealed that higher solubilities are more beneficial for surfactant recovery, and lower solubilities are more beneficial for enrichment of the foamate in a fractionation process. Systems with lower initial concentrations benefited more from reflux in terms of both recovery of surfactant and enrichment.

In summary, previous work [1] looked at the insoluble case. In Rajabi and Grassia [2], solubility was taken into account, but in the limit of small $\mathrm{Pe}\,\Delta$ (rapid surfactant

diffusion across films, applicable for relatively small surfactant molecules and very thin films). Here, we worked out another relevant limit, namely soluble surfactant with large $\mathrm{Pe}\,\Delta$ (convection-dominated limit, for bulky surfactant molecules within films that are not quite so thin). However in reality systems will presumably be in between these two limits. Moreover, just as Vitasari et al. [1], Rajabi and Grassia [2] did, we simplified the film's shape, using instead the assumption of a flat film. As a result, even though we captured Marangoni and film drainage effects to an extent, the flow fields we determined are simplified ones. The adsorption isotherm has also been simplified as has been mentioned. Furthermore Plateau borders are treated as if they were surfactant reservoirs. However, despite the simplifying assumptions and the particular limit assumed, we were able to obtain predictions of fractionation performance, which can help to guide the separation by fractionation of surface-active materials, such as proteins.

There is an important point here however for a practitioner aiming to use fractionation to separate a big bulky molecule like a protein (likely to have a large $\mathrm{Pe}\,\Delta$ and hence involve convection-dominated transport): relying on convective transport to enrich a foam film significantly could well be challenging. Indeed convection is only able to enrich a bulk foam film to the extent that bulk liquid is transferred between a film and a surrounding surfactant rich Plateau border. Since the amount of liquid convected is always less than the total amount of liquid in the film's bulk, the extent of enrichment could therefore be rather limited. A less bulky molecule (e.g. a smaller surfactant molecule, instead of a protein) with a small $\mathrm{Pe}\,\Delta$ can be transported into the bulk of foam films via diffusion, and might therefore become enriched more readily.

The predictions however come with a number of caveats, that are important to mention. Although we have considered only convective surfactant transport in the film bulk, in reality $\mathrm{Pe}\,\Delta$ is large but finite (on the order of 1000 or so according to Table 7.3). This means weak diffusion of surfactant will actually be present concurrently with the

convection. That diffusion will of course be active where concentration gradients are largest. Clearly there are large concentration gradients at the separatrix itself, so a sharp concentration front there will be smeared out by diffusion even as the separatrix advects. Diffusion will also be present near the film surface. Material in the subsurface (immediately below the surface) can be in equilibrium with the surface, but is not in equilibrium with the remainder of the bulk slightly further from the surface.

However weak diffusion (whether near the separatrix or near the surface) can also couple with the convective flow fields. If diffusion causes surfactant to diffuse a small distance away from what is nominally a sharp front, then spatiotemporal differences in velocity will exist between the actual position of the surfactant and the nominal position of the front. Depending on the velocity gradients present in the flow field, this potentially could advect the surfactant even further away from the nominal position of the front.

Another caveat is that despite some similarities between the insoluble surfactant case of Vitasari et al. [1] and the large $\mathrm{Pe}\,\Delta$ case considered here (i.e. in both cases limitations are placed on surfactant exchange between surface and bulk), there are also differences. In the insoluble case, i.e. small values of $\mathcal{S}$, even if surfactant did manage to transfer from surface to bulk, according to Eq. (6.17) there would never be much of it in the bulk, even if surface and bulk were to equilibrate. In the present situation, i.e. large values of $\mathrm{Pe}\,\Delta$, it is merely the case that Eq. (6.9) predicts surfactant diffuses off or onto the surface comparatively slowly, certainly on time scales longer than any Marangoni or film drainage flows might proceed. After several units of dimensionless time then, the separatrix will have reached a steady configuration (or in the case when film drainage is present, a quasi-steady configuration), and convection will have have come almost to a stop or at least will have slowed significantly. Even after that though, diffusion is still ongoing: provided $\mathcal{S}$ is not too small, significant amounts of surfactant can still eventually manage to enter the bulk diffusively, albeit as we have said, this

occurs slowly compared to the prior convective transport. The surfactant distribution that results at the end of the convective transport stage is an initial condition for the diffusive transport stage.

In fact based on Eq. (6.9) we would need dimensionless times on the order of several multiples of $\mathrm{Pe}\,\Delta$ to see significant diffusion. A single unit of dimensionless time in the present problem, when converted back to dimensional variables (see Table 7.2) is however only around 0.01 s. This is short compared to a typical residence time expected for a foam film rising through a fractionation column in a laboratory experiment, which could be on the order of seconds or even more. Hence the end of the convective stage is reached quickly, at least on a laboratory time scale. The dimensionless time scale for diffusion meanwhile is, as we have said, several multiples of $\mathrm{Pe}\,\Delta$. With $\mathrm{Pe}\,\Delta$ values on the order of 1000 as given by Table 7.3 this corresponds to a time scale up to the order of a minute. On that sort of time scale, diffusive transport cannot be ignored, and the model already considered by Rajabi and Grassia [2] (which incorporates significant diffusive surfactant transfer effects right from the outset) arguably then becomes more pertinent than the convective transport dominated model that has been considered here.

Chapter 7

Transport of convected soluble surfactants on and within the foam film in the context of a foam fractionation process: Supplementary material

"This chapter consists of published material: [H. Rajabi, R. Rosario, P. Grassia, "Transport of convected soluble surfactants on and within the foam film in the context of a foam fractionation process," Chemical Engineering Science, vol.281, 119100, 2023. https://doi.org/10.1016/j.ces.2023.119100]"

Abstract

In this supplementary section, we present some additional information used to develop a model for convected soluble surfactant transport on and within the foam film. In Sec. 7.1 we review the nondimensionalisation process. Sec. 7.2 is an important section to progress our simulations: in that section we explain how to manage the numerical complications that arise due to the singularity of the flow field at early times. The

numerical approach applied after that very early time is then presented in Sec. 7.3. Sec. 7.4 provides the physical and physicochemical data used in the simulations and also the benchmarking procedure used to set numerical parameters. Finally Sec. 7.5 considers the possible role of having a non-linear adsorption isotherm.

7.1 Nondimensionalization

Here we show how to nondimensionalise the parameters and equations used in our model, as presented in Sec. 6.2 in the main text.

- We make x (distance along the film) dimensionless with respect to the film half-length (L), and z (distance across the film) dimensionless with respect to the initial film half-thickness (δ_0).
- Velocities u in the x direction are nondimensionalised with respect to $\mathcal{G}\delta_0/\mu L$ (a characteristic Marangoni velocity with $\mathcal{G}$ being Gibbs parameter and μ being viscosity), while velocities w in the z direction are nondimensionalised with respect to $\mathcal{G}\delta_0^2/\mu L^2$.
- Times t are made dimensionless with respect to $\mu L^2/\mathcal{G}\delta_0$.
- Surfactant concentrations in the film c are made dimensionless with respect to the surfactant concentration in the bulk of the Plateau border c_{Pb}. Note that the Plateau border is treated as a surfactant reservoir. Thus, its concentration is assumed to be constant.
- Surfactant concentration on the film surface Γ is made dimensionless with respect to the Plateau border's surface concentration Γ_{Pb}.
- When films are draining, we make instantaneous film half-thicknesses δ dimensionless with respect to the initial film half-thickness δ_0.
- Cross sectional areas A_b and A_t within films (or strictly speaking within each

film half-length and half-thickness) are made dimensionless with respect to the initial film cross sectional area $A_t|_{t=0}$ or equivalently $\delta_0 L$.

7.2 Early time evolution

In this work, we are trying to track the material points which form the boundary between material that was originally in the film and material that was originally in the Plateau border. These material points form the so called separatrix. Due to a step change in concentration between Plateau border and film at initial time, the velocity field Eq. (6.5) is singular, i.e. initially velocity turns out to be infinite [220]. Hence, at early times, the numerics are difficult to handle, and we need to specify a method to proceed. Subsequently, the early-time results obtained from the present section will be needed to continue tracking material points at later times. Hence we discuss the early-time case in some detail here.

In Sec. 7.2.1 we work out an analytical formula to find the position, after the first time step, of the material points that were initially at $x = 1$. Essentially what we find is that if we can track the material point at the top of the separatrix on the film surface, we can also track material points on the separatrix in the bulk: the situation on the film surface is therefore explained in Sec. 7.2.2. Interestingly, as will be discussed later, the material point that separates initial material on the film surface from newly arrived Plateau border material turns out to correspond to the point on the surface with maximum velocity: the derivation of this result can also be found in Sec. 7.2.2. Finally, the dependency of the accuracy of this first time step upon the size of the time step itself is calculated in Sec. 7.2.3.

7.2.1 Early-time evolution during the initial time step

In the limit of interest, i.e. very early times, Marangoni flow on the surface is the dominant transport mechanism. Hence, we can ignore film drainage for this specific

time, and use instead the analytical solution involving complementary error functions for the evolution of surfactant surface concentration Γ, introduced by Vitasari et al. [1]. However, for the purpose of our calculations, using one term of the complementary error function solution is sufficient, as follows:

$$\Gamma \approx \Gamma_0 + (1 - \Gamma_0)\ \mathrm{erfc}\left[\frac{\sqrt{3}(1-x)}{2\sqrt{t}}\right], \tag{7.1}$$

where Γ_0 is initial surface concentration, and Eq. (7.1) is in dimensionless form. As film drainage early on is ignored, the velocity field in the x-direction Eq. (6.5) in the main text, is reduced to the following equation:

$$u = \left(\frac{1}{6} - \frac{z^2}{2}\right)\frac{1}{\Gamma}\frac{\partial \Gamma}{\partial x}, \tag{7.2}$$

again in dimensionless form. Moreover, $\partial\Gamma/\partial x$ can be obtained from Eq. (7.1) as:

$$\frac{\partial \Gamma}{\partial x} = \sqrt{\frac{3}{\pi t}}\exp\left(-\frac{3(1-x)^2}{4t}\right)(1 - \Gamma_0). \tag{7.3}$$

Thus, a horizontal velocity field equation can be obtained from the combination of Eqs. (7.2) and (7.3) as:

$$u = \left(\frac{1}{6} - \frac{z^2}{2}\right)\frac{\sqrt{3}\exp\left(-\frac{3(1-x)^2}{4t}\right)(1-\Gamma_0)}{\sqrt{\pi t}\left(\Gamma_0 + \mathrm{erfc}\left(\frac{\sqrt{3}(1-x)}{2\sqrt{t}}\right)(1-\Gamma_0)\right)} \tag{7.4}$$

and, by substituting z by unity, the equation for surface velocity field would be:

$$u_s = \frac{-\exp\left(-\frac{3(1-x)^2}{4t}\right)(1-\Gamma_0)}{\sqrt{3\pi t}\left(\Gamma_0 + \mathrm{erfc}\left(\frac{\sqrt{3}(1-x)}{2\sqrt{t}}\right)(1-\Gamma_0)\right)}. \tag{7.5}$$

We can simplify Eq. (7.5), by introducing the variable $\beta = \Gamma_0/(1-\Gamma_0)$ as follows:

$$u_s = \frac{-\exp\left(-\frac{3(1-x)^2}{4t}\right)}{\sqrt{3\pi t}\,\left(\beta + \operatorname{erfc}\left(\frac{\sqrt{3}(1-x)}{2\sqrt{t}}\right)\right)}. \tag{7.6}$$

We find that u scales similarly to $Kt^{-1/2}$ at early times, where K is a quantity that depends on z and also on Γ_0. Moreover, K has a well-defined limit at $t \to 0$. Therefore, it is possible to estimate the final position of separatrix points after the first time step (Δt) by integrating the velocity component associated with the x-direction as follows:

$$x_{\text{end}} = x_{\text{start}} + \int_0^{\Delta t} u \, \mathrm{d}t \tag{7.7}$$

where x_{start} and x_{end} are the positions of the material points initially and after the first time step, respectively. Substitution of u from Eq. (7.4) into Eq. (7.7) gives:

$$\left.\begin{aligned} x_{\text{end}} &= x_{\text{start}} + 2K\Delta t^{1/2} \\ u_{\text{end}} &= K\Delta t^{-1/2} \end{aligned}\right\} \Longrightarrow x_{\text{end}} = x_{\text{start}} + 2u_{\text{end}}\,\Delta t \tag{7.8}$$

where $x_{\text{start}} = 1$ and where u_{end} is the horizontal velocity field at the material point position after the first time step. In particular we suppose

$$u_{\text{end}} \approx u(x_m, z_{\text{start}}, \Delta t), \tag{7.9}$$

where x_m denotes the particular x value after time Δt of the specific material point that was located at $x = 1$ and $z = 1$ at $t = 0$ (i.e. x_m gives the top boundary of the separatrix, at least at early times). Meanwhile, z_{start} can be any arbitrary z location. Note however from Eq. (7.4) if we know u_{end} at any one z_{start} location, e.g. at $z_{\text{start}} = 1$, then we know it at all z locations. Our challenge therefore is to estimate x_m.

Notice that we focus on the x-component of velocity here. In the initial state, since the separatrix (dividing film from Plateau border) is vertical, even if material points

on this boundary do acquire a non-zero vertical velocity component w, this velocity component is initially tangential to the separatrix and hence has no impact upon the evolving shape of the separatrix during the first time step. This then is the reason why u_{end} in equation Eq. (7.8) can be evaluated at z_{start} at least for this first time step. Points at different z_{start} will of course displace horizontally by different amounts according to the shape of the velocity profile u from equation Eq. (7.4). As alluded to above, we do however need to find x_m. This is discussed next.

7.2.2 Behaviour at the film surface for the initial time step

Here, we are trying to identify a particular material point at the topmost end of the separatrix (on the surface of the film), ideally such that its trajectory in (x, t) space is particularly easy to track. What we are working towards here turns out to be a very simple result (Eq. (7.20)) but the detailed derivation of it is given below.

For convenience, we define χ which is a similarity variable, as below:

$$\chi = (1 - x)/\sqrt{t}. \tag{7.10}$$

The following equation is the rate of change of χ with time:

$$\frac{\mathrm{d}\chi}{\mathrm{d}t} = -\frac{\mathrm{d}x/\mathrm{d}t}{\sqrt{t}} - \frac{\chi}{2t} \tag{7.11}$$

where $\mathrm{d}x/\mathrm{d}t$ is the speed of a material point. It is convenient to try to find a material point which always has the same value of χ, because that material point then can be shown to have a very simple trajectory for x. Indeed, to find the particular material point which has always the same χ value, the time rate of change for χ following that specific material point should be zero.

More generally, we know that a material point on the surface moves with the velocity of the fluid on the surface, u_s. As a result, the time rate of change of χ following any

material point on the surface can be obtained by substituting $\mathrm{d}x/\mathrm{d}t$ with u_s, as follows:

$$\frac{\mathrm{d}\chi}{\mathrm{d}t} = -\frac{u_s(x,t)}{\sqrt{t}} - \frac{\chi}{2t}. \tag{7.12}$$

Now, at early times and using Eq. (7.6), it is possible to write u_s, as below:

$$u_s(x,t) = -\frac{V(\chi)}{\sqrt{t}} \tag{7.13}$$

where

$$V(\chi) = \frac{\exp\left(-\frac{3}{4}\chi^2\right)}{\sqrt{3\pi}\left(\beta + \operatorname{erfc}\left(\frac{\sqrt{3}}{2}\chi\right)\right)}. \tag{7.14}$$

Hence, Eq. (7.12) can be rewritten as

$$\frac{\mathrm{d}\chi}{\mathrm{d}t} = \frac{V(\chi)}{t} - \frac{\chi}{2t}. \tag{7.15}$$

Now, suppose there is a particular χ value that we call χ_m, such that χ following a material point does not change with time. To find it, as has been mentioned, $\mathrm{d}\chi/\mathrm{d}t$ should be equal to zero. This then requires

$$V(\chi_m) = \frac{\chi_m}{2}. \tag{7.16}$$

Eq. (7.16) is a non-linear equation which can be solved numerically to find χ_m (the particular χ value that always corresponds to the same material point on the surface). Note that Eq. (7.16) when coupled with Eq. (7.8) and Eq. (7.13) is sufficient to ensure that x_{end} at the top within Eq. (7.8) retains the value $\chi = \chi_m$, so the equations are all consistent.

However it turns out that χ_m is also the χ corresponding to maximum surface velocity. To work out the χ corresponding to maximum velocity, denoted $\chi_{\max}$ say, we set

$\mathrm{d}V/\mathrm{d}\chi|_{\chi=\chi_{\max}} = 0$. In general, from Eq. (7.14), we first evaluate as follows:

$$\frac{\mathrm{d}V(\chi)}{\mathrm{d}\chi} = \frac{\exp\left(-\frac{3\chi^2}{2}\right)}{\pi\left(\mathrm{erfc}\left(\frac{\sqrt{3}\chi}{2}\right)+\beta\right)^2} - \frac{\sqrt{3}\,\chi\exp\left(-\frac{3\chi^2}{4}\right)}{2\sqrt{\pi}\left(\mathrm{erfc}\left(\frac{\sqrt{3}\chi}{2}\right)+\beta\right)}. \tag{7.17}$$

Eq. (7.17) simplifies as:

$$\frac{\mathrm{d}V(\chi)}{\mathrm{d}\chi} = 3V^2(\chi) - 3\chi\frac{V(\chi)}{2}. \tag{7.18}$$

Then, setting $\mathrm{d}V/\mathrm{d}\chi|_{\chi=\chi_{\max}} = 0$, using Eq. (7.18) results in:

$$V(\chi_{\max}) = \frac{\chi_{\max}}{2}. \tag{7.19}$$

We can see that Eq. (7.16) and Eq. (7.19) are identical. Thus, the material point χ_m, turns out to correspond to the point of maximum velocity $\chi_{\max}$. Interestingly, as time evolves, the point $\chi = \chi_{\max}$ does not remain at $x = 1$.

To understand why the maximum velocity is not at $x = 1$, we can consult Eq. (7.2). According to Eq. (7.2), as x falls below 1, the value of $1/\Gamma$ rises (from 1 to $1/\Gamma_0$). Likewise, as x falls below 1, the value of $\partial\Gamma/\partial x$ falls. For a small set of x values the rise in $1/\Gamma$ can outweigh the fall in $\partial\Gamma/\partial x$. Hence the maximum velocity is not exactly at $x = 1$. It is clear now, in any case, that the point of maximum velocity is itself also a material point.

We now convert from coordinate χ to coordinate x. The point of maximum velocity certainly must coincide with $x = 1$ exactly at $t = 0$. As time evolves though, we can identify x_m, the location at the top of the separatrix, with $x_{\max}$, which is the point of maximum velocity. However at $\chi = \chi_m$, the relationship between x and χ following a material point is very simple. Because $\chi = (1 - x)/\sqrt{t}$ does not change for that

material point, the equation for x_m becomes simply:

$$x_m = 1 - \chi_m \sqrt{t} \tag{7.20}$$

which is the key equation we have been aiming to derive here.

It still remains to find the numerical value of χ_m as a function of β or equivalently as a function of Γ_0. By combining Eq. (7.14) and Eq. (7.16) we obtain:

$$\chi_m = \frac{2\exp\left(-\frac{3}{4}\chi_m^2\right)}{\sqrt{3\pi}\left(\beta + \operatorname{erfc}\left(\frac{\sqrt{3}}{2}\chi_m\right)\right)}. \tag{7.21}$$

This can be solved numerically, remembering that $\beta = \Gamma_0/(1-\Gamma_0)$. In Fig. 7.1 we can see the graph of χ_m vs Γ_0 over the domain $0.01 \leq \Gamma_0 \leq 0.99$.

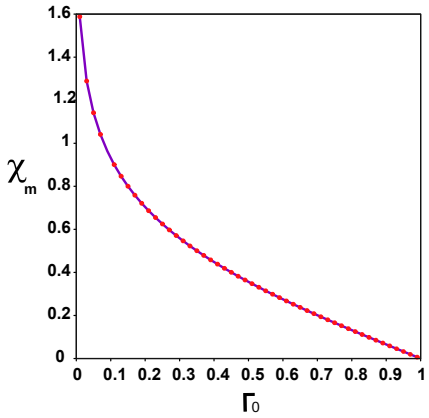

Figure 7.1: $\chi_m = (1 - x_m)/\sqrt{t}$ versus Γ_0, plotted over the domain $0.01 \leq \Gamma_0 \leq 0.99$.

As we can see, χ_m decreases as Γ_0 increases. Fig. 7.1 tells us that as initial surfactant surface concentration increases, Marangoni flow driving material points along decreases due to less driving force on the surface. This then causes x_m to stay closer to unity, owing to having a smaller χ_m.

As already alluded to, we can see that Eq. (7.20) is consistent with Eqs. (7.7) to (7.9). At the top, $2K$ is equivalent to χ_m, and K is equivalent to $V(\chi_m)$. Moreover at the end of the time step, $V(\chi_m)\Delta t^{-1/2}$ is equivalent to u_s (the velocity on the surface at $x = x_m$).

As Sec. 7.2.1 already mentions, once we know where the top of the separatrix has reached during the initial time step (which is exactly what Eq. (7.20) gives us), we also know where the rest of the separatrix has reached. This is because we know the horizontal velocity at any z value relative to the horizontal velocity at the top (Eq. (7.2)). Thus the shape of the separatrix after the first time step has now been characterised, which is what we set out here to achieve.

Nonetheless, it turns out that the value chosen for initial time step Δt can affect the accuracy of the calculations of the position of material on the surface after the completion of that first time step. The calculation of the difference of separatrix location using different size of time steps can be found in the next section.

7.2.3 Accuracy for the initial time step

Due to singular behaviour during the first time step, we are at risk of making significant truncation error, if we do not choose time steps small enough. Hence, one thing we need to do is to assess the accuracy of the initial time step.

Here, we evaluate the difference which occurs if we use half of the original time step size or $\Delta t/2$ (instead of Δt), for the initial time step calculations. To do this, we first calculate the material point position on the surface at $t = \Delta t$, using Eq. (7.8), as below:

$$x_{\text{end}} = x_{\text{start}} + 2\, u_{\text{end}}\, \Delta t \tag{7.22}$$

where $x_{\text{start}} = 1$. Now, we calculate the analogous position, but using instead two steps. Consequently, we use the same method as Eq. (7.22) for the first step, which gives us the position at time $\Delta t/2$, which we will denote x_{mid}. Then we use Heun's method for the second step to calculate x_{end}, or more precisely a new estimate $x_{\text{end,New}}$. Thus we have for the first step:

$$x_{\text{mid}} = x_{\text{start}} + 2\, u_{\text{mid}}\, \Delta t/2 \tag{7.23}$$

where u_{mid} is the velocity at $t = \Delta t/2$, and where $x_{\mathrm{start}} = 1$. Now, for the second step (Heun's method) we have:

$$x_{\mathrm{end,New}} = x_{\mathrm{mid}} + u_{\mathrm{mid}}\,\Delta t/4 + u_{\mathrm{end}}\,\Delta t/4 \tag{7.24}$$

where, as mentioned, $x_{\mathrm{end,New}}$ is the final position using the two-step calculation. Hence:

$$x_{\mathrm{end,New}} = x_{\mathrm{start}} + 2\,u_{\mathrm{mid}}\,\Delta t/2 + u_{\mathrm{mid}}\,\Delta t/4 + u_{\mathrm{end}}\,\Delta t/4. \tag{7.25}$$

We know from Eq. (7.13) that at the early stages when Eq. (7.1) is applicable, u scales proportionally to $1/\sqrt{t}$. Thus by substitution of u_{mid} with $\sqrt{2}\,u_{\mathrm{end}}$, the difference of using half of the size instead of the original time steps (i.e. $x_{\mathrm{end,New}} - x_{\mathrm{end}}$) turns out to be $0.0178\,u_{\mathrm{end}}\,\Delta t$. Therefore, this analysis reveals the importance of using a greater number of time steps or small enough time intervals to have a more accurate simulation. Fortunately, the numerical prefactor 0.0178 is actually relatively small.

7.3 Numerical approach (Heun's method) after the initial time step

In this section, we present the numerical method that has been used for the purpose of simulating soluble surfactant transport in the bulk of a foam film as a result of convective flow. This method is used to update the position of the material points forming the so called separatrix after the first time step, the very first time step having already been considered in Sec. 7.2. Recall that the separatrix is made up of points that separate material located originally in the film from material that has newly arrived from the Plateau border. Note that the evolution of surfactant on the surface itself (Eq. (6.10) in the main text) has been solved using a spectral method which is explained in detail elsewhere [2]. Hence we focus solely on the method for updating the separatrix location here.

The position of the separatrix (in the bulk) is computed using Heun's method [291]. This is a second-order Runge-Kutta method so the local truncation error is therefore of order $\mathcal{O}(\Delta t^3)$ [292]. This method is implemented by representing the separatrix as a collection of individual material points. Each material point is tracked during a time step starting from some time t as follows [291]:

$$x_{\text{est,end}} = x_{\text{start}} + u_{\text{start}}\,\Delta t \tag{7.26}$$

$$z_{\text{est,end}} = z_{\text{start}} + w_{\text{start}}\,\Delta t \tag{7.27}$$

where $x_{\text{est,end}}$ and $z_{\text{est,end}}$ are estimates of the position in the x-coordinate and z-coordinate directions, respectively, at the instant $t + \Delta t$, based on the position (x_{start}, z_{start}) and the velocity field (u_{start},w_{start}) at the instant t: the subscript "start" here denotes now just the start of the time step (not the start of the entire process). An estimate of the dimensionless velocity at the estimated final position is then as follows:

$$u_{\text{est,end}} = u(x_{\text{est,end}}, z_{\text{est,end}}, t + \Delta t) \tag{7.28}$$

$$w_{\text{est,end}} = w(x_{\text{est,end}}, z_{\text{est,end}}, t + \Delta t) \tag{7.29}$$

where $u_{\text{est,end}}$ and $w_{\text{est,end}}$ are the components of the estimated velocity field at the instant $t + \Delta t$. The final coordinates of the material points, at the instant $t + \Delta t$, are now calculated as follows:

$$x_{\text{end}} = x_{\text{start}} + (u_{\text{start}}/2 + u_{\text{est,end}}/2)\,\Delta t \tag{7.30}$$

$$z_{\text{end}} = z_{\text{start}} + (w_{\text{start}}/2 + w_{\text{est,end}}/2)\,\Delta t. \tag{7.31}$$

The process now iterates to the next time step. By using this method, the position of separatrix at each instant can be obtained. Although we envisage the above equations

as applying in the film bulk, we can also apply them right at the top of the separatrix where it meets the film surface. However there is an alternate method to locate this particular point. The aforementioned spectral method describing the state of the surface tells us how surfactant on the surface evolves. We know moreover how much surface material must be to the left of the separatrix, because that is all material that was originally on the surface. We will exploit this idea later on (Eq. (7.32)) as a way of gauging the accuracy of the computed separatrix shape.

This completes our presentation of the numerical method. A discussion around parameter values employed to carry out the simulations, and how we obtained those parameters are the subject of the next section.

7.4 Simulation parameters and benchmarking

In this section, we supply parameters employed in the simulations. In Sec. 7.4.1, the physical data used within the simulations are explained. Data are given in dimensional form in the first instance, and then dimensionless groups are defined. Moreover, to ensure accurate simulations we benchmarked our simulations using various choices of numerical parameters. The results of the benchmarking and a discussion related to how to select the parameters in question are given in Sec. 7.4.2.

7.4.1 Physicochemical data used in the simulations

Although we often employ the generic term "surfactant" throughout the present study, we chose to look at parameters relevant to β-LG (β-lactoglobulin) protein as it is a common protein which makes up 50–55% of whey proteins [281], and its foaming and adsorption properties have been widely studied [76, 149, 158, 161]. For simplicity, we consider that β-LG is the only surface active species present, although in fractionation it is sometimes the case [103, 273] that we have a main species that we aim to separate, and a second species present as foam booster, merely to increase the volume of foam.

The surfactant transport model that is studied in the present work is only sensitive to the flow field that is set up in the presence of surface active material: it does not matter whether this flow field is due to a single surface active species or multiple species. Of course, for a convective mass transport model to apply (as is considered here), the transport of all species must be dominated by convection. If large bulky protein molecules (as a main species) are mixed with much smaller surfactant molecules (as a foam booster), diffusive [2] rather than convective transport might be relevant to the booster, and the model would then need to change. With just a single species though, i.e. β-LG as considered in the present work, that sort of issue does not arise.

The molecular mass of β-LG is $18.3\mathrm{kDa}$ [293, 294]. It exhibits good foaming properties due to its specific molecular structure [76]. In particular β-LG strongly adsorbs at the air/water interface forming viscoelastic layers and stabilises foam films. This then provides stability to foams preventing coalescence [152, 282].

Typically, the adsorption isotherm of a protein [288] is much more complicated than a simpler surfactant, such as SDS. Moreover, large area and large number of conformations of an adsorbed protein can increase the complexity of the system. For this reason, the most simple isotherm models (e.g. Henry or more generally Langmuir adsorption isotherms [289]) do not usually describe protein adsorption accurately [159, 163, 288].

That said, all we need for the purposes of the present study is a reasonable estimation of a typical amount of a protein, such as β-LG, dissolved in the Plateau border's bulk and the corresponding concentration on the Plateau border surface. Common β-LG concentrations used in fractionation and other separation applications are reported to be on the order of 10^{-4}–$10^{-1}\,\mathrm{mol.m^{-3}}$ in literature [24, 61, 159, 282, 284]. Consulting experimental data from Gochev et al. [159] (Table 7.1), we have therefore chosen data which are likely to be relevant in a foam fractionation process. This provided us with some typical values of both c and Γ. It is clear from Table 7.1 that the relationship between c and Γ is non-linear, so Γ/c is not a constant. Nonetheless having selected

typical surfactant concentrations Γ_{Pb} and c_{Pb} on and within the Plateau border (both richer than the concentrations in the film owing to the underlying assumption of reflux through the Plateau borders) and hence having selected the ratio between them $\Gamma_{\mathrm{Pb}}/c_{\mathrm{Pb}}$, we can make a very crude approximation that the initial concentrations for the film Γ_0 and c_0 are in a comparable ratio and hence $c_0 \sim (\Gamma_0/\Gamma_{\mathrm{Pb}})c_{\mathrm{Pb}}$.

This corresponds to assuming a so called global Henry constant in Rajabi and Grassia [2], denoted $K_{H(\mathrm{glob})}$ and defined as $K_{H(\mathrm{glob})} \equiv \Gamma_{\mathrm{Pb}}/c_{\mathrm{Pb}}$. A more general relation would be to assume a so called local Henry constant (again see Rajabi and Grassia [2]), which contemplates the value of $\mathrm{d}\Gamma/\mathrm{d}c$ near the Plateau border concentration. However all that would do in the present model is change the value of c_0 for a given Γ_0, assuming fixed Γ_{Pb} and c_{Pb}. Note that in the present model, although Γ can evolve away from Γ_0, the value of c is held at either c_0 or c_{Pb} depending on whether a point in the film is to the left or right of the separatrix. Hence qualitatively we expect to see similar results regardless of whether a global isotherm (a crude estimate) or a local isotherm (a better estimate) or indeed a more complex relation entirely is used to estimate c_0. For simplicity, we assume the global isotherm case. Note that in the main text, it was mentioned that the model for foam fractionation with reflux as considered here largely carries over to foam fractionation in stripping mode [91, 94, 103]. Global isotherms tend to be especially relevant for low surfactant concentrations in both films and Plateau borders, a situation which is likely to be particularly relevant to stripping mode: the purpose of stripping mode is to reduce surfactant concentration in say a wastewater stream down to a comparatively low level.

Table 7.1: Experimental data for β-LG surface concentration Γ at selected bulk concentration c taken from Gochev et al. [159].

$c\,[\mathrm{mol.m^{-3}}]$	$\Gamma\,[\mathrm{mol.m^{-2}}]$	$\Gamma/c\,[\mathrm{m}]$
10^{-4}	6.4×10^{-8}	6.4×10^{-4}
10^{-2}	8.1×10^{-8}	8.1×10^{-6}
10^{-1}	1.1×10^{-7}	1.1×10^{-6}

The values in Table 7.1 indicate that compared to a small surfactant molecule such as

sodium dodecyl sulphate (SDS) (data reported in Rajabi and Grassia [2]), the values for the ratio Γ/c for proteins such as β-LG, are larger. This implies, even though bigger molecules like proteins can exist in solution in the film, they are not quite as soluble as SDS would be. For our case of interest, we have chosen c_{Pb} to be $10^{-2}\,\mathrm{mol.m^{-3}}$ and Γ_{Pb} to be $8.1 \times 10^{-8}\,\mathrm{mol.m^{-2}}$ (see Table 7.2). Even though, in principle, the protein concentration can affect the rheology of the foam film [155], in many cases, the film's viscosity μ can be comparable to that of water [158] around $10^{-3}\,\mathrm{Pa.s}$. Gibbs elasticity $\mathcal{G}$ of β-LG is taken from Fainerman et al. [283], and remains almost constant even for concentrations up to $0.1\,\mathrm{mol.m^{-3}}$ as stated by Lexis and Willenbacher [158], Gochev et al. [162]. The value of $\mathcal{G}$ is taken as $85 \times 10^{-3}\,\mathrm{N.m^{-1}}$. In addition, for the particular concentration that we have chosen, surface tension at the Plateau border γ_{Pb} for β-LG is reported to be approximately $42 \times 10^{-3}\,\mathrm{N.m^{-1}}$ [205]. The diffusion coefficient $\mathcal{D}$ of β-LG is taken to be $5 \times 10^{-11}\,\mathrm{m^2.s^{-1}}$, which has been reported by Miller et al. [280].

In addition to the above mentioned physicochemical parameters, we also need geometric parameters, the film half-length L, the initial film half-thickness δ_0, and the curvature radius a of the Plateau border attaching to the film. These are chosen (see Table 7.2) to have typical values $L = 5 \times 10^{-3}\,\mathrm{m}$, $\delta_0 = 2.5 \times 10^{-5}\,\mathrm{m}$ and $a = 5 \times 10^{-4}\,\mathrm{m}$. Thus the film is comparatively long and slender, and is also thin compared to the Plateau border, but can become yet more slender over time as liquid drains out of it. Note that with these choices of L, δ_0 and a there is actually a comparable amount of liquid in the film and in the Plateau border (unlike the case with a much smaller δ_0, in which the amount of liquid in the film is much less than the amount in the Plateau border). Despite this we will persist with our simplifying assumption that the Plateau border can be treated as a reservoir of surfactant. We bear in mind here that liquid is also draining down through the network of Plateau borders. Even as a Plateau border in contact with a given film starts to become depleted, the depleted liquid will drain out through the network, and be replenished by less depleted liquid from higher up in the Plateau border network.

Table 7.2: Dimensional parameters for β-lactoglobulin (β-LG), available from Lexis and Willenbacher [158], Gochev et al. [159, 162], Pradines et al. [205], Miller et al. [280], Fainerman et al. [283]. A number of geometric parameters for foam films are also reported.

Dimensional Parameters	Symbol	Value	Unit
Characteristic time scale	$\mu L^2/\mathcal{G}\,\delta_0$	1.18×10^{-2}	s
Film half-length	L	5×10^{-3}	m
Initial film half-thickness	δ_0	2.5×10^{-5}	m
Liquid viscosity	μ	1×10^{-3}	Pa.s
Surfactant surface excess at Plateau border	Γ_{Pb}	8.1×10^{-8}	$\mathrm{mol.m^{-2}}$
Bulk concentration in Plateau border	c_{Pb}	1×10^{-2}	$\mathrm{mol.m^{-3}}$
Radius of curvature of Plateau border	a	5×10^{-4}	m
Surface tension at Plateau border	γ_{Pb}	42×10^{-3}	$\mathrm{N.m^{-1}}$
Gibbs parameter	$\mathcal{G}$	85×10^{-3}	$\mathrm{N.m^{-1}}$
Diffusion coefficient	$\mathcal{D}$	5×10^{-11}	$\mathrm{m^2.s^{-1}}$
Global Henry constant	$K_{H(\mathrm{glob})}$	8.1×10^{-6}	m

Having gathered together all the dimensional variables for the purpose of our simulations (Table 7.2), we worked out base case values of various dimensionless groups using definitions in Sec. 6.2.1. Data are reported in Table 7.3. These include Péclet number Pe, film aspect ratio Δ, a solubility parameter $\mathcal{S}$ and a drainage parameter V_R.

Table 7.3: Dimensionless parameters, calculated using the data from Table 7.2. Values of Pe and $\mathrm{Pe}\,\Delta$ are comparatively large, so surfactant transport is assumed to be dominated by advection.

Péclet number	Pe	2.13×10^5
(Initial) aspect ratio	Δ	5×10^{-3}
Value of $\mathrm{Pe}\,\Delta$	$\mathrm{Pe}\,\Delta$	1.06×10^3
Solubility parameter	$\mathcal{S}$	3.09
Film drainage velocity parameter	V_R	1.65×10^{-2}

Within Table 7.3, values for $\mathrm{Pe}\,\Delta$ are relevant as they appear in the surfactant mass transfer equations (see Eqs. (6.8) and (6.9) in the main text). Note that $\mathrm{Pe}\,\Delta$ is a large parameter here (unlike the work of Rajabi and Grassia [2] which considered SDS not β-LG, leading to a different parameter set with a small $\mathrm{Pe}\,\Delta$, so had rather different physics). The mass transfer equations also include a term in $\mathrm{Pe}\,/\Delta$, but this is a very large parameter indeed.

Table 7.3 also contains a base case value of the solubility parameter $\mathcal{S}$, although in the

main text we also allow $\mathcal{S}$ to vary. Note that in the present model (unlike the work of Rajabi and Grassia [2]) varying $\mathcal{S}$ does not actually change the computations for how mass is transferred in any way. All varying $\mathcal{S}$ does is to change a post-processing step, changing the weighting between material on the surface and material in the bulk. A film drainage velocity parameter V_R is also included in Table 7.3. Clearly it is a relatively small parameter, meaning film drainage is a comparatively weak effect. In the main text we consider situations both without film drainage and with film drainage.

Note also that the dimensionless analogues of Γ_{Pb}, c_{Pb} and $K_{H(\mathrm{glob})}$ are all unity by definition so these do not appear in Table 7.3. The only other dimensionless parameters affecting the system are then the dimensionless analogues Γ_0 and c_0 of the initial film concentrations. For compactness of notation, we use the same symbol for these dimensionless analogues and the original dimensional concentrations. Indeed we already considered dimensionless Γ_0 back in Sec. 7.2. In the present work, these dimensionless quantities Γ_0 and c_0 are equal to each other, and (since the film is less surfactant rich than the Plateau border which is subject to reflux) they necessarily take values between zero and unity.

We have now specified all the various physical parameters which influence the model. In the next section we move on to numerical aspects.

7.4.2 Benchmarking the simulations and selecting numerical parameters

To benchmark our simulations, we carry out the following steps. In general, there are three numerical parameters which contribute to the accuracy of our simulations. One is the number of Fourier terms used in the spectral method calculations [2]. This parameter must be set to obtain evolution of Γ for the surface using Eq. (6.10) in the main text. The Γ thereby obtained will then be used in the calculation of the velocity fields Eqs. (6.5) and (6.6), which are then used to determine how material points move

around in the bulk. As Rajabi and Grassia [2] also found, using a larger number of Fourier terms improves accuracy at earlier times. However using more Fourier terms than needed leads to little further improvement, but on the other hand, extends the simulation run time considerably.

The second important parameter is the size of the time steps. Due to the model's boundary conditions, the initial changes are very rapid and the changes slow down over time. Owing to this, we can make a significant error at the initial time if we do not use small enough time intervals. The size of time steps can affect not just what happens on the surface, but also what happens in the bulk, particularly while calculating the separatrix evolution. Especially, as can be seen in Sec. 7.2.3, it influences in particular the calculation of the separatrix evolution during the very first time step.

The third parameter is the number of material points that we consider in the separatrix. Including and following more material points gives a more accurate shape of the separatrix, improving the accuracy of the quadratures used to find the areas of regions either side of the separatrix which govern the amount of material in the film (see Fig. 6.1b in the main text for a sketch). Of course including more material points also makes calculations more expensive.

The main focus of the present work is to investigate the evolution of the separatrix with time. As a result, to identify a sufficient number of Fourier terms to represent the system, a sufficiently small size of time step size, and also sufficient material points on the separatrix, we have run many different simulations considering various ranges of the mentioned parameters. Then, we have devised several ways of measuring differences between the various results to assess the numerical accuracy, specifically in regards to how accuracy impacts the separatrix.

Firstly, we have performed a comparison of the shape of the separatrix. To to this, we have plotted the separatrix and visually compared the shapes obtained using different numerical parameters. We have also used an alternative numerical calculation to track

the position of the specific material point on the surface x_{surf} which separates the material that has always been on the surface from the newly arrived surface material from the Plateau border[1]. That calculation is determined as follows.

We know that the separatrix is a boundary between a region with initial bulk concentration c_0 and a region with the Plateau border's concentration c_{Pb}, normalised to unity in the dimensionless system considered here. The region with concentration c_0 starts off in contact with the film surface with a concentration Γ_0. In our dimensionless system, c_0 and Γ_0 are equal. Over time, surface concentration Γ evolves away from Γ_0. However the amount of surfactant on the surface to the left of x_{surf} ideally always equals the total initial amount Γ_0. This is due to the fact that because of the lack of diffusion in the model, surfactants on the surface remain there throughout the process. Hence, x_{surf} at each instant can be calculated by solving the following equation:

$$\left(\int_0^1 \Gamma \,\mathrm{d}x\right)\Bigg|_{t=0} = \int_0^{x_{\mathrm{surf}}} \Gamma \,\mathrm{d}x \tag{7.32}$$

where Γ at the initial time ($t = 0$) ideally should be Γ_0 everywhere for $0 \leq x < 1$. To increase the accuracy of the x_{surf} calculation using Eq. (7.32), the value of Γ in Eq. (7.32) has been calculated using a large number 1000 Fourier terms (by contrast with Sec. 7.4.2.1 below which considers fewer terms) and the size of time steps has been chosen to be comparatively small 5×10^{-4} (by contrast with Sec. 7.4.2.2 later on which considers larger time steps).

Note that using our Fourier approach the left-hand side of Eq. (7.32) is close to Γ_0, but is not exactly Γ_0 as a finite number of Fourier terms has still been used in our calculations. Having calculated x_{surf}, we have measured and compared the difference between the values of x_{surf} (the position of the material point on the surface along the x-axis obtained from Eq. (7.32)), with the values obtained from the simulations that

[1]The material point x_m in Sec. 7.2.1 is analogous to x_{surf} considered here, although x_m was considered only for early times, whereas x_{surf} applies for arbitrary times.

calculate the trajectory of the separatrix at each instant, looking specifically at the top of the separatrix. This then is one measure of the accuracy of the simulation.

The value of x_{surf} of course only measures the top of the separatrix and not the accuracy of the shape of the separatrix as a whole. As a global measure of accuracy of the separatrix shape, we considered root mean square difference (denoted rmsd) as below:

$$\mathrm{rmsd} = \sqrt{\int_{x_{\mathrm{surf}}}^{1} (z_{\mathrm{sep},1} - z_{\mathrm{sep},2})^2 \, \mathrm{d}x} \tag{7.33}$$

where $z_{\mathrm{sep},1}$ and $z_{\mathrm{sep},2}$ correspond to the z positions of the material points on the separatrix with the same x positions, calculated using different numerical parameters.

Remember also that the purpose of computing the separatrix is to determine the area A_b (to the right of the separatrix) occupied by material with a surfactant concentration equal to that in the Plateau border, and how that then compares with the area A_t of the film as a whole. Accordingly we have computed the ratio between these (A_b/A_t), based on finding A_b via a numerical (trapezoidal rule) integration of the points on the separatrix. Comparing A_b/A_t for different sets of numerical parameters is then another measure of the accuracy of the simulations.

To summarise, we have changed number of Fourier terms, size of time steps and number of material points on the separatrix, and compared the simulation results. Based on the data presented in what follows, ultimately we decided that 30 Fourier terms, 10^{-3} as the dimensionless time step and 50 material points on the separatrix would give us a reasonable accuracy without causing the simulation time to become excessively long. On an ASUS laptop computer (3.3 GHz processor with 16 GByte RAM), a simulation with those parameters took around an hour per dimensionless time unit to complete. Some of the comparisons that were done are mentioned below as examples of our benchmarking procedure.

7.4.2.1 Number of Fourier terms

Fig. 7.2 is a comparison between the separatrix shapes produced using respectively 3, 30 and 100 Fourier terms in the simulations. The points marked with a cross ($\times$) on the graphs correspond to x_{surf}, calculated for each instant using Eq. (7.32).

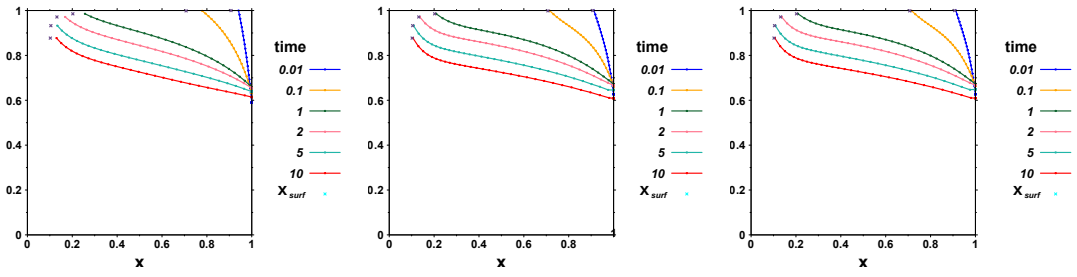

(a) 3 Fourier terms **(b)** 30 Fourier terms **(c)** 100 Fourier terms

Figure 7.2: The difference in the shape of the separatrix calculated using 3, 30 and 100 Fourier terms. In all three cases, size of time steps is 2×10^{-3} and 50 material points have been used on the separatrix. The dimensionless initial surface concentration (Γ_0) in all the simulations is assumed to be 0.1.

We have also calculated using Eq. (7.33) the root mean square difference between the position of the material points on the separatrix using different numbers of Fourier terms as presented in Fig. 7.3.

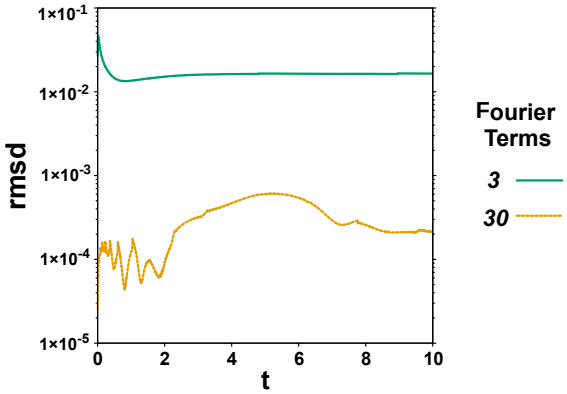

Figure 7.3: Root mean square difference between position of the material points calculated with 3 and 30 Fourier terms with the one calculated with 100 Fourier terms. In all calculations time steps of 2×10^{-3} and 50 material points have been used.

It can be seen that the shapes of the separatrix produced with 30 and 100 Fourier terms are visually at least almost identical. Moreover, Fig. 7.2 also shows that the material points on the surface calculated with the simulations using 30 and 100 Fourier terms are much closer to the corresponding x_{surf} obtained from Eq. (7.32), than the one

calculated with only 3 Fourier terms. Furthermore, the calculated root mean square difference between the position of the material points on the separatrix with 30 Fourier terms and with 100 Fourier terms (less than 1×10^{-3} for all times) in Fig. 7.3 confirms this. Hence, we have decided to use 30 Fourier terms in the simulations.

7.4.2.2 Size of time steps

Table 7.4 shows the difference in the calculations of x_{surf} using simulations with 30 Fourier terms, but different size of time steps at three times, e.g. 0.1, 1 and 10.

Table 7.4: In this table, the difference is reported at various times between the top of the separatrix calculated using simulations with 30 Fourier terms and different sizes of dimensionless time steps ($1 \times 10^{-2}, 2 \times 10^{-3}, 1 \times 10^{-3}$ and 5×10^{-4}) and the material point on the surface x_{surf} calculated using Eq. (7.32). Initial surfactant concentration on the surface (Γ_0) in all the simulations is assumed to be 0.1.

Δt	0.01	0.002	0.001	0.0005
Time				
0.1	1.55×10^{-2}	0.88×10^{-2}	0.64×10^{-2}	0.44×10^{-2}
1	1.44×10^{-2}	0.65×10^{-2}	0.46×10^{-2}	0.31×10^{-2}
10	0.79×10^{-2}	0.35×10^{-2}	0.24×10^{-2}	0.16×10^{-2}

It can be seen from Table 7.4 that using smaller time steps increases the accuracy of the calculations. Here, by utilisation of time steps equal to 2×10^{-3}, the difference in x_{surf} using simulation (i.e. the point computed at the top of the separatrix) is never further than 10^{-2} from the one calculated using Eq. (7.32). On the other hand, using time steps equal 5×10^{-4} leads at most to around 4.4×10^{-3} difference from x_{surf} values, but increases the simulation run times by a factor of four. Thus, choosing time step equal to 1×10^{-3} is selected as a compromise between accuracy and a reasonable simulation run time.

7.4.2.3 Number of material points in separatrix

By using more material points on the separatrix, we capture the separatrix shape more accurately, but the simulation becomes more expensive to run. Ultimately we are using the separatrix to compute areas of regions with specified surfactant concentration (area

A_b with concentration of the Plateau border, area $A_t - A_b$ with initial concentration of the film, and A_t as area overall). Accuracy of computing areas is therefore what we must assess.

We have evaluated as a function of time the ratio A_b/A_t calculated using 10, 20, 30, 50 and 100 material points. Then we calculated at each instant the difference in A_b/A_t obtained using 10, 20, 30 and 50 material points compared to the area calculated with 100 material points.

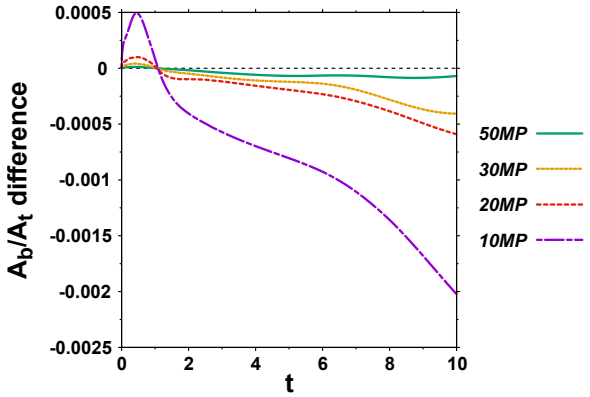

Figure 7.4: The difference between area ratio A_b/A_t calculated with 10, 20, 30 and 50 material points and area ratio calculated with 100 material points (MP in the legend here denotes material points). In all calculations 30 Fourier terms and a time step of 2×10^{-3} have been used.

As can be seen in Fig. 7.4, as the number of material points increases, the difference between the A_b/A_t values becomes smaller. Clearly using more material points improves the accuracy of trapezoidal rule integration. In particular the difference between A_b/A_t calculated using 50 material points and the one calculated with 100 material points is always smaller than 10^{-4}, so we selected in the end 50 material points.

7.5 Non-linear adsorption isotherm

As alluded to in Sec. 6.2.5.2 (in the main text), throughout the study thus far we have used a global Henry adsorption isotherm (i.e. a linear isotherm) to relate the equilibrium amount of surfactant on the surface to the equilibrium amount of surfactant in the bulk. Using a linear adsorption isotherm would also be in line with what Rajabi and

Grassia [2] have previously done. Nonetheless we can also use a non-linear isotherm when required. In this section, we investigate what the effect of a non-linear adsorption isotherm would be on the performance of a fractionation process assuming (as has been done throughout the present study) a large $\mathrm{Pe}\,\Delta$ limit.

7.5.1 Specifying the non-linear isotherm

Remember here that we work with a dimensionless system, such that for the Plateau border, the dimensionless surface concentration Γ_{Pb} and dimensionless bulk concentration c_{Pb} are both unity. What this means then for a non-linear adsorption isotherm, such as e.g. a Langmuir isotherm, is that the equilibrium surfactant concentration on the film surface, Γ is higher than the corresponding amount in the film bulk, c. Of course in the large $\mathrm{Pe}\,\Delta$ limit, surfactant transfer between surface and bulk is considered slow, so that, in the film itself, we only impose equilibrium between initial surface concentration Γ_0 and initial bulk concentration c_0. A non-linear isotherm then requires that dimensionless Γ_0 exceeds dimensionless c_0 (equivalently c_0 is below Γ_0), but both are less than unity.

Exactly how much c_0 falls below any given Γ_0 depends on exactly how much the isotherm departs from linearity. This depends in turn upon exactly where Plateau border conditions lie on an original non-linear isotherm. If dimensional Γ_{Pb} and c_{Pb} are increased, the departure from linearity is greater. Here though we work in a dimensionless system with $\Gamma_{\mathrm{Pb}} = c_{\mathrm{Pb}} = 1$ as mentioned.

In view of the discussion above, we have chosen three initial surface concentrations, i.e. $\Gamma_0 = 0.1, 0.5$ and 0.9. For the lowest surfactant surface concentration, namely, $\Gamma_0 = 0.1$, we only used surfactant bulk concentration $c_0 = 0.1$ which corresponds to using the global Henry adsorption isotherm, i.e. a linear isotherm. However, for $\Gamma_0 = 0.5$, besides using $c_0 = 0.5$, which corresponds again to using the global Henry adsorption isotherm, we have also used $c_0 = 0.1$ as if a non-linear isotherm had been

selected. The same approach has been taken for $\Gamma_0 = 0.9$ with $c_0 = 0.9, 0.5$ and 0.1, which corresponds to using a linear adsorption isotherm and two non-linear ones with differing extent of non-linearity.

7.5.2 Expected behaviours for non-linear isotherm

Before proceeding with examining data, it is useful to make some general predictions as to how the system might behave. For example the initial total amount of surfactant recovered in the film satisfies $S_{T,0} = \Gamma_0 + \mathcal{S}\, c_0$ where $\mathcal{S}$ is solubility parameter. Reducing c_0 at fixed Γ_0 (i.e. making the isotherm increasingly non-linear) clearly makes $S_{T,0}$ reduce. The final amount of surfactant recovered on the film is expected to be around

$$S_T \approx 1 + \mathcal{S}\left(\frac{A_b}{A_t} + \left(1 - \frac{A_b}{A_t}\right) c_0\right) \tag{7.34}$$

at least if film drainage is ignored, and where we assume A_b/A_t here specifically is a final ratio of areas (area brought in from the Plateau border divided by area of the film). The value of A_b/A_t (which is always less than unity) depends on Γ_0 (it reduces as Γ_0 increases), but does not depend on c_0. Reducing c_0 at fixed Γ_0 of course reduces S_T.

Note that the maximum value of $S_T/S_{T,0}$ is also the maximum relative amount that recovery can increase over time. If solubility $\mathcal{S}$ is small, this can be on the order of Γ_0^{-1}. On the other hand, if solubility $\mathcal{S}$ is large and bulk concentration c_0 is low, the maximum value that $S_T/S_{T,0}$ can reach will be on the order of $A_b/(A_t c_0)$. This is always less than c_0^{-1}. In fact it might be substantially less than that: values of Γ_0 close to unity give values of A_b/A_t much smaller than unity. Conversely an effective way of increasing $A_b/(A_t c_0)$ is of course to reduce Γ_0. Another way of increasing $A_b/(A_t c_0)$, even at fixed Γ_0, is to reduce c_0, in other words to make the isotherm increasingly non-linear.

We now turn to consider enrichment. Films are richer than bulk solution even prior

to any effect of reflux. Initial enrichment is $S_{T,0}/(\mathcal{S}\, c_0)$. If solubility $\mathcal{S}$ is small, then initial enrichment is $\Gamma_0/(\mathcal{S}\, c_0)$. Making the isotherm non-linear, in other words making c_0 smaller than Γ_0 clearly benefits initial enrichment. On the other hand, when $\mathcal{S}$ is large, the initial enrichment is close to unity.

Turning now to the final state (still ignoring film drainage though) in the low solubility limit, final enrichment can reach $(\mathcal{S}\, c_0)^{-1}$. In the high solubility limit, final enrichment might reach instead $A_b/(A_t c_0)$, where remember that the value of A_b/A_t depends on Γ_0 but not on c_0. In this case, decreasing Γ_0 benefits enrichment, and also, even at fixed Γ_0, making the isotherm non-linear benefits enrichment too.

The various estimates provided above ignore film drainage of course, whereas the results to be presented in what follows will include drainage. Nonetheless to the extent that film drainage is a relatively weak effect compared to Marangoni, the trends predicted by the above estimates will be borne out.

7.5.3 Non-linear isotherm data for $S_T/S_{T,0}$

The graphs of $S_T/S_{T,0}$ for the various above mentioned initial concentrations (see Sec. 7.5.1) are plotted in cases with different solubility parameters, i.e. $\mathcal{S}$ equal to either 0.3, 3 or 30 in Fig. 7.5.

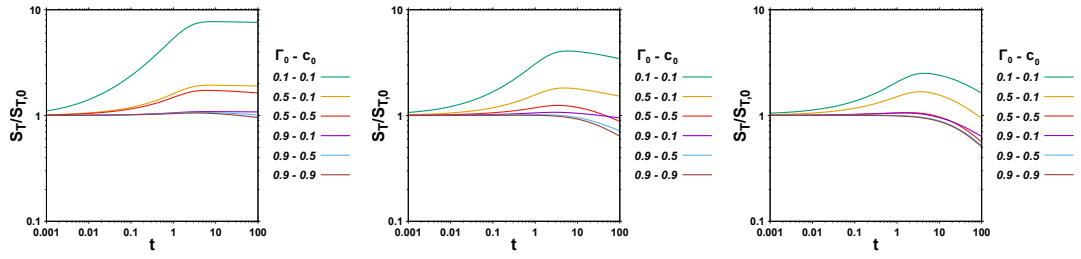

(a) $\mathcal{S} = 0.3$ **(b)** $\mathcal{S} = 3$ **(c)** $\mathcal{S} = 30$

Figure 7.5: Total amount of surfactant (S_T) relative its initial value ($S_{T,0}$) versus time, calculated for surfactants with solubility parameters, 0.3, 3 and 30 and for various values of Γ_0 using linear $c_0 = \Gamma_0$ and non-linear $c_0 < \Gamma_0$ isotherms.

Looking first at low solubilities (Fig. 7.5a), we see that decreasing Γ_0 leads to increased $S_T/S_{T,0}$, whereas setting Γ_0 close to unity keeps $S_T/S_{T,0}$ close to unity also: this is

what Sec. 7.5.2 anticipated. On the other hand, for a given Γ_0, switching to a non-linear isotherm also increases $S_T/S_{T,0}$ albeit slightly. This increase follows because, as was anticipated (Sec. 7.5.2), using a non-linear adsorption isotherm reduces the initial total amount of surfactant, $S_{T,0}$, i.e. the amount of surfactant in the bulk is less than when using a linear adsorption isotherm.

Switching now to moderate solubilities (Fig. 7.5b), we see that $S_T/S_{T,0}$ exhibits non-monotonic behaviour with time: a decrease is seen at late times due to loss of surfactant from the bulk due to film drainage. The smallest Γ_0 values still lead to the largest $S_T/S_{T,0}$, but $S_T/S_{T,0}$ does not now reach anywhere near Γ_0^{-1} as it would in a low solubility case. Meanwhile at a given Γ_0, we now see a greater difference between the non-linear and linear isotherm cases. This is in part due to $S_{T,0}$ being larger in the linear isotherm cases. The difference in $S_T/S_{T,0}$ between non-linear and linear cases is also more significant when Γ_0 is smaller: this follows because the value of A_b/A_t in Eq. (7.34) is itself more significant when Γ_0 is smaller. In essence, using a linear isotherm increases the recovery of a fractionation column (increases S_T) but reduces the relative effect of reflux (reduces $S_T/S_{T,0}$).

Switching again to the highest solubility (Fig. 7.5c), we now see a much clearer effect of film drainage reducing the value of $S_T/S_{T,0}$ at late times. Small Γ_0 still gives higher $S_T/S_{T,0}$ compared to large Γ_0. Moreover for a given Γ_0, the non-linear isotherm again gives higher $S_T/S_{T,0}$ than the linear one, the difference between the non-linear and linear cases again being more significant when Γ_0 is smaller.

7.5.4 Non-linear isotherm data for recovery and enrichment

Now, we compare recovery and enrichment for $\Gamma_0 = 0.1$, using a linear adsorption isotherm, with $\Gamma_0 = 0.5$, for both linear and non-linear adsorption isotherms.

From Fig. 7.6 and in particular Fig. 7.6a, we can see that overall there is more benefit over time in the case with lower initial surface concentration (i.e. lower Γ_0), in terms

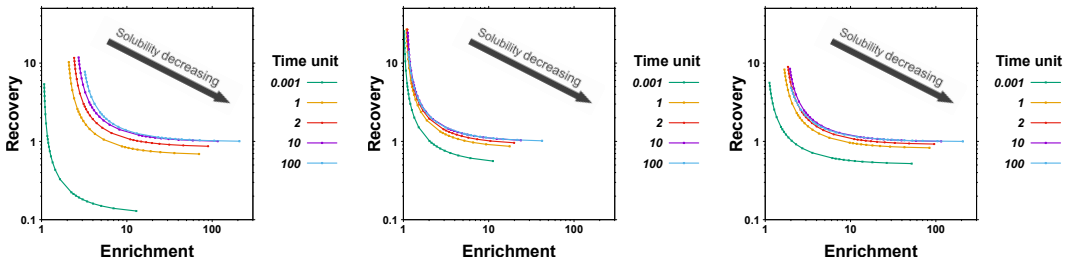

(a) $\Gamma_0 = 0.1, c_0 = 0.1$ (Linear isotherm)

(b) $\Gamma_0 = 0.5, c_0 = 0.5$ (Linear isotherm)

(c) $\Gamma_0 = 0.5, c_0 = 0.1$ (Non-linear isotherm)

Figure 7.6: Recovery versus enrichment, plotted for various solubility parameters, at different times. Linear adsorption isotherm has been used for $\Gamma_0 = 0.1$, while both linear and non-linear isotherms have been used for $\Gamma_0 = 0.5$.

of relative increase over time in recovery and enrichment. This is just as Sec. 7.5.2 anticipated.

However, comparing different adsorption isotherms for $\Gamma_0 = 0.5$, e.g. Fig. 7.6b (linear) and Fig. 7.6c (non-linear) can reveal some interesting findings. First, we can see that in the non-linear isotherm case (Fig. 7.6c), generally, enrichment is higher, while recovery is a little lower than in the linear isotherm case (Fig. 7.6b). This is due to the fact that the amount of bulk surfactant in the non-linear isotherm case is less than for the linear isotherm. However, both cases recover more or less comparable total amounts of surfactant at long time. As a result, the case that is leaner in the bulk initially (i.e. the non-linear isotherm case) is found to be more enriched.

The other interesting finding is that in the high solubility region, there is, in relative terms, more benefit from Plateau-border-to-film mass transfer induced by reflux over time in the case with a non-linear isotherm. This is in line with what Sec. 7.5.2 anticipated, and is due to the fact that, for a non-linear isotherm we are replacing material from the film with a very low dimensionless concentration c_0, with material with unit concentration from the Plateau border. However, in the low solubility region despite the fact that the case with a non-linear isotherm has higher initial enrichment, the benefit from reflux (in terms of relative change in recovery and enrichment over time) is not really any different in the non-linear and linear adsorption isotherm cases, at least if Γ_0 is held fixed: this is again in line with what Sec. 7.5.2 anticipated.

In summary, for surfactants with a linear adsorption isotherm, in the high solubility region, there is a limited benefit from Plateau-border-to-film mass transfer induced by reflux, unless films are initially very depleted in surfactant. That said, less soluble surfactants (smaller $\mathcal{S}$) manage to benefit more over time from reflux than more soluble surfactants (larger $\mathcal{S}$) do. On the other hand, when using a non-linear adsorption isotherm, surfactants with all solubilities can benefit from reflux. Despite reflux being beneficial in such cases, the important effect for non-linear isotherms is higher enrichment. Recovery however in the case of non-linear isotherms can actually be lower than with linear ones.

Chapter 8

Summary and conclusions

As discussed in Sec. 2.1, surface-active materials are widely used in industrial processes. This is due to their characteristics which make them suitable for various applications, e.g., food industry, oil recovery and pharmaceuticals. This widespread use of surface-active materials can also create a great demand for their separation within the abovementioned industrial processes. The tendency of surfactants to adsorb on a gas/liquid interface is one of their main characteristics. Therefore, using a separation method that takes advantage of this characteristic can be worthwhile [9].

As discussed in Sec. 2.2, foam fractionation is a separation method that works based on the adsorption of surfactants on bubbles surfaces. Moreover in a fractionation column with reflux, rising bubbles are in contact with richer interstitial liquid. This then causes a driving force for mass transfer to happen between these regions [26].

As mentioned in Sec. 2.1, because of their structure, surfactants tend to report to the surface of foam films. Previous work has treated surfactants as being entirely on the surface [1]. However, each surfactant has a specific solubility in water. Within a given foam film, the newly-introduced solubility parameter, $\mathcal{S}$, represents the typical amount of dissolved surfactant in the bulk relative to the typical amount on the surface. The purpose of the present study has been to model surfactant transport on and within a

foam film in a fractionation column with reflux, but accounting now for solubility.

As discussed in Sec. 2.4, in the system of interest here, foam is considered to be comparatively dry, i.e. with low liquid content. In this case, bubbles are polyhedral, foam films are thin and almost flat, and three of them join each other in a so-called Plateau border. In contrast, Plateau borders' surfaces are curved. According to the Young-Laplace law, this difference in curvature between foam films and the adjacent Plateau borders causes the so-called foam film drainage. Hence, since surfactants are now present in the bulk, film drainage from the bulk contributes to mass transport during the fractionation process.

The other important mechanism for surfactant transport though is the Marangoni effect. The fact that there is a difference, due to the reflux, in the surface concentrations on the films and on the neighbouring Plateau borders leads to differences in surface tensions. These in turn now act to produce a driving force to bring surfactants from the surface (and also bulk) of the Plateau borders towards the centre of the film. Thus, Marangoni flow has a significant effect on the evolution of surfactant distribution on the surface and consequently also, when surfactant is soluble, in the bulk of the foam films.

Modelling of insoluble surfactants transported on the foam film surface accounting for the mentioned effects, i.e. Marangoni flow and film drainage, has previously been developed, as has been mentioned, by Vitasari et al. [1]. Behaviour has been considered both in the absence and the presence of film drainage. However, as discussed already, surfactants are in reality soluble. This then is what has led us to consider the current model, in which surfactant solubility and its transport inside the bulk are included. Moreover, in line with Vitasari et al. [1], we consider cases both with and without film drainage.

Just as Vitasari et al. [1] did, we consider the lubrication approximation to the Navier-Stokes equations. Then, we numerically solve mass transport equations based on the approximation made. However, to do that, we need to know the relationship between

surface and bulk concentrations. Here, we use an adsorption isotherm. In this study, to avoid complications associated with non-linear adsorption isotherms, we use a linear isotherm based on data taken from relevant literature [1, 165, 202, 247]. Having employed all the aforementioned models, we can obtain an equation for the evolution of surfactant concentration with time, considering both the film surface as well as the bulk. We then solve numerically the obtained equations using a so-called spectral method, and simulate the system to obtain results. In addition to the evolution of surfactants at specified locations on the surface and within the film, the overall surfactant concentration of the films, and the resulting recovery and enrichment have been calculated and analysed. The latter enables us to predict the performance of a fractionation column with respect to its length or else with respect to the foam film residence time.

In this study, we consider two limits to carrying out our modelling. The two limits differ according to whether or not we take into account diffusive transport from the surface to bulk. Generally, the diffusive transport from the surface to bulk can in principle occur at different rates relative to Marangoni and film drainage flow. In the first particular limit we look at, surfactants can diffuse very quickly across a thin film, even though any diffusion along the film is very slow. Therefore, surfactants are distributed uniformly across the film thickness. Mathematically, we can express this in terms of the product of a Péclet number (Pe) and a film aspect ratio, Δ, with this product being a small parameter. This then is known as the small $\mathrm{Pe}\,\Delta$ limit. The important findings of the abovementioned limit are as below:

- The reflux produces a Marangoni flow that drives surfactant onto the film.
- Higher initial surfactant concentration Γ_0, leads to slower Marangoni flows and as a result less rapid improvement in recovery and enrichment.
- Higher solubilities slow down the Marangoni evolution of the overall amount of surfactant.
- The so-called local Henry isotherm (effectively a local tangent line to a more

general isotherm) leads to even more slow down than the global Henry isotherm.

- In film drainage cases, the amount of surfactant recovered by the film is less, but the effective concentration, i.e. enrichment, is higher. This is due to the fact that, as the film drains, the contribution from the surface relative to the bulk, increases.

- In cases with significantly slowed down Marangoni flows (high solubilities with local Henry isotherm), the film drainage might even cause a reduction of the total amount of surfactant recovered after a sufficiently long time on the time scales we examined.

However, there could be an opposite limit in which $\mathrm{Pe}\,\Delta$ is relatively large: transport within films is now dominated by convection. This is the second limit we consider. This limit is relevant in cases with relatively small diffusivity coefficients, e.g. for bigger molecules such as proteins [280]. It could also be relevant for foam films shortly after they are formed, such that the film is still in the process of draining, and hence could be quite some way from a final thickness. In this part of the study, within the bulk, we tracked a locus that we call a separatrix, which forms a boundary between two regions with uniform, but different concentrations. The findings in this second limit can be summarized below:

- The top of the separatrix is pulled towards the centre of the film, while for locations closer to the midplane of the film, the separatrix is pulled instead towards the Plateau border.

- Higher initial surfactant concentration Γ_0, and higher solubility parameter $\mathcal{S}$, lead to having a more initial overall amount of surfactant on and within the film, but less overall amount of surfactant relative to the initial amount.

- In the no film drainage case, the overall amount of surfactant relative to the initial amount increases up to a point and then reaches a steady state. However, in the

present case with large $\mathrm{Pe}\,\Delta$, this increase is not as much as was seen in the first limit (with small $\mathrm{Pe}\,\Delta$).

- In the case with film drainage, the surfactant amount relative to the initial amount decreases after reaching a maximum.
- In the cases with higher initial surfactant concentration Γ_0, and higher solubility parameter $\mathcal{S}$, the time to reach maximum recovery is less and the amount of surfactant being lost from the film afterwards is greater.
- Higher solubilities are more beneficial for surfactant recovery, and lower solubilities are more beneficial for the enrichment of the foamate in a fractionation process.

Having discussed the results of each limit separately, now the difference between them is considered. As far as the surfactant transport onto the surface is concerned, the two limits are comparable. This means that the dominant mechanism for increasing the amount of surfactant on the surface is the Marangoni flow. As a result, the difference between the surfactant surface concentration initially on the film and that of the Plateau border is an essential parameter governing how surfactant transport happens on the surface. However, in the first limit, the rate of surfactant increase on the surface is also dependent on the solubility parameter as some of the surfactants diffuse into the bulk, along with being transported on the surface by Marangoni flow. On the other hand, there is no solubility dependence in the second limit, at least when surfactant transport on the surface itself is concerned: results on the surface are then identical to the insoluble case of Vitasari et al. [1].

The difference between the two models is much more obvious in the bulk. This is due to the fact that in the first limit, different positions in the bulk have uniform concentrations across the thickness of the bulk. This concentration is determined by the surfactant concentration on the surface. However, in the second limit, there are two regions in the bulk with different but uniform concentrations. These concentrations

are the Plateau border bulk concentration and the initial film bulk concentration. The shape of the boundary that separates the two regions needs to be computed.

It is expected that the insights gained from the models developed here should assist design of foam fractionation processes with reflux, and should also help to make existing processes more efficient by indicating how process performance depends on operating parameters.

Chapter 9

Future work

Although this thesis has provided insights into foam fractionation with reflux, there is still more work that can be done. In this thesis, the various assumptions and simplifications used to develop the models have been discussed in-depth. However, regardless of how much effort is employed to make the assumptions closer to real physical conditions, they certainly can affect the accuracy of the mathematical models developed and consequently the accuracy of the final results. Therefore, a general statement for future work could be to reconsider such simplifications wherever possible. Now, we discuss some of them in brief.

One significant assumption has been to consider Marangoni-driven flow in the foam films solely for films treated as being flat and uniform thickness, albeit with that thickness changing with time (specifically via a film drainage model that assumed rigid interfaces). In reality though, the Marangoni flow and film drainage flow are coupled, with the film thickness becoming non-uniform. A normal stress boundary condition then relates a pressure jump across the film to surface tension and surface curvature. The film drainage flow and film thinning rate must then be obtained as part of the solution to the Marangoni flow problem [51, 222, 223], not as a drainage flow that is externally imposed (imposed from e.g. empirical observations of film thinning rates).

Even in the context of a film drainage flow that is externally imposed as mentioned previously, in the present thesis, two extreme limits regarding the diffusion of surfactant across the film relative to the Marangoni flow along it have been considered. However, despite the fact that these cases could be reasonable approximations under particular conditions, the real case should always be somewhere in between them. As a result, one potential direction for future work would be to model and simulate the finite $\mathrm{Pe}\,\Delta$ case or "in-between" case (in-between the small $\mathrm{Pe}\,\Delta$ and large $\mathrm{Pe}\,\Delta$ limits) considering thereby all the relevant terms in the governing equations.

Moreover, in this thesis, we carried out a study of surfactant transport both on and within the foam films. Hence, we needed a relationship between surfactant surface and bulk concentrations which has been done by using an adsorption isotherm. Particular simple isotherms were selected here. The future work related to this part could thereby concern using more complicated adsorption isotherms to expand the model to the surface active components with different adsorption behaviours.

In addition, in the large $\mathrm{Pe}\,\Delta$ limit, we have looked just at convective transport and ignored the diffusion between two regions in the bulk separated by the separatrix. This is a good approximation for early stages of the process as long as convective flow in the film dominates the diffusion transport in the aforementioned regions. However, we know that convection can decay comparatively quickly as Marangoni forces decay away (see e.g. the characteristic time scale in Table 7.2): the surfactant diffusion that happens long times (once convection has in effect ceased) still needs to be considered.

Furthermore, we have looked at just the impact of reflux on enhancing surfactant transport on the film scale. This understanding of the film scale needs, in the future, to be incorporated into a model on the entire process scale for foam fractionation with reflux. Finally, the impact of this thesis would be greater if the obtained results were to be experimentally tested and investigated. Here, the scope of the project did not include any experimental analysis, but it should be considered in the future.

References

[1] D. Vitasari, P. Grassia, and P. Martin, "Surfactant transport onto a foam lamella," *Chemical Engineering Science*, vol. 102, pp. 405–423, Oct. 2013.

[2] H. Rajabi and P. Grassia, "Transport of soluble surfactant on and within a foam film in the context of a foam fractionation process," *Chemical Engineering Science*, vol. 265, p. 118171, Jan. 2023.

[3] H. Neurath and H. B. Bull, "The surface activity of proteins," *Chemical Reviews*, vol. 23, no. 3, pp. 391–435, Dec. 1938.

[4] Z. Shafiei, A. A. Hamid, T. Fooladi, and W. M. W. Yusoff, "Surface active components: Review," *Current Research Journal of Biological Sciences*, vol. 6, no. 2, pp. 89–95, Mar. 2014.

[5] C. C. Blesken, T. Strümpfler, T. Tiso, and L. M. Blank, "Uncoupling foam fractionation and foam adsorption for enhanced biosurfactant synthesis and recovery," *Microorganisms*, vol. 8, no. 12, p. 2029, Dec. 2020.

[6] M. Pletnev, "Chemistry of surfactants," in *Surfactants: chemistry, interfacial properties, applications*, ser. Studies in interface science, V. B. Fainerman, D. Möbius, and R. Miller, Eds. Amsterdam, New York: Elsevier Science Ltd, 2001, vol. 13, pp. 1–98.

[7] I. Anestopoulos, D. E. Kiousi, A. Klavaris, A. Galanis, K. Salek, S. R. Euston, A. Pappa, and M. I. Panayiotidis, "Surface active agents and their health-promoting properties: Molecules of multifunctional significance," *Pharmaceutics*, vol. 12, no. 7, p. 688, Jul. 2020.

[8] D. J. Burgess and N. O. Sahin, "Interfacial rheological and tension properties of protein films," *Journal of Colloid and Interface Science*, vol. 189, no. 1, pp. 74–82, May 1997.

[9] R. J. Farn, Ed., *Chemistry and technology of surfactants*. Oxford, UK, Ames, Iowa: Blackwell Pub, 2006.

[10] N. Kumar and R. Tyagi, "Industrial applications of dimeric surfactants: A review," *Journal of Dispersion Science and Technology*, vol. 35, no. 2, pp. 205–214, Feb. 2014.

[11] D. R. Karsa, *Industrial applications of surfactants IV*. Cambridge: Royal Society of Chemistry, 1999.

[12] M. Kumari, U. K. Singh, A. B. Khan, M. A. Malik, and R. Patel, "Effect of bovine serum albumin on the surface properties of ionic liquid-type gemini surfactant," *Journal of Dispersion Science and Technology*, vol. 39, no. 10, pp. 1462–1468, Oct. 2018.

[13] P. G. De Gennes, F. Brochard-Wyart, and D. Quéré, *Capillarity and wetting phenomena: drops, bubbles, pearls, waves*. New York: Springer, 2010.

[14] W. Liu, M. Zhang, Y. Lv, S. Tian, N. Li, and Z. Wu, "Foam fractionation for recovering whey soy protein from whey wastewater: Strengthening foam drainage using a novel internal component with superhydrophobic surface," *Journal of the Taiwan Institute of Chemical Engineers*, vol. 78, pp. 39–44, Sep. 2017.

[15] T. Buckley, X. Xu, V. Rudolph, M. Firouzi, and P. Shukla, "Review of foam

fractionation as a water treatment technology," *Separation Science and Technology*, vol. 57, no. 6, pp. 929–958, Apr. 2022.

[16] J. P. Maity, Y. M. Huang, C. M. Hsu, C. I. Wu, C. C. Chen, C. Y. Li, J. S. Jean, Y. F. Chang, and C. Y. Chen, "Removal of Cu, Pb and Zn by foam fractionation and a soil washing process from contaminated industrial soils using soapberry-derived saponin: A comparative effectiveness assessment," *Chemosphere*, vol. 92, no. 10, pp. 1286–1293, Aug. 2013.

[17] T. M. Schmitt, *Analysis of surfactants*, 2nd ed. Boca Raton: CRC Press, Jan. 2001.

[18] S. M. Shaban, J. Kang, and D. H. Kim, "Surfactants: Recent advances and their applications," *Composites Communications*, vol. 22, p. 100537, Dec. 2020.

[19] T. Kinoshita, S. Akita, Y. Ishigaki, K. Yamaguchi, Y. Yamada, S. Nii, F. Kawaizumi, and K. Takahashi, "Continuous foam separation of metals enhanced by down-flowing surfactant solution from column top," *Chemical Engineering Research and Design*, vol. 85, no. 2, pp. 229–233, Jan. 2007.

[20] J. F. Scamehorn, *Surfactant-based separation processes*. Boca Raton: CRC Press, Nov. 2020.

[21] L. Shedlovsky, "A review of fractionation of mixtures by foam formation," *Annals of the New York Academy of Sciences*, vol. 49, no. 2, pp. 279–294, 1948.

[22] L. Du, V. Loha, and R. D. Tanner, "Modeling a protein foam fractionation process," *Applied Biochemistry and Biotechnology*, vol. 84, pp. 1087–1099, 2000.

[23] G. Mukhopadhyay, J. Khanam, and A. Nanda, "Protein removal from whey waste by foam fractionation in a batch process," *Separation Science and Technology*, vol. 45, no. 9, pp. 1331–1339, May 2010.

[24] B. Cheang and A. L. Zydney, "Separation of β-lactalbumin and β-lactoglobulin using membrane ultrafiltration," *Biotechnology and Bioengineering*, vol. 83, no. 2, pp. 201–209, Jul. 2003.

[25] J. F. Scamehorn and J. H. Harwell, Eds., *Surfactant-based separations: Science and technology*, ser. ACS symposium. Washington, DC: American Chemical Society, Nov. 1999, vol. 740.

[26] R. Lemlich and E. Lavi, "Foam fractionation with reflux," *Science (New York)*, vol. 134, no. 3473, p. 191, Jul. 1961.

[27] B. Grieves, "Foam separations: A review," *Chemical Engineering Journal*, vol. 9, no. 2, pp. 93–106, Jan. 1975.

[28] I. Kowalska, "Nanofiltration: Ion exchange system for effective surfactant removal from water solutions," *Brazilian Journal of Chemical Engineering*, vol. 31, no. 4, pp. 887–894, Dec. 2014.

[29] H. Duan, W. Liu, W. Liu, Y. Shen, X. Gu, J. Qiu, and S. Zhou, "Selective adsorption of a novel x-shaped surfactant dioctyl di-hydroxamic acid on fluorite surface leading the effective flotation separation of fluorite from calcite and barite," *Journal of Molecular Liquids*, vol. 344, p. 117941, Dec. 2021.

[30] B. Burghoff, "Foam fractionation applications," *Journal of Biotechnology*, vol. 161, no. 2, pp. 126–137, Oct. 2012.

[31] R. Lemlich, "Adsorptive bubble separation method-foam fractionation and allied techniques," *Industrial & Engineering Chemistry*, vol. 60, no. 10, pp. 16–29, Oct. 1968.

[32] R. A. Leonard and R. Lemlich, "A study of interstitial liquid flow in foam. Part I. Theoretical model and application to foam fractionation," *AIChE Journal*, vol. 11, no. 1, pp. 18–25, Jan. 1965.

[33] P. Stevenson and G. J. Jameson, "Modelling continuous foam fractionation with reflux," *Chemical Engineering and Processing: Process Intensification*, vol. 46, no. 12, pp. 1286–1291, Dec. 2007.

[34] P. Stevenson, X. Li, and G. M. Evans, "A mechanism for internal reflux in foam fractionation," *Biochemical Engineering Journal*, vol. 39, no. 3, pp. 590–593, May 2008.

[35] P. J. Martin, H. M. Dutton, J. B. Winterburn, S. Baker, and A. B. Russell, "Foam fractionation with reflux," *Chemical Engineering Science*, vol. 65, no. 12, pp. 3825–3835, Jun. 2010.

[36] P. Stevenson, *Foam engineering: fundamentals and applications*. New York: John Wiley & Sons, Jan. 2012.

[37] L. N. Brush and S. H. Davis, "A new law of thinning in foam dynamics," *Journal of Fluid Mechanics*, vol. 534, pp. 227–236, Jun. 2005.

[38] D. Weaire and S. Hutzler, *The physics of foams*. Oxford, New York: Clarendon Press, Oxford University Press, 1999.

[39] S. Hutzler and W. Drenckhan, "The structure of liquid foams," in *Foam films and foams*, 1st ed., D. Exerowa, G. Gochev, D. Platikanov, L. Liggieri, and R. Miller, Eds. Boca Raton: CRC Press, Jul. 2018, pp. 295–307.

[40] C. J. W. Breward and P. D. Howell, "The drainage of a foam lamella," *Journal of Fluid Mechanics*, vol. 458, pp. 379–406, May 2002.

[41] O. Reynolds, "IV. On the theory of lubrication and its application to Mr. Beauchamp tower's experiments, including an experimental determination of the viscosity of olive oil," *Philosophical Transactions of the Royal Society of London*, vol. 177, pp. 157–234, Dec. 1886.

[42] A. W. Adamson, *Physical chemistry of surfaces*, 2nd ed. New York: Interscience Publishers, 1967.

[43] C. V. Sternling and L. E. Scriven, "Interfacial turbulence: Hydrodynamic instability and the Marangoni effect," *AIChE Journal*, vol. 5, no. 4, pp. 514–523, 1959.

[44] D. Exerowa, G. Gochev, D. Platikanov, L. Liggieri, and R. Miller, *Foam Films and Foams: Fundamentals and Applications*. Boca Raton: CRC Press, Jul. 2018.

[45] L. Y. Yeo, O. K. Matar, E. S. Perez de Ortiz, and G. F. Hewitt, "Film drainage between two surfactant-coated drops colliding at constant approach velocity," *Journal of Colloid and Interface Science*, vol. 257, no. 1, pp. 93–107, 2003.

[46] P. Grassia, S. Ubal, M. D. Giavedoni, D. Vitasari, and P. J. Martin, "Surfactant flow between a Plateau border and a film during foam fractionation," *Chemical Engineering Science*, vol. 143, pp. 139–165, Apr. 2016.

[47] G. Verbist, D. Weaire, and A. M. Kraynik, "The foam drainage equation," *Journal of Physics: Condensed Matter*, vol. 8, no. 21, pp. 3715–3731, May 1996.

[48] P. S. Stewart and S. H. Davis, "Dynamics and stability of metallic foams: Network modeling," *Journal of Rheology*, vol. 56, no. 3, pp. 543–574, May 2012.

[49] S. I. Karakashev and A. V. Nguyen, "Effect of sodium dodecyl sulphate and dodecanol mixtures on foam film drainage: Examining influence of surface rheology and intermolecular forces," *Colloids and Surfaces A: Physicochemical and Engineering Aspects*, vol. 293, no. 1–3, pp. 229–240, Feb. 2007.

[50] P. Stewart and S. H. Davis, "Self-similar coalescence of clean foams," *Journal of Fluid Mechanics*, vol. 722, pp. 645–664, May 2013.

[51] L. Y. Yeo, O. K. Matar, E. P. de Ortiz, and G. F. Hewitt, "The dynamics of Marangoni-driven local film drainage between two drops," *Journal of Colloid and Interface Science*, vol. 241, no. 1, pp. 233–247, Sep. 2001.

[52] T. Gambaryan-Roisman, "Dynamics of free liquid films during formation of polymer foams," *Colloids and Surfaces A: Physicochemical and Engineering Aspects*, vol. 382, no. 1–3, pp. 113–117, Jun. 2011.

[53] M. Roché, Z. Li, I. M. Griffiths, S. Le Roux, I. Cantat, A. Saint-Jalmes, and H. A. Stone, "Marangoni flow of soluble amphiphiles," *Physical Review Letters*, vol. 112, no. 20, p. 208302, May 2014.

[54] V. B. Fainerman, D. Möbius, and R. Miller, Eds., *Surfactants: Chemistry, interfacial properties, applications*, ser. Studies in interface science. Amsterdam, New York: Elsevier Science, Ltd, 2001, vol. 13.

[55] M. Tanaka, S. Kaneshina, T. Tomida, K. Noda, and K. Aoki, "The effect of pressure on solubilities of ionic surfactants in water," *Journal of Colloid and Interface Science*, vol. 44, no. 3, pp. 525–531, 1973.

[56] A. M. Schwartz and J. W. Perry, *Surface active agents: Their chemistry and technology*. New York: Interscience Publishers, 1949.

[57] J. J. Sheng, "Surfactant flooding," in *Modern Chemical Enhanced Oil Recovery*. Amsterdam: Elsevier, 2011, pp. 239–335.

[58] M. Rieger, *Surfactants in cosmetics*. New York: Routledge, Sep. 2017.

[59] J. D. Desai and I. M. Banat, "Microbial production of surfactants and their commercial potential," *Microbiology and Molecular Biology Reviews*, vol. 61, pp. 47–64, 1997.

[60] J. R. Lu, T. J. Su, and J. Penfold, "Adsorption of serum albumins at the air/water interface," *Langmuir*, vol. 15, no. 20, pp. 6975–6983, Sep. 1999.

[61] A. P. Shea, C. L. Crofcheck, F. A. Payne, and Y. L. Xiong, "Foam fractionation of α-lactalbumin and β-lactoglobulin from a whey solution," *Asia-Pacific Journal of Chemical Engineering*, vol. 4, no. 2, pp. 191–203, Mar. 2009.

[62] H. Cheng and D. A. Sabatini, "Separation of organic compounds from surfactant solutions: A review," *Separation Science and Technology*, vol. 42, no. 3, pp. 453–475, Feb. 2007.

[63] F. Prud'homme, M. Morency, K. Freyer, H. Weiss, J. Bourne, B. Daus, D. Fontaine, J. Mattusch, R. Mineau, M. Préda, H. C. Treutler, and R. Wennrich, "Surfactant separation as a technique for physical and chemical characterization of ore processing residues," *Science of The Total Environment*, vol. 243–244, pp. 9–20, Dec. 1999.

[64] R. J. Pearce, "Whey protein recovery and whey protein fractionation," in *Whey and Lactose Processing*, J. G. Zadow, Ed. Dordrecht: Springer Netherlands, 1992, pp. 271–316.

[65] H. M. Schoen, "Foam separation as a purification and preparative tool," *Annals of the New York Academy of Sciences*, vol. 137, no. 1, pp. 148–161, Jan. 1966.

[66] I. Kowalska, "Separation of anionic surfactants in a sequential ultrafiltration – ion exchange purification system," *Polish Journal of Environmental Studies*, vol. 21, pp. 677–684, 2012.

[67] J. G. Speight, "Thermodynamics of water," in *Natural Water Remediation*. Amsterdam: Elsevier, 2020, pp. 131–163.

[68] T. Cosgrove, Ed., *Colloid science: principles, methods and applications*. Oxford, UK, Ames, Iowa: Blackwell Publisheres, 2005.

[69] J. Bergfreund, S. Siegenthaler, V. Lutz-Bueno, P. Bertsch, and P. Fischer, "Surfactant adsorption to different fluid interfaces," *Langmuir*, vol. 37, no. 22, pp. 6722–6727, Jun. 2021.

[70] D. Exerowa and P. M. Kruglyakov, *Foam and foam films: Theory, experiment, application*. Amsterdam: Elsevier, Dec. 1997.

[71] J. Zhou, P. G. Ranjith, and W. A. M. Wanniarachchi, "Different strategies of foam stabilization in the use of foam as a fracturing fluid," *Advances in Colloid and Interface Science*, vol. 276, p. 102104, Feb. 2020.

[72] R. Miller and V. B. Fainerman, "Surfactant adsorption layers at liquid-fluid interfaces," in *Handbook of Surfaces and Interfaces of Materials*. Amsterdam: Elsevier, 2001, pp. 383–421.

[73] P. Mukerjee, *Critical micelle concentrations of aqueous surfactant systems*. NSRDS-NBS, 1971.

[74] O. Massarweh and A. S. Abushaikha, "The use of surfactants in enhanced oil recovery: A review of recent advances," *Energy Reports*, vol. 6, pp. 3150–3178, Nov. 2020.

[75] H. Esmaeili, S. M. Mousavi, S. A. Hashemi, C. W. Lai, W. H. Chiang, and S. Bahrani, "Application of biosurfactants in the removal of oil from emulsion," in *Green Sustainable Process for Chemical and Environmental Engineering and Science*. Amsterdam: Elsevier, 2021, pp. 107–127.

[76] R. Baeza, C. Carrera Sanchez, A. M. R. Pilosof, and J. M. Rodríguez Patino, "Interactions of polysaccharides with β-lactoglobulin adsorbed films at the air-water interface," *Food Hydrocolloids*, vol. 19, no. 2, pp. 239–248, Mar. 2005.

[77] F. M. Doyle, "Ion flotation-its potential for hydrometallurgical operations,"

International Journal of Mineral Processing, vol. 72, no. 1–4, pp. 387–399, Sep. 2003.

[78] C. Huang, "Precipitate flotation of fluoride-containing wastewater from a semiconductor manufacturer," *Water Research*, vol. 33, no. 16, pp. 3403–3412, Nov. 1999.

[79] S. D. Huang, T. P. Wu, C. H. Ling, G. L. Sheu, C. C. Wu, and M. H. Cheng, "Adsorbing colloid flotation of heavy metal ions with activators," *Journal of Colloid and Interface Science*, vol. 124, no. 2, pp. 666–672, Aug. 1988.

[80] R. B. Grieves and D. Bhattacharyya, "The effect of temperature upon foam fractionation," *Journal of the American Oil Chemists' Society*, vol. 42, no. 3, pp. 174–176, Mar. 1965.

[81] F. Capponi, M. Sartori, M. Souza, and J. Rubio, "Modified column flotation of adsorbing iron hydroxide colloidal precipitates," *International Journal of Mineral Processing*, vol. 79, no. 3, pp. 167–173, Jun. 2006.

[82] S. L. de Lucena, E. Alves Miranda, and C. Costapinto Santana, "The effect of external reflux on the foam fractionation of proteins," *Applied Biochemistry and Biotechnology*, vol. 57, pp. 47–65, 1996.

[83] P. Stevenson, *Foam fractionation: Principles and process design*. Boca Raton: CRC Press, Feb. 2014.

[84] W. Ostwald, A. Siehr, and H. Erbring, "Enrichment of substances dissolved in liquids in the foam phase," German Patent DE691 618C, Jul., 1940.

[85] V. Bergeron and P. Walstra, "Foams," in *Fundamentals of interface and colloid science*, ser. Soft Colloids, J. Lyklema, Ed. London: Academic Press, Jan. 2005, vol. 5, pp. 7.1–7.38.

[86] D. Linke, H. Zorn, B. Gerken, H. Parlar, and R. G. Berger, "Laccase isolation

by foam fractionation: New prospects of an old process," *Enzyme and Microbial Technology*, vol. 40, no. 2, pp. 273–277, Jan. 2007.

[87] D. M. Ackermann, M. L. Stedman, S. Ko, A. Prokop, D. H. Park, and R. D. Tanner, "Effect of invertase on the batch foam fractionation of bromelain," *Biotechnology and Bioprocess Engineering*, vol. 8, no. 3, pp. 167–172, Jun. 2003.

[88] C. Crofcheck, M. Loiselle, J. Weekley, I. Maiti, S. Pattanaik, P. M. Bummer, and M. Jay, "Histidine tagged protein recovery from tobacco extract by foam fractionation," *Biotechnology Progress*, vol. 19, no. 2, pp. 680–682, Apr. 2003.

[89] M. Backleh-Sohrt, P. Ekici, G. Leupold, and H. Parlar, "Efficiency of foam fractionation for the enrichment of nonpolar compounds from aqueous extracts of plant materials," *Journal of Natural Products*, vol. 68, no. 9, pp. 1386–1389, Sep. 2005.

[90] C. E. Lockwood, P. M. Bummer, and M. Jay, "Purification of proteins using foam fractionation," *Pharmaceutical Research*, vol. 14, no. 11, pp. 1511–1515, Nov. 1997.

[91] P. Datta, A. Ghosh, P. Chakraborty, and A. Gangopadhyay, "Foam fractionation in separation of pharmaceutical biomolecules: A promising unit operation for industrial process and waste control," *Journal of Fundamental Pharmaceutial Research*, vol. 3, pp. 33–41, 2015.

[92] A. D. Jones and C. Robinson, "Solvent extraction and adsorptive bubble separation of metal ions from aqueous solution. II: Adsorptive bubble separation of nickel(II) using carboxylic acids and their salts as collectors," *Journal of Inorganic and Nuclear Chemistry*, vol. 36, no. 8, pp. 1871–1875, 1974.

[93] C. H. Chang and E. I. Franses, "Adsorption dynamics of surfactants at the

air/water interface: A critical review of mathematical models, data, and mechanisms," *Colloids and Surfaces A: Physicochemical and Engineering Aspects*, vol. 100, pp. 1–45, Jul. 1995.

[94] E. Rubin and D. Melech, "Foam fractionation of solutions containing two surfactants in stripping and reflux columns," *Canadian Journal of Chemical Engineering*, vol. 50, no. 6, pp. 748–753, Dec. 1972.

[95] L. Du, A. Prokop, and R. D. Tanner, "Effect of bubble size on foam fractionation of ovalbumin," *Applied Biochemistry and Biotechnology*, vol. 98–100, p. 17, 2002.

[96] J. Wang, G. Liu, Z. Wu, and L. Zhang, "Intensified effect of reduced pressure on the foam fractionation process of bovine serum albumin," *Separation Science and Technology*, vol. 45, no. 16, pp. 2489–2496, Nov. 2010.

[97] L. Du, A. Prokop, and R. D. Tanner, "Effect of pH on the startup of a continuous foam fractionation process containing ovalbumin," *Separation Science and Technology*, vol. 38, no. 5, pp. 1093–1109, Jan. 2003.

[98] V. Burapatana, E. A. Booth, A. Prokop, and R. D. Tanner, "Effect of buffer and pH on detergent-assisted foam fractionation of cellulase," *Industrial & Engineering Chemistry Research*, vol. 44, no. 14, pp. 4968–4972, Jul. 2005.

[99] G. T. Jeong, E. S. Park, V. L. Wahlig, V. Burapatana, D. H. Park, and R. D. Tanner, "Effect of pH on the foam fractionation of mimosa pudica L. seed proteins," *Industrial & Engineering Chemistry Research*, vol. 43, no. 2, pp. 422–427, Jan. 2004.

[100] S. Ko, J. Cherry, A. Prokop, and R. D. Tanner, "Effect of a natural contaminant on foam fractionation of bromelain," *Applied Biochemistry and Biotechnology*, vol. 91–93, pp. 405–411, 2001.

[101] C. C. Stowers, V. Makarov, A. Walker, R. A. Edwards, and R. D. Tanner,

"Effect of air flow rate on the foam fractionation of a mixture of egg white and egg yolk," *Asia-Pacific Journal of Chemical Engineering*, vol. 4, no. 2, pp. 180–183, Mar. 2009.

[102] S. Hutzler, S. T. Tobin, A. J. Meagher, A. Marguerite, and D. Weaire, "A model system for foam fractionation," *Proceedings of the Royal Society A*, vol. 469, no. 2154, p. 20120727, Jun. 2013.

[103] I. D. Kamalanathan and P. J. Martin, "Competitive adsorption of surfactant-protein mixtures in a continuous stripping mode foam fractionation column," *Chemical Engineering Science*, vol. 146, pp. 291–301, 2016.

[104] I. L. Jashnani and R. Lemlich, "Transfer Units in Foam Fractionation," *Industrial & Engineering Chemistry Process Design and Development*, vol. 12, no. 3, pp. 312–321, Jul. 1973.

[105] W. McCabe, J. Smith, and P. Harriott, *Unit Operations of Chemical Engineering*. McGraw-Hill Education, 2004.

[106] C. A. Brunner and R. Lemlich, "Foam fractionation. Standard separator and refluxing columns," *Industrial & Engineering Chemistry Fundamentals*, vol. 2, no. 4, pp. 297–300, Nov. 1963.

[107] Z. S. Saleh and M. M. Hossain, "A study of the separation of proteins from multicomponent mixtures by a semi-batch foaming process," *Chemical Engineering and Processing: Process Intensification*, vol. 40, no. 4, pp. 371–378, Jul. 2001.

[108] B. Gerken, A. Nicolai, D. Linke, H. Zorn, R. Berger, and H. Parlar, "Effective enrichment and recovery of laccase-C using continuous foam fractionation," *Separation and Purification Technology*, vol. 49, no. 3, pp. 291–294, May 2006.

[109] A. Dinache, M. L. Pascu, and A. Smarandache, "Spectral properties of foams and emulsions," *Molecules*, vol. 26, no. 24, p. 7704, Dec. 2021.

[110] K. Engelhardt, M. Lexis, G. Gochev, C. Konnerth, R. Miller, N. Willenbacher, W. Peukert, and B. Braunschweig, "pH effects on the molecular structure of β-lactoglobulin modified air-water interfaces and its impact on foam rheology," *Langmuir*, vol. 29, no. 37, pp. 11 646–11 655, Sep. 2013.

[111] S. Hilgenfeldt, S. A. Koehler, and H. A. Stone, "Dynamics of coarsening foams: Accelerated and self-limiting drainage," *Physical Review Letters*, vol. 86, no. 20, pp. 4704–4707, May 2001.

[112] A. I. Rusanov and V. V. Krotov, "Gibbs elasticity of free thin liquid films," *Doklady Physical Chemistry*, vol. 393, no. 4-6, pp. 350–352, Dec. 2003.

[113] A. Saint-Jalmes, "Physical chemistry in foam drainage and coarsening," *Soft Matter*, vol. 2, no. 10, pp. 836–849, 2006.

[114] I. Cantat, S. Cohen-Addad, F. Elias, F. Graner, R. Höhler, O. Pitois, F. Rouyer, and A. Saint-Jalmes, *Foams: Structure and dynamics*, 1st ed. Oxford, New York: Oxford University Press, 2013.

[115] W. Y. Jang, A. M. Kraynik, and S. Kyriakides, "On the microstructure of open-cell foams and its effect on elastic properties," *International Journal of Solids and Structures*, vol. 45, no. 7-8, pp. 1845–1875, Apr. 2008.

[116] S. Hutzler, D. Weaire, A. Saugey, S. Cox, and N. Peron, "The physics of foam drainage," in *Proceedings 52nd SEPAWA Congress, 12th–14thOct.*, K. Henning, Ed., Wuerzburg, 2005, pp. 191–206.

[117] E. B. Matzke, "The three-dimensional shape of bubbles in foam: an analysis of the role of surface forces in three-dimensional cell shape determination," *American Journal of Botany*, vol. 33, no. 1, pp. 58–80, 1946.

[118] D. Weaire, S. Hutzler, G. Verbist, and E. Peters, "A review of foam drainage," *Advances in Chemical Physics*, vol. 102, pp. 315–374, 1997.

[119] S. Vafaei and D. Wen, "Modification of the Young-Laplace equation and prediction of bubble interface in the presence of nanoparticles," *Advances in Colloid and Interface Science*, vol. 225, pp. 1–15, Nov. 2015.

[120] S. Goldman, "Generalizations of the Young-Laplace equation for the pressure of a mechanically stable gas bubble in a soft elastic material," *Journal of Chemical Physics*, vol. 131, no. 18, p. 184502, Nov. 2009.

[121] J. B. M. Hudales and H. N. Stein, "Profile of the Plateau border in a vertical free liquid film," *Journal of Colloid and Interface Science*, vol. 137, no. 2, pp. 512–526, Jul. 1990.

[122] K. Feitosa and D. J. Durian, "Gas and liquid transport in steady-state aqueous foam," *European Physical Journal E*, vol. 26, no. 3, pp. 309–316, Jul. 2008.

[123] J. J. Bikerman, *Foams*. Berlin, Heidelberg: Springer, 1973.

[124] J. Stavans, "The evolution of cellular structures," *Reports on Progress in Physics*, vol. 56, no. 6, pp. 733–789, Jun. 1993.

[125] S. A. Koehler, S. Hilgenfeldt, and H. A. Stone, "A generalized view of foam drainage: Experiment and theory," *Langmuir*, vol. 16, no. 15, pp. 6327–6341, Jul. 2000.

[126] R. Braun, S. Snow, and U. Pernisz, "Gravitational drainage of a tangentially-immobile thick film," *Journal of Colloid and Interface Science*, vol. 219, no. 2, pp. 225–240, Nov. 1999.

[127] I. I. Gol'dfarb, K. B. Kann, and I. R. Shreiber, "Liquid flow in foams," *Fluid Dynamics*, vol. 23, no. 2, pp. 244–249, 1988.

[128] S. A. Koehler, S. Hilgenfeldt, and H. A. Stone, "Liquid flow through aqueous

foams: The node-dominated foam drainage equation," *Physical Review Letters*, vol. 82, no. 21, pp. 4232–4235, May 1999.

[129] S. J. Cox, D. Weaire, S. Hutzler, J. Murphy, R. Phelan, and G. Verbist, "Applications and generalizations of the foam drainage equation," *Proceedings of the Royal Society of London. Series A: Mathematical, Physical and Engineering Sciences*, vol. 456, no. 2002, pp. 2441–2464, Oct. 2000.

[130] R. Tsekov, "The $r^{4/5}$-problem in the drainage of dimpled thin liquid films," *Colloids and Surfaces A: Physicochemical and Engineering Aspects*, vol. 141, no. 2, pp. 161–164, Nov. 1998.

[131] N. Politova, S. Tcholakova, K. Golemanov, N. D. Denkov, M. Vethamuthu, and K. P. Ananthapadmanabhan, "Effect of cationic polymers on foam rheological properties," *Langmuir*, vol. 28, no. 2, pp. 1115–1126, Jan. 2012.

[132] N. D. Denkov, P. Cooper, and J. Y. Martin, "Mechanisms of action of mixed solid-liquid antifoams. 1. Dynamics of foam film rupture," *Langmuir*, vol. 15, no. 24, pp. 8514–8529, Nov. 1999.

[133] A. Sheludko, "Thin liquid films," *Advances in Colloid and Interface Science*, vol. 1, no. 4, pp. 391–464, Dec. 1967.

[134] P. Claesson, T. Ederth, V. Bergeron, and M. Rutland, "Techniques for measuring surface forces," *Advances in Colloid and Interface Science*, vol. 67, pp. 119–183, Sep. 1996.

[135] J. E. Coons, P. . Halley, S. A. McGlashan, and T. Tran-Cong, "A review of drainage and spontaneous rupture in free standing thin films with tangentially immobile interfaces," *Advances in Colloid and Interface Science*, vol. 105, no. 1–3, pp. 3–62, Sep. 2003.

[136] G. Debrégeas, P. G. de Gennes, and F. Brochard-Wyart, "The life and death of

'bare' viscous bubbles," *Science*, vol. 279, no. 5357, pp. 1704–1707, Mar. 1998.

[137] E. Manev, R. Tsekov, and B. Radoev, "Effect of thickness non-homogeneity on the kinetic behaviour of microscopic foam film," *Journal of Dispersion Science and Technology*, vol. 18, no. 6–7, pp. 769–788, Sep. 1997.

[138] A. Sharma and E. Ruckenstein, "Stability, critical thickness, and the time of rupture of thinning foam and emulsion films," *Langmuir*, vol. 3, no. 5, pp. 760–768, Sep. 1987.

[139] R. Narayanan, Ed., *Interfacial processes and molecular aggregation of surfactants*, ser. Advances in Polymer Science. Berlin, Heidelberg: Springer, 2008, vol. 218.

[140] R. K. Prud'homme, *Foams: Theory: Measurements: Applications*. Boca Raton: CRC Press, Oct. 1995.

[141] A. Wilson and A. W. Robards, Eds., *Foams: Physics, chemistry and structure*, ser. Springer Series in Applied Biology. London: Springer, 1989.

[142] L. L. Schramm, *Emulsions, foams, and suspensions: Fundamentals and applications*, 1st ed. New York: Wiley, Jul. 2005.

[143] V. V. Yaminsky, S. Ohnishi, E. A. Vogler, and R. G. Horn, "Stability of aqueous films between bubbles. Part 1. The effect of speed on bubble coalescence in purified water and simple electrolyte solutions," *Langmuir*, vol. 26, no. 11, pp. 8061–8074, Jun. 2010.

[144] N. D. Denkov and K. G. Marinova, "Antifoam effects of solid particles, oil drops and oil-solid compounds in aqueous foams," in *Colloidal Particles at Liquid Interfaces*, 1st ed., B. P. Binks and T. S. Horozov, Eds. Cambridge: Cambridge University Press, Aug. 2006, pp. 383–444.

[145] L. Wang and R. H. Yoon, "Effects of surface forces and film elasticity on foam stability," *International Journal of Mineral Processing*, vol. 85, no. 4, pp. 101–110, Jan. 2008.

[146] E. H. Lucassen-Reynders, "Interfacial viscoelasticity in emulsions and foams," *Food Structure*, vol. 12, no. 1, p. 13, 1993.

[147] D. Langevin, "On the rupture of thin films made from aqueous surfactant solutions," *Advances in Colloid and Interface Science*, vol. 275, p. 102075, Jan. 2020.

[148] S. J. McClellan and E. I. Franses, "Effect of concentration and denaturation on adsorption and surface tension of bovine serum albumin," *Colloids and Surfaces B: Biointerfaces*, vol. 28, no. 1, pp. 63–75, Apr. 2003.

[149] P. J. Atkinson, E. Dickinson, D. S. Horne, and R. M. Richardson, "Neutron reflectivity of adsorbed β-casein and β-lactoglobulin at the air/water interface," *Journal of the Chemical Society, Faraday Transactions*, vol. 91, no. 17, pp. 2847–2854, 1995.

[150] A. G. Richter and I. Kuzmenko, "Using in situ X-ray reflectivity to study protein adsorption on hydrophilic and hydrophobic surfaces: Benefits and limitations," *Langmuir*, vol. 29, no. 17, pp. 5167–5180, Apr. 2013.

[151] A. Stocco, W. Drenckhan, E. Rio, D. Langevin, and B. P. Binks, "Particle-stabilised foams: An interfacial study," *Soft Matter*, vol. 5, no. 11, pp. 2215–2222, 2009.

[152] E. Bouyer, G. Mekhloufi, N. Huang, V. Rosilio, and F. Agnely, "β-lactoglobulin, gum arabic, and xanthan gum for emulsifying sweet almond oil: Formulation and stabilization mechanisms of pharmaceutical emulsions," *Colloids and Surfaces A: Physicochemical and Engineering Aspects*, vol. 433, pp. 77–87, Sep. 2013.

[153] G. V. Lubarsky, M. R. Davidson, and R. H. Bradley, "Hydration–dehydration of adsorbed protein films studied by AFM and QCM-D," *Biosensors and Bioelectronics*, vol. 22, no. 7, pp. 1275–1281, Feb. 2007.

[154] K. E. Sapsford and F. S. Ligler, "Real-time analysis of protein adsorption to a variety of thin films," *Biosensors and Bioelectronics*, vol. 19, no. 9, pp. 1045–1055, Apr. 2004.

[155] K. Engelhardt, A. Rumpel, J. Walter, J. Dombrowski, U. Kulozik, B. Braunschweig, and W. Peukert, "Protein adsorption at the electrified air-water interface: Implications on foam stability," *Langmuir*, vol. 28, no. 20, pp. 7780–7787, May 2012.

[156] E. Guzmán, A. Maestro, C. Carbone, F. Ortega, and R. G. Rubio, "Dilational rheology of fluid/fluid interfaces: foundations and tools," *Fluids*, vol. 7, no. 10, p. 335, Oct. 2022.

[157] E. H. Lucassen-Reynders, V. B. Fainerman, and R. Miller, "Surface dilational modulus or Gibbs' elasticity of protein adsorption layers," *Journal of Physical Chemistry B*, vol. 108, no. 26, pp. 9173–9176, Jul. 2004.

[158] M. Lexis and N. Willenbacher, "Relating foam and interfacial rheological properties of β-lactoglobulin solutions," *Soft Matter*, vol. 10, no. 48, pp. 9626–9636, 2014.

[159] G. G. Gochev, V. I. Kovalchuk, E. V. Aksenenko, V. B. Fainerman, and R. Miller, "β-lactoglobulin adsorption layers at the water/air surface: 5. Adsorption isotherm and equation of state revisited, impact of pH," *Colloids and Interfaces*, vol. 5, no. 1, p. 14, Mar. 2021.

[160] M. A. Bos and T. van Vliet, "Interfacial rheological properties of adsorbed protein layers and surfactants: A review," *Advances in Colloid and Interface Science*, vol. 91, no. 3, pp. 437–471, Jul. 2001.

[161] J. Krägel, M. O'Neill, A. V. Makievski, M. Michel, M. E. Leser, and R. Miller, "Dynamics of mixed protein-surfactant layers adsorbed at the water/air and water/oil interface," *Colloids and Surfaces B: Biointerfaces*, vol. 31, no. 1–4, pp. 107–114, Sep. 2003.

[162] G. G. Gochev, I. Retzlaff, E. V. Aksenenko, V. B. Fainerman, and R. Miller, "Adsorption isotherm and equation of state for β-lactoglobulin layers at the air/water surface," *Colloids and Surfaces A: Physicochemical and Engineering Aspects*, vol. 422, pp. 33–38, Apr. 2013.

[163] V. B. Fainerman and R. Miller, "Equilibrium and dynamic characteristics of protein adsorption layers at gas-liquid interfaces: Theoretical and experimental data," *Colloid Journal*, vol. 67, no. 4, pp. 393–404, Jul. 2005.

[164] M. Durand and D. Langevin, "Physicochemical approach to the theory of foam drainage," *European Physical Journal E*, vol. 7, no. 1, pp. 35–44, Jan. 2002.

[165] M. Durand and H. A. Stone, "Relaxation time of the topological T1 process in a two-dimensional foam," *Physical Review Letters*, vol. 97, p. 226101, 2006.

[166] E. H. Lucassen-Reynders, A. Cagna, and J. Lucassen, "Gibbs elasticity, surface dilational modulus and diffusional relaxation in nonionic surfactant monolayers," *Colloids and Surfaces*, vol. 186, no. 1, pp. 63–72, 2001.

[167] G. J. Elfring, L. G. Leal, and T. M. Squires, "Surface viscosity and Marangoni stresses at surfactant laden interfaces," *Journal of Fluid Mechanics*, vol. 792, pp. 712–739, Apr. 2016.

[168] R. Miller, V. B. Fainerman, A. V. Makievski, J. Krägel, D. O. Grigoriev, V. N. Kazakov, and O. V. Sinyachenko, "Dynamics of protein and mixed protein/surfactant adsorption layers at the water/fluid interface," *Advances in Colloid and Interface Science*, vol. 86, no. 1–2, pp. 39–82, May 2000.

[169] C. Marangoni, "Ueber die ausbreitung der tropfen einer flüssigkeit auf der

oberfläche einer anderen," *Annalen der Physik und Chemie*, vol. 219, no. 7, pp. 337–354, 1871.

[170] D. Vitasari, P. Grassia, and P. Martin, "Surfactant transport onto a foam film in the presence of surface viscous stress," *Applied Mathematical Modelling*, vol. 40, no. 3, pp. 1941–1958, Feb. 2016.

[171] E. Rio and A. L. Biance, "Thermodynamic and mechanical timescales involved in foam film rupture and liquid foam coalescence," *ChemPhysChem*, vol. 15, no. 17, pp. 3692–3707, Dec. 2014.

[172] S. I. Karakashev, D. S. Ivanova, Z. K. Angarska, E. D. Manev, R. Tsekov, B. Radoev, R. Slavchov, and A. V. Nguyen, "Comparative validation of the analytical models for the Marangoni effect on foam film drainage," *Colloids and Surfaces A: Physicochemical and Engineering Aspects*, vol. 365, no. 1–3, pp. 122–136, Aug. 2010.

[173] E. H. Lucassen-Reynders, "Surface equation of state for ionized surfactants," *The Journal of Physical Chemistry*, vol. 70, no. 6, pp. 1777–1785, Jun. 1966.

[174] M. J. Rosen and J. T. Kunjappu, *Surfactants and interfacial phenomena*, 4th ed. Hoboken, N.J: Wiley, 2012.

[175] R. A. Latour, "The Langmuir isotherm: A commonly applied but misleading approach for the analysis of protein adsorption behavior," *Journal of Biomedical Materials Research Part A*, vol. 103, no. 3, pp. 949–958, Mar. 2015.

[176] E. A. Guggenheim, *Thermodynamics: An advanced treatment for chemists and physicists*, 8th ed. Amsterdam, New York: North-Holland Publishing Co, Aug. 1988.

[177] P. A. Rock and W. H. Casey, "Gibbs–Duhem equation," in *Geochemistry*. Dordrecht: Springer Netherlands, 1998, pp. 308–309.

[178] R. G. Mortimer, *Physical chemistry*. London: Academic Press, 2000.

[179] H. Guangze and M. Jianjia, "Extension of Gibbs–Duhem equation including influences of external fields," *Continuum Mechanics and Thermodynamics*, vol. 30, no. 4, pp. 817–823, Jul. 2018.

[180] P. Nikitas, "Applications of the Gibbs–Duhem equation," *Journal of Chemical Education*, vol. 78, pp. 1070–1075, Aug. 2001.

[181] T. Tadros, "Gibbs adsorption isotherm," in *Encyclopedia of Colloid and Interface Science*, T. Tadros, Ed. Berlin, Heidelberg: Springer, 2013, pp. 626–626.

[182] J. W. Gibbs, *The collected works of J. Willard Gibbs: Thermodynamics*. New York, London, Toronto: Longmans, Green and Company, 1928, vol. 1.

[183] R. Lemlich, "Adsubble processes: Foam fractionation and bubble fractionation," *Journal of Geophysical Research*, vol. 77, no. 27, pp. 5204–5210, 1972.

[184] D. K. Chattoraj and K. S. Birdi, *Adsorption and the Gibbs surface excess*. New York, London: Plenum Press, 1984.

[185] F. Menger and S. Rizvi, "Relationship between surface tension and surface coverage," *Langmuir*, vol. 27, pp. 13 975–7, Dec. 2011.

[186] J. Eastoe and J. S. Dalton, "Dynamic surface tension and adsorption mechanisms of surfactants at the air-water interface," *Advances in Colloid and Interface Science*, vol. 85, no. 2-3, pp. 103–144, Mar. 2000.

[187] N. O. Mchedlov-Petrossyan, "Adsorption of ionic surfactants on water/air interface: One more transformation of the Gibbs equation," *Surface Engineering and Applied Electrochemistry*, vol. 50, no. 2, pp. 173–182, Mar. 2014.

[188] M. Przyborowski, T. Hibiya, M. Eguchi, and I. Egry, “Surface tension measurement of molten silicon by the oscillating drop method using electromagnetic levitation,” *Journal of Crystal Growth*, vol. 151, no. 1–2, pp. 60–65, May 1995.

[189] S. Ebnesajjad, “Surface tension and its measurement,” in *Handbook of Adhesives and Surface Preparation*, ser. Plastics Design Library, S. Ebnesajjad, Ed. Oxford: William Andrew Publishing, Jan. 2011, pp. 21–30.

[190] W. Henry, “Experimental and theoretical statics of liquids subject to molecular forces only,” *Philosophical Transactions of the Royal Society of London*, vol. 93, pp. 29–42, 1803.

[191] K. F. Loughlin and D. Abouelnasr, “Adsorption Henry constants calculated from the entire isotherm,” *Adsorption*, vol. 19, no. 6, pp. 1189–1196, Dec. 2013.

[192] H. Swenson and N. P. Stadie, “Langmuir’s theory of adsorption: A centennial review,” *Langmuir*, vol. 35, no. 16, pp. 5409–5426, Apr. 2019.

[193] J. H. Chun, K. H. Ra, and N. Y. Kim, “Qualitative analysis of the Frumkin adsorption isotherm of the over-potentially deposited hydrogen at the poly-Ni/KOH aqueous electrolyte interface using the phase-shift method,” *Journal of the Electrochemical Society*, vol. 149, no. 9, p. E325, Jul. 2002.

[194] V. B. Fainerman, R. Miller, R. Wüstneck, and A. V. Makievski, “Adsorption isotherm and surface tension equation for a surfactant with changing partial molar area. 1. Ideal surface layer,” *Journal of Physical Chemistry*, vol. 100, no. 18, pp. 7669–7675, Jan. 1996.

[195] V. B. Fainerman and R. Miller, “Surface tension isotherms for surfactant adsorption layers including surface aggregation,” *Langmuir*, vol. 12, no. 25, pp. 6011–6014, Jan. 1996.

[196] V. B. Fainerman, R. Wüstneck, and R. Miller, "Surface tension of mixed surfactant solutions," *Tenside, Surfactants, Detergents*, vol. 38, pp. 224–229, Jul. 2001.

[197] V. B. Fainerman, E. V. Aksenenko, N. Mucic, A. Javadi, and R. Miller, "Thermodynamics of adsorption of ionic surfactants at water/alkane interfaces," *Soft Matter*, vol. 10, no. 36, pp. 6873–6887, Aug. 2014.

[198] Y. Liu and L. Shen, "From Langmuir kinetics to first- and second-order rate equations for adsorption," *Langmuir*, vol. 24, no. 20, pp. 11 625–11 630, Oct. 2008.

[199] S. Salvestrini, "A modification of the langmuir rate equation for diffusion-controlled adsorption kinetics," *Reaction Kinetics, Mechanisms and Catalysis*, vol. 128, no. 2, pp. 571–586, Dec. 2019.

[200] B. Von Szyszkowski, "Experimentelle studien über kapillare eigenschaften der wasserigen losungen von fettsauren. (experimental studies of the capillary properties of aqueous solutions of fatty acids)," *Zeitschrift für Physikalische Chemie*, vol. 64, pp. 385–414, 1908.

[201] A. A. Sonin, A. Bonfillon, and D. Langevin, "Thinning of soap films: The role of surface viscoelasticity," *Journal of Colloid and Interface Science*, vol. 162, no. 2, pp. 323–330, 1994.

[202] C. H. Chang, N. H. L. Wang, and E. I. Franses, "Adsorption dynamics of single and binary surfactants at the air/water interface," *Colloids and Surfaces*, vol. 62, no. 4, pp. 321–332, Mar. 1992.

[203] K. Tajima, M. Muramatsu, and T. Sasaki, "Radiotracer studies on adsorption of surface active substance at aqueous surface. I. Accurate measurement of adsorption of tritiated sodium dodecylsulfate," *Bulletin of the Chemical Society of Japan*, vol. 43, no. 7, pp. 1991–1998, Jul. 1970.

[204] S. Damodaran and K. B. Song, "Kinetics of adsorption of proteins at interfaces: Role of protein conformation in diffusional adsorption," *Biochimica et Biophysica Acta (BBA): Protein Structure and Molecular Enzymology*, vol. 954, pp. 253–264, Jan. 1988.

[205] V. Pradines, J. Krägel, V. B. Fainerman, and R. Miller, "Interfacial properties of mixed β-lactoglobulin-SDS layers at the water/air and water/oil interface," *Journal of Physical Chemistry B*, vol. 113, no. 3, pp. 745–751, Jan. 2009.

[206] J. Hu, J. Yang, Y. Xu, K. Zhang, K. Nishinari, G. O. Phillips, and Y. Fang, "Comparative study on foaming and emulsifying properties of different beta-lactoglobulin aggregates," *Food & Function Journal*, vol. 10, no. 9, pp. 5922–5930, 2019.

[207] M. Zahid, N. Z. Khan, A. M. Siddiqui, S. Iqbal, A. Muhammad, and I. Tlili, "Analysis of the lubrication approximation theory in the calendering/sheeting process of upper convected Jeffery's material," *Journal of Plastic Film & Sheeting*, vol. 37, no. 2, pp. 128–159, Apr. 2021.

[208] E. Guyon, J. P. Hulin, L. Petit, and C. D. Mitescu, *Physical hydrodynamics, 2nd Edn*. Oxford: Oxford University Press, Jan. 2015.

[209] R. L. Panton, *Incompressible flow*, 4th ed. Hoboken, NJ: John Wiley & Sons, 2013.

[210] I. Ivanov, *Thin liquid films*, 1st ed. New York: Routledge, Jan. 2023.

[211] I. B. Ivanov, "Effect of surface mobility on the dynamic behavior of thin liquid films," *Pure and Applied Chemistry*, vol. 52, no. 5, pp. 1241–1262, Jan. 1980.

[212] K. S. Birdi, Ed., *Handbook of surface and colloid chemistry*, 3rd ed. Boca Raton: CRC Press/Taylor & Francis, 2009.

[213] K. Matsuoka, Y. Sato, S. Takashima, and Y. Goto, "Removal of ionic dyes with

different charges by foam separation," *Journal of Molecular Liquids*, vol. 355, p. 118994, Jun. 2022.

[214] B. Keshavarzi, T. Krause, S. Sikandar, K. Schwarzenberger, K. Eckert, M. B. Ansorge-Schumacher, and S. Heitkam, "Protein enrichment by foam fractionation: Experiment and modeling," *Chemical Engineering Science*, vol. 256, p. 117715, 2022.

[215] Z. Li, A. L. Williams, and M. J. Rood, "Influence of soluble surfactant properties on the activation of aerosol particles containing inorganic solute," *Journal of the Atmospheric Sciences*, vol. 55, no. 10, pp. 1859–1866, May 1998.

[216] O. E. Jensen and J. B. Grotberg, "Insoluble surfactant spreading on a thin viscous film: Shock evolution and film rupture," *Journal of Fluid Mechanics*, vol. 240, pp. 259–288, Jul. 1992.

[217] G. Bruell and R. Granero-Belinchón, "On a thin film model with insoluble surfactant," *Journal of Differential Equations*, vol. 268, no. 12, pp. 7582–7608, Jun. 2020.

[218] O. E. Jensen, "The spreading of insoluble surfactant at the free surface of a deep fluid layer," *Journal of Fluid Mechanics*, vol. 293, pp. 349–378, Jun. 1995.

[219] M. Roché, Z. Li, I. M. Griffiths, S. Le Roux, I. Cantat, A. Saint-Jalmes, and H. A. Stone, "Marangoni flow of soluble amphiphiles," *Physical Review Letters*, vol. 112, p. 208302, 2014.

[220] R. B. Bird, W. E. Stewart, and E. N. Lightfoot, *Transport phenomena*. New York, London: John Wiley & Sons, 1960.

[221] D. Dowson, "Osborne Reynolds centenary (1886– 1986)," *Proceedings of the*

Institution of Mechanical Engineers, Part C: Journal of Mechanical Engineering Science, vol. 201, no. 2, pp. 75–96, Mar. 1987.

[222] S. P. Frankel and K. J. Mysels, "On the dimpling during the approach of two interfaces," *Journal of Physical Chemistry*, vol. 66, no. 1, pp. 190–191, 1962.

[223] J. L. Joye, G. J. Hirasaki, and C. A. Miller, "Dimple formation and behavior during axisymmetrical foam film drainage," *Langmuir*, vol. 8, pp. 3083–3092, 1992.

[224] S. Ubal, C. H. Harrison, P. Grassia, and W. J. Korchinsky, "Numerical simulation of mass transfer in circulating drops," *Chemical Engineering Science*, vol. 65, no. 10, pp. 2934–2956, 2010.

[225] E. L. Cussler, *Diffusion: Mass transfer in fluid systems*, 3rd ed. Cambridge, New York: Cambridge University Press, 2009.

[226] H. A. Stone, "A simple derivation of the time-dependent convective-diffusion equation for surfactant transport along a deforming interface," *Physics of Fluids A: Fluid Dynamics*, vol. 2, no. 1, pp. 111–112, Jan. 1990.

[227] I. Cantat and B. Dollet, "Liquid films with high surface modulus moving in tubes: Dynamic wetting film and jumpy motion," *Soft Matter*, vol. 8, no. 30, p. 7790, 2012.

[228] D. P. Gaver and J. B. Grotberg, "The dynamics of a localized surfactant on a thin film," *Journal of Fluid Mechanics*, vol. 213, pp. 127–148, Apr. 1990.

[229] P. C. Hiemenz and R. Rajagopalan, *Principles of colloid and surface chemistry*, 3rd ed. New York: Marcel Dekker, 1997.

[230] E. D. Shchukin, A. V. Pertsov, E. A. Amelina, and A. S. Zelenev, *Colloid and surface chemistry*, ser. Studies in Interface Science. Amsterdam: Elsevier, 2001, vol. 12.

[231] M. Brio, G. M. Webb, and A. R. Zakharian, "Chapter 2: Discretization methods," in *Numerical time-dependent partial differential equations for scientists and engineers*, ser. Mathematics in Science and Engineering, M. Brio, A. Zakharian, and G. M. Webb, Eds. Amsterdam: Elsevier, 2010, vol. 213, pp. 59–108.

[232] K. J. Ruschak, "Boundary conditions at a liquid-air interface in lubrication flows," *Journal of Fluid Mechanics*, vol. 119, pp. 107–120, 1982.

[233] K. Ruschak, "Coating flows," *Annual Review of Fluid Mechanics*, vol. 17, pp. 65–89, 1985.

[234] F. I. El-Dossoki, E. A. Gomaa, and O. K. Hamza, "Solvation thermodynamic parameters for sodium dodecyl sulfate (SDS) and sodium lauryl ether sulfate (SLES) surfactants in aqueous and alcoholic-aqueous solvents," *SN Applied Sciences*, vol. 1, no. 8, p. 933, Aug. 2019.

[235] P. H. Elworthy and K. J. Mysels, "The surface tension of sodium dodecylsulfate solutions and the phase separation model of micelle formation," *Journal of Colloid and Interface Science*, vol. 21, no. 3, pp. 331–347, Mar. 1966.

[236] C. M. Johnson and E. Tyrode, "Study of the adsorption of sodium dodecyl sulfate (SDS) at the air/water interface: Targeting the sulfate headgroup using vibrational sum frequency spectroscopy," *Physical Chemistry Chemical Physics*, vol. 7, no. 13, pp. 2635–2640, 2005.

[237] V. L. Kolev, K. D. Danov, P. A. Kralchevsky, G. Broze, and A. Mehreteab, "Comparison of the van der Waals and Frumkin adsorption isotherms for sodium dodecyl sulfate at various salt concentrations," *Langmuir*, vol. 18, no. 23, pp. 9106–9109, Nov. 2002.

[238] S. Llamas, E. Santini, L. Liggieri, F. Salerni, D. Orsi, L. Cristofolini, and F. Ravera, "Adsorption of sodium dodecyl sulfate at water–dodecane interface

in relation to the oil in water emulsion properties," *Langmuir*, vol. 34, no. 21, pp. 5978–5989, May 2018.

[239] D. Mańko, A. Zdziennicka, and B. Jańczuk, "Adsorption and aggregation activity of sodium dodecyl sulfate and rhamnolipid mixture," *Journal of Surfactants and Detergents*, vol. 20, no. 2, pp. 411–423, Mar. 2017.

[240] R. Matuura, H. Kimizuka, S. Miyamoto, R. Shimozawa, and K. Yatsunami, "The study of adsorption of detergents at a solution-air interface by radiotracer method. II. The kinetics of adsorption of sodium alkyl sulfates," *Bulletin of the Chemical Society of Japan*, vol. 32, no. 4, pp. 404–407, Apr. 1959.

[241] K. J. Mysels and A. T. Florence, "The effect of impurities on dynamic surface tension-basis for a valid surface purity criterion," *Journal of Colloid and Interface Science*, vol. 43, no. 3, pp. 577–582, Jun. 1973.

[242] K. M. Sachin, S. A. Karpe, M. Singh, and A. Bhattarai, "Study on surface properties of sodiumdodecyl sulfate and dodecyltrimethylammonium bromide mixed surfactants and their interaction with dyes," *Heliyon*, vol. 5, no. 4, p. e01510, Apr. 2019.

[243] A. Q. Shen, B. Gleason, G. H. McKinley, and H. A. Stone, "Fiber coating with surfactant solutions," *Physics of Fluids*, vol. 14, no. 11, pp. 4055–4068, Nov. 2002.

[244] D. Vollhardt and G. Emrich, "Coadsorption of sodium dodecyl sulfate and medium-chain alcohols at the air-water interface," *Colloids and Surfaces A: Physicochemical and Engineering Aspects*, vol. 161, no. 1, pp. 173–182, Jan. 2000.

[245] A. Wołowicz and K. Staszak, "Study of surface properties of aqueous solutions of sodium dodecyl sulfate in the presence of hydrochloric acid and heavy metal ions," *Journal of Molecular Liquids*, vol. 299, p. 112170, Feb. 2020.

[246] L. Martínez-Balbuena, A. Arteaga-Jiménez, E. Hernández-Zapata, and C. Márquez-Beltrán, "Applicability of the Gibbs adsorption isotherm to the analysis of experimental surface-tension data for ionic and nonionic surfactants," *Advances in Colloid and Interface Science*, vol. 247, pp. 178–184, Sep. 2017.

[247] G. Nilsson, "The adsorption of tritiated sodium dodecyl sulfate at the solution surface measured with a windowless, high humidity gas flow proportional counter," *Journal of Physical Chemistry*, vol. 61, no. 9, pp. 1135–1142, Sep. 1957.

[248] J. D. Hines, "The preparation of surface chemically pure sodiumn-dodecyl sulfate by foam fractionation," *Journal of Colloid and Interface Science*, vol. 180, no. 2, pp. 488–492, Jun. 1996.

[249] E. Weißenborn and B. Braunschweig, "Specific ion effects of dodecyl sulfate surfactants with alkali ions at the air–water interface," *Molecules*, vol. 24, no. 16, p. 2911, Aug. 2019.

[250] W. H. Press, S. A. Teukolsky, W. T. Vetterling, and B. P. Flannery, *Numerical recipes: The art of scientific computing*, 2nd ed. Cambridge: Cambridge University Press, 1992.

[251] K. A. Stroud and D. J. Booth, *Advanced engineering mathematics*, 6th ed. London: Red Globe Press, 2020.

[252] J. P. Boyd, *Chebyshev and Fourier spectral methods*, 2nd ed. Mineola, NY: Dover Publications, Inc., 2000.

[253] H. S. Carslaw, "A historical note on Gibbs' phenomenon in Fourier's series and integrals," *Bulletin of the American Mathematical Society*, vol. 31, no. 8, pp. 420–424, 1925.

[254] V. G. Levich and V. S. Krylov, "Surface tension-driven phenomena," *Annual Review of Fluid Mechanics*, vol. 1, pp. 293–316, 1969.

[255] Z. A. Zell, A. Nowbahar, V. Mansard, L. G. Leal, S. S. Deshmukh, J. M. Mecca, C. J. Tucker, and T. M. Squires, "Surface shear inviscidity of soluble surfactants," *Proceedings of the National Academy of Sciences*, vol. 111, no. 10, pp. 3677–3682, Mar. 2014.

[256] H. N. Stein, "The drainage of free liquid films," *Colloids and Surfaces A: Physicochemical and Engineering Aspects*, vol. 79, no. 1, pp. 71–80, Oct. 1993.

[257] B. V. Derjaguin, N. V. Churaev, V. M. Muller, and V. I. Kisin, *Surface forces*. New York: Springer, 1987.

[258] A. Scheludko, "Thin liquid films," *Advances in Colloid and Interface Science*, vol. 1, pp. 391–464, 1967.

[259] B. Mercier, *An introduction to the numerical analysis of spectral methods*, ser. Lecture Notes in Physics. Berlin Heidelberg: Springer-Verlag, 1989.

[260] R. A. Bernatz, *Fourier series and numerical methods for partial differential equations*. Hoboken, NJ: John Wiley & Sons, Jul. 2010.

[261] M. Renardy and R. C. Rogers, *An introduction to partial differential equations*. New York: Springer Science & Business Media, Apr. 2006.

[262] I. P. Stavroulakis and S. A. Tersian, *Partial differential equations: An introduction with Mathematica and MAPLE*, 2nd ed. River Edge, NJ: World Scientific, 2004.

[263] J. N. Reddy, *An introduction to the finite element method*, 3rd ed., ser. McGraw-Hill Series in Mechanical Engineering. New York: McGraw-Hill Higher Education, 2006.

[264] X. Liu and J. H. Duncan, “An experimental study of surfactant effects on spilling breakers,” *Journal of Fluid Mechanics*, vol. 567, pp. 433–455, Nov. 2006.

[265] C. H. Wong, M. M. Hossain, and C. E. Davies, “Performance of a continuous foam separation column as a function of process variables,” *Bioprocess and Biosystems Engineering*, vol. 24, no. 2, pp. 73–81, Sep. 2001.

[266] C. J. King, *Separation processes*, 2nd ed., ser. McGraw-Hill Chemical Engineering Series. New York: McGraw-Hill, 1980.

[267] D. L. Husband, J. H. Masliyah, and M. R. Gray, “Cell and surfactant separation by column flotation,” *Canadian Journal of Chemical Engineering*, vol. 72, no. 5, pp. 840–847, Oct. 1994.

[268] R. Grieves and S. Wang, “Foam separation of bacteria with a cationic surfactant,” *Biotechnology and Bioengineering*, vol. 9, no. 2, pp. 187–194, Apr. 1967.

[269] R. B. Grieves and S. L. Wang, “Foam separation of pseudomonas fluorescens and bacillus subtilis var. niger,” *Journal of Applied Microbiology*, vol. 15, pp. 76–81, 1996.

[270] W. A. Boyles and R. E. Lincoln, “Separation and concentration of bacterial spores and vegetative cells by foam flotation,” *Applied Microbiology*, vol. 6, pp. 327–334, 1958.

[271] S. B. Lee and D. D. Y. Ryu, “Separation of gentamicin by foaming,” *Biotechnology and Bioengineering*, vol. 21, no. 11, pp. 2045–2059, Nov. 1979.

[272] R. Dieter Gehle and K. Schiigerl, “Penicillin recovery from aqueous solutions by continuous foam flotation,” *Applied Microbiology and Biotechnology*, vol. 19, no. 6, pp. 373–375, Jun. 1984.

[273] D. Vitasari, P. Grassia, and P. Martin, "Simulation of dynamics of adsorption of mixed protein-surfactant on a bubble surface," *Colloids and Surfaces A: Physicochemical and Engineering Aspects*, vol. 438, pp. 63–73, 2013.

[274] P. Xanthopoulos and K. Binnemans, "Removal of cadmium, zinc, and manganese from dilute aqueous solutions by foam separation," *Journal of Sustainable Metallurgy*, vol. 7, no. 1, pp. 78–86, Mar. 2021.

[275] W. Shao, Y. Lin, and Y. Lu, "Study on the extraction technology of candida antarctica lipase b by foam separation," *Processes*, vol. 9, no. 1, p. 14, Dec. 2020.

[276] S. T. Tobin, D. Weaire, and S. Hutzler, "Theoretical analysis of the performance of a foam fractionation column," *Proceedings of the Royal Society A: Mathematical, Physical and Engineering Sciences*, vol. 470, p. 20130625, 2014.

[277] L. Brown, G. Narsimhan, and P. C. Wankat, "Foam fractionation of globular proteins," *Biotechnology and Bioengineering*, vol. 36, no. 9, pp. 947–959, Nov. 1990.

[278] P. Grassia, "Quasistatic model for foam fractionation," *Chemical Engineering Science*, vol. 275, p. 118721, 2023.

[279] P. Grassia, J. J. Cilliers, S. J. Neethling, and E. Ventura-Medina, "Quasi-one-dimensional foam drainage," *European Physical Journal E*, vol. 6, pp. 325–348, 2001.

[280] R. Miller, V. B. Fainerman, M. E. Leser, and M. Michel, "Kinetics of adsorption of proteins and surfactants," *Current Opinion in Colloid & Interface Science*, vol. 9, pp. 350–356, Dec. 2004.

[281] X. Xiong and N. Bansal, "β-Lactoglobulin," in *Encyclopedia of Dairy Sciences*. Amsterdam: Elsevier, 2022, pp. 860–869.

[282] G. Gochev, E. Scoppola, R. A. Campbell, B. A. Noskov, R. Miller, and E. Schneck, "β-lactoglobulin adsorption layers at the water/air surface: 3. Neutron reflectometry study on the effect of pH," *Journal of Physical Chemistry B*, vol. 123, no. 50, pp. 10 877–10 889, Dec. 2019.

[283] V. B. Fainerman, E. V. Aksenenko, A. V. Makievski, D. V. Trukhin, S. Yeganehzad, G. Gochev, and R. Miller, "Surface tension and dilational rheology of mixed β-casein– β-lactoglobulin aqueous solutions at the water/air interface," *Food Hydrocolloids*, vol. 106, p. 105883, Sep. 2020.

[284] F. J. Lech, "Foam properties of proteins, low molecular weight surfactants and their complexes," Ph.D. dissertation, Wageningen University, 2016.

[285] L. G. Leal, *Advanced transport phenomena: Fluid mechanics and convective transport processes*, ser. Cambridge Series in Chemical Engineering Book 7. Cambridge: Cambridge University Press, 2007.

[286] B. Tang, K. Chong, W. Massefski, and R. Evans, "Quantitative interpretation of protein diffusion coefficients in mixed protiated-deuteriated aqueous solvents," *Journal of Physical Chemistry B*, vol. 126, no. 31, pp. 5887–5895, Aug. 2022.

[287] C. Canuto, M. Y. Hussaini, A. Quarteroni, and T. A. Zang, *Spectral methods. Fundamentals in single domains*. Berlin, Heidelberg: Springer-Verlag, 2006.

[288] V. B. Fainerman, E. H. Lucassen-Reynders, and R. Miller, "Description of the adsorption behaviour of proteins at water/fluid interfaces in the framework of a two-dimensional solution model," *Advances in Colloid and Interface Science*, vol. 106, no. 1–3, pp. 237–259, Dec. 2003.

[289] J. A. V. Butler, "The thermodynamics of the surfaces of solutions," *Proceedings of the Royal Society of London. Series A, Containing Papers of a Mathematical and Physical Character*, vol. 135, no. 827, pp. 348–375, Mar. 1932.

[290] V. B. Fainerman and E. H. Lucassen-Reynders, "Adsorption of single and

mixed ionic surfactants at fluid interfaces," *Advances in Colloid and Interface Science*, vol. 96, no. 1–3, pp. 295–323, Feb. 2002.

[291] N. W. Loney, *Applied mathematical methods for chemical engineers*, 2nd ed. Boca Raton: CRC/Taylor & Francis, 2007.

[292] K. Atkinson, W. Han, and D. Stewart, *Numerical solution of ordinary differential equations*. New York: John Wiley & Sons, 2009.

[293] J. Y. Won, G. Gochev, V. Ulaganathan, J. Krägel, E. V. Aksenenko, V. B. Fainerman, and R. Miller, "Effect of solution pH on the adsorption of BLG at the solution/tetradecane interface," *Colloids and Surfaces A: Physicochemical and Engineering Aspects*, vol. 519, pp. 161–167, Apr. 2017.

[294] V. Ulaganathan, I. Retzlaff, J. Y. Won, G. Gochev, C. Gehin-Delval, M. Leser, B. A. Noskov, and R. Miller, "β-lactoglobulin adsorption layers at the water/air surface: 1. Adsorption kinetics and surface pressure isotherm: Effect of pH and ionic strength," *Colloids and Surfaces A: Physicochemical and Engineering Aspects*, vol. 519, pp. 153–160, Apr. 2017.

[295] A. V. Nguyen, "Historical note on the Stefan–Reynolds equations," *Journal of Colloid and Interface Science*, vol. 231, no. 1, p. 195, Nov. 2000.

[296] V. B. Fainerman and D. Vollhardt, "Surface pressure isotherm for the fluid State of Langmuir monolayers," *Journal of Physical Chemistry B*, vol. 110, no. 21, pp. 10 436–10 440, Jun. 2006.

[297] R. Miller, V. B. Fainerman, A. V. Makievski, J. Krägel, and R. Wüstneck, "Adsorption characteristics of mixed monolayers of a globular protein and a non-ionic surfactant," *Colloids and Surfaces A: Physicochemical and Engineering Aspects*, vol. 161, no. 1, pp. 151–157, Jan. 2000.

[298] E. H. Lucassen-Reynders, "Competitive adsorption of emulsifiers 1. Theory for

adsorption of small and large molecules," *Colloids and Surfaces A: Physicochemical and Engineering Aspects*, vol. 91, pp. 79–88, Nov. 1994.

[299] C. Kotsmar, V. Pradines, V. S. Alahverdjieva, E. V. Aksenenko, V. B. Fainerman, V. I. Kovalchuk, J. Krägel, M. E. Leser, B. A. Noskov, and R. Miller, "Thermodynamics, adsorption kinetics and rheology of mixed protein-surfactant interfacial layers," *Advances in Colloid and Interface Science*, vol. 150, no. 1, pp. 41–54, Aug. 2009.

[300] V. B. Fainerman, S. A. Zholob, M. Leser, M. Michel, and R. Miller, "Competitive adsorption from mixed nonionic surfactant/protein solutions," *Journal of Colloid and Interface Science*, vol. 274, no. 2, pp. 496–501, Jun. 2004.

[301] V. B. Fainerman, V. I. Kovalchuk, E. V. Aksenenko, M. Michel, M. E. Leser, and R. Miller, "Models of two-dimensional solution assuming the internal compressibility of adsorbed molecules: A comparative analysis," *Journal of Physical Chemistry B*, vol. 108, no. 36, pp. 13 700–13 705, Sep. 2004.

Appendix

The appendix section includes some extra information used when carrying out this study. In Sec. A 1, the derivation of the thinning rate equation for a rigid interface is presented. In Sec. A 2, we review the adsorption isotherm used in the case of a protein, while in Sec. A 3, we try to simplify the obtained isotherm and present it in the form of a Langmuir adsorption isotherm. Finally, in Sec. A 4, we analyse the resulting non-linear isotherm.

A 1 Thinning rate equation for a rigid interface

In this section, we aim to derive Eq. (2.9) known as the thinning rate equation. The presented two-dimensional model for film drainage derives from the work developed originally by Reynolds [41], under a set of assumptions known as the lubrication approximation (see also [135, 295]):

- The film-thickness or half-thickness δ, is very small when compared to its length (or half-length, L), i.e. $\delta \ll L$;
- Gravity and inertial forces are negligible when compared to viscous forces;
- The film fluid is assumed to be Newtonian (with constant viscosity) and also incompressible;

- The liquid-gas interfaces are rigid and parallel;
- The transversal velocity (along the z-axis) w, is small in comparison to the longitudinal velocity (along the x-axis) u;
- The variation of u with respect to z, is much higher than that of u with respect to x, i.e. $\partial u/\partial z \gg \partial u/\partial x$.

In the analytical estimate for thinning rate presented here, the film is assumed to be flat, non-deformable and in a quasi-steady state (as far as momentum balance is concerned), with also a boundary condition of zero velocity at the film interface (no-slip). Due to this, the fluid velocity field within the film will present a profile similar to a Poiseuille flow [171].

By applying the lubrication approximation to the momentum conservation equations for a two-dimensional thin film in Cartesian coordinates, we obtain:

$$\frac{\partial P}{\partial x} = \mu \frac{\partial^2 u}{\partial z^2}, \tag{A 1.1}$$

$$\frac{\partial P}{\partial z} = 0, \tag{A 1.2}$$

where P is the pressure within the film, and μ is the liquid viscosity. The film pressure varies only along the film length, being uniform across the film thickness, for any given position on the x-axis. The aforementioned equations have the following boundary conditions, due to symmetry with respect to the x- and z-axes:

$$\left.\frac{\partial u}{\partial z}\right|_{z=0} = w|_{z=0} = \left.\frac{\partial P}{\partial x}\right|_{x=0} = u|_{x=0} = 0. \tag{A 1.3}$$

The no-slip boundary condition at the liquid-gas interface is expressed as follows:

$$u|_{z=\pm\delta} = 0. \tag{A 1.4}$$

Finally, the initial film half-thickness, and the instantaneous film drainage velocity and pressure at the film boundaries are:

$$\delta|_{t=0} = \delta_0, \tag{A 1.5}$$

$$w|_{z=\pm\delta} = \pm\frac{\mathrm{d}\delta}{\mathrm{d}t} \tag{A 1.6}$$

$$P|_{x=L} = P_0. \tag{A 1.7}$$

In these circumstances, there are three dependent variables in the aforementioned equations that need to be solved to obtain an expression for the drainage rate of the film $\mathrm{d}\delta/\mathrm{d}t$. These dependent variables are the velocity along the x-axis u, the velocity along the z-axis w, and the pressure field along the film P. An analytical solution for u is obtained by integrating Eq. (A 1.1) twice, with the boundary condition Eq. (A 1.3) $\partial u/\partial z|_{z=0} = 0$, and the no-slip boundary condition in Eq. (A 1.4), $u|_{z=\pm\delta} = 0$, as follows:

$$u(x,z,t) = -\frac{1}{2\mu}\frac{\partial P}{\partial x}(\delta^2 - z^2). \tag{A 1.8}$$

The continuity equation in Cartesian coordinates is:

$$\frac{\partial u}{\partial x} + \frac{\partial w}{\partial z} = 0. \tag{A 1.9}$$

By substituting the expression for u found in Eq. (A 1.8) into the continuity equation (Eq. (A 1.9)), and integrating with the boundary condition in Eq. (A 1.3) $w|_{z=0} = 0$, we can now derive an expression for the transversal velocity w, as follows:

$$w(x,z,t) = \frac{1}{2\mu}\frac{\partial^2 P}{\partial x^2}\left(\delta^2 z - \frac{z^3}{3}\right). \tag{A 1.10}$$

We can now relate pressure P, with the film thinning rate $\mathrm{d}\delta/\mathrm{d}t$, and the film half-thickness δ, by applying the boundary condition Eq. (A 1.6), to the expression

just obtained for w, in Eq. (A 1.10):

$$\frac{\partial^2 P}{\partial x^2} = \frac{3\mu}{\delta^3}\frac{\mathrm{d}\delta}{\mathrm{d}t}. \tag{A 1.11}$$

A solution for the pressure along the film, $P(x)$, is obtained by integrating Eq. (A 1.11) twice, with the boundary conditions from Eq. (A 1.3) $\partial P/\partial x|_{x=0} = 0$, and also Eq. (A 1.7) $P|_{x=L} = P_0$:

$$P = -\frac{3\mu}{\delta^3}\frac{\mathrm{d}\delta}{\mathrm{d}t}\left(\frac{L^2}{2} - \frac{x^2}{2}\right) + P_0. \tag{A 1.12}$$

Here, δ and hence $\mathrm{d}\delta/\mathrm{d}t$ are treated as spatially uniform. The film drainage rate $\mathrm{d}\delta/\mathrm{d}t$, can now be expressed as a function of the pressure change between the centre of the thin film and its boundary with the Plateau border $\Delta P = P|_{x=0} - P_0$, thereby obtaining the so-called Stefan-Reynolds equation [41, 49, 133, 171, 295]:

$$\frac{\mathrm{d}\delta}{\mathrm{d}t} = -\frac{2\delta^3 \Delta P}{3\mu L^2}, \tag{A 1.13}$$

where δ is the film half-thickness at an instant t, L is the film half-length, μ is the film bulk viscosity, and ΔP is the excess pressure driving the drainage mechanism within the film.

Generally speaking, the excess pressure ΔP involves combining a capillary pressure P_c, and a disjoining pressure Π_d. At a sufficiently large δ, the disjoining pressure Π_d, is small compared to capillary P_c, therefore the excess pressure in the film will be approximately the capillary pressure. Thus $\Delta P \approx \gamma_{\mathrm{Pb}}/a$, where γ_{Pb} is surface tension and a is the radius of curvature of the Plateau border. We can now rewrite $\mathrm{d}\delta/\mathrm{d}t$ as follows:

$$\frac{\mathrm{d}\delta}{\mathrm{d}t} = -\frac{2\gamma_{\mathrm{Pb}}\delta^3}{3\mu L^2 a}. \tag{A 1.14}$$

It is now possible to derive an expression to estimate the film half-thickness δ, by

rearranging and integrating Eq. (A 1.14), using initial condition Eq. (A 1.5):

$$\delta = \delta_0 \left(1 + \frac{4}{3}\frac{\gamma_{\mathrm{Pb}}\delta_0^2}{\mu L^2 a}t\right)^{-1/2}. \tag{A 1.15}$$

where δ_0 is the film half-thickness at the initial time. This then is the expression for evolution of film thickness which we employ here.

A 2 Equilibrium adsorption behaviour of proteins

This section provides extra information to support the discussion in Sec. 2.5.4 on how adsorption isotherms for proteins are calculated. The large area and large number of conformations of an adsorbed protein molecule can be modelled as a significant increase in the non-ideality of the system. This is the reason why the simplest adsorption isotherms, e.g. Henry, and Langmuir adsorption isotherms do not always describe protein adsorption with high accuracy [163, 288].

Components of a mixture cover surface area A, with their partial molar surface areas ω_i, and moles adsorbed values $\mathcal{N}_i^s$ [163], related as expressed below:

$$\omega_0\mathcal{N}_0^s + \omega_1\mathcal{N}_1^s + \omega_2\mathcal{N}_2^s + ... = A \tag{A 2.16}$$

where the partial molar surface areas are defined as $\omega_i = \partial A/\partial\mathcal{N}_i^s$ at fixed $\mathcal{N}_{j\neq i}^s$ values. Here as mentioned $\mathcal{N}_i^s$ is the number of moles of i^{th} component in the surface layer. In addition, we define $\Gamma_i = \mathcal{N}_i^s/A$ and also the respective fractions of surface coverage $\theta_i = \omega_i\Gamma_i$. Moreover, ω_0 is the molar area of the solvent, although its value may depend on the choice of the position of the dividing surface [296]. From Eq. (A 2.16) we obtain:

$$\omega_0\Gamma_0 + \omega_1\Gamma_1 + \omega_2\Gamma_2 + ... = \theta_0 + \theta_1 + \theta_2 + ... = 1 \tag{A 2.17}$$

where subscript 0 refers to the solvent. In what follows, the subscript P stands for protein, where Γ_P is the total adsorption of proteins in all n available states. For macromolecules such as proteins, since they typically have an actual molar area much larger than that of the solvent, the notation makes a distinction between values of the area ω_0, on the solvent and the areas ω_j, corresponding to all the dissolved species (or conformational states thereof). Thus to distinguish ω_P from ω_0, the following relations are used [297, 298]:

$$\omega_0 \neq \omega_P = \frac{\sum_{i=1}^{n} \omega_i \Gamma_i}{\sum_{i=1}^{n} \Gamma_i} = \frac{\omega_1 \Gamma_1 + \omega_2 \Gamma_2 + ...}{\Gamma_1 + \Gamma_2 + ...} \tag{A 2.18}$$

$$\Gamma_P = \sum_{i=1}^{n} \Gamma_i. \tag{A 2.19}$$

Here clearly ω_P is the weighted-average molar surface area, and depends on the total protein adsorption. Moreover we define

$$\theta_P = \omega_P \Gamma_P = \sum_{i=1}^{n} \omega_i \Gamma_i. \tag{A 2.20}$$

Here, $\theta_P = \sum_{i \geq 1} \theta_i = 1 - \theta_0$ is the total fraction of the surface covered with protein. The following equation of state can be used for the protein's surface layer [299]:

$$\Pi = -\frac{RT}{\omega_0} \left[\ln(1 - \theta_P) + \theta_P (1 - \omega_0/\omega_P) + \alpha_P \theta_P^2 \right] \tag{A 2.21}$$

where Π denotes surface pressure (i.e. the difference in surface tension arising due to adsportion), α_P is the parameter of non-ideality (Frumkin's parameter, $\alpha_P > 0$ implies intermolecular attraction [159]). This is associated with an adsorption isotherm equation for each state j of the protein molecule in the surface layer, as follows [300]:

$$b_{Pj} c_P = \frac{\omega_P \Gamma_j}{(1 - \theta_P)^{\omega_j/\omega_P}} \exp[-2\alpha_P (\omega_j/\omega_P) \theta_P] \tag{A 2.22}$$

where c_P is the concentration of the protein in the subsurface layer, and the b_{Pj} terms

are the adsorption equilibrium constant of protein in the state j. Here specifically, b_{Pj} is the adsorption equilibrium constant for the protein in the j^{th} state; ω_P is the average molar surface area of the protein (see Eq. (A 2.18)). Also $\omega_j = \omega_1 + (j-1)\omega_0$ is the molar surface area of the protein in the j^{th} state, assuming that the increment of molar surface area upon transition from a given state to a neighbour state is equal to ω_0, such that $\omega_1 = \omega_{min}$ and $\omega_{max} = \omega_1 + (n-1)\omega_0$. For solutions of single surfactants adsorbed in a single state at the surface, this equation transforms into a Frumkin model equation [301].

It is known that the surface activity of adsorbed proteins increases with increasing the partial molar area ω_j, according to a power law with a constant exponent α, as below [194]:

$$b_{Pj} = b_{P_{min}} \left(\frac{\omega_j}{\omega_{min}} \right)^{\alpha}. \tag{A 2.23}$$

Note that $b_{P_{min}}$ is the adsorption equilibrium constant for the protein molecules in the first (i.e. smallest area) state. Then, combining Eqs. (A 2.22) and (A 2.23), one can obtain [159]:

$$b_{P_{min}} c_P = \frac{\omega_P \Gamma_j}{(\omega_j/\omega_{min})^{\alpha}(1-\theta_P)^{\omega_j/\omega_P}} \exp[-2\alpha_P(\omega_j/\omega_P)\theta_P]. \tag{A 2.24}$$

To summarise, in this section, a set of parameters, relationships and equations have been presented to demonstrate just how complicated protein adsorption behaviour can be. Generally, these adsorption isotherms contain numerous unknowns and are required to be matched with experimental data to enable us to calculate parameters values. A simpler (albeit less accurate) approach is proposed in the next section.

A 3 Simpler approach to protein adsorption isotherm

In this section, we indicate how to simplify the very complicated protein adsorption isotherm discussed in Sec. A 2 by fitting a Langmuir isotherm to it (effectively

replacing Eq. (A 2.22) with something much simpler). Even though we are aware that this is not a perfect fit, it nonetheless allows us to obtain adsorption parameters in our model and as a result to carry out mass transport calculations.

First, we obtain an average value for b_{Pj} over the concentration domain of interest and name it b_{avg}. Then, we average all the ω_j (for $j \geq 1$) to obtain ω_{avg}. Next, starting from Eq. (A 2.22), we determine θ_P values in the domain of interest, and we use an average for it (θ_{avg}) within the exponential term. This results in replacing $\exp(-2\alpha_P\theta_P)$ with $\exp(-2\alpha_P\theta_{avg})$. As long as θ_P does not change too much in the range of interest, this assumption can be reasonable [162].

By replacing b_{Pj} by b_{avg}, ω_j by ω_{avg} and ω_P by ω_{avg} in Eq. (A 2.22), the following equation will be obtained:

$$b_{avg}c_P = \frac{\omega_{avg}\Gamma_j}{(1-\theta_P)}\exp(-2\alpha_P\theta_{avg}). \tag{A 3.25}$$

If we sum over j and by using $B_P = n\, b_{avg}$, we obtain the following expression:

$$B_P c_P = \frac{\omega_{avg}\Gamma_P}{(1-\omega_{avg}\Gamma_P)}\exp(-2\alpha_P\theta_{avg}). \tag{A 3.26}$$

We define an effective B_P as $\bar{B}_{Peff} = B_P\exp(2\alpha_P\theta_{avg})$, which can be considered an analogue to the Langmuir parameter ($\bar{K}_L$), we now have:

$$\bar{B}_{Peff}c_P = \frac{\omega_{avg}\Gamma_P}{(1-\omega_{avg}\Gamma_P)} \tag{A 3.27}$$

and maximum packing is $\bar{\Gamma}_{Pmax} = 1/\omega_{avg}$. Rearranging Eq. (A 3.27) leads to the following equation:

$$\Gamma_P = \frac{\bar{\Gamma}_{Pmax}\bar{B}_{Peff}c_P}{1+\bar{B}_{Peff}c_P}. \tag{A 3.28}$$

This then is a simple way to replace the complicated protein isotherm with a simple approximate Langmuir one. However, as mentioned previously it cannot predict

protein concentration behaviour on the surface and in the bulk quite so accurately. Nonetheless it has the advantage that it can be used easily in our modelling study.

A 4 Analysing non-linear isotherm for β-LG

In the small $\mathrm{Pe}\,\Delta$ case discussed in Chapter 4, we used both global and local Henry isotherms when relating surfactant surface and bulk concentrations, with the local Henry isotherm taking account, at least to some extent, of rather more complicated isotherm shapes. In the large $\mathrm{Pe}\,\Delta$ case discussed in Chapter 6 however, we focussed mostly on a local Henry isotherm. However, the large $\mathrm{Pe}\,\Delta$ case is special in that fluid elements in the bulk retain their bulk concentration throughout the evolution. Given that we typically normalise the system by respective surface and bulk concentrations in the Plateau border, all the information we really need from an isotherm is to obtain bulk concentration in the film given initial surface concentration of the film. However, in this case, we can also easily substitute a non-linear isotherm, such as the Langmuir adsorption isotherm (see Fig. 2.6) instead of a linear one (see Sec. 7.5.1 for example). In what follows we estimate some typical parameter values that could be used in an analysis like that in Sec. 7.5.1.

To obtain a simplified Langmuir adsorption isotherm for β-LG, we used the procedure explained in Sec. A 3. We have also taken β-LG relevant adsorption data from [159, 162, 205]. Doing this results in the following parameters, $B_P = 1.9 \times 10^3\,\mathrm{m^3.mol^{-1}}$, $\alpha_P = 0.4$, $\theta_{avg} = 0.9$ and $\omega_{avg} = 10^7\,\mathrm{m^2.mol^{-1}}$. This will then result in an amount for $\bar{B}_{Peff} \approx 3900\,\mathrm{m^3.mol^{-1}}$ and for $\bar{\Gamma}_{Pmax} = 10^{-7}\,\mathrm{mol.m^{-2}}$. We also set c_{Pb} equal $1 \times 10^{-2}\,\mathrm{mol.m^{-3}}$ to be consistent with data assumed in Tables 7.2 and 7.3. Using this c_{Pb}, the value of Γ_{Pb} turns out to be $9.75 \times 10^{-8}\,\mathrm{mol.m^{-2}}$. As can be seen, the obtained Γ_{Pb} is slightly different from what had been used in Chapters 6 and 7 as now a Langmuir isotherm is fitted to the β-LG adsorption data (rather than reading from data directly as Table 7.1 did).

Now, we convert to dimensionless variables, effectively normalising by the c_{Pb} and Γ_{Pb} mentioned above. For compactness of notation we use the same symbols c_P and Γ_P as before. The nondimensional Langmuir adsorption isotherm is:

$$\Gamma_P = \frac{\Gamma_{Pmax} B_{Peff} c_P}{1 + B_{Peff} c_P} \tag{A 4.29}$$

where Γ_{Pmax} and B_{Peff} are dimensionless analogues of $\bar{\Gamma}_{Pmax}$ and $\bar{B}_{Peff}$, and turn out to be 1.0256 and 39, respectively, from the nondimensionalization procedure explained in Sec. 5.5. Using Eq. (A 4.29) and the aforementioned variables will lead to the β-LG adsorption isotherm in dimensionless form as plotted in Fig. A 4.1.

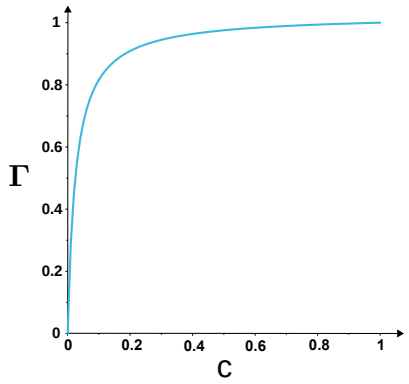

Figure A 4.1: β-LG approximation to Langmuir adsorption isotherm cast in dimensionless form

Table A 4.1 (again in dimensionless form) shows surfactant concentrations on the surface for various initial surfactant bulk concentrations.

Table A 4.1: Values of various initial surfactant bulk concentrations and their corresponding surface concentrations are taken from Eq. (A 4.29). Data are presented in dimensionless form.

c_0	Γ_0
0.1	0.816
0.3	0.945
0.5	0.976
0.7	0.989
0.9	0.997

Alternatively Table A 4.2 shows surfactant concentrations in the bulk for various initial surfactant surface concentrations.

Table A 4.2: Values of various initial surfactant surface concentrations and their corresponding bulk concentrations are taken from Eq. (A 4.29). Data are presented in dimensionless form.

Γ_0	c_0
0.1	0.00277
0.3	0.01060
0.5	0.02439
0.7	0.05512
0.9	0.18367

As can be seen from Tables A 4.1 and A 4.2, dimensionless surfactant surface concentration is always higher than the corresponding dimensionless bulk concentration or alternatively, for the same initial surfactant surface concentration, initial surfactant bulk concentrations are always much smaller. Remember (see Secs. 6.3.3 and 6.3.4) that to have significant surfactant exchange between the bulk of the film and the bulk of the Plateau border, it was necessary for an area ratio A_b/A_t (film area cross section exchanged divided by total film cross section) to be not too small, and the way to achieve that was to have comparatively small Γ_0. It is clear though that, for the isotherm considered here, this only occurs for extremely low initial surfactant bulk concentrations (even lower than $c_0 = 0.1$).